博士論文

Computational design with bending behavior of wood
- explored through simulations on pliability of wood

(木材の曲げを用いたコンピュテーショナルデザイン

－木材の屈撓性に関するシミュレーションを通じて)

江　莱

Acknowledgement

I would like to express my special appreciation and gratitude to my supervisor Professor Obuchi Yusuke for his encouraging comments and precious time spent on improving my research. I would also like to thank the committee members Professor Sato Jun, Professor Tsunetsugu Yuko, Professor Otsuki Toshio and Professor Fujita Kaori for their patience and brilliant comments and suggestions. My sincere thanks also go to Professor Shida Satoshi, Dr. Maeda and Mr. Furuichi Shohei for providing me materials and giving me access to the laboratory and research facilities. This thesis is not possible without their precious support. I would also like to show my gratitude to Professor Kuma Kengo, Dr. Hirano Toshiki and staff from Haseko Corporation, Kabushiki Nittax and Kabushiki Aruku whom I worked together with on Project URO-CO, for their great support throughout the whole project.

Last but not least, I would also like to thank my family, friends and Mr Kurihara Moritsune for their endless encouragement and support during my hardship. Both of my grandmothers passed away during my doctoral study. I wish they rest in peace.

Table of Contents

Abstract

Wood has been a common construction material for the human beings since ancient times. While lamination technology has driven wood to become stronger and less prone to undesired deformations, people also never stop bending wood for various uses as it is a pliable material when certain conditions apply. However, the way to bend wood did not change much since ancient times. As a common practice in building industry, steam and much external force, equipment and spaces are usually required to bend wood. Thus, by taking advantage of the heterogeneous properties of wood, this research investigates into new ways to engineer wood surfaces and simulate their bending behaviors. The bending behavior is discussed in two categories: self-actuated bending and kerf bending of wood. The former utilizes the hygroscopicity and anisotropy of wood to manipulate the curvature of the bent wood, allowing for a 2-dimensional to 3-dimensional transformation; while the latter demonstrated a reverse process in which anisotropy is created in the homogeneous plywood. For either approach, physical prototypes and digital simulations were explored while the latter had a furniture-scaled physical output. By evaluating these two approaches for bending, design scenarios could be composed for using individual and combination of these bending methods by taking advantage of both of them.

Introduction

Human beings have been working with wood for a long time. Wood is widely used through our life from small objects such as housewares and tools to large items such as furniture and construction materials. People love to use wood not only because of its soft touch, warmth and fragrance that is unique to the material, but also because of the flexibility and strength that it provides. Japan has a long history of using wood as a construction material. In Japanese traditional folk houses, columns and beams were carefully selected to be used as the same condition as they were grown so that undesirable deformations due to the change in the environment was minimized.

Wood has been treated as a living material which can respond to the environmental changes in Japan. Due to its microstructure, water molecules entering and leaving the microfibrils of cellulose of cell walls, causes the dimensional expansion and shrinkage of wood. This hygroscopic property is a double-edged sword. On the one hand, this property has escalated the standardization of wood used in the construction industry, thus homogenization of wood as a material. For a long time, wood was used and shaped by paying extra care to the expansion and shrinkage of wood due to the change in the environment. Lamination is one of the efficient ways to minimize this deformation of wood. Attempts trying to use lamination as a way to fabricate a material that is dimensional stable and strong in all directions can be found back to 3500 years ago in ancient Egypt (Figure a). It is not until the invention of water-proof glue towards the end of 19th century that laminated wood could be afforded and accessible to ordinary people. The development of technology such as cross laminated timber (CLT) and establishment of regulations such as JAS (Japanese Agricultural Standard) for plywood since 1953, enabled standardization in the industry, allowing for minimum deformation of wood due to the change in environment (Hayashi 2012).

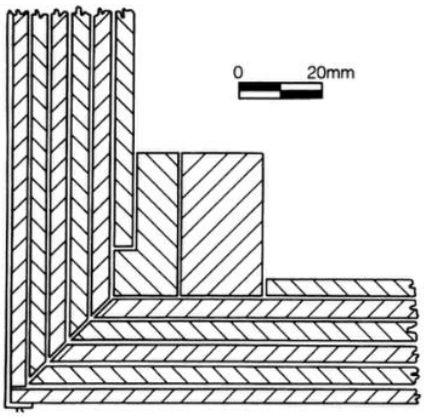

Figure a. Plywood construction on a coffin found in Gallery V under eastern part of the Third-Dynasty Step Pyramid of Djoser at Saqqara. (Nicholson & Shaw, 2000)

However, on the other hand, this deformation is not necessarily bad. By taking advantage of this hygroscopic property of wood due the adsorption and desorption of water, the spa buckets in Japan, for example, utilized this property of wood to make it watertight (Figure b).

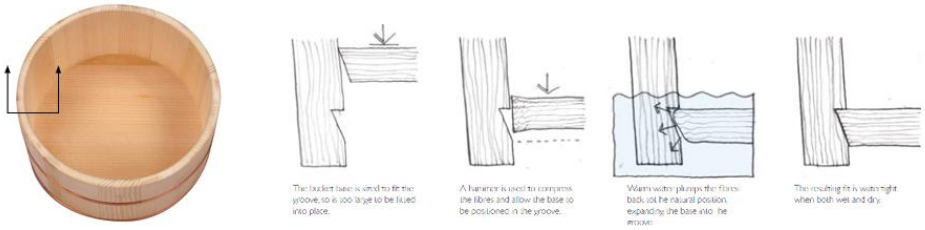

Figure b. Left: A watertight foot spa bucket. (Kodai Sangyo Co. Ltd 2007)
Right: The making process taking advantage of the hygroscopic property of wood. The change in the dimension due to the moisture change locks the base into the groove, making it watertight. (Miller 2015)

Furthermore, by taking advantage of this property of wood, bending technologies are developed to bend wood to a specific form. While wood itself has the property of being able to deform with environmental changes, extreme conditions were also applied to bend wood to a form that could be reproduced i.e. mass production. With the help of steam box and a positive form, wood can be bent to different curves. Thonet chair produced in the 1850s has marked the mass production of bent wood making use of hygroscopicity of wood (Figure c)

Figure c. Thonet Chair mass produced in 1850s, denoting the standardization of wood bending technology. (THONET, n.d.)

This method of bending, steam bending, is most commonly used today. Although the principle is to make use of the hygroscopicity of wood, however, much external forces, formwork, extreme conditions, equipment and manpower were required for the bending. Especially, formworks have to be used to control the geometry of the final outcome. However, with the advancements in computational technologies and machinery, recent researches have demonstrated the possibility of bending wood without formwork and minimum external forces and energy – self-actuated bending using hygroscopicity and anisotropy of wood and kerf pattern introducing anisotropy into wood for it to bend.

Thus, this research aims to investigate into these two ways of bending wood surfaces with minimum extra energy, equipment and manpower -

Pioneered by Menges (Menges & Reichert, 2012), the self-actuated mechanism of wood makes use of hygroscopicity of wood, making wood a smart material with embedded intelligence. Different from the existing bending technologies which bend the wood using much external forces, manpower and equipment, by combining two layers of wood cut in different directions from tree log and a change in relative humidity, anisotropy of wood will automatically give rise to different stress in both layers, hence causing an automatic bend.

Other than this 'low-tech' bending, another technique, kerf pattern is also a way to bend wood with minimum energy and manpower. It is a technique used back since the old times when people scoring on wood strips to make it soft enough to bend. The emergence of cutting machines in the 1930s has enabled wood to bend like rubber by introducing cuttings in wood pieces at Bauhaus (Moholy-Nagy, 1975). With the aid of computer-controlled machines, this subtractive process can be conveniently applied to wood materials ranging from MDF to wood panels. The patterns can be designed to create anisotropy into any homogeneous or non-homogeneous material.

This research thesis is structured with an introduction of background and key knowledge to understand the following sections in the beginning, followed by precedent studies regarding two approaches of bending wood – self-actuated and kerf bending. These two methods were particularly looked into because of their minimum requirement for bending a wood surface. For self-actuated bending, it has been researched extensively only in recent years. By making use of the bi-layer theory developed by Timoshenko (Timoshenko, 1925) on thermal metal and learning from the pioneers in this field, experiments were designed to adapt this methodology for single species and for simulation of the bending behavior. For kerf patterned bending, the precedents so far focused mainly on applying it partially to wood or plywood. The relationship pattern and bending radius was not explored. Hence, this research will explore a full kerf bending with considerations on the extent of bending as well. The outcome will be a furniture-scale full kerf pattern object.

The goals of this research are:

- To explore methodologies for making simulations from physical investigations of the two different bending behaviour of wood – self-actuated bending and kerf bending
- To evaluate the two approaches of bending wood and discuss the possible design scenarios applicable.

Below is an illustration of the structure of the research (Figure d):

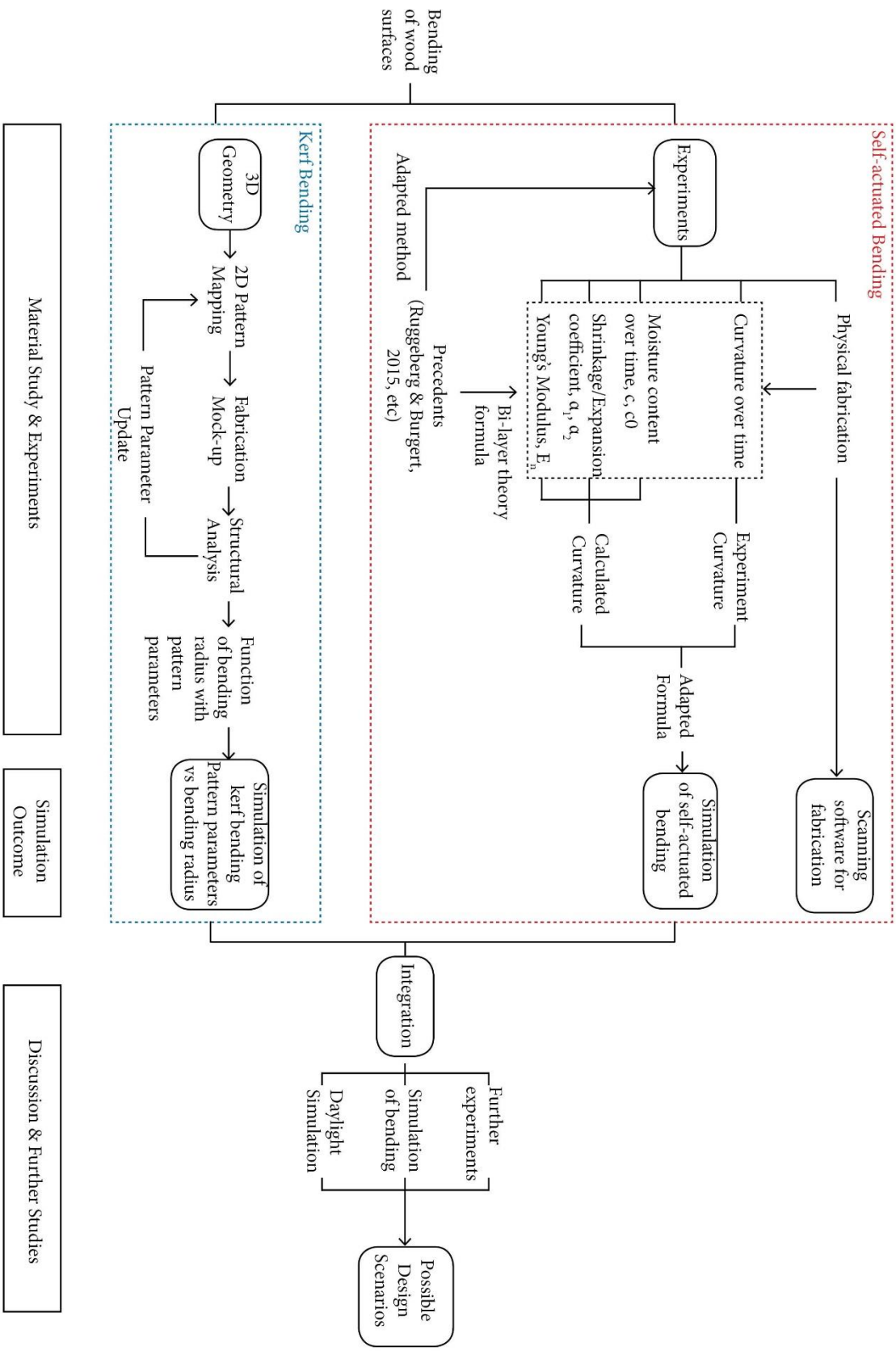

Figure d. Structure of research

Chapter 1 – Background

Pliability is defined as the ability to bend easily into a new shape without breaking or cracking, or the degree to which a substance can do this (Dictionary.cambridge.org, 2019). Wood has been well known for its pliability since ancient times. This ability exists in many forms. Figure 1-1 illustrated a brief history of using the techniques of bending wood. In ancient Egypt, steam was used to bend wood to make bows for military use. Since ancient Japan, wood was sliced into thin layers and bent to make well formworks since Heian Era (Iwai, 1994). Human beings have been dealt with bending wood for a long time. However, it is not until the emergence of Thonet chair No. 14 created by Michael Thonet that the bending of wood could achieve a consistent shape and ready for mass production.

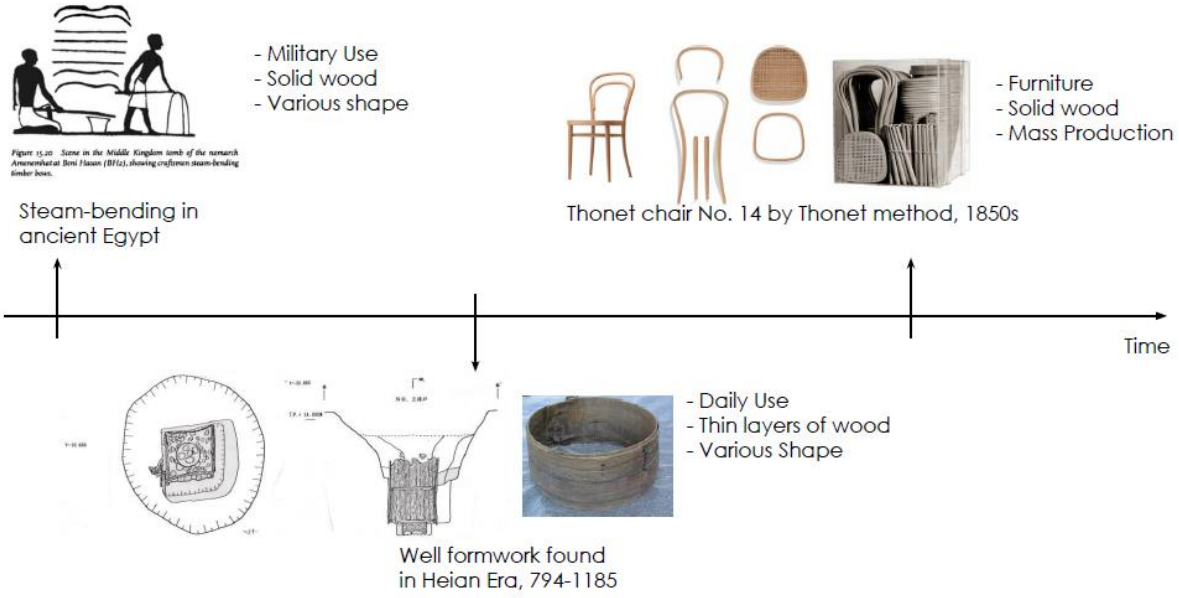

Figure 1-1. Brief history of bending wood. Top left: Scene in the Middle Kingdom Tomb of the Nomarch Amenemhat at Beni Hasan, showing craftsman steam-bending timber bows (Nicholson & Shaw, 2000). Bottom: Well formwork of Heian Era made by bending thin layers of wood found in Nara Prefecture (*Well formwork found in 2013*, n.d.). Top right: Thonet chair marks the mass production of wood bending technology (THONET, n.d.).

In architecture industry, one of the most famous pieces using pliability of wood for construction is the Mannheim Multihalle designed by Frei Otto back in the 1970s. The laths structure was flat at first and pushed from the bottom and lifted by scaffolds to create the bending stress in the wood laths to form the

double-curved geometry (Figure 1-2). Four layers of wood laths of 50mm x 50mm was used instead of ones with larger sectional area so as to allow them to be bent easily (Happold & Liddell, 1975). Another example making use of the pliability of wood is wood shingles used for the onion roof for the church on Kizhi Island of Russia. Each piece of wood shingles was customized to fit the curvature of the onion shaped roof.

Figure 1-2. Mannheim Multihalle, 1974. Designed by Frei Otto with Ove Arup and Partners (Happold & Liddell, 1975) The photo on the right was illustrating the lifting process of the wood laths.

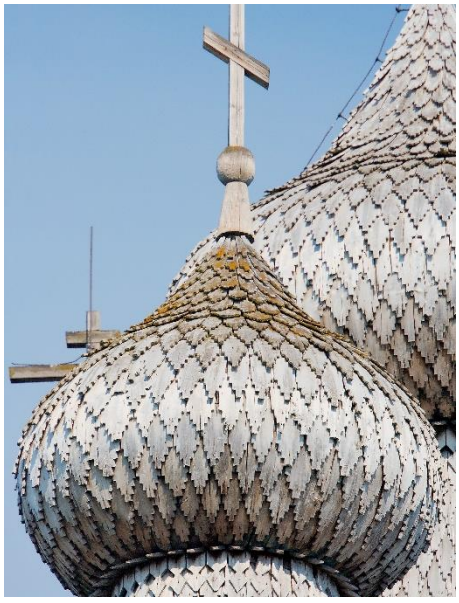

Figure 1-3. Onion roof of The Church of Transfiguration from Kizhi Island, Russia. The roof was made from steam-bent wood shingles (Kabel, 2008)

The history and examples have demonstrated that wood is a pliable material. The pliability of wood is highly related to its microstructure. In this chapter,

microstructure of wood that results in the inherited properties of wood and the bending technologies that utilized the properties of wood will be explained.

1.1 Hygroscopicity of wood

Hygroscopicity is the tendency of a solid substance to absorb moisture from the surrounding atmosphere (Richardson, 2011). Wood by its nature is a hygroscopic substance which is able to adsorb and desorb water molecules from and to its surrounding environment.

The adsorption and desorption mechanisms are achieved by the specific cellular structure of wood. The cell walls of wood consist of cellulose, hemicellulose and lignin in which cellulose and hemicellulose are able to bond with water molecules. Cellulose molecules bundle together to form microfibrils which is the major structural component of wood. Water entering between the microfibrils of cellulose and in between the crystallites of microfibrils makes wood start to swell.

Water entering the cell walls is known as bound water while that entering cell cavities after cell wall is saturated is known as free water. Fiber saturation point (FSP) is reached when there is no water in the cell cavities while the cell wall is completely saturated. When wood is dried beyond FSP, bound water starts to leave microfibrils, shortening the distance between them. Wood starts to shrink. Free water has little effect on the dimensional change of wood while bound water does. Thus, only beyond FSP dimensional change occurs (Figure 1-4). The moisture content (MC) of FSP of most wood is around 25% to 30% disregarding of tree species (Hayashi 2012). Wood swells when bound water increases and shrinks when bound water decreases. The expansion and shrinkage processes are reversible.

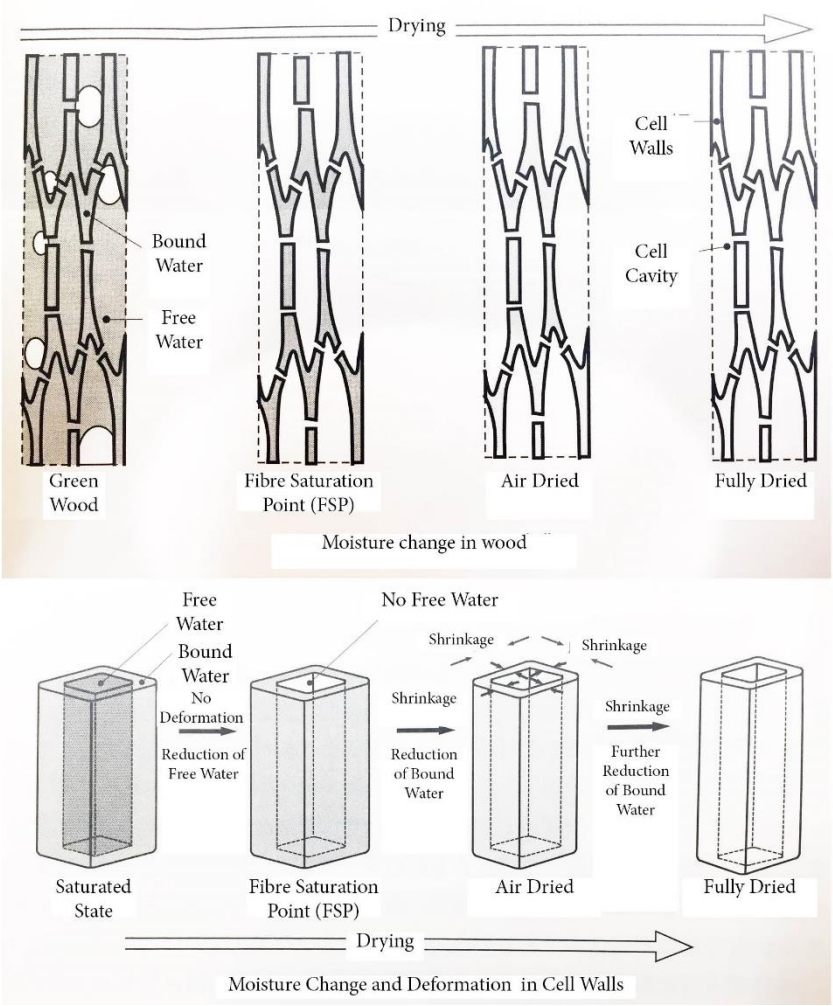

Figure 1-4. Microstructure of wood. (Hayashi 2012) (Translated).

The moisture content (u) of wood refers to the total amount of water in the wood and is calculated by the following equation

$$u = \frac{m_u - m_{dr}}{m_{dr}} \cdot 100\% \qquad \text{(Eq.1)}$$

where m_u is the mass of wood at moisture content u and m_{dr} is the mass of wood when it is fully dried.

The moisture content will stop changing in constant environment when equilibrium moisture content (EMC) is reached. Equilibrium moisture content is the moisture level when there is neither gain nor loss in moisture content as it is at equilibrium condition with the surrounding environments. Although under the same relative humidity, EMC is almost the same for

different tree species around 12-15%, once the environmental condition is changed, this mechanism will start work again until it reaches another equilibrium (Hayashi 2012). In other words, it is closely related to the relative humidity of the environment. EMC can be calculated:

$$EMC = 1800/W*[KH/(1-KH) + (K_1KH + 2K_1K_2K^2H^2)/(1 + K_1KH + K_1K_2K^2H^2)] \quad \text{(Eq. 2)}$$

where:
M = moisture content (%)
T = temperature (oF)
H = relative humidity (%) / 100
$W = 330 + 0.452T + 0.00415T^2$
$K = 0.791 + 0.000463T - 0.000000844T^2$
$K1 = 6.34 + 0.000775T - 0.0000935T^2$
$K2 = 1.09 + 0.0284T - 0.0000904T^2$
(Mitchell, 2017)

Thus, the dimensional change of wood is due to this change in moisture content at micro-level. From here it is understood that the hygroscopic property of wood is highly dependent on the environment condition such as temperature and relative humidity. It is also a reversible phenomenon resulting from its hierarchical structure.

1.2 Technology of bending wood

As mentioned above, human beings have been trying to bend wood for military, daily use and design for a long time. The bending technologies has also been advancing. Various bending technologies has been developed to bend the wood to the target geometry, all of which utilize the hygroscopic properties and physical properties of wood. Regardless of how the technology has developed, the principles of bending wood have not been changed. The most commonly known method is still

steaming bending but with pressure and better and automated set-ups (Figure 1-5). To pass steam through wood using a steam box helps to plasticize lignin of wood, making it soften. After clamping the wood to the shape desired and wait for it to cool down, wood will stay as bent. Wood can also be bent when the thickness is small enough. Hence, bending wood using a jig before the veneers are laminated together is another method commonly used for making furniture and architectural beams (Figure 1-6). After the glue has dried, wood can stay curved. This method requires much extra formwork and manpower for bending one piece of wood. Pressurized ammonia is also used to complete extreme bending for wood. This method changes the appearance and microstructure irreversibly. As it has higher requirement for processing, it is not so widely used (Figure1-7). Heat bending is another way for bending wood, too. Wood is soaked in water before bending it on a bending iron (Figure 1-8.). This method allows for detailed manipulation of curvatures. Hence, it is commonly used for making musical instruments.

Figure 1-5. Automated steam bending. Bending requires much external energy, equipment and force. (GHEBavaria, 2012)

Figure 1-6. Steam bending wood with jigs and manpower (Making curved beams, 2017)

Figure 1-7. Pressurized bending. (Applied Science, 2015)

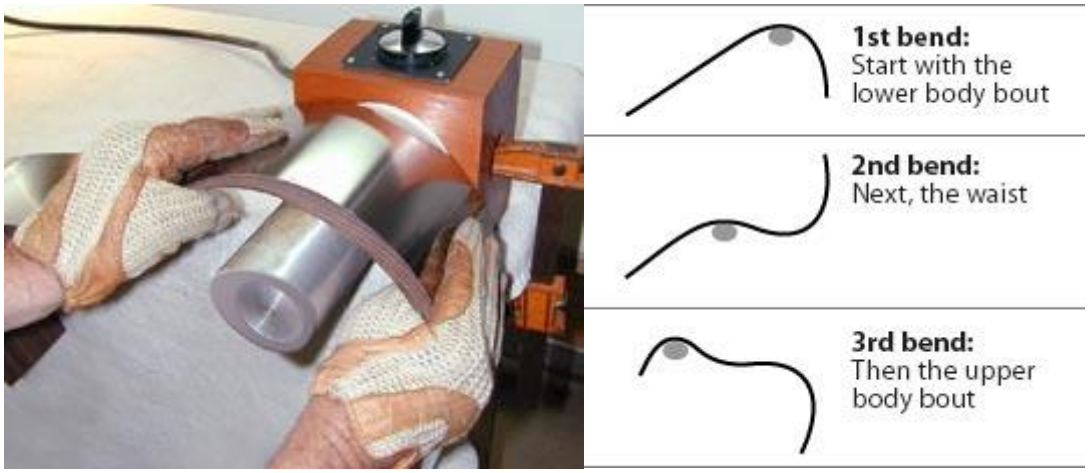

Figure 1-8. Heat bending using an electrical bending iron (Stew MacDonald, n.d.)

However, all the methods mentioned above require extra equipment, energy, formwork and certain amount of manpower. The need for extra equipment also limits the size of wood that is able to be processed as well. In order to process the wood, there is a need to build supporting steam box or jig that is much larger than the final product. And most of it fall into the category of craftsmanship, which is still mainly by trial and error and experience. Furthermore, from the traditional bending skills to modern bending technologies, most of the applications apply on wood with rod-like shape which gains the moment easily to be bent instead of treating on a surface. This limits the possibility of wood of being further widely used.

Therefore, it is necessary to fully utilize the potential of the properties of wood to reduce the need for extra input of equipment and materials during the bending process. With the development of computational technology and fabrication methods, it has become possible to predict the bending behavior of the wood through simulations. By utilizing the properties of wood, minimum extra energy,

equipment and formworks are required for producing a desired curvature. The next chapter will review the recent research result of these cutting-edge fabrication methods.

Chapter 2 – Precedent Studies

2.1 Self-actuated bending

Due to the hygroscopicity and anisotropy of wood, wood can absorb and desorb water from the environment depending on its moisture content and the relative humidity of the surroundings, resulting in different dimensional changes in longitudinal (ΔL), radial (ΔR) and tangential(ΔT) directions (Figure 2-1). The dimensional change in these three directions ΔL: ΔR: ΔT is approximately 0.5-1: 5: 10 (Hayashi 2012). In addition, wood with higher density such as hardwood has more cell walls per unit volume, the swell and shrinkage rate is also higher than that with lower density such as softwood. These properties make wood a smart material of which the dimensional changes can be controlled through manipulations on moisture content, relative humidity and fiber orientations.

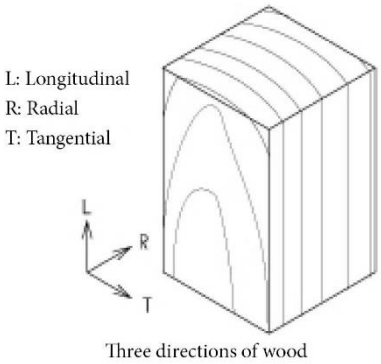

Figure 2-1. Diagram showing the three fiber directions of wood. L: longitudinal, R: radial, T: tangential. (Hokkaido Research Organization, Forest Research Department Products Research Institute, 2006) (Translated)

This embedded intelligence of wood has been explored extensively in recent years amongst the pioneers such as Wood & Menges (Wood, Correa, Krieg & Menges, 2016) and Ruggeberg & Burgert (Rüggeberg & Burgert, 2015). By adapting Timoshenko's bi-layer theory on thermal metal (Timoshenko, 1925) which stated that when a composite with two layers bonded together it would bend when they expand unequally, two layers of wood, beech in tangential direction and spruce in longitudinal direction, with various thicknesses were combined to produce curvature (Figure 2-2). Beech, which is a hardwood with higher density, producing

larger deformation due to moisture content change served as an active layer, while spruce which is a softwood that is less prone to dimensional changes due to moisture content change served as restrictive layer. The wood pieces were equilibrated in a constant environment of relative humidity 85% for at least 72 hours for them to reach a moisture content 18% and 35% relative humidity to reach an equilibrium moisture content of 10% (Figure 2-2). The curvature change was measured by tracking the dots marked on the samples using python program.

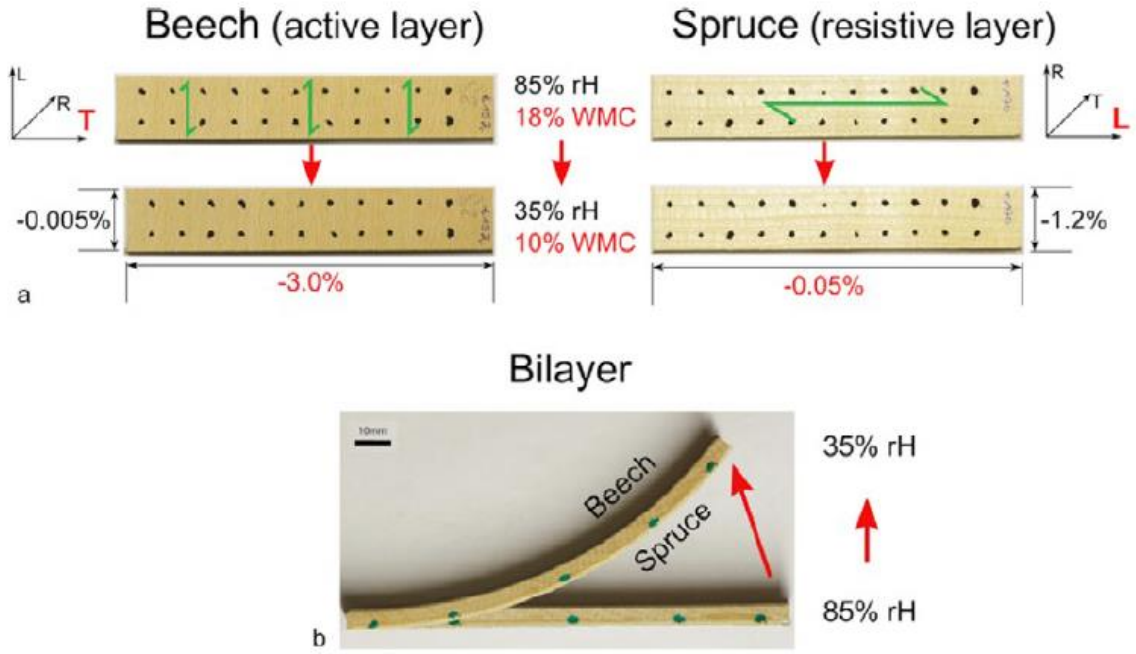

Figure 2-2. Experiment conditions of the research by ETH (Rüggeberg & Burgert, 2015)

The expansion rate was substituted and testified with shrinkage when combining active layer with larger shrinkage coefficient and restrictive layer with smaller shrinkage coefficient, the composite could bend into a surface with a curvature which could be calculated using the following formula:

$$\frac{1}{\rho} = \frac{6(1+m)^2}{\left(3(1+m)^2 + (1+mn)\left(m^2 + \frac{1}{mn}\right)\right)} \frac{(\alpha_2 - \alpha_1)(c - c_0)}{h} = k\frac{\Delta\alpha\Delta c}{h}, \qquad \text{(Eq.3)}$$

$$m = \frac{h_1}{h_2}, n = \frac{E_1}{E_2}$$

where

h1 = thickness of restrictive layer

h2 = thickness of active layer

h = h1+ h2

E1 = Young's Modulus of restrictive layer

E2 = Young's Modulus of active layer

c = initial moisture content

c0 = final moisture content

α1 = shrinking coefficient of restrictive layer

α2 = shrinking coefficient of active layer

The parameters were re-adapted to wood and verified. The angle change could be calculated:

$$\varphi = \frac{l}{\rho} \cdot \frac{360}{2\pi} \qquad \text{(Eq.4)}$$

The result was compared with that of Timoshenko's formula and it has been proved that the bi-layer theory formula could be used to predict the curvature change of wood due to moisture change (Figure 2-3).

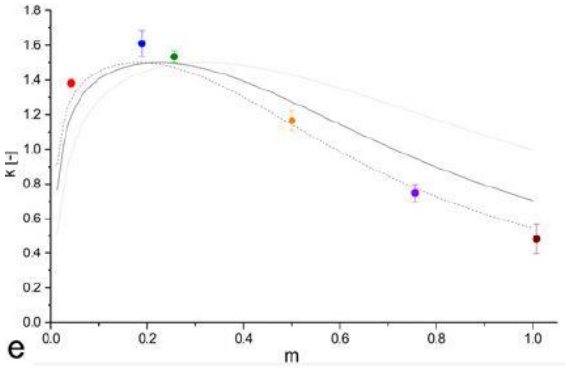

Figure 2-3. Obtained curvature was compared with bi-layer theory formula. The result demonstrated a good fit for the adapted formula. (Rüggeberg & Burgert, 2015)

Research by Wood & Menges involved material selection, wood processing technology, digitally controlled fabrication and post actuation analysis. The goal was trying to scale up the self-actuated bending by joining the small self-actuated wood pieces together. Starting with testing a 0.2m x 0.3m sample of 1.2mm-thick maple veneer with glass fiber textile of 40g/m^2 fabricated below 6% moisture

content, the environment oscillates between 30% and 60% relative humidity for 1-hour cycles (Figure 2-4). The result was extended for making a large-scale piece of 1.5m x 1.0m size, joining 12mm beech triangular pieces with glass fiber textile of 80g/m^2. The sample was fabricated under at 10-15% moisture content and each piece of the element was robotic milled to achieve a range of thickness of 6mm – 12mm (Figure 2-5). Samples were then equilibrated in a condition of 90% relative humidity. Finally, both layers were changed to wood with 10mm maple used as active layer while 2.0mm spruce as restrictive layer. They were produced under 30% moisture content and equilibrated under 30% relative humidity. The joints were 3D printed (Figure 2-5).

Figure 2-4. Research by Wood and Menges. Small scale experiment using 1.2mm maple veneer and glass fiber textile of 40g/m^2. The relative humidity was oscillated for 1-hour cycle between 30% and 60%. (Wood, Correa, Krieg & Menges, 2016).

Figure 2-5. Left: combination of 12mm beech wood with glass fiber textile of 80g/m2. Thickness of each elemental pieces were robotic milled to achieve the curvature. Right: combination of 10mm maple and 2.0mm spruce.

Both researches have provided valuable information in understanding the bi-layer system, the methodology of experiment and fabrication methods. In summary, although the researches used different dimensions for the experiment samples, the common experiment set-ups were:

- Each experiment sample combined a piece of hardwood such as beech with tangential direction as the active layer, and softwood such as spruce with longitudinal direction as the restrictive layer.
- Samples were glued together with polyurethane glue which absorbs water as it takes effect.
- The moisture content of the samples was equilibrated for at least 72 hours under a constant condition i.e. temperature and relative humidity. Mass was taken to calculate the moisture content change.
- Samples started with relatively high relative humidity to obtain high moisture content, then they were naturally dried at in constant conditions as well, enabling bending of different samples.
- Curvature changes were measured either by analog way or digital way.

- Curvature difference were achieved by changing the thickness of layers which involved the use of CNC machines or robotic mills.

For analysis, the following curves were plotted to examine the trend.

- Moisture content change over time
- Curvature over time

The curvature obtained from the experiments were compared against the calculated curvature using the equation 3.

For research conducted by Ruggeberg & Burgert (Rüggeberg & Burgert, 2015), cyclic conditions were also investigated for various relative humidity. Samples were also exposed under full weather for a period of 9 months, testing their durability over time. The change in curvature decreased slightly in the end but that was mainly due to the rain and UV light which caused physical damage to the samples. This reversible process of adsorption and desorption of water caused almost no fatigue in the material itself. (Abdelmohsen et al., 2019)

For the research conducted by Wood & Menges (Wood, Correa, Krieg & Menges, 2016), together with legacy from the series of explorations conducted and led by Menges, other than the experiment set-up stated above, the focus was mainly on treating the surface and complete fabrication process for scaling up the self-actuated wood surfaces to as large as 1.5m x 1.0m for potential architectural usage. In a further study by Wood (Wood, Vailati, Menges & Rüggeberg, 2018), large pieces were formed by combining small pieces with fiber orientations calculated specifically for the curvature at their respective positions. Glass fiber instead of wood was used for the restrictive layer. 3D printed joints were also made to facilitate bending the components into complex shapes.

However, for all the researches, as the changes in bending curvatures depended much on the thickness and species of wood, it provided certain limitations on

applicability of the process to a more common use. For instance, the processing of wood involved the use of robotic arm which is not readily available for anyone to use. The requirement of different species to be used made it limited geographically to regions with the specific species. Thus, this research would like to address the difficulty in processing wood, making it more ready for common use. Single species will be used for easiness of obtaining the material.

2.2 Kerf bending

Kerf denotes a slit or notch made by a saw or a cutting torch ("Definition of KERF", 2019). In the context of current computer-controlled printer technology, kerf almost equates a unit of a cut by laser. Kerf pattern is the cutting pattern for treating a surface by laser cutting or CNC machines to make surface material soft and pliable. To soften a surface by scoring is a traditional technique in Japan dates back to Heian Era (794 – 1185 A.D.). Parallel or diamond-shape scores were made to make the bending of wood easier (Iwai, 1994). With the invention of wood cutting machines, wood treatment gained more freedom and expression (Figure 2-2). Hin Bredendieck in 1937 brought surface treatment to another world by making wood flexible like rubber (Figure 2-6) (Moholy-Nagy, 1975). With the availability of computer-controlled machine, kerf pattern nowadays is widely used as a living hinge to make craft products. There were researches on the use of kerf pattern using laser-cutting and CNC machines. I will introduce them in the following sub-sections.

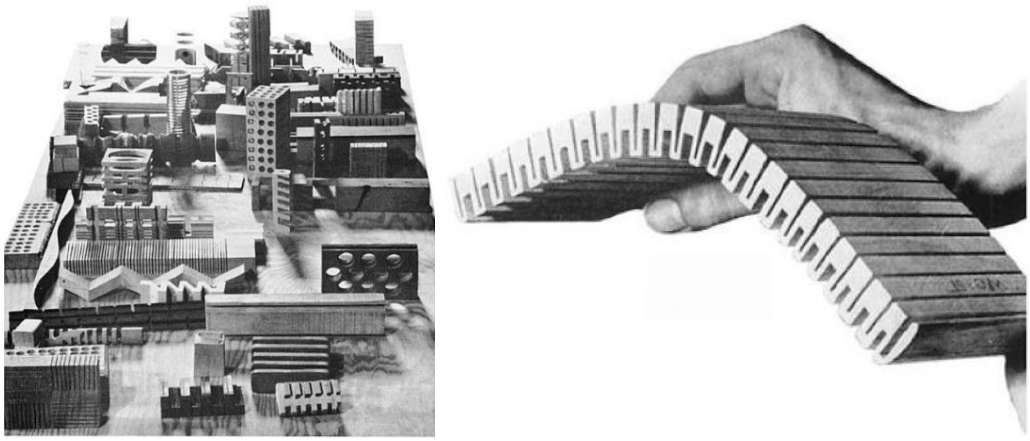

Figure 2-6. Left: wood cutting by William Worst. Right: wood cutting makes wood flexible like rubber in 1937. (Moholy-Nagy, 1975)

2.2.1 Built pavilion projects

There are several built pavilion projects from other research institutions.

a. Kerf-Based Complex Wood System

This is project completed by Harvard GSD in 2010. In this project, the combination of steam bending and designed kerf pattern were used to bend the wooded slats. The former was used to control the overall geometry and the latter was used to make more elaborated bending at some locations. The cuts were made by robotic sawing where the depth of the cuts could be varied in order to produce desired curvature (Figure 2-7). Cuts were made to be perpendicular to the fiber direction so as to keep the aesthetic strengths of the wood.

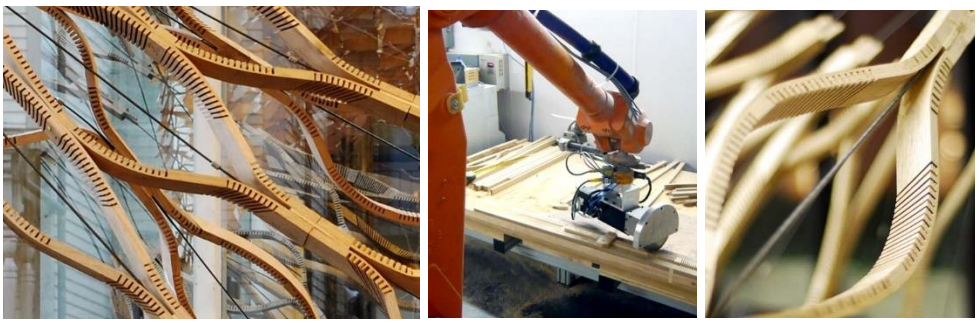

Figure 2-7. Components were made by steam bending for overall geometry and robotic sawing for deliberate bending at specific location. (Harvard GSD, 2010)

b. Kerf Pavilion

This is a project completed by MIT Department of Architecture in 2012. Instead of wooded slats which was anisotropic used in the previous project, plywood which is a more homogeneous material was used to produce this project. As a result, any bending behavior produced were mainly because of the kerf pattern applied. This also means that the bending did not require extra techniques or tools (Figure 2-8). This pattern is produced by CNC router.

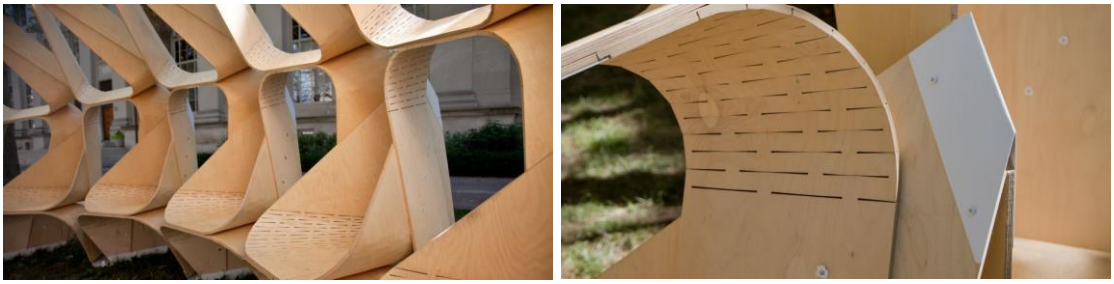

Figure 2-8. Bending purely on kerf pattern with homogeneous plywood. (MIT Architecture, 2012)

c. Active-Joint System

This is an installation project by an architect Zaqi Fathis in 2017. Kerf pattern was used as an element of a joint component. Different from the projects above, simple cuts were made by laser cuts. While the density of the cuts controlled the degree of the possible curve, the direction of the cuts was made to control the twisting of each elements (Figure 2-9). Similar to project in section 2.2.1a, the cuts were also made perpendicular to fiber direction of wood to retain the strength of the material. The axial forces of the components could be analyzed, and a double-curved shape with negative Gaussian curvature could be achieved by connecting the specific components together.

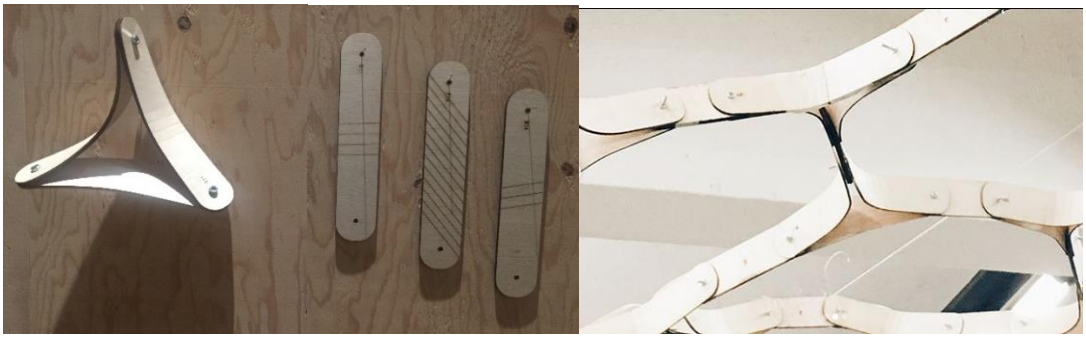

Figure 2-9. Each element in one component is designated specifically for certain axial change controlled by the density and direction of the kerf pattern. (Fathis, 2018)

2.2.2 Parametric pattern study

There were studies on forming pattern such as Porterfield's summary of a series of patterns (Porterfield, 2016) and qualitative studies of the

relationship between pattern and bending curvature using MDF boards by Guzelci (Guzelci, Alaçam & Bacınoğlu, 2017). Both of the studies demonstrated the potential of using computational method to create patterns in 2D surface and mapping them onto 3D surfaces. Through fabrication in laser-cutting machine, material could them into a 3D form. While the former provided qualitative descriptions of each pattern, the latter established a 3-step system to study the relationship between pattern and curvatures through physical and digital experimentations – cut 2D patterns on planar surfaces, mapping patterns onto 3D surfaces and forming new 3D patterns through both physical and digital methods. The first step involves explorations through model making to gain the knowledge, followed by the second step in which the 2D planar surfaces were mapped onto 3D surfaces for predictions. Finally, make 3D physical models to verify the predictions in digital spaces.

The above studies remained in a small scale of handy size with materials easy to implement. In this research, a larger scale with proper construction material plywood will be used for investigations. In Chapter 4, the above 2D to 3D, physical to digital loop of acquiring relationship of pattern and curvature was modified and adopted for this research. Not only the relationship between pattern and curvature but also the relationship of pattern and structural strength will be explored quantitatively.

The series of built projects (section 2.2.1) used computer-controlled technologies to either add anisotropy to the anisotropic wood or create anisotropy in the homogeneous plywood. The methods of fabrications were mainly using CNC routers or laser cutters. Components were made first and joint together to scale up it into architectural scale. In all projects, kerf pattern was used as an assist for composing the components. The treatments were minimum so that the structural strength the components and overall geometry of was mainly dependent on untreated part of wood. As the projects were temporary pavilion, hence the geometry study was the focus. In Chapter 4, the relationship between kerf pattern

and structural property will be studied, and the outcome was a furniture-scaled architecture produced with full kerf patterned plywood.

Chapter 3 – Self-actuated bending

Material selection in Japanese context

While in the precedent studies in Chapter 2, all the samples were made from a combination of hardwood and softwood. However, each country has a different condition for available materials, especially in Japan, where hardwood comprises only 2.4% of the planted forest ("Overview of the survey (31 March 2012): MAFF", 2012). Although in total, natural forest still outnumbered planted forest. However, the area of planted forest stock expanded 6 times over the past 50 years and continued increasing (Figure3-1) ("Breakdown of Country and Forest Area, Trend of Growth of Forest Stock (From MAFF)", 2018) Amongst the planted forest, 'Sugi', Japanese Cedar, comprises approximately 44% of the forest (Figure 3-1).

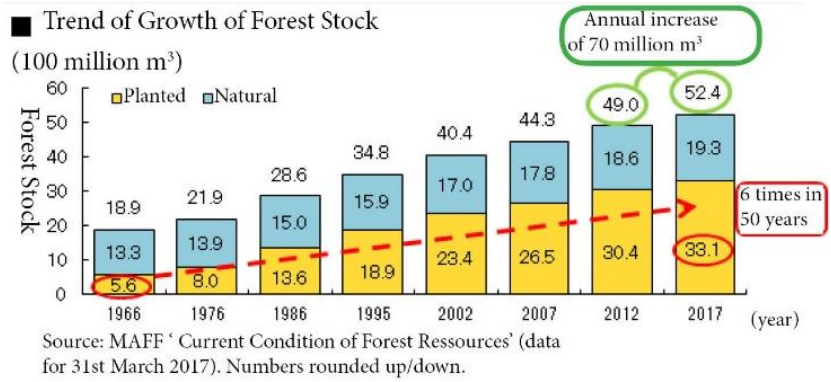

Source: MAFF ' Current Condition of Forest Ressources' (data for 31st March 2017). Numbers rounded up/down.

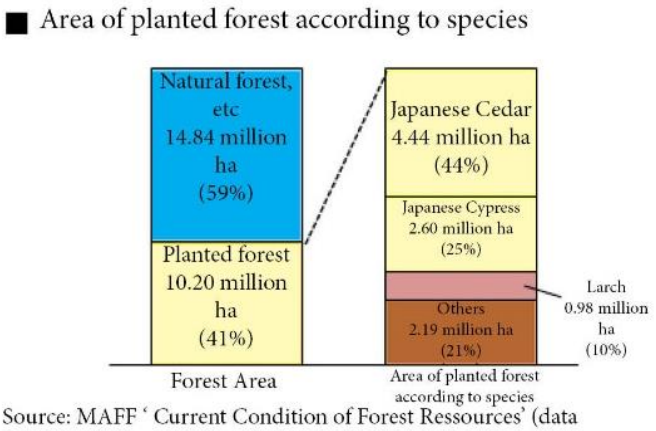

Source: MAFF ' Current Condition of Forest Ressources' (data for 31st March 2017). Numbers rounded up/down.

Figure 3-1. Top: Planted forest stock increased 6 times over the past 50 years. Bottom: Japanese cedar comprises of 44%, which is the top of the planted stock ("Breakdown of Country and Forest Area, Trend of Growth of Forest Stock (From MAFF)", 2018)

As a result, while hardwood has a larger rate of deformation due to its fibril structure, with the extraordinarily high and growing availability and usage of cedar in Japan, cedar is selected as the material for the experiment.

Cedar in Japan has a relatively small diameter. It is difficult to get an intact piece larger than 150mm x 150mm from a 'futomaru', a tree log, by slicing. The most widely used manufacturing method for making surface wood such as plywood is to make from rotary-cut veneer (Figure 3-2). The advantage of using rotary-cut veneer is that there is no limitation to the length of the material, which in turn greatly enlarges the possibility of obtaining a larger piece for experiment.

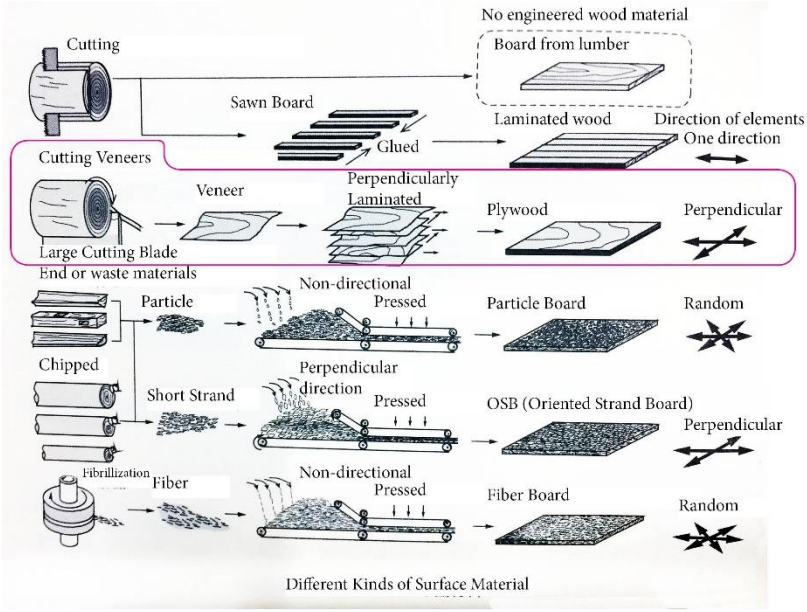

Figure 3-2. To obtain surface material, rotary-cut veneers are most commonly used (Hayashi 2012).

3.1 Experiments

To design the experiment with single material, softwood Japanese cedar, there were several considerations. With rotary cut, all the pieces were cut in tangential direction. Referring to the precedent studies, no unequal shrinkage could be created by bonding the two layers of the same material and direction together as they would have the same shrinkage coefficient. Thus, in order to overcome the issue of single material, different initial moisture content was designed to create

the unequal shrinkage for bending. Although all the rotary-cut wood is in tangential direction, there was a clear fiber direction on each piece. Thus, different fiber orientations could be used for active and restrictive layers respectively to generate variations in the curvature. The differences between the precedents and this research are summarized in the table below (Table 3-1).

	Precedents	This research
Method to process wood	Slicing	Rotary cut
Species	Hardwood + Softwood	Softwood
Fiber orientation	Longitudinal + Tangential	Tangential + Tangential
Moisture content of the two layers	Same	Different

Table 3-1. Difference in the set-up between precedents and this research.

Thus, the goal of the experiments was to find out whether the new bi-layer theory formula (equation 3) deducted by Ruggeberg & Burgert (Rüggeberg & Burgert, 2015) could be used for this new condition as well. If not, it may be required to find out a newly adapted formula.

Referring to equation 3 in Chapter 2, shrinkage coefficient and Young's Modulus in longitudinal and tangential direction used in precedent studies were extracted from other sources. However, in this case, when both layers were tangential, there were no studies on the shrinkage coefficient or Young's Modulus according to specific fiber orientation. As a result, the following experiments and measurements are necessary:

1. To find out the relationship between the parameters, **moisture content, curvature with time**, and if the curvature trend follows the bi-layer theory.
2. To find out the **shrinkage coefficient** for different fiber orientations when they are all in tangential condition.
3. To find out the **Young's Modulus of wood in different fiber orientations**.

3.1.1 Bi-layer experiment

3.1.1a. Experiment Setup

Square-shaped bi-layer samples with dimension 250mm x 250mm were planned. Active layers are designated to provide various fiber orientations from 0 degree, 90 degree, 30 degree, 45 degree and 60 degree. The restrictive layers remain for 0 degree.

The moisture content of active layers was adjusted to 24% in climate chamber with 90% relative humidity and 20 degree Celsius for one week to make them equilibrated. Two types of moisture content were used for restrictive layers, 5% and 12%. These two initial moisture contents were particularly used because of accessibility of the material. 5% moisture content is a typical moisture content after kiln-dried wood which is readily available 12% moisture content is a typical moisture content air-dried wood in the case of Japan.

The method is summarized in Figure 3-3. Active and restrictive layers are combined with different fiber directions, different moisture content and different thicknesses (Figure 3-3).

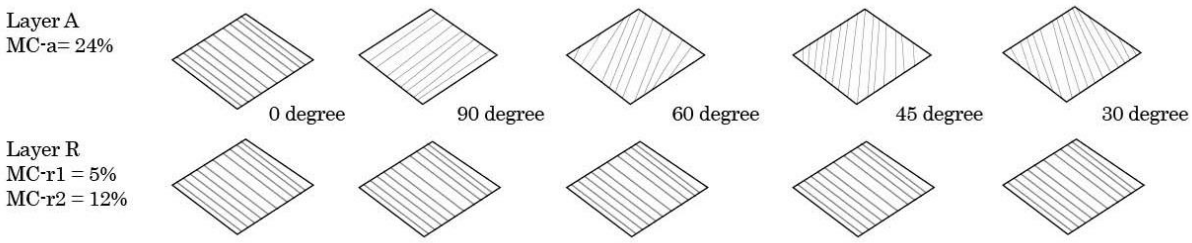

Figure 3-3. Active layers, Layer A were equilibrated at moisture content of 24% while restrictive layers, Layer R, were equilibrated at moisture content of 5% and 12%.

Layer A and Layer R will be combined with following conditions:

a) Combine layers of the same thickness

   3mm x 3mm, 3.5mm x 3.5mm 4mm x 4mm

b) Combine layers with different thicknesses
3mm x 4mm

c) Combine with other controlled material - 0.2mm veneer and glass fiber.

3.1.1b. Experiment method and measurements

1. Preparation
Veneers were received as green wood with high moisture content. Each piece was scanned and documented for fiber direction and knot condition and average thickness of each piece. In general, the pieces came in with the thickness of 3mm, 3.5mm and 4mm and the size was 900mm x 900mm

2. The experiment samples were drawn and cut, taking care of the knot condition. The sample size obtained were 250mm x 250mm as shown in Figure 3-4. There were 37 pieces of 900mm x 900mm veneers examined and 80 pieces of samples cut for further experiments. Veneers with drawings are shown in Appendix 1.

Figure 3-4. Examples showing typical drawings on layer of each thickness. Each sample was labeled with thickness followed by fiber orientation.
The samples were then cut according to the drawing.

3. The cut experiment samples were then put in constant temperature room and temperature chamber (Figure 3-5) to adjust the moisture content to the desired value. The moisture content of active layers was adjusted to 24% in climate chamber with 90% relative humidity and 20 degree Celsius for one

week to make them equilibrated. Moisture content 5% was reached by placing wood samples into oven of relative humidity 22% and 33.1 degree Celsius and 12% was reached and equilibrated by placing the wood under room conditions of relative humidity 71% and 20.7 degree Celsius (Figure 3-5). The thermo recorder used was TR-72U from T&D corporation (Appendix 2, Figure p-2a).

Figure 3-5. Left: climate chamber for equilibrate active layers. Center: condition of oven to dry the restrictive layers to 5%. Right: condition to dry restrictive layers to 12%

4. Experiment samples were glued under the condition of temperature 20 degree Celsius and humidity 65%. As the actuated bending happens fast, super glue called 'Ultra Multi-purpose SU Premium Soft' comprised mainly of silylated urethane resin from the manufacturer Konishi was used to bond the two layers together to allow for quick fixation within 15 mins and settled within 3 hours ("Ultra Multi-purpose Special Site / Konishi Corporation", 2019)(Appendix 2, Figure p-2c). Mass of each sample was taken before and after glue so that the calculations later would exclude the mass of glue used.

5. Mass and deformation were measured at more frequent intervals such as 1.5 hours or 2.5 hours for the first 10 hours and less frequent intervals of 6 hours or 12 hours between 10 to 24 hours. Mass was measured using scale with precision to 0.01 gram while deformation was measured by using digital measure tape Bosch Professional GLM 50C with precision of 0.1mm (Appendix 2, Figure p-2b). A jig was made to fit the size of the digital measure to make sure that each measurement was taken at the same location. The measurements results were recorded via Bluetooth in excel sheet. In total, 25 points were taken for each sample with each

measurement 50mm apart (Figure 3-6). Measurements for deformation were taken using the jig with an order shown in Figure 3-7.

Figure 3-6. Left: top view of the jig. Measurements were taken for 25 points for each sample. Center & Right: using the digital measure tape to take measurements. The data could be linked with excel via Bluetooth.

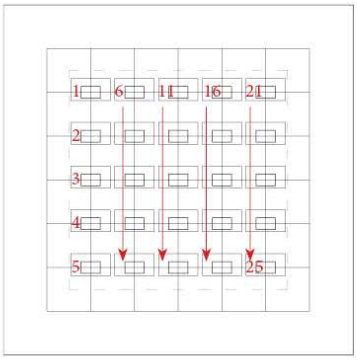

Figure 3-7. Order of deformation measurements.

6. Moisture content of each layer was measured by a moisture meter Shinwa 78636 with precision of 0.1% (Appendix 2, Figure p-2d) together with mass. As the moisture measure could only measure the surface moisture content ("Digital Moisture Meter for Wood - Hold function for max/min values - Shinwa Sokutei Co., Ltd.", n.d.), the moisture content measured was double checked with decrease in mass and compared with precedents for result verification (Appendix 4b).

   As the place for the experiment was a shared space, people coming in and out may change the relative humidity and temperature. Relative humidity and temperature were also measured at the same interval with mass and deformation using the same thermo recorder.

Measurements

In all the tables, samples are named by thickness of layers and 'a' represents the combination of moisture content 24% and 5% while 'b' represents the combination 24% and 12%. The suffix number 1 to 5 represent the active layer orientation from 0-degree, 90-degree, 60-degree, 45-degree and 30-degree respectively.
For example, sample 3-3-a3 means a combination of a 3mm-thick layer to a 3mm-thick layer of the active layer with moisture content 24% and restrictive layer of moisture content 5%. The fiber orientation of the active layer is 60 degrees.

The measurement data for mass is shown in the tables below for sample 3-3, sample 4-4 and sample 3-4 (Table 3-2). Mass of glue has been deducted from the mass measured. The original data of all samples can be found in Appendix 3.

Name	Combination		Mass before glue(g)	Mass after glue(g)	Mass of glue (g)	Mass after 1.5 hr(g)	Mass after 3 hrs(g)	Mass after 4.5 hrs(g)	Mass after 6.0 hrs(g)	Mass after 16.0 hrs(g)	Mass after 19.5.hrs(g)	Mass after 24.5hrs(g)	Mass after 28hrs(g)	Mass after 52.5hrs(g)	Mass after 76hrs(g)	Mass after 111hrs(g)
3-3-a1	3-A0-mc5-1	3-A0-mc30-1	102.96	108.25	5.29	102.20	101.98	101.90	102.63	102.32	102.80	99.71	99.89	98.37	98.38	100.60
3-3-a2	3-A0-mc5-2	3-A90-mc30-1	101.59	106.77	5.18	102.06	101.13	100.04	101.89	100.84	99.54	98.01	98.38	96.87	96.90	98.16
3-3-a3	3-A0-mc5-3	3-A60-mc30-1	105.84	112.58	6.74	105.27	104.44	106.18	104.24	105.96	104.18	103.30	102.71	101.13	101.05	103.16
3-3-a4	3-A0-mc5-4	3-A45-mc30-1	106.68	113.05	6.37	105.14	106.59	106.45	105.14	106.41	104.82	104.68	103.41	101.80	101.73	103.73
3-3-a5	3-A0-mc5-5	3-A30-mc30-1	109.20	113.69	4.49	109.85	107.81	107.62	109.23	108.31	107.31	106.41	105.99	104.20	104.16	106.27
3-3-b1	3-A0-mc15-1	3-A0-mc30-2	106.22	111.89	5.67	105.86	103.58	104.50	102.89	103.89	102.51	100.58	100.78	98.71	98.40	100.53
3-3-b2	3-A0-mc15-2	3-A90-mc30-2	106.62	114.80	8.18	106.02	105.09	104.00	102.91	102.23	102.95	101.82	100.86	98.39	98.25	100.01
3-3-b3	3-A0-mc15-3	3-A60-mc30-2	113.14	120.28	7.14	112.19	111.76	111.23	109.33	109.56	108.42	107.06	106.90	104.32	104.16	106.87
3-3-b4	3-A0-mc15-4	3-A45-mc30-2	111.32	117.90	6.58	109.73	109.17	108.53	108.75	108.28	107.36	105.43	105.83	102.83	102.62	104.93
3-3-b5	3-A0-mc15-5	3-A30-mc30-2	108.37	113.02	4.65	107.02	105.53	105.30	104.62	106.21	105.34	103.71	103.04	100.33	100.16	102.41
Relative Humidity			78%	78%	na	78%	78%	78%	76%	75%	60%	56%	55%	54%	54%	73%
Temperature (C)			15.0	15.0	na	15.0	15.0	15.0	15.3	14.9	24.0	25.6	26.6	20.5	20.3	15.4

Table 3-2. Measurement of mass after glue is deducted for sample 3-3, 4-4 and 3-4. The original data of all samples is in Appendix 3.

Name	Combination		Mass before glue(g)	Mass after glue(g)	Mass of glue (g)	Mass after 2.5 hrs(g)	Mass after 5.0 hrs(g)	Mass after 7.0 hrs(g)	Mass after 9.0 hrs(g)	Mass after 24 hrs(g)	Mass after 48 hrs(g)	Mass after 96 hrs(g)
4-4-a1	4-A0-mc5-1	4-A0-mc30-1	145.85	153.18	7.33	141.86	139.73	138.86	140.49	138.76	142.12	138.30
4-4-a2	4-A0-mc5-2	4-A90-mc30-1	143.68	150.71	7.03	139.76	140.08	138.88	138.10	137.57	140.81	138.26
4-4-a3	4-A0-mc5-3	4-A60-mc30-1	136.16	143.03	6.87	133.48	130.80	130.48	131.49	131.45	133.97	130.52
4-4-a4	4-A0-mc5-4	4-A45-mc30-1	141.51	146.91	5.40	137.85	137.66	136.33	137.15	135.88	139.16	135.43
4-4-a5	4-A0-mc5-5	4-A30-mc30-1	143.38	150.24	6.86	139.28	138.63	138.24	138.83	139.25	140.88	136.85
4-4-b1	4-A0-mc15-1	4-A0-mc30-2	155.07	161.01	5.94	149.02	146.72	146.67	144.56	145.66	147.55	141.67
4-4-b2	4-A0-mc15-2	4-A90-mc30-2	150.22	158.00	7.78	145.51	143.48	140.59	140.06	140.28	142.48	138.89
4-4-b3	4-A0-mc15-3	4-A60-mc30-2	147.54	151.80	4.26	143.35	141.31	140.66	140.16	138.59	141.47	136.03
4-4-b4	4-A0-mc15-4	4-A45-mc30-2	142.69	147.72	5.03	136.69	135.26	134.57	134.73	135.30	136.50	130.61
4-4-b5	4-A0-mc15-5	4-A30-mc30-2	142.50	148.85	6.35	137.94	134.66	134.94	134.21	134.13	136.37	130.27

Relative Humidity			52%	50%	na	50%	49%	53%	51%	54%	74%	41%
Temperature (C)			19.9	19.7	na	19.8	19.9	20.2	19.8	19.6	15.4	22.6

Name	Combination		Mass before glue(g)	Mass after glue(g)	Mass of glue (g)	Mass after 2.0 hr(g)	Mass after 4.5 hrs(g)	Mass after 6.5 hrs(g)	Mass after 8.5 hrs(g)	Mass after 24 hrs(g)	Mass after 48 hrs(g)	Mass after 96 hrs(g)
3-4-a1	3-A0-mc5-6	4-A0-mc30-3	125.00	132.15	7.15	121.22	119.42	118.00	118.66	118.26	120.85	117.36
3-4-a2	3-A0-mc5-7	4-A90-mc30-3	123.51	131.15	7.64	121.45	120.70	120.21	118.01	118.87	120.32	117.73
3-4-a3	3-A0-mc5-8	4-A60-mc30-3	124.36	131.37	7.01	123.20	120.61	120.81	119.10	119.37	121.85	118.48
3-4-a4	3-A0-mc5-9	4-A45-mc30-3	131.06	139.08	8.02	129.01	127.27	126.61	127.10	126.67	128.14	124.55
3-4-a5	3-A0-mc5-10	4-A30-mc30-3	131.12	138.27	7.15	126.58	124.48	124.91	123.91	124.83	127.06	123.07
3-4-b1	3-A0-mc15-6	4-A0-mc30-4	128.14	132.95	4.81	121.52	121.09	119.41	118.39	118.71	121.01	116.76
3-4-b2	3-A0-mc15-7	4-A90-mc30-4	128.87	134.78	5.91	123.48	123.28	122.79	120.66	121.38	122.33	118.96
3-4-b3	3-A0-mc15-8	4-A60-mc30-4	120.74	126.70	5.96	114.79	114.56	114.03	114.45	112.28	115.00	111.04
3-4-b4	3-A0-mc15-9	4-A45-mc30-4	126.10	132.68	6.58	120.66	119.23	118.68	118.27	118.61	120.09	115.86
3-4-b5	3-A0-mc15-10	4-A30-mc30-4	133.81	138.95	5.14	127.69	125.71	125.40	123.63	124.07	126.50	121.64

Relative Humidity			53%	54%	na	51%	50%	51%	52%	56%	76%	42%
Temperature (C)			19.5	19.8	na	19.9	20.0	19.9	19.9	19.8	15.4	22.5

Table 3-2. Measurement of mass after glue is deducted for sample 3-3, 4-4 and 3-4. The original data of all samples is in Appendix 3. (continued)

Measurements of deformation involved large quantity of data. Part of the measurements for deformation are shown in Appendix 6.

3.1.1c. Experiment Result and Analysis

3.1.1c-1. Moisture content over time

Moisture content of active layer and restrictive layer was measured separately and the results were shown below. Graph of moisture over time was plotted (Figure 3-8). The data of sample group 3-3-a and 3-3-b were shown below (Table 3-3). The other samples had an identical trend on moisture content change over time. The results of other samples are in Appendix 4a. Both active layers and restrictive layers showed a typical trend of water adsorption and desorption. Equilibrium moisture content were reached within 24 hours due to a stabilization

of mass and moisture content. Hence, the data was collated for the first 24 hours only.

Due to the limitation of moisture meter stated in section 3.1.1b, moisture content was double confirmed both quantitatively and qualitatively, with decrease in mass and compared with graphs of precedents and compared with other researches (Appendix 4b). Generally, the result of mass comparison has shown a reliable moisture content obtained from moisture meter with correlation coefficient between 0.75 to 0.99. The variations in the coefficient is mainly due to the limitation in equipment that could only measure the moisture content of the surface of samples. However, the samples were not very thick so that the overall results demonstrated a reliable experiment result. Group 3-3-a showed the lowest correlation coefficients. This may be due to the exchange of moisture content between the layers, especially the inexperienced application of glue at the start of the experiment.

Although data 3.5mmx3.5mm samples was taken in the experiments, they were not used in the analysis as there was too little difference between 3mmx 3mm and 4mm x4mm samples, and they were insignificant in providing further information on the impact of thickness of layers as well.

Sample 3-3-a Moisture Content over time

Time (hours)	0	1.5	3	4.5	6	16	19.5	24.5
RH	78%	78%	78%	78%	76%	75%	60%	56%
Temp (C)	15.0	15.0	15.0	15.0	15.3	14.9	24.0	25.6
3-3-a1	0-0							
MC-A_a1	24.0%	17.2%	15.3%	14.9%	14.8%	14.6%	14.0%	13.0%
MC-R_a1	5.0%	9.0%	11.0%	12.7%	12.6%	12.9%	12.3%	10.3%
3-3-a2	0-90							
MC-A_a2	24.0%	18.4%	16.4%	15.7%	14.9%	15.6%	14.9%	13.0%
MC-R_a2	5.0%	9.2%	10.9%	11.4%	12.1%	12.1%	11.4%	10.8%
3-3-a3	0-60							
MC-A_a3	24.0%	17.2%	15.8%	15.5%	15.2%	15.5%	14.9%	12.9%
MC-R_a3	5.0%	10.5%	11.6%	11.8%	12.1%	12.1%	11.5%	10.5%
3-3-a4	0-45							
MC-A_a4	24.0%	18.0%	15.9%	15.9%	15.7%	15.8%	15.3%	13.3%
MC-R_a4	5.0%	9.5%	12.9%	12.9%	13.1%	13.1%	12.6%	11.6%
3-3-a5	0-30							
MC-A_a5	24.0%	18.3%	16.3%	16.2%	16.1%	16.3%	15.7%	13.1%
MC-R_a5	5.0%	9.9%	11.4%	11.4%	11.5%	11.5%	10.9%	10.4%

Sample 3-3-b Moisture Content over time

Time (hours)	0	1.5	3	4.5	6	16	19.5	24.5
RH	78%	78%	78%	78%	76%	75%	60%	56%
Temp (C)	15.0	15.0	15.0	15.0	15.3	14.9	24.0	25.6
3-3-b1	0-0							
MC-A_b1	24.0%	20.1%	18.9%	17.8%	17.0%	16.2%	15.2%	14.7%
MC-R_b1	12.0%	12.5%	12.6%	12.8%	12.9%	13.0%	13.1%	10.5%
3-3-b2	0-90							
MC-A_b2	24.0%	20.1%	18.9%	17.8%	17.0%	16.2%	15.2%	13.6%
MC-R_b2	12.0%	12.5%	12.6%	12.8%	12.9%	13.0%	13.1%	11.6%
3-3-b3	0-60							
MC-A_b3	24.0%	19.5%	17.9%	16.7%	15.9%	15.2%	14.5%	12.4%
MC-R_b3	12.0%	12.6%	12.8%	12.9%	13.0%	13.1%	12.8%	11.7%
3-3-b4	0-45							
MC-A_b4	24.0%	20.2%	16.7%	15.4%	14.4%	13.5%	13.2%	12.0%
MC-R_b4	12.0%	12.5%	12.7%	12.8%	13.0%	13.1%	13.0%	11.7%
3-3-b5	0-30							
MC-A_b5	24.0%	20.5%	18.9%	17.7%	16.8%	15.9%	15.4%	13.3%
MC-R_b5	12.0%	12.4%	12.6%	12.8%	12.9%	13.0%	12.9%	12.3%

Table 3-3. Measurement of moisture content over time of 3-3-a and 3-3-b group, the other data is shown in Appendix 4a.

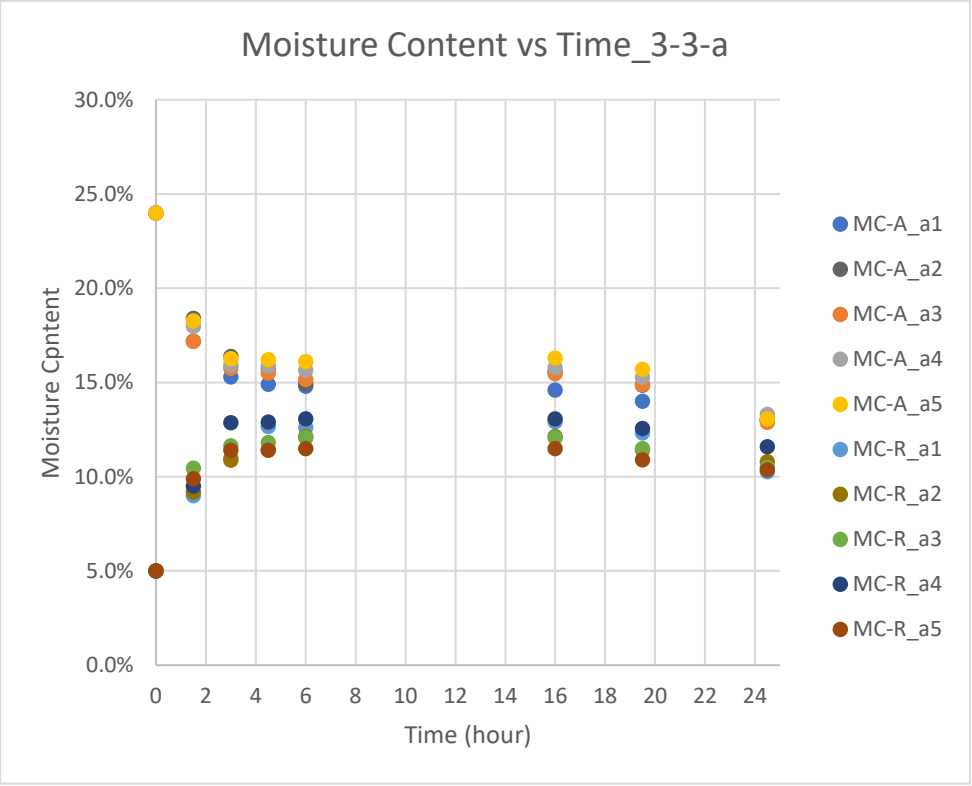

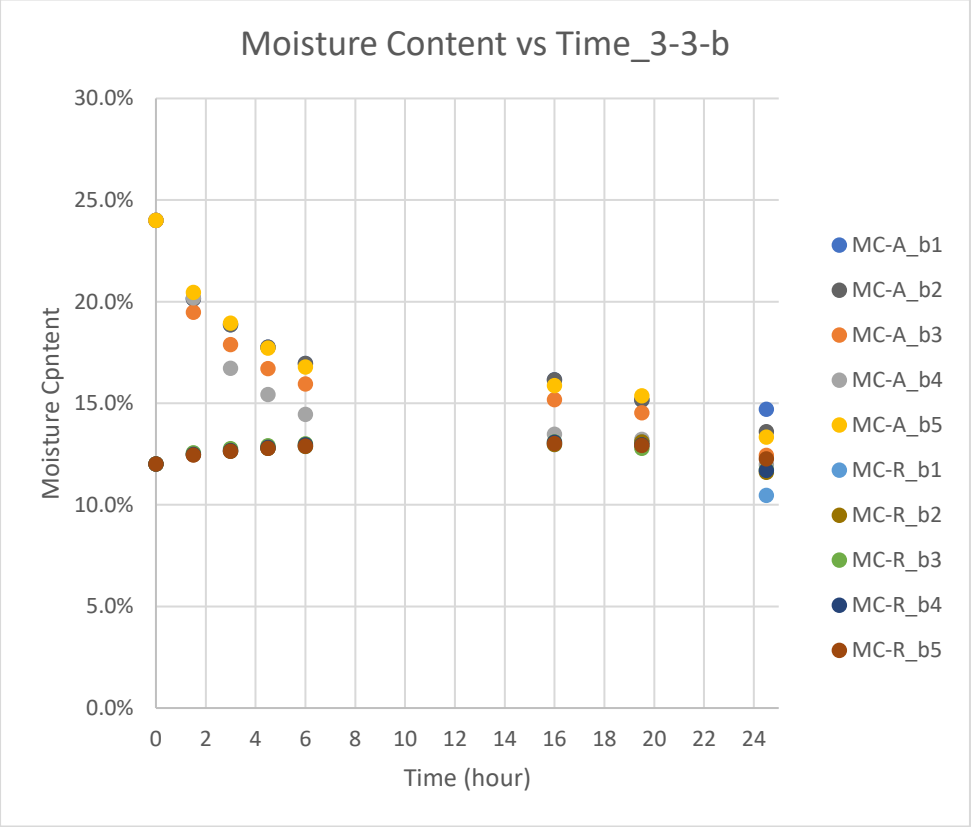

Figure 3-8. Graph of moisture content over time of sample group 3-3-a and 3-3-b. Graphs of other samples are shown in Appendix 4b - ii).

3.1.1c-2. Curvature over time

The bending of the samples is shown in Figure 3-9.

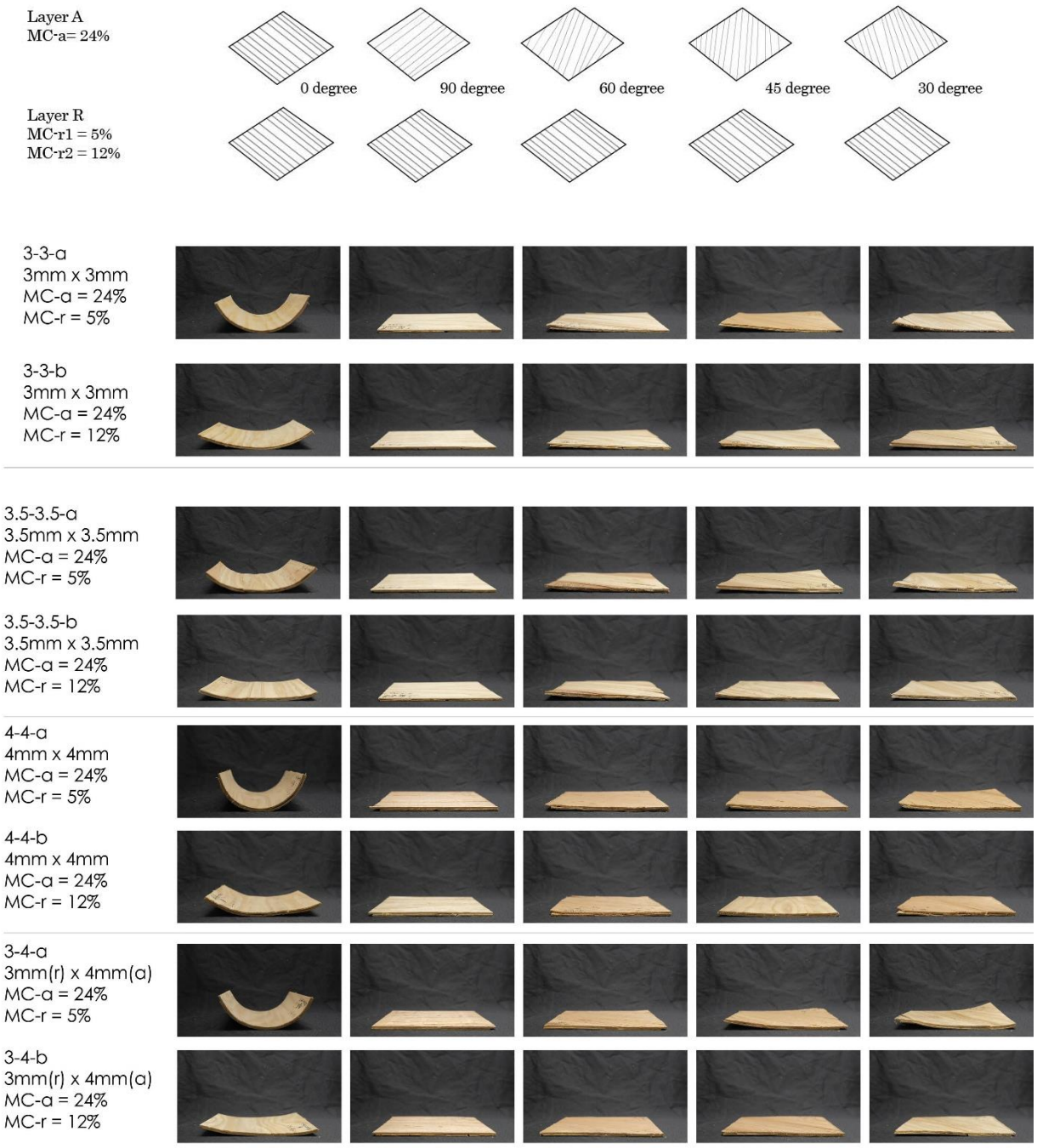

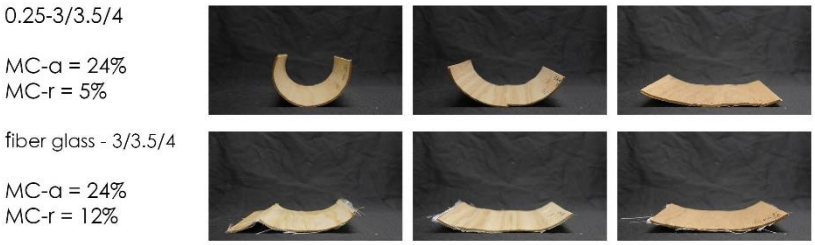

Figure 3-9. Deformation of the samples.

The deformation measurements could be imported to software Rhinoceros and form a surface to approximate the deformation via grasshopper. Below is visualization of curvature vs time of sample 3-3-a1 in rhino interface (Figure 3-10).

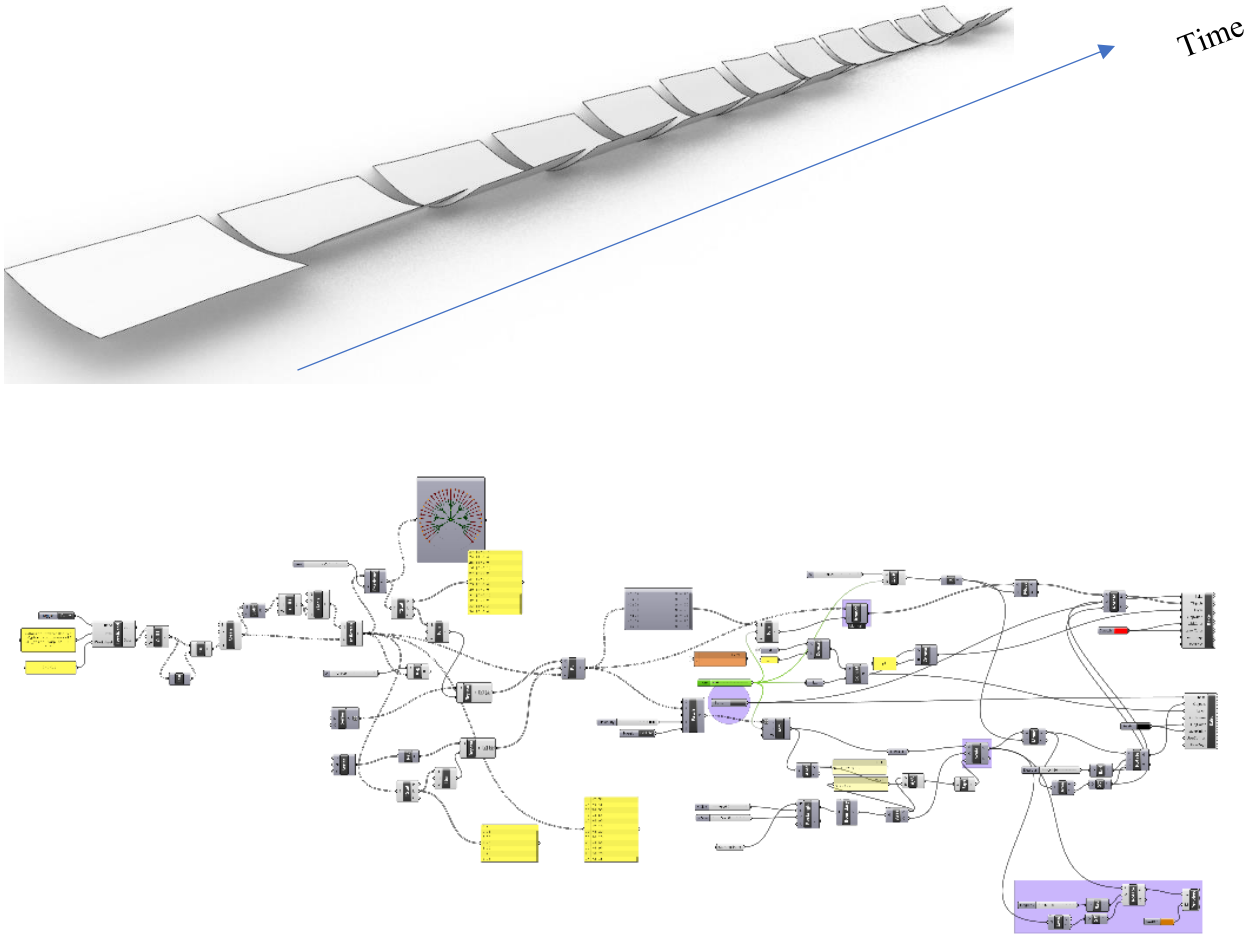

Figure 3-10. Top: visualization of the curvature changes over time of sample 3-3-a1 in Rhinoceros. Bottom: grasshopper definition

Following the method by Wood (Wood, Vailati, Menges & Rüggeberg, 2018), the main curvatures were measured by fitting a circle and represented as $r^{-1}(mm^{-1})$. The same applied here. By fitting circles along the main curvatures of the samples (Figure 3-11).

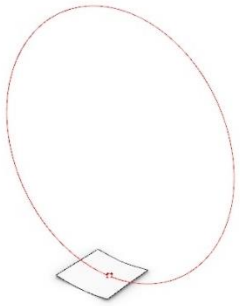

Figure 3-11. Finding the major curvatures by fitting the circle.

The data for curvature over time could be obtained (Table 3-4), the first shows the time passed. As when the two pieces were combined perpendicularly, the piece stays flat. Hence, all the a2 samples were removed from the data.

Time (h) / Sample	0	1.5	3	4.5	6	16	19.5	24.5	28	52.5	76	111
3-3-a1	0.00000	0.00500	0.00670	0.00763	0.00766	0.00849	0.00851	0.00864	0.00851	0.00823	0.01034	0.01039
3-3-a5	0.00000	0.00103	0.00133	0.00155	0.00164	0.00167	0.00178	0.00201	0.00200	0.00205	0.00191	0.00185
3-3-a4	0.00000	0.00082	0.00126	0.00135	0.00147	0.00172	0.00175	0.00178	0.00173	0.00165	0.00165	0.00162
3-3-a3	0.00000	0.00064	0.00081	0.00093	0.00102	0.00115	0.00112	0.00108	0.00102	0.00089	0.00090	0.00102
3-3-a2	0.00000	0.00000	0.00000	0.00000	0.00000	0.00000	0.00000	0.00000	0.00000	0.00000	0.00000	0.00000

Time (h) / Sample	0	1.5	3	4.5	16	19.5	24.5	28	52.5	76	111
3-3-b1	0.00000	0.00156	0.00223	0.00258	0.00324	0.00338	0.00339	0.00546	0.00510	0.00479	0.00460
3-3-b5	0.00000	0.00036	0.00050	0.00060	0.00068	0.00072	0.00076	0.00084	0.00081	0.00081	0.00070
3-3-b4	0.00000	0.00033	0.00041	0.00052	0.00061	0.00072	0.00076	0.00078	0.00078	0.00070	0.00075
3-3-b3	0.00000	0.00029	0.00038	0.00041	0.00044	0.00044	0.00045	0.00045	0.00042	0.00032	0.00032
3-3-b2	0.00000	0.00000	0.00000	0.00000	0.00000	0.00000	0.00000	0.00000	0.00000	0.00000	0.00000

Time (h) / Sample	0	2	4.5	6.5	8.5	24	48	96
3.5-3.5-a1	0.00000	0.00244	0.00372	0.00455	0.00479	0.00504	0.00522	0.00604
3.5-3.5-a5	0.00000	0.00040	0.00062	0.00069	0.00075	0.00078	0.00084	0.00089
3.5-3.5-a4	0.00000	0.00054	0.00052	0.00054	0.00051	0.00054	0.00014	0.00044
3.5-3.5-a3	0.00000	0.00002	0.00008	0.00008	0.00009	0.00014	0.00004	0.00015
3.5-3.5-a2	0.00000	0.00000	0.00000	0.00000	0.00000	0.00000	0.00000	0.00000

Time (h) / Sample	0	2	4.5	6.5	8.5	24	96
3.5-3.5-b1	0.00000	0.00126	0.00153	0.00162	0.00171	0.00179	0.00187
3.5-3.5-b5	0.00000	0.00030	0.00033	0.00035	0.00036	0.00030	0.00027
3.5-3.5-b4	0.00000	0.000124	0.000154	0.000174	0.000217	0.000227	0.000096
3.5-3.5-b3	0.00000	0.00009	0.00013	0.00015	0.00018	0.00023	0.00028
3.5-3.5-b2	0.00000	0.00000	0.00000	0.00000	0.00000	0.00000	0.00000

Time (h) / Sample	0	2.5	5	7	9	24	48	96
4-4-a1	0.00000	0.007981	0.0095	0.009668	0.009867	0.010389	0.010209	0.010782
4-4-a5	0.00000	0.000756	0.000988	0.001101	0.001048	0.001242	0.001459	0.001283
4-4-a4	0.00000	0.000131	0.000255	0.000442	0.000534	0.000539	0.000103	5.78E-06
4-4-a3	0.00000	0.0002	0.000348	0.000406	0.000471	0.00051	0.000617	0.000325
4-4-a2	0.00000	0.00000	0.00000	0.00000	0.00000	0.00000	0.00000	0.00000

Table 3-4. Data for curvature over time.

Time (h) / Sample	0	2.5	5	7	9	24	48	96
4-4-b1	0.00000	0.002863	0.003823	0.004151	0.004307	0.004337	0.004605	0.003819
4-4-b5	0.00000	0.000038	0.000065	0.000078	0.00011	0.000082	0.000051	0.000219
4-4-b4	0.00000	0.000152	0.000206	0.000252	0.000264	0.00024	0.000225	0.000139
4-4-b3	0.00000	0.000036	0.00007	0.000079	0.000081	0.000096	0.000059	0.000097
4-4-b2	0.00000	0.00000	0.00000	0.00000	0.00000	0.00000	0.00000	0.00000

Time (h) / Sample	0	2.5	4.5	6.5	8.5	24	48	96
3-4-a1	0.00000	0.00632	0.00909	0.00989	0.00980	0.01024	0.01062	0.01071
3-4-a5	0.00000	0.00087	0.00098	0.00109	0.00102	0.00138	0.00161	0.00111
3-4-a4	0.00000	0.00017	0.00029	0.00037	0.00043	0.00049	0.00038	0.00012
3-4-a3	0.00000	0.00027	0.00034	0.00036	0.00038	0.00041	0.00042	0.00023
3-4-a2	0.00000	0.00000	0.00000	0.00000	0.00000	0.00000	0.00000	0.00000

Time (h) / Sample	0	2.5	4.5	6.5	8.5	24	48	96
3-4-b1	0.00000	0.003118	0.004478	0.004883	0.004861	0.004851	0.004548	0.004832
3-4-b5	0.00000	0.000362	0.000472	0.000498	0.000497	0.000655	0.000744	0.000435
3-4-b4	0.00000	0.00012	1.70E-04	0.00022	2.80E-04	0.00036	0.00059	0.00097
3-4-b3	0.00000	0.000061	0.000092	0.000124	0.00013	0.00014	0.000193	0.000086
3-4-b2	0.00000	0.00000	0.00000	0.00000	0.00000	0.00000	0.00000	0.00000

Time (h) / Sample	0	2	4	6	24	72
3-0.25	0.00000	0.006426	0.009201	0.010322	0.011834	0.013481
3.5-0.25	0.00000	0.003283	0.003926	0.004154	0.003717	0.005561
4-0.25	0.00000	0.000953	0.001072	0.001203	0.001028	0.002584

Table 3-4. Data for curvature over time. (continued)

Curvature over time graph were plotted over a period of 24 hours as the samples reached equilibrium within 24 hours. (Figure 3-12).

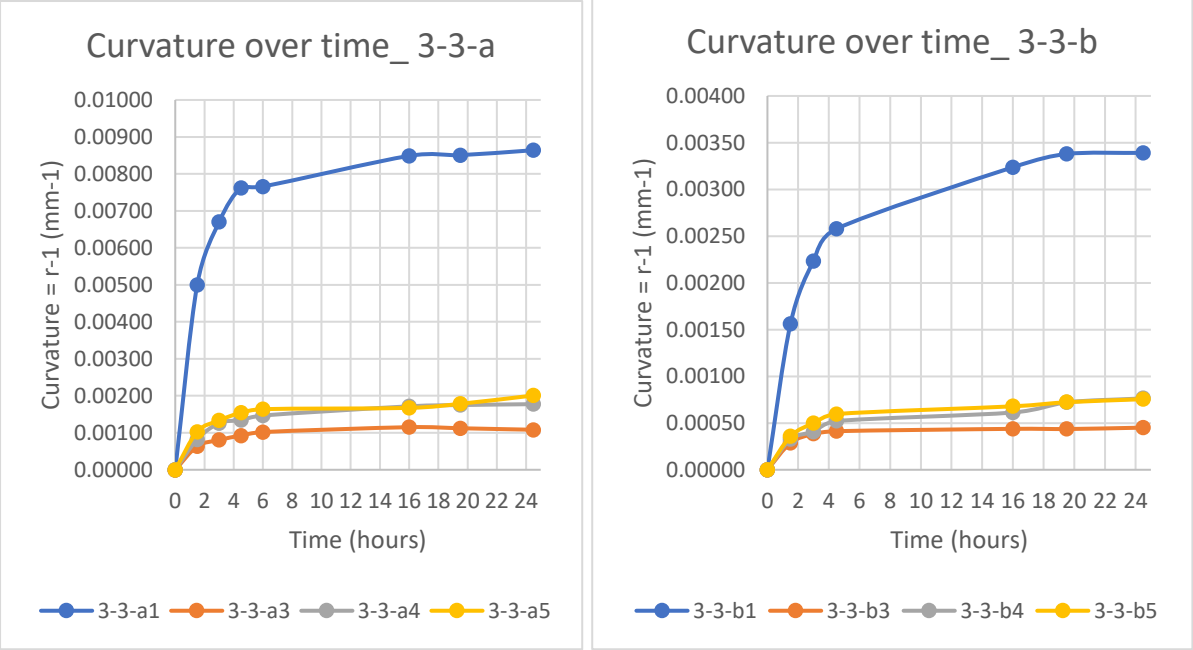

Figure 3-12. Graph of curvature over time.

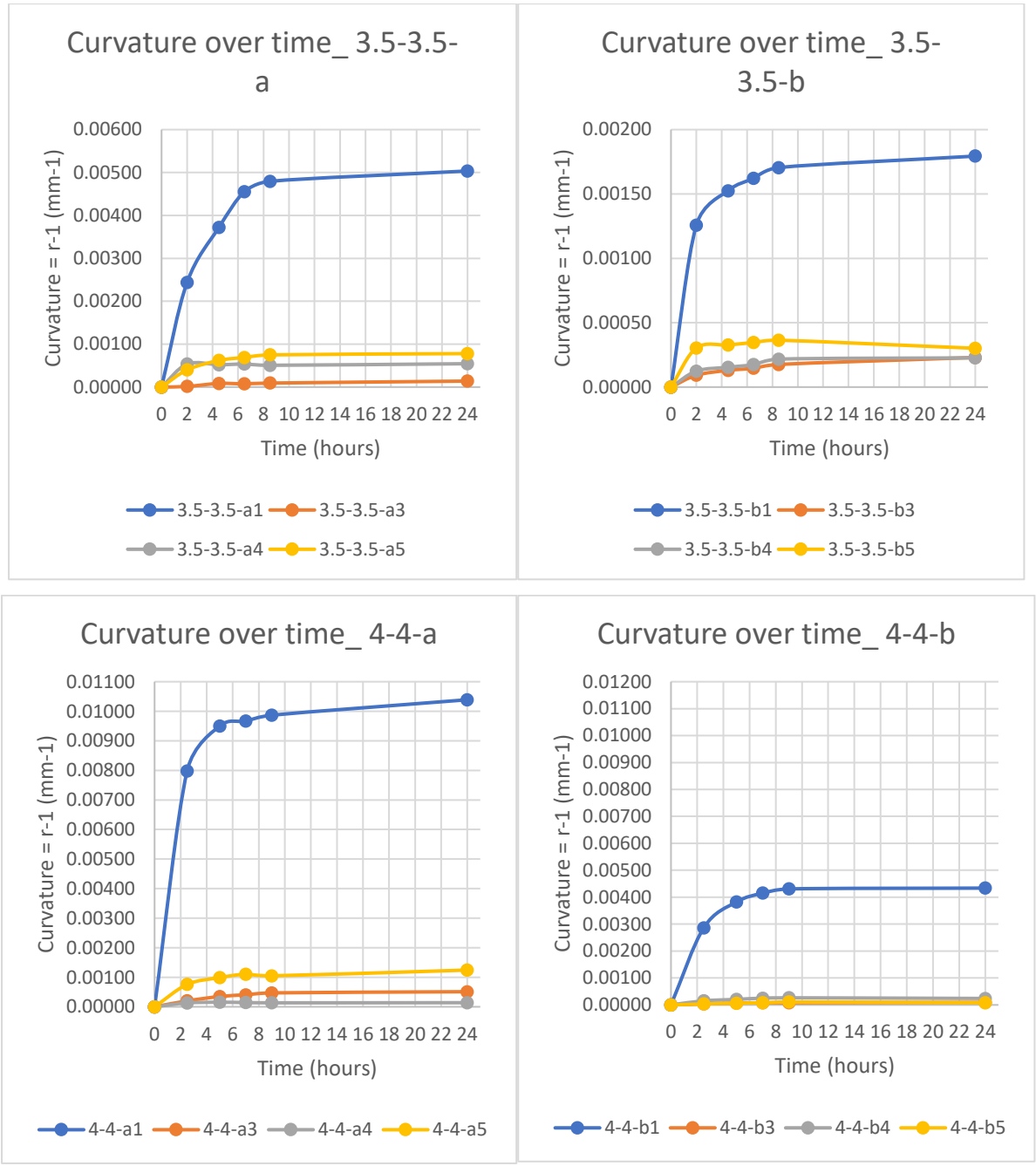

Figure 3-12. Graph of curvature over time (continued)

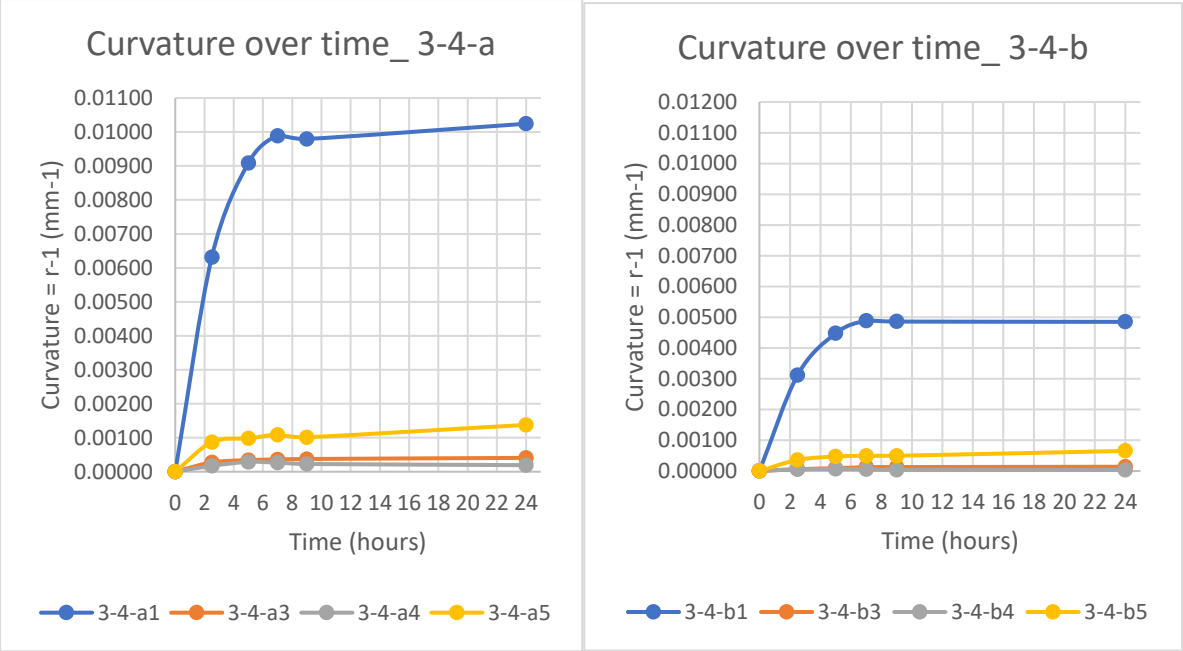

Figure 3-12. Graph of curvature over time for all samples.

The graph above has shown a drastic change in the curvature for the first 6 hours for all samples. The change reached plateau after 6 hours. In addition, group a1 and b1 (0-degree with 0-degree) showed a different trend from other groups. The relationship betewen curvature and time should be analysed in separate groups and with 6 hour as a break point for separating the groups as well (Figure 3-13). This way of seperating of groups will aslo be used in defining the relationship between curvature and time in section 3.2.1c. Other graphs are shown in Appendix 5a. Graphs were also plotted with samples of same fiber orientation and moisture content but diffferent thickness (Appendix 5b).

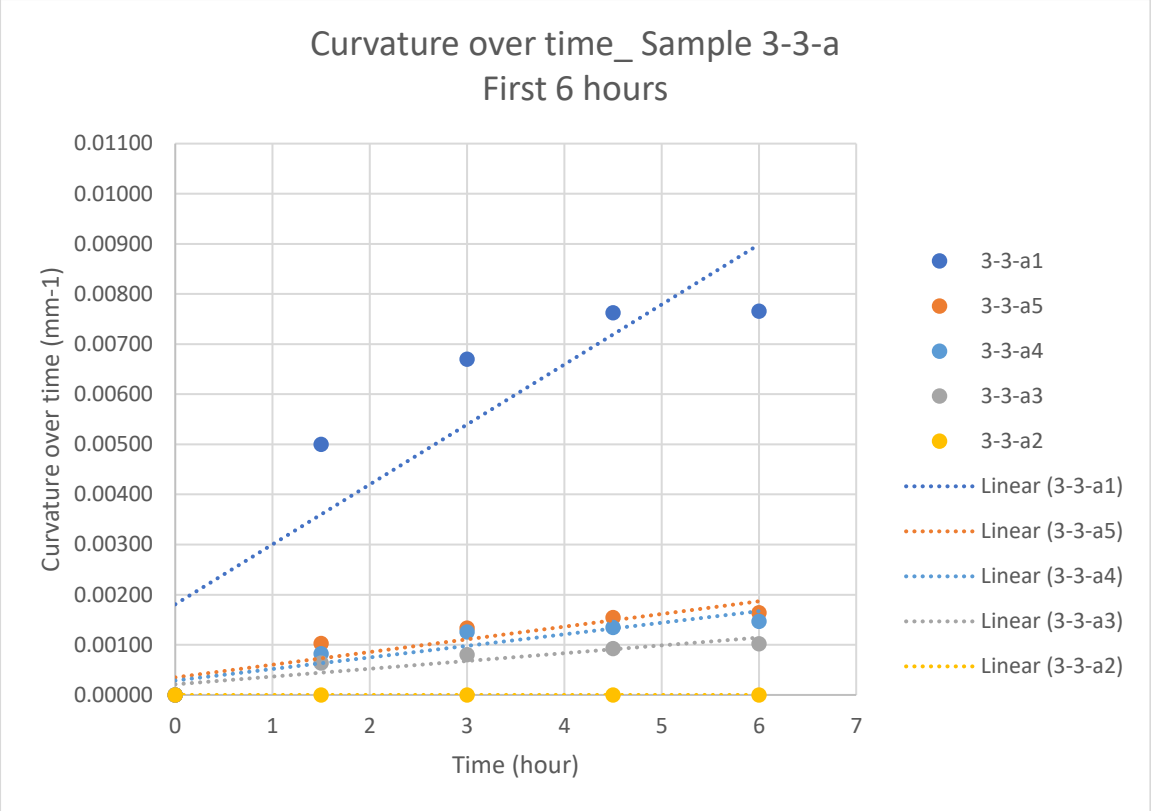

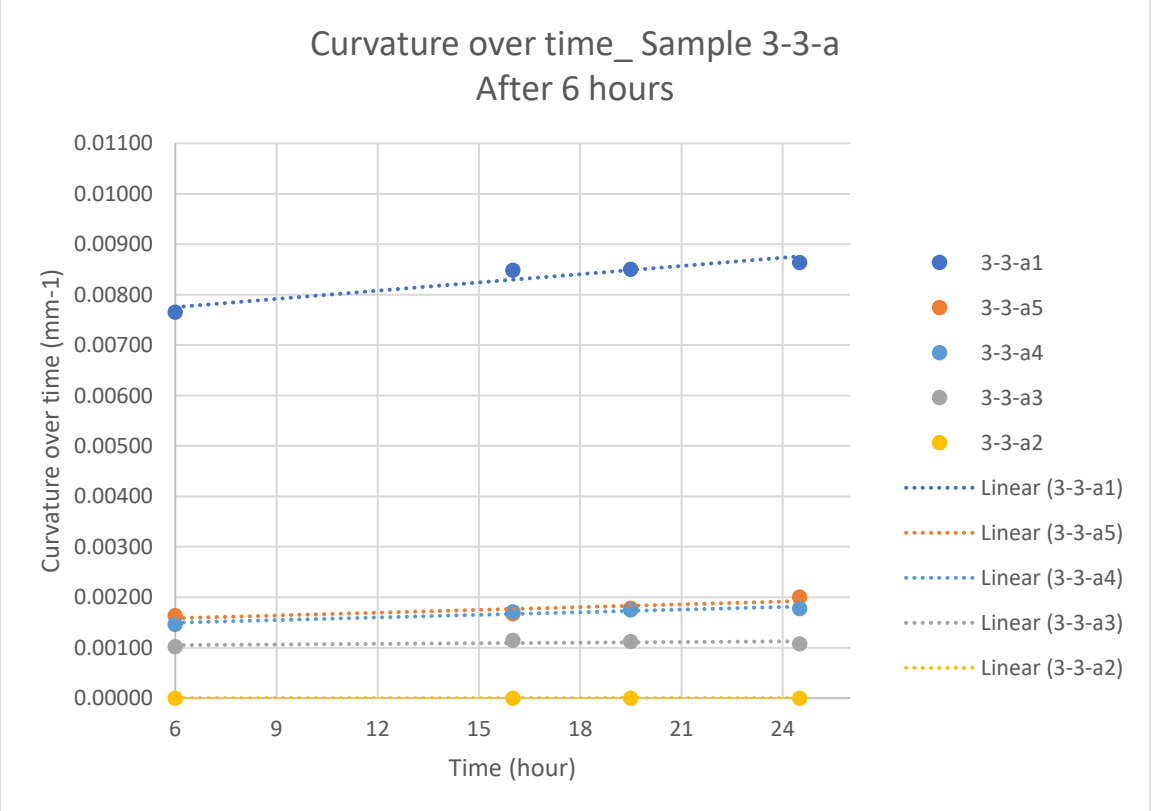

Figure 3-13. Curvature over time of Group a before and after 6 hours. Other graphs can be found in Appendix 5a.

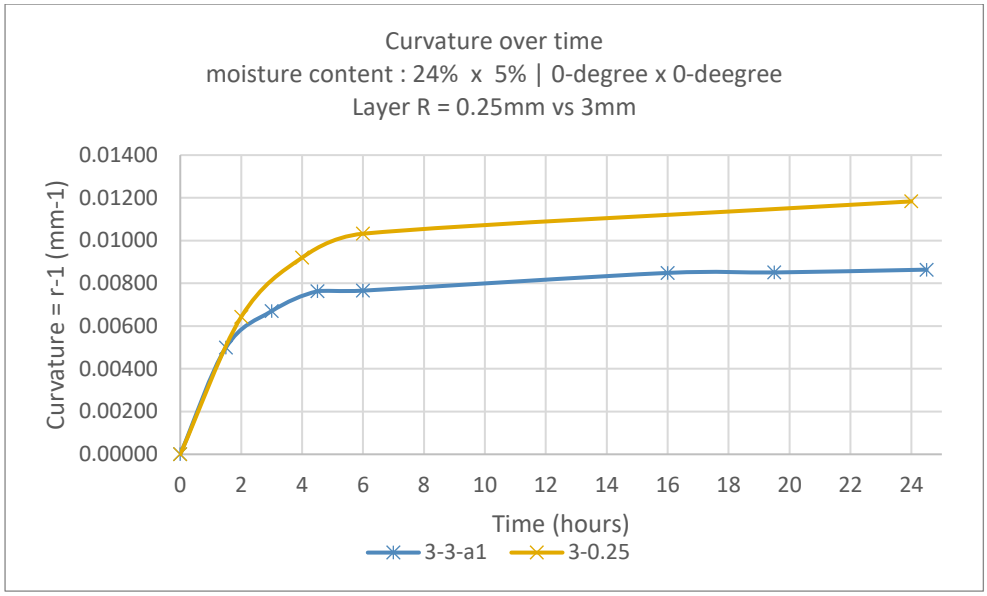

Figure 3-14. curvature over time of sample 3-3-a1 and 3-0.25

From Figure 3-14, the difference in restrictive layer resulted in an obvious difference in curvature which stands in line with bi-layer's theory. However, from Figure 3-15, while 3-4-a1 and 4-4-a1 with the same thickness of active, had almost the same curvature, 3-4-a1 generated a larger curvature than 3-3-a1. With the same thickness of restrictive layer, the active layer dominates the bending. This stands in line with the moisture content measurement that the decrease in moisture content of active layer is plays the major role in creating the stress in bending process.

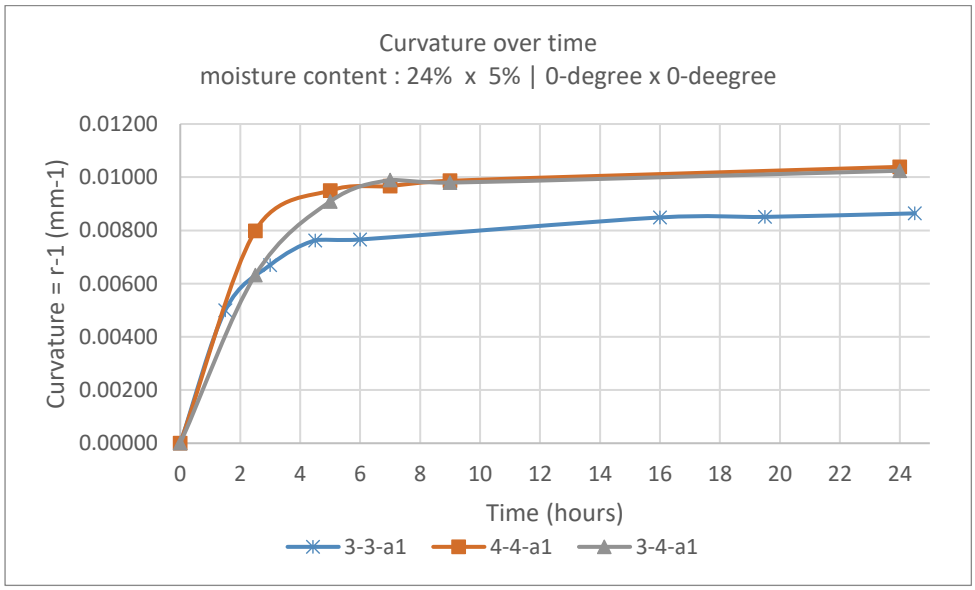

Figure 3-15 curvature over time of sample 3-3-a1, 4-4-a1 and 3-4-a1.

As the moisture and curvature over time was reaching equilibrium within 24 hours, the data with relative humidity, temperature data for the first 24 hours were collated in Appendix 4c.

3.1.1c-3. Shrinkage Coefficient

Recalling equation 3 in Chapter 2, shrinkage coefficient is needs to be obtained in order to apply the formula for simulation. Shrinkage of the samples were measured by fitting a strip of paper to the sample and measured with ruler.

The shrinkage/expansion coefficient α can be calculated by adopting the formula below.

$$\alpha_1 = \frac{n}{c - c0} \quad \text{for shrinkage}$$

$$\alpha_2 = \frac{n}{c0 - c} \quad \text{for expansion}$$

where:

n = percentage shrinkage/expansion

c = initial moisture content

c0 = final moisture content

The percentage shrinkage can be obtained by

$$n = \frac{l_1 - l_2}{l_1} \times 100\ (\%) \quad \text{for shrinkage}$$

$$n = \frac{l_2 - l_1}{l_1} \times 100\ (\%) \quad \text{for expansion}$$

where:

l_1 = initial length

l_2 = final length

(Edited from "Hygroexpansion in wood – shrinkage and swelling", n.d.)

The measurements and calculations are summarized in Table 3-5 below for group 3-3-a and 3-3-b. Other data are shown in Appendix 7. The length was measured as shown in Figure 3-16. After bending, the length was measured by fitting a strip

of paper to the same side of the curved surfaces and measure the length of the paper using a ruler. Graph was plotted separately to show the shrinkage coefficient of the active layers of the two groups 3-3-a and 4-4-a separately. The graph has demonstrated that shrinkage coefficient is a property of wood that is affected by the moisture content but not by thickness of the material (Figure 3-17). In this case, since layer A has various orientations, Layer A has unique shrinkage coefficient corresponding to the fiber orientation while Layer R remained almost constant as there was no change in the fiber orientation (Appendix 7). As a result, shrinkage coefficient will be related to fiber orientation in the simulation later in Section 3.2.1.

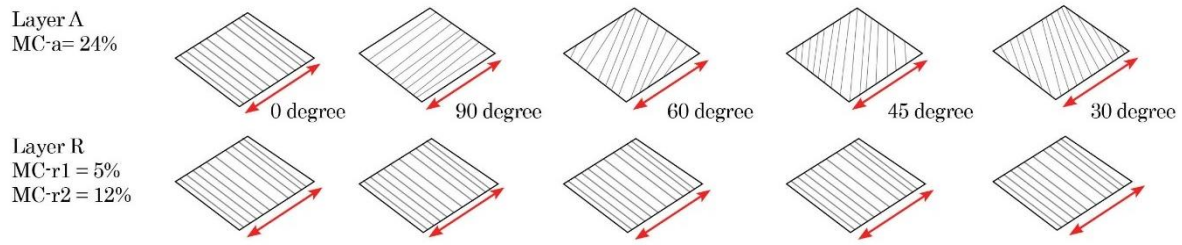

Figure 3-16. Side of the measurements taken for the length change due to shrinkage or expansion.

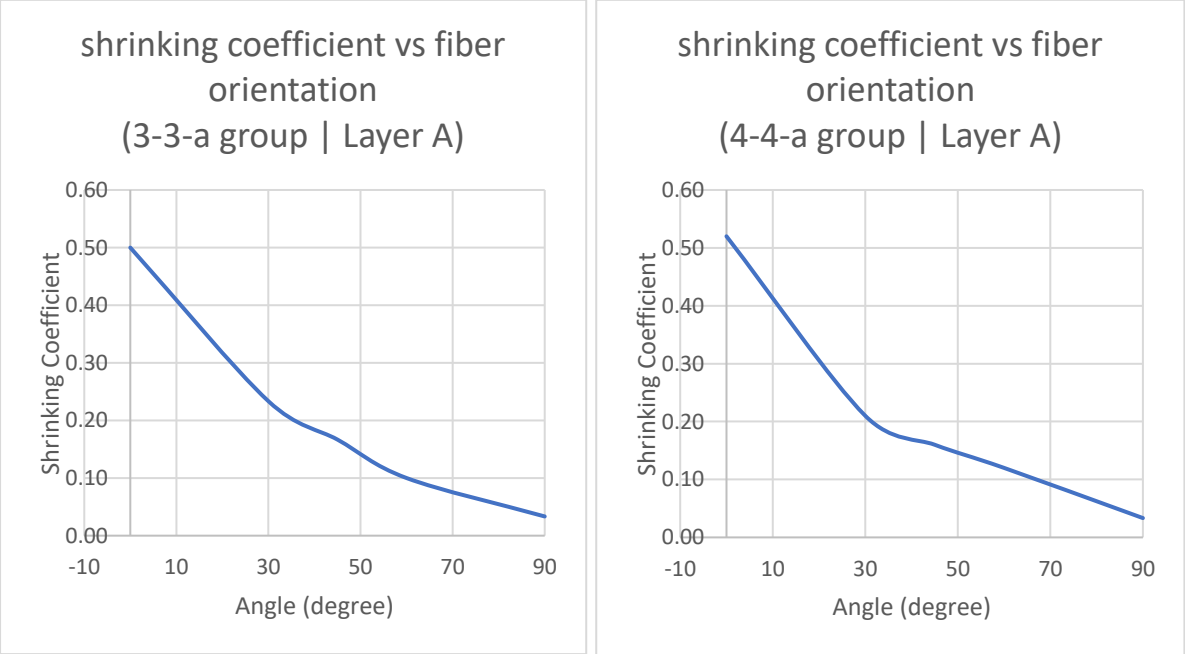

Figure 3-17. Graph of shrinking coefficient of group 3-3-a and 4-4-a. The shrinkage coefficient is a property of the material and it is not much affected by the thickness.

Type a = 24% x 5%

3mm x 3mm

Active Layer	orientation (degree)	initial moisture content	final moisture content	initial length (mm)	final length (mm)	percentage shrinkage	shrinkage coefficient
		c	c0	l1	l2	n	α1
3-3-a1-A	0	24.0%	12.80%	25.0	23.5	5.6%	0.500
3-3-a5-A	30	24.0%	13.10%	25.0	24.3	2.5%	0.233
3-3-a4-A	45	24.0%	13.30%	25.0	24.5	1.8%	0.167
3-3-a3-A	60	24.0%	12.90%	25.0	24.7	1.1%	0.100
3-3-a2-A	90	24.0%	13.03%	25.0	24.9	0.4%	0.033
Restrictive Layer	orientation (degree)	initial moisture content	final moisture content	initial length (mm)	final length (mm)	percentage expansion	expansion coefficient
		c	c0	l1	l2	n	α2
3-3-a1-R	0	5.0%	10.5%	25.0	25.1	0.6%	0.100
3-3-a5-R	0	5.0%	10.4%	25.0	25.1	0.4%	0.080
3-3-a4-R	0	5.0%	11.6%	25.0	25.1	0.5%	0.078
3-3-a3-R	0	5.0%	10.5%	25.0	25.1	0.3%	0.059
3-3-a2-R	0	5.0%	10.8%	25.0	25.1	0.4%	0.065

Type b = 24% x 12%

Active Layer	orientation (degree)	initial moisture content	final moisture content	initial length (mm)	final length (mm)	percentage shrinkage	shrinkage coefficient
		c	c0	l1	l2	n	α1
3-3-b1-A	0	24.0%	14.7%	25.0	23.7	4.0%	0.433
3-3-b5-A	30	24.0%	13.3%	25.0	24.9	0.4%	0.033
3-3-b4-A	45	24.0%	13.8%	25.0	24.8	0.7%	0.067
3-3-b3-A	60	24.0%	12.4%	25.0	24.6	1.5%	0.133
3-3-b2-A	90	24.0%	13.6%	25.0	24.3	2.4%	0.233
Restrictive Layer	orientation (degree)	initial moisture content	final moisture content	initial length (mm)	final length (mm)	percentage expansion /shrikage	expansion /shrinkage coefficient
		c	c0	l1	l2	n	α2
3-3-b1-R	0	12.0%	10.5%	25.0	25.0	0.1%	0.049
3-3-b5-R	0	12.0%	12.3%	25.0	25.0	0.0%	0.047
3-3-b4-R	0	12.0%	11.7%	25.0	25.0	0.0%	0.042
3-3-b3-R	0	12.0%	11.7%	25.0	25.0	0.0%	0.048
3-3-b2-R	0	12.0%	11.6%	25.0	25.0	0.0%	0.043

Table 3-5. Measurements taken for the five samples of 3-3-a group and those of 3-3-b group. Shrinkage coefficient of active layer, Layer A, is affected by fiber orientation while that of restrictive layer, Layer R, showed an almost constant value as they remained in the same orientations.

3.1.2 Structural Test for Young's Modulus for different fiber orientations

3.1.2a. Experiment

Purpose

The purpose of structural test was to find out

1. Young's Modulus, Ei (i = orientation angle of the active layer) of the timber pieces when they are combined with different orientations, i.e. 0-degree x 30 degree, 0-degree x 45-degree etc
2. To find out the effect of glue on strength of the laminated wood.

Experiment Set-up

Since there are a lot of combinations of not only different fiber orientations, but also the facing of the surface and glue types. To simplify the experiment, the pieces are combined with same orientations and perpendicular orientations (Figure 3-18). The other orientations can be derived.

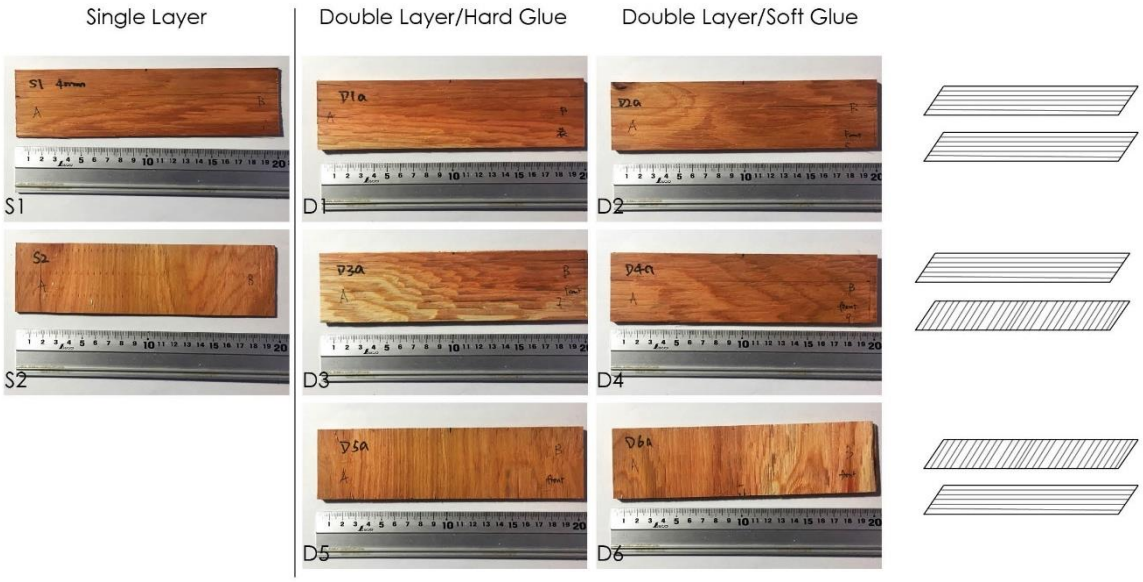

Figure 3-18. Experiment samples. S1 and S2 are single layers with different fiber orientation, D1 to D6 are double layers with fiber orientations shown on the right side of the figure. D1, D3 & D5 were glued using hard glue while D2, D4 and D6 were glued using soft glue, which was a the same as what was used in making the prototypes in the previous section.

Masses were weighed before and after glue, and also wood moisture content was equilibrated at 24 degree Celsius and relative humidity of 52% for over a month. Each test piece was measured for length, width and thickness. Width and thickness were measure at three points of each test piece (Figure 3-19). This information was collated in Table 3-6.

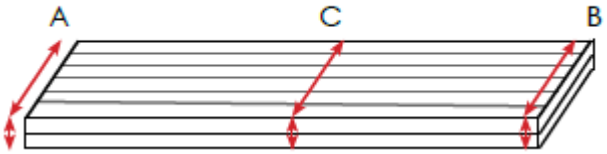

Figure 3-19. Method of measurements for the width and thickness of the samples

	2018/11/12			2018/12/14						
	Mass (g)			Length(mm)	Width (mm)			Thickness (mm)		
	before glue(g)	after glue(g)	Reach Equilibrium		A	C	B	A	C	B
S1	14	NA	13	200.5	51.0	51.0	51.0	3.8	3.8	3.8
S2	19	NA	18	197.0	52.5	53.5	53.5	3.8	4.0	3.5
D1	28	30	28	200.8	51.5	51.5	51.0	7.5	7.5	7.0
D2	30	31.5	29	201.0	50.5	51.5	50.5	7.5	7.5	7.5
D3	29	31	29	201.0	51.5	51.5	51.5	7.5	8.0	7.5
D4	32	33	31	200.5	51.5	51.5	51.5	7.5	8.0	7.2
D5	36	37	35	200.5	53.0	53.5	53.5	7.5	7.5	7.0
D6	30	31	29	200.5	53.5	53.5	53.0	8.0	7.5	7.0

Table 3-6. Preparation of the samples for testing. Average width and thickness were calculated for further calculations.

The experiment was done by exert load at the center of the test samples (Figure 3-20). The load applied and the displacement were recorded (Appendix 8)

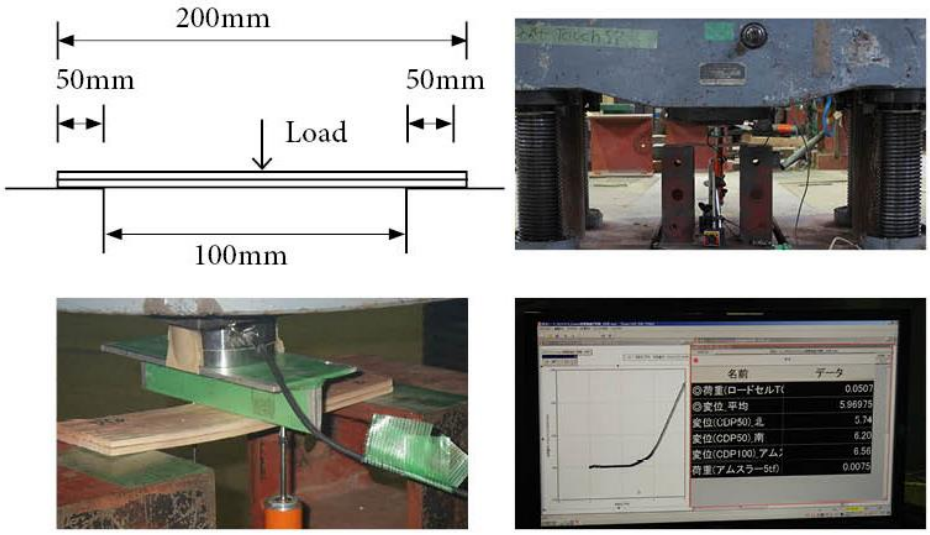

Figure 3-20. Bending test set up

Experiment Result

Graphs are plotted as load(N) versus vertical displacement(mm). Experiment data is shown in Appendix 6.

Single Layer Samples

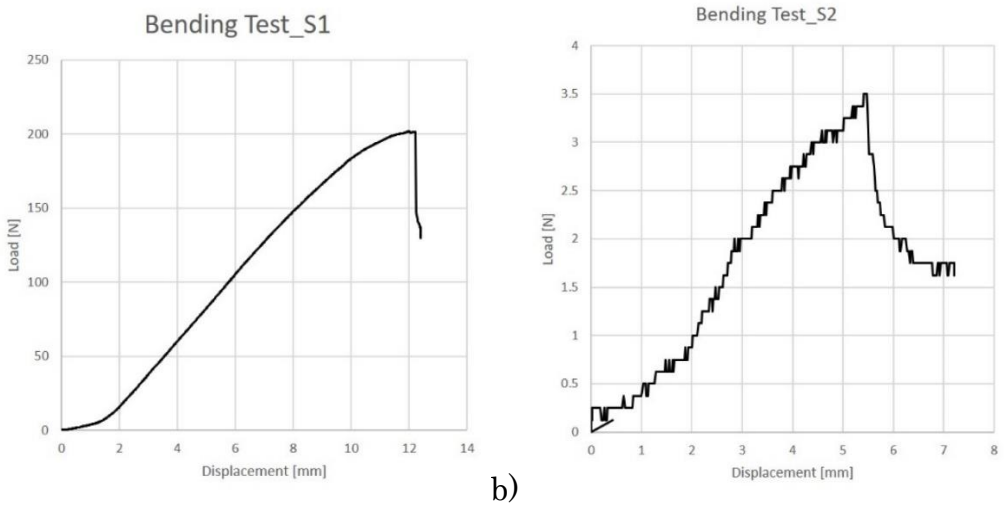

a) b)

Figure 3-21. Graph of load vs displacement to obtain Young's modulus (E). a) S1 graph. b) S2 graph. c) D1 graph. d) D2 graph e) D3 graph f) D4 graph. g) D5 graph. h) D6 graph

Double Layer Samples

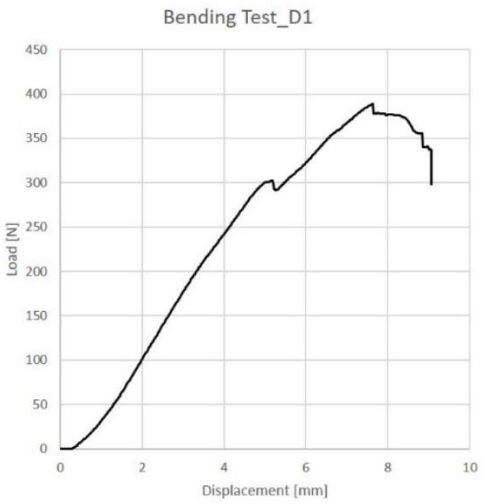

c)

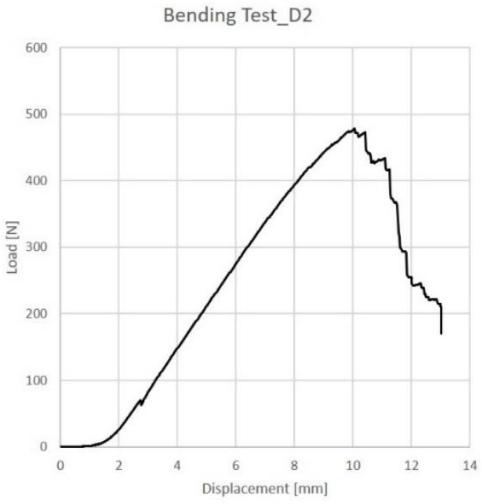

d)

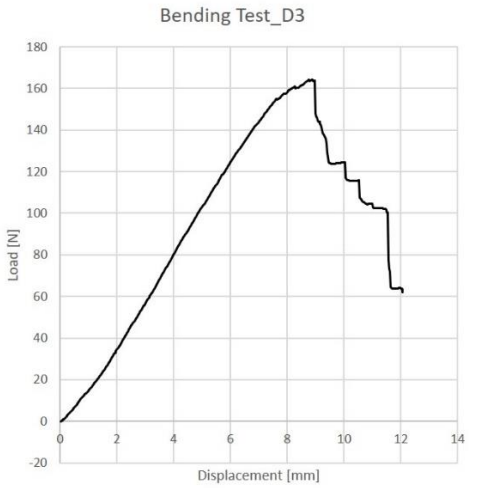

e)

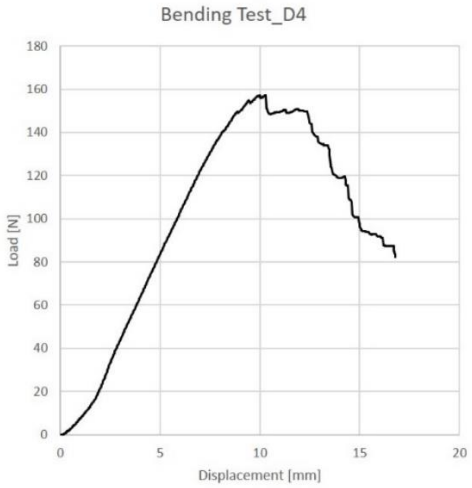

f)

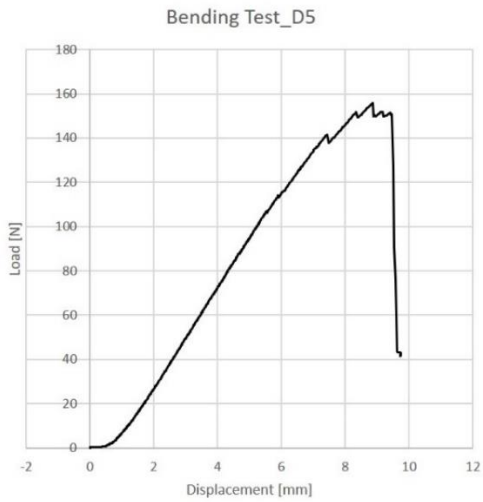

g)

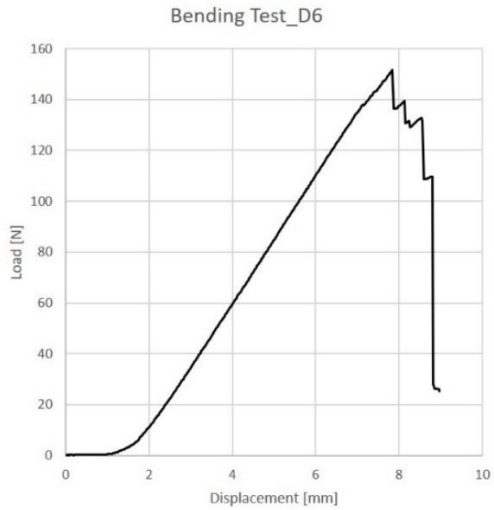

h)

Figure 3-21. Graph of load vs displacement to obtain Young's modulus (E). a) S1 graph. b) S2 graph. c) D1 graph. d) D2 graph e) D3 graph f) D4 graph. g) D5 graph. h) D6 graph (continued)

3.1.2b Calculations

Calculation of Young's Modulus of each sample

Sample	スパン(mm) Span (mm) L	荷重増分(N) Load Increment(N) Pi	鉛直変位(mm) Vertical Displacement(mm) D	断面二次モーメント (mm4) Area Moment of Inertia (mm4) I=wt^3/12	ヤング係数(N/mm2) Young's Modulus (N/mm2) E=Pi*L^3/48/I/D
S1	100.5	66.9	3.0	233.2	2045.6
S2	47.0	0.9	1.0	236.8	8.0
D1	100.8	88.6	1.2	1687.0	957.8
D2	101.0	76.0	1.2	1787.1	760.5
D3	101.0	50.4	2.2	1934.0	256.7
D4	100.5	47.9	2.1	1859.3	254.5
D5	100.5	35.9	1.6	1752.8	275.7
D6	100.5	31.0	1.2	1875.0	284.3

Table 3-7. Calculation of Young's Modulus of each sample.

For the double layered samples, D1 and D2 with the same horizontal fiber orientations are obviously different from the other samples. Amongst D3, D4, D5 and D6, there is no significant difference, i.e. neither glue nor the order of the placement of the two layers results in a significant difference in the stiffness of the sample. The Young's Modulus (E) for the parallel (0 degree) and vertical (90 degree) orientations are obtained from the table above (Table 3-7). As the previous experiments used the soft glue, the E of S1, S2, D2 and D6 are taken for further calculations (Figure 3-22).

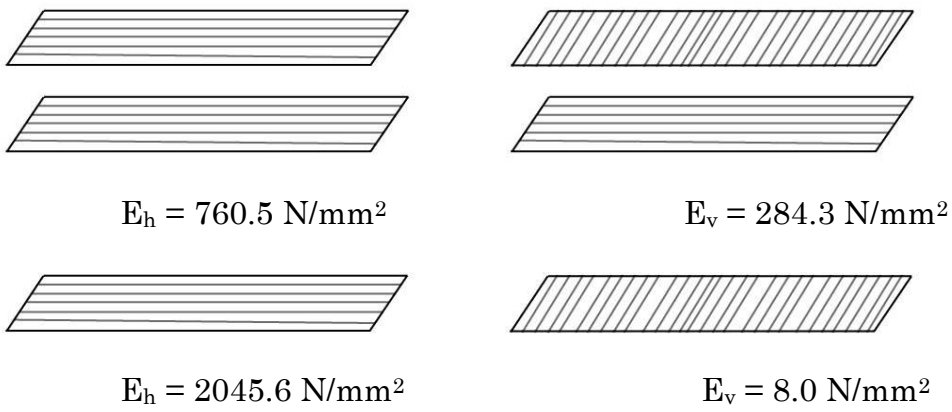

Figure 3-22. Top left: sample D2. Top right: sample D6. Bottom left: sample S1. Bottom right: sample S2

Subsequently, the relationship between the rest of fiber orientations and Young's Modulus can be inferred as follows:

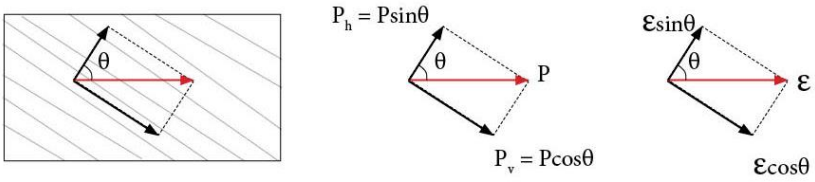

Figure 3-23. Illustration of principle of calculation using Hooke's Law

According to Hooke's Law,

P = Eε, where P = stress, E is modulus of elasticity (Young's Modulus), ε represents strain.

$P = PCos^2\theta + PSin^2\theta$

$= E_h\varepsilon Cos^2\theta + E_v\varepsilon Sin^2\theta$

$= (E_h Cos^2\theta + E_v Sin^2\theta)\varepsilon$

$= E'\varepsilon$

Hence, the equation for E and fiber orientation is as follows

$E' = E_h Cos^2\theta + E_v Sin^2\theta$ (Eq. 5)

As a result, the Young's Modulus of the test samples in Section 3.1.2 can be derived in the following Table:

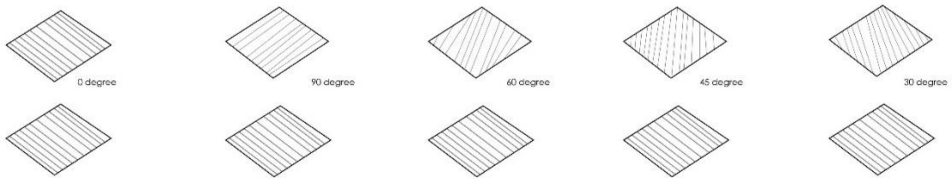

Young's Modulus of Single-Layered samples					
combination	E_0 (N/mm2)	E_{90} (N/mm2)	E_{60} (N/mm2)	E_{45} (N/mm2)	E_{30} (N/mm2)
Single layer	2045.6	8.0	517.4	1026.8	1536.2
Stiffness of double-layered samples					
combination	δ_0 (N/mm2)	δ_{90} (N/mm2)	δ_{60} (N/mm2)	δ_{45} (N/mm2)	δ_{30} (N/mm2)
3x3	570.4	213.2	302.5	391.8	481.1
3.5x3.5	665.4	248.7	352.9	457.1	561.2
4x4	760.5	284.3	403.3	522.4	641.4
3x4	665.4	248.7	352.9	457.1	561.2

Table 3-8. Young's Modulus of each single-layered samples. Stiffness of double-layered samples.

As Young's Modulus is a property of material, it will not change due to the thickness change. When it is double-layered, the thickness affects the stiffness of the samples. The values obtained for double-layered samples were just for the completion of the experiment but not used in the derivation of the function or simulation later. Only the values for the single-layered samples were used for further calculations.

3.2 Digital Simulation

In order to propose a simulation, first of all, it is important to verify the experimental data with the equation 3 in Chapter 2 to find out if further adaptations should be done.

3.2.1 Derivation of formula

3.2.1a. Adaptation of bi-layer theory formula

With the experimental data obtained above, experiment values are compared with the calculated values. Recalling the modified bi-layer equation 3 in Chapter 2, samples of 3x3mm, 4x4mm, and 3x4mm groups were used as an example for calculation (Table 3-9a&b).

TYPE a_24% x 5%

3 x 3mm	Fiber orientation degree		shrinkage coefficient active α1	expansion coefficient restrictive α2	Young's Modulus active E2	Young's Modulus restrictive E1	initial moisture content c	Final moisture content c0	m	n	k	calculated curvature 1/ρ	experiment curvature
3-3-a1	0	0	0.500	0.100	2.0456	2.0456	0.24	0.130	1	1.000	1.500	0.01100	0.00864
3-3-a5	30	0.5235988	0.233	0.080	1.5362	2.0456	0.24	0.131	1	1.332	1.492	0.00416	0.00291
3-3-a4	45	0.7853982	0.167	0.078	1.0268	2.0456	0.24	0.133	1	1.992	1.455	0.00230	0.00178
3-3-a3	60	1.0471976	0.100	0.059	0.5174	2.0456	0.24	0.129	1	3.954	1.318	0.00100	0.00108
3-3-a2	90	1.5707963	0.033	0.065	0.008	2.0456	0.24	0.131	1	255.700	0.089	-0.00005	0.00000

4 x 4mm	Fiber orientation degree		shrinkage coefficient active α1	expansion coefficient restrictive α2	Young's Modulus active E2	Young's Modulus restrictive E1	initial moisture content c	Final moisture content c0	m	n	k	calculated curvature 1/ρ	experiment curvature
4-4-a1	0	0	0.520	0.100	2.0456	2.0456	0.24	0.122	1	1.000	1.500	0.01239	0.01039
4-4-a5	30	0.5235988	0.210	0.090	1.5362	2.0456	0.24	0.143	1	1.332	1.492	0.00290	0.00124
4-4-a4	45	0.7853982	0.160	0.082	1.0268	2.0456	0.24	0.146	1	1.992	1.455	0.00178	0.00054
4-4-a3	60	1.0471976	0.120	0.067	0.5174	2.0456	0.24	0.148	1	3.954	1.318	0.00107	0.00051
4-4-a2	90	1.5707963	0.033	0.090	0.008	2.0456	0.24	0.142	1	255.700	0.089	-0.00008	0.00000

3 x 4mm	Fiber orientation degree		shrinkage coefficient active α1	expansion coefficient restrictive α2	Young's Modulus active E2	Young's Modulus restrictive E1	initial moisture content c	Final moisture content c0	m	n	k	calculated curvature 1/ρ	experiment curvature
3-4-a1	0	0	0.510	0.100	2.0456	2.0456	0.24	0.100	0.75	1.000	1.469	0.01406	0.01024
3-4-a5	30	0.5235988	0.190	0.090	1.5362	2.0456	0.24	0.103	0.75	1.332	1.492	0.00341	0.00138
3-4-a4	45	0.7853982	0.166	0.078	1.0268	2.0456	0.24	0.121	0.75	1.992	1.499	0.00262	0.00049
3-4-a3	60	1.0471976	0.120	0.063	0.5174	2.0456	0.24	0.127	0.75	3.954	1.441	0.00155	0.00041
3-4-a2	90	1.5707963	0.033	0.070	0.008	2.0456	0.24	0.117	0.75	255.700	0.155	-0.00012	0.00000

Table 3-9a. calculations using equation 3, the bi-layer theory equation, of Type a

TYPE b_24% x 12%

3 x 3mm	Fiber orientation degree		shrinkage coefficient active α1	expansion coefficient restrictive α2	Young's Modulus active E2	Young's Modulus restrictive E1	initial moisture content c	Final moisture content c0	m	n	k	calculated curvature 1/ρ	experiment curvature
3-3-b1	0	0	0.433	0.049	2.0456	2.0456	0.24	0.147	1	1.000	1.500	0.00894	0.00339
3-3-b5	30	0.5235988	0.233	0.047	1.5362	2.0456	0.24	0.133	1	1.332	1.492	0.00496	0.00076
3-3-b4	45	0.7853982	0.133	0.042	1.0268	2.0456	0.24	0.138	1	1.992	1.455	0.00226	0.00076
3-3-b3	60	1.0471976	0.067	0.048	0.5174	2.0456	0.24	0.124	1	3.954	1.318	0.00048	0.00045
3-3-b2	90	1.5707963	0.033	0.043	0.008	2.0456	0.24	0.122	1	255.700	0.089	-0.00002	0.00000

4 x 4mm	Fiber orientation degree		shrinkage coefficient active α1	expansion coefficient restrictive α2	Young's Modulus active E2	Young's Modulus restrictive E1	initial moisture content c	Final moisture content c0	m	n	k	calculated curvature 1/ρ	experiment curvature
4-4-b1	0	0	0.425	0.050	2.0456	2.0456	0.24	0.114	1	1.000	1.500	0.01181	0.004337
4-4-b5	30	0.5235988	0.211	0.080	1.5362	2.0456	0.24	0.123	1	1.332	1.492	0.00381	0.00082
4-4-b4	45	0.7853982	0.125	0.078	1.0268	2.0456	0.24	0.142	1	1.992	1.455	0.00112	0.00024
4-4-b3	60	1.0471976	0.069	0.060	0.5174	2.0456	0.24	0.131	1	3.954	1.318	0.00022	0.000096
4-4-b2	90	1.5707963	0.031	0.060	0.008	2.0456	0.24	0.113	1	255.700	0.089	-0.00005	0.00000

3 x 4mm	Fiber orientation degree		shrinkage coefficient active α1	expansion coefficient restrictive α2	Young's Modulus active E2	Young's Modulus restrictive E1	initial moisture content c	Final moisture content c0	m	n	k	calculated curvature 1/ρ	experiment curvature
3-4-b1	0	0	0.412	0.047	2.0456	2.0456	0.24	0.107	1	1.000	1.500	0.01214	0.004851
3-4-b5	30	0.5235988	0.200	0.070	1.5362	2.0456	0.24	0.111	1	1.332	1.492	0.00417	0.000655
3-4-b4	45	0.7853982	0.128	0.078	1.0268	2.0456	0.24	0.128	1	1.992	1.455	0.00136	0.00036
3-4-b3	60	1.0471976	0.067	0.063	0.5174	2.0456	0.24	0.116	1	3.954	1.318	0.00010	0.00014
3-4-b2	90	1.5707963	0.028	0.050	0.008	2.0456	0.24	0.122	1	255.700	0.089	-0.00004	0.00000

Table 3-9b. calculations using equation 3, the bi-layer theory equation, of Type b (bottom).

By comparing the calculated curvature and experiment curvature by groups (Table 3-10), they showed a strong linear relationship between them (Figure 3-24). This means that the experiment result can be obtained by adapting Equation 3.

Type a	Calculated	Experiment
3-3-a1	0.01100	0.00864
3-3-a5	0.00416	0.00291
3-3-a4	0.00230	0.00178
3-3-a3	0.00100	0.00108
3-3-a2	-0.00005	0.00000
4-4-a1	0.01239	0.01039
4-4-a5	0.00290	0.00124
4-4-a4	0.00178	0.00054
4-4-a3	0.00107	0.00051
4-4-a2	-0.00008	0.00000
3-4-a1	0.01406	0.01024
3-4-a5	0.00341	0.00138
3-4-a4	0.00262	0.00049
3-4-a3	0.00155	0.00041
3-4-a2	-0.00012	0.00000

Type b	Calculated	Experiment
3-3-b1	0.00894	0.00339
3-3-b5	0.00496	0.00076
3-3-b4	0.00226	0.00076
3-3-b3	0.00048	0.00045
3-3-b2	-0.00002	0.00000
4-4-b1	0.01181	0.00434
4-4-b5	0.00381	0.00082
4-4-b4	0.00112	0.00024
4-4-b3	0.00022	0.00010
4-4-b2	-0.00005	0.00000
3-4-b1	0.01214	0.00485
3-4-b5	0.00417	0.00066
3-4-b4	0.00136	0.00036
3-4-b3	0.00010	0.00014
3-4-b2	-0.00004	0.00000

Table 3-10. Calculated curvature vs experiment curvature summarized for Type a and Type b

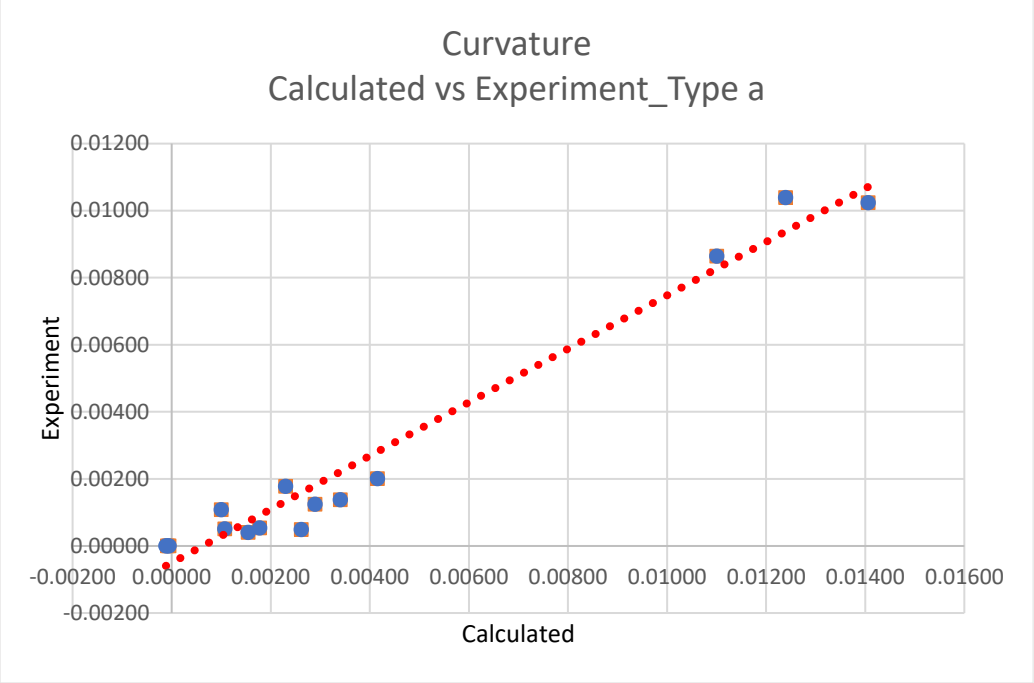

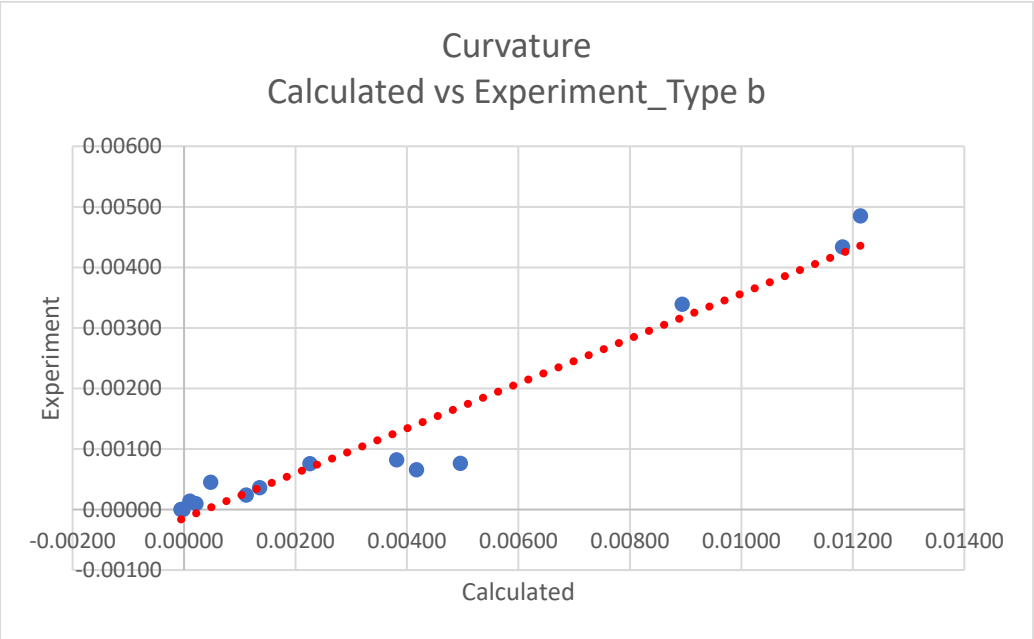

Figure 3-24. Top: Calculated curvature vs experiment curvature for Type a (24% x 5%). Bottom: Calculated curvature vs experiment curvature for Type b (24% x 12%)

As the graphs almost passed origin, let $\hat{y}$ = New Equation, x = Equation 3, and let $\hat{y} = b_1 * x$, the coefficient b_1 can be obtained using least squares method using Data Analysis in Microsoft Excel. The result is shown in Table 3-11. Type a showed coefficient of determination R Square of 0.976 while that of Type b was 0.957. 97.6% and 95.7% of the variation in experiment curvature was explained by independent variables in calculated curvature for Type a and b respectively,

showing a strong linear relationship between the calculated and experiment curvature for both types.

Type a		Type b	
Regression Statistics		*Regression Statistics*	
Multiple R	0.988	Multiple R	0.978
R Square	0.976	R Square	0.957
Adjusted R Square	0.905	Adjusted R Square	0.885
Standard Error	0.001	Standard Error	0.000
Observations	15	Observations	15

Table 3-11. Result of regression analysis for Type a and Type b. Type a showed coefficient of determination R Square of 0.976 while that of Type b was 0.957.

As both Significance F and P-value were below 0.05, the result is reliable i.e. statistically significant.

Type a
ANOVA

	df	*SS*	*MS*	*F*	*Significance F*
Regression	1	0.000297	0.000297	569.9944	4.02417E-12
Residual	14	7.3E-06	5.22E-07		
Total	15	0.000305			

	Coefficients	*tandard Erro*	*t Stat*	*P-value*	*Lower 95%*	*Upper 95%*	*ower 95.0%*	*Upper 95.0%*
Intercept	0	#N/A	#N/A	#N/A	#N/A	#N/A	#N/A	#N/A
Calculated	0.750	0.031397	23.87456	9.63E-13	0.682255964	0.816937	0.682256	0.816937

Type b
ANOVA

	df	*SS*	*MS*	*F*	*Significance F*
Regression	1	5.41E-05	5.41E-05	308.3911	1.94666E-10
Residual	14	2.45E-06	1.75E-07		
Total	15	5.65E-05			

	Coefficients	*tandard Erro*	*t Stat*	*P-value*	*Lower 95%*	*Upper 95%*	*ower 95.0%*	*Upper 95.0%*
Intercept	0	#N/A	#N/A	#N/A	#N/A	#N/A	#N/A	#N/A
Calculated	0.354	0.020152	17.56107	6.22E-11	0.310665162	0.397108	0.310665	0.397108

Table 3-12. Significance F for Type a & b was both below 0.05, which means that the data is statistically significant

Hence, the adapted equation for Type a and b can be obtained respectively as:

$$\frac{1}{\rho} = 0.750 * \frac{6(1+m)^2}{\left(3(1+m)^2 + (1+mn)\left(m^2 + \frac{1}{mn}\right)\right)} \frac{(\alpha_2 - \alpha_1)(c - c_0)}{h} = k' \frac{\Delta\alpha \Delta c}{h},$$

(Eq.6a)

$$\frac{1}{\rho} = 0.354 * \frac{6(1+m)^2}{\left(3(1+m)^2 + (1+mn)\left(m^2 + \frac{1}{mn}\right)\right)} \frac{(\alpha_2 - \alpha_1)(c - c_0)}{h}$$

$$= k'' \frac{\Delta\alpha\Delta c}{h},$$

(Eq. 6b)

$$m = \frac{h_1}{h_2}, n = \frac{E_1}{E_2}$$

where

h1 = thickness of restrictive layer

h2 = thickness of active layer

h = h1+ h2

E1 = Young's Modulus of restrictive layer

E2 = Young's Modulus of active layer

c = initial moisture content

c0 = final moisture content

α1 = shrinkage coefficient of restrictive layer

α2 = expansion coefficient of active layer

However, the resulting equations have shown that the curvature of Type a and b was 0.75 and 0.354 of the result calculated by the original equation Eq.3. This is mainly because that the condition for Eq.3 used different species and a combination of tangential and longitudinal direction to maximize the shrinkage difference between active and restrictive layer. While in this experiment, only single species and a combination of tangential and tangential direction was used due to the prioritization of local context and simplifying the processing of wood. Hence, the potential difference in shrinkage between the two layers was reduced, resulting in smaller curvature value generated by experiment compared to the calculated one. It also means that different species and a combination of tangential and longitudinal direction of wood is a more powerful set of tools to generate curvature through self-actuated bending as compared to single species and tangential and tangential combination.

Attempts were also made to find a universal equation regardless of the Type i.e. initial moisture content of the restrictive layer (Appendix 9). However, the coefficient of determination R square was only 0.87 which is not good enough for such a small amount of sample. As a result, Type a and b were discussed separately.

As for the difference in the coefficient 0.75 and 0.354 for Type a and b, the possible reason could be the difference in the initial moisture content of the restrictive layer. While coefficient of the curvature of Type a is almost 0.75/0.354 = 2.12 times of that of Type b, the initial moisture content of restrictive layer of Type b is almost 0.12/0.05 = 2.4 times of that of Type a. There observes almost an inverse relationship. However, the experiment was only limited to these two types so that it is difficult to draw a conclusion as such. As the goal of this research is to complete the system of simulation based on the physical explorations, the deeper relationship between the coefficients and the parameters could be studied in future research.

In order to make the simulation compatible to the experiment result, the simulation was designed such that it could switch between two modes Type a and b for application of the equations.

3.2.1b. Relationship between shrinkage coefficient and fiber orientation angle

With the adapted equations, the simulations could be completed by input thickness, Young's Modulus, moisture contents and shrinkage coefficient of layers. In order for the simulation to be meaningful for simple inputs which do not require extra information that needs to be verified. Young's Modulus and can be linked to the orientation of active layer as explained in previous section. Shrinkage coefficient can be linked to orientation of active layer as follows: by determining a relationship between the fiber orientation angle and the average of the shrinkage coefficients of various samples of the same angle (Table 3-13).

TYPE a_Layer A

Sample	Angle (degree)	Angle (radians)	Shrinkage Coefficient			
			3x3	4x4	3x4	average
a1-A	0	0.000	0.500	0.520	0.510	0.510
a5-A	30	0.524	0.233	0.210	0.190	0.211
a4-A	45	0.785	0.167	0.160	0.166	0.164
a3-A	60	1.047	0.100	0.120	0.120	0.113
a2-A	90	1.571	0.033	0.033	0.033	0.033

TYPE b_Layer A

Sample	Angle (degree)	Angle (radians)	Shrinkage Coefficient			
			3x3	4x4	3x4	average
b1-A	0	0.000	0.433	0.425	0.412	0.423
b5-A	30	0.524	0.233	0.211	0.200	0.215
b4-A	45	0.785	0.133	0.125	0.128	0.129
b3-A	60	1.047	0.067	0.069	0.067	0.067
b2-A	90	1.571	0.033	0.031	0.028	0.031

Table 3-13. Summary of shrinkage coefficient and angle in radians for various samples.

By plotting the graph and regression line between angle and average shrinkage coefficient, the R-square was only 0.88 which is not good enough for such a small sample, i.e., the regression line does not fit the data well (Appendix 10). Exponential curve is then used for prediction.

Let $\alpha_1 = a \times e^{b\theta}$,

where θ = fiber orientation angle in radian, α_1 = average shrinkage coefficient, a and b are constants. Then it is obtained that:

$\Rightarrow ln\alpha_1 = lna + bx$

$\Rightarrow \alpha_1' = lna + bx$

θ (angle in radian)	α1'
0.000	-0.673
0.524	-1.555
0.785	-1.807
1.047	-2.177
1.571	-3.401

Table 3-14. value of θ and α1.

By applying the regression analysis, coefficient b could be obtained by covariance.p / variance.p operation in Microsoft Excel, lna = average of α_1' – b*(average of θ) = -0.602. Hence, a = 0.548

Thus, the function obtained for shrinkage coefficient was:

$$\alpha_1 = 0.548 \times e^{(-1.682\theta)} \qquad \text{(Eq. 7)}$$

where θ = fiber orientation angle of active layer in radian.

To verify equation 5, the calculated values 'α_1-hat' is compared with average shrinkage coefficient.

TYPE a

average shrinkage coefficient	α1-hat	correlation
0.510	0.548	0.997
0.211	0.227	
0.164	0.146	
0.113	0.094	
0.033	0.039	

TYPE b

average shrinkage coefficient	α1-hat	correlation
0.423	0.548	0.993
0.215	0.227	
0.129	0.146	
0.067	0.094	
0.031	0.039	

Table 3-15. comparison between average shrinkage coefficient and the calculated result using formula obtained. The correlation was 0.997 and 0.993 respectively for Type a and b, indicating the formula fits the data well.

As for the expansion coefficients of the restrictive layer, as shown in the table below, as there was no change in the fiber orientation, they remained almost constant throughout. Hence, average was taken to carry out simulation in the next section (Table 3-16) - α2 of Type a is 0.081 while that of Type b is 0.058.

TYPE a_Layer R

Sample	Angle (degree)	Angle (radians)	Expansion Coefficient 3x3	4x4	3x4	average
a1-R	0	0.000	0.100	0.100	0.100	0.100
a5-R	0	0.000	0.080	0.090	0.090	0.087
a4-R	0	0.000	0.078	0.082	0.078	0.079
a3-R	0	0.000	0.059	0.067	0.063	0.063
a2-R	0	0.000	0.065	0.090	0.070	0.075
					Average	0.081

TYPE b_Layer R

Sample	Angle (degree)	Angle (radians)	Expansion Coefficient 3x3	4x4	3x4	average
b1-R	0	0.000	0.049	0.050	0.047	0.049
b5-R	0	0.000	0.047	0.080	0.070	0.066
b4-R	0	0.000	0.042	0.078	0.078	0.066
b3-R	0	0.000	0.048	0.060	0.063	0.057
b2-R	0	0.000	0.043	0.060	0.050	0.051
					Average	0.058

Table 3-16. Calculation of expansion coefficient used for restrictive layer, Layer R.

3.2.1c. Relationship between curvature and time

As the time passed and moisture content changed, the curvature also changed with time. The final curvature at the point of 24 hours could be obtained by equation 6a & 6b above, curvature over time has a more complicated relationship. From the result in sub-section 3.1.1c-2, within the 24 hours, curvature changed drastically for the first six hours and slowly changed after that for all samples. Sample group a1 and b1 (0-degree x 0-degree) also behave differently from other samples. It is difficult to find a universal relationship for all the conditions for such a small sample. Hence, the data of the relationship between curvature and time should be discussed in different for different type a and b, before and after 6 hours and for group a1&b1 and others.

From the graph of curvature and time in Appendix 5a, the relationship between curvature and time can be defined as $1/\rho = p*t+q$ in general where p is the coefficient of time, q is a constant. The coefficient of b is related to the fiber orientation. Thus, to find this relationship, curvature over time were summarized in Table 3-17 for group a1. The same was done for all the other groups and the data is in Appendix 11.

3-3
4-4
3-4

Group a1_0x0

First 6 hours

Time (hour)	Curvature (mm-1)
0	0.00000
1.5	0.00500
3	0.00670
4.5	0.00763
6	0.00766
0	0.00000
2.5	0.00798
5	0.00950
7	0.00967
0	0.00000
2.5	0.00632
4.5	0.00909
6.5	0.00989

After 6 hours

Time (hour)	Curvature (mm-1)
6	0.00766
16	0.00849
19.5	0.00851
24.5	0.00864
7	0.00967
9	0.00987
24	0.01039
6.5	0.00989
8.5	0.00980
24	0.01024

Table 3-17. Data and regression analysis of curvature over time for group a1

SUMMARY OUTPUT

First 6 hours_Group a1

Regression Statistics	
Multiple R	0.966967
R Square	0.935026
Adjusted R Square	0.851692
Standard Error	0.001882
Observations	13

ANOVA

	df	*SS*	*MS*	*F*	*ignificance F*
Regression	1	0.000612	0.000612	172.6882	4.55E-08
Residual	12	4.25E-05	3.54E-06		
Total	13	0.000654			

	Coefficients	*andard Erro*	*t Stat*	*P-value*	*Lower 95%*	*Upper 95%*	*ower 95.0%*	*Upper 95.0%*
Intercept	0	#N/A	#N/A	#N/A	#N/A	#N/A	#N/A	#N/A
X Variable 1	0.001681	0.000128	13.14109	1.75E-08	0.001402	0.00196	0.001402	0.00196

SUMMARY OUTPUT

After 6 hours_Group a1

Regression Statistics	
Multiple R	0.121019
R Square	0.014646
Adjusted R Square	-0.10852
Standard Error	0.000964
Observations	10

ANOVA

	df	*SS*	*MS*	*F*	*ignificance F*
Regression	1	1.1E-07	1.1E-07	0.118907	0.739114
Residual	8	7.43E-06	9.29E-07		
Total	9	7.54E-06			

	Coefficients	*andard Erro*	*t Stat*	*P-value*	*Lower 95%*	*Upper 95%*	*ower 95.0%*	*Upper 95.0%*
Intercept	0.009112	0.000662	13.77397	7.45E-07	0.007587	0.010638	0.007587	0.010638
X Variable 1	1.4E-05	4.05E-05	0.344829	0.739114	-7.9E-05	0.000107	-7.9E-05	0.000107

Table 3-17. Data and regression analysis of relationship between curvature over time for group a1 before and after 6 hours. (continued)

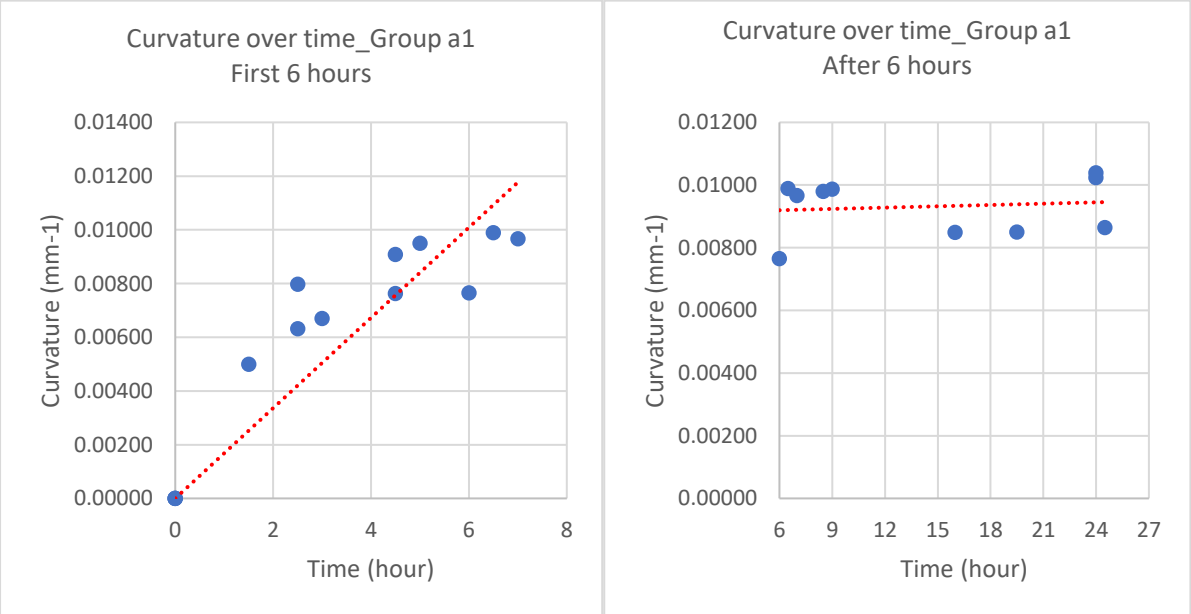

Figure 3-25. Graph of regression analysis of relationship between curvature over time for group a1 before and after 6 hours.

The equations for group a1 before and after 6 hours could be derived as:

$\frac{1}{\rho} = 0.00168 \times t$ and $\frac{1}{\rho} = 0.00001 \times t + 0.00911$ respectively.

For the other groups, results are shown in Table 3-18.

For the first 6 hours, curvature depends on time while it is affected little by time after 6 hours. Thus, for curvature for the first 6 hours, $1/\rho = p_1*t+q$ while for curvature after 6 hours, $1/\rho = p_2*t+q$.

Since the curvature over time has a strong relationship with fiber orientation, it is meaningful to link the equations with fiber orientation angle θ for simulation. Regression analysis was conducted again to express coefficient p1 and constant q in θ. For coefficient p2, there is no obvious relationship with angle and the impact is almost negligible, average is taken as 0.00002 for Type and 0.00001 for Type b. The coefficient p or constant q for all groups can be derived as:

First 6 hours

Group	θ (degree)	θ (radians)	Coefficient p1
a5	30	0.52	0.000233
a4	45	0.79	0.000132
a3	60	1.05	0.000108
a2	90	1.57	0.000000
After 6 hours			
Group	θ (degree)	θ (radians)	Coefficient p2
a5	30	0.52	0.000024
a4	45	0.79	0.000026
a3	60	1.05	0.000013
a2	90	1.57	0.000000
Group	θ (degree)	θ (radians)	Constant q
a5	30	0.52	0.001047
a4	45	0.79	0.000576
a3	60	1.05	0.000500
a2	90	1.57	0.000000

First 6 hours

Group	θ (degree)	θ (radians)	Coefficient p1
b5	30	0.52	0.000066
b4	45	0.79	0.000054
b3	60	1.05	0.000032
b2	90	1.57	0.000000
After 6 hours			
Group	θ (degree)	θ (radians)	Coefficient p2
b5	30	0.52	0.000010
b4	45	0.79	0.000011
b3	60	1.05	0.000005
b2	90	1.57	0.000000
Group	θ (degree)	θ (radians)	Constant q
b5	30	0.52	0.000328
b4	45	0.79	0.000266
b3	60	1.05	0.000166
b2	90	1.57	0.000000

Table 3-18. Result of coefficient p1, p2 and constant q for Group a2~a5, b2~b5.

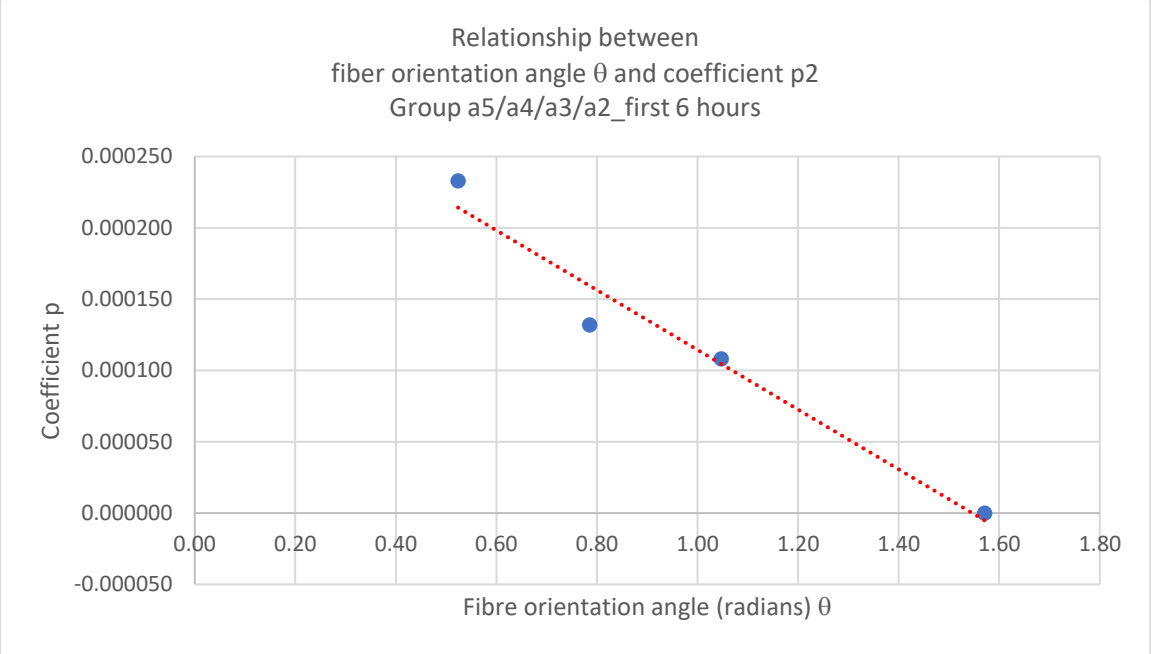

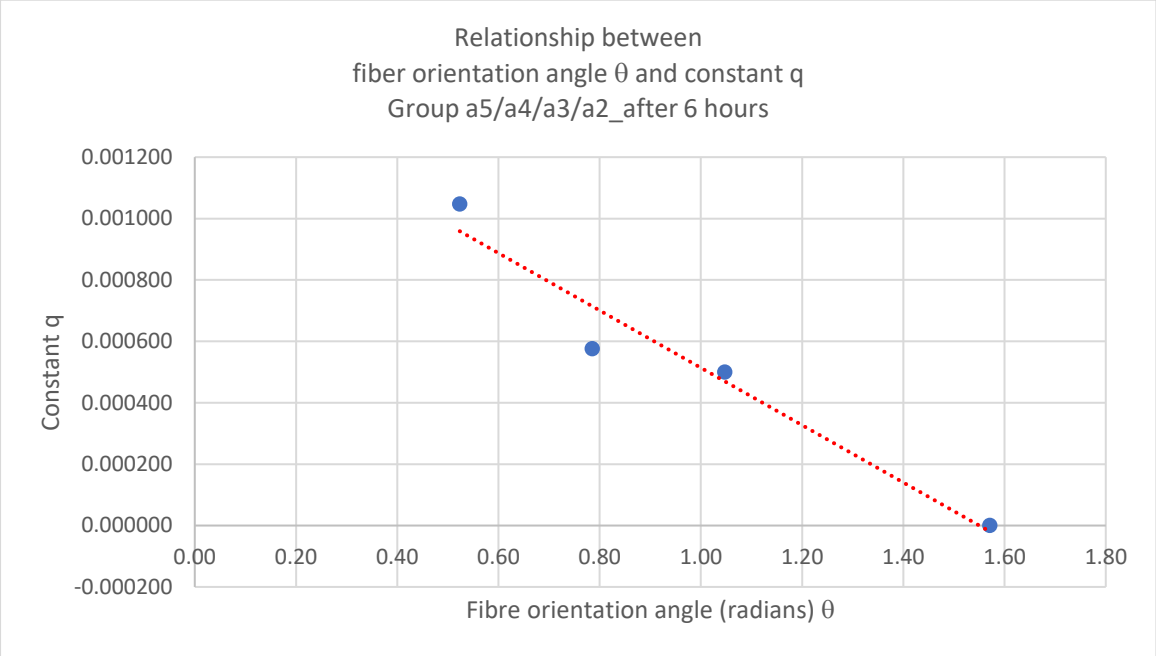

Figure 3-26. Regression analysis of relationship between fiber orientation angle θ and coefficient p or constant q before and after 6 hours for Type a and b

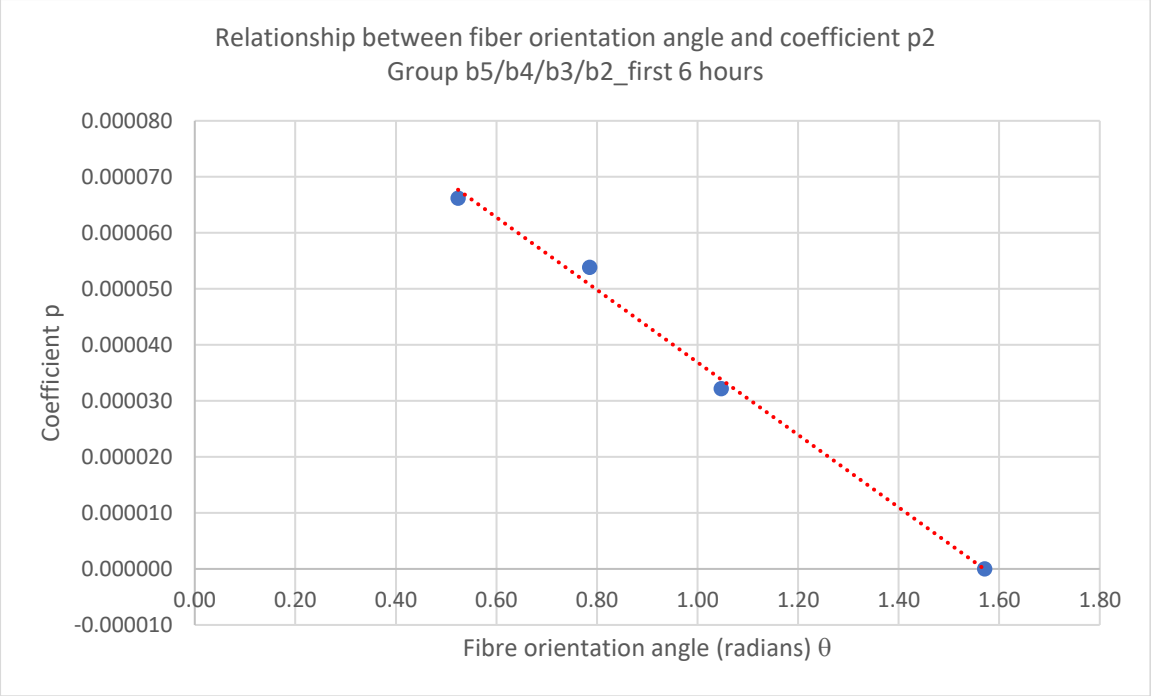

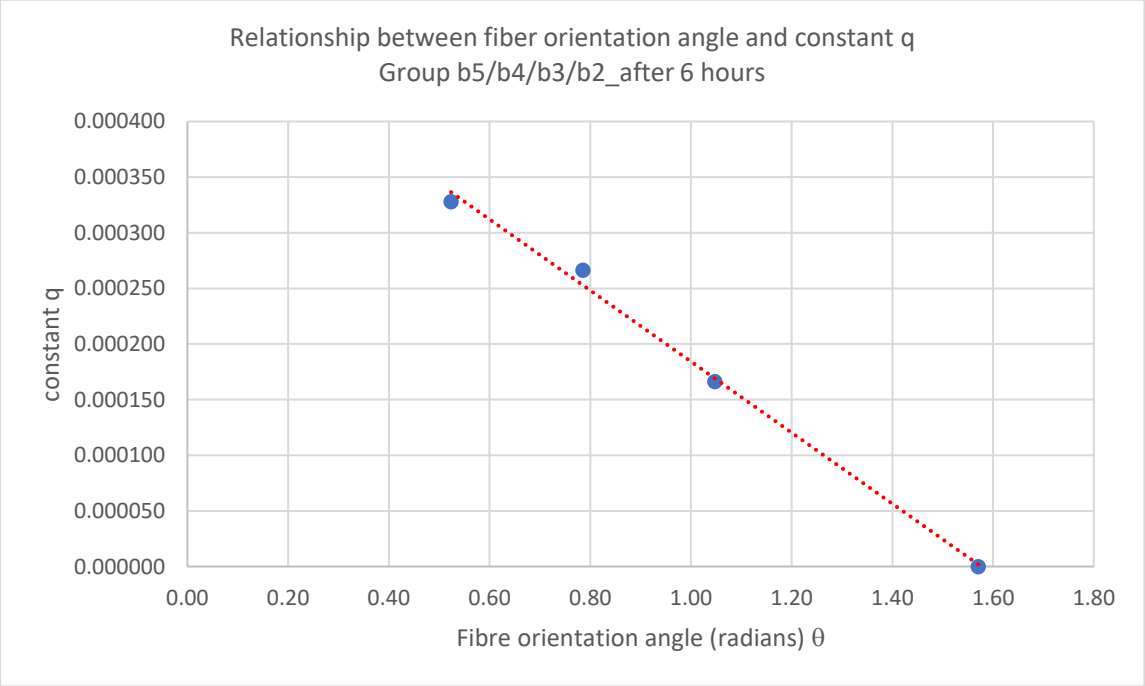

Figure 3-26. Regression analysis of relationship between fiber orientation angle θ and coefficient p or constant q before and after 6 hours for Type a and b. (continued)

SUMMARY OUTPUT

θ vs coefficient p_First 6 hours_Group a

Regression Statistics	
Multiple R	0.978997
R Square	0.958435
Adjusted R Square	0.937652
Standard Error	2.39E-05
Observations	4

ANOVA

	df	*SS*	*MS*	*F*	*ignificance F*
Regression	1	2.63E-08	2.63E-08	46.11733	0.021003
Residual	2	1.14E-09	5.7E-10		
Total	3	2.74E-08			

	Coefficients	*andard Erro*	*t Stat*	*P-value*	*Lower 95%*	*Upper 95%*	*ower 95.0%*	*Upper 95.0%*
Intercept	0.000324	3.25E-05	9.950661	0.009949	0.000184	0.000464	0.000184	0.000464
X Variable 1	-0.00021	3.08E-05	-6.79097	0.021003	-0.00034	-7.7E-05	-0.00034	-7.7E-05

SUMMARY OUTPUT

θ vs constant q_After 6 hours_Group a

Regression Statistics	
Multiple R	0.97397
R Square	0.948617
Adjusted R Square	0.922926
Standard Error	0.000119
Observations	4

ANOVA

	df	*SS*	*MS*	*F*	*ignificance F*
Regression	1	5.23E-07	5.23E-07	36.92373	0.02603
Residual	2	2.83E-08	1.42E-08		
Total	3	5.52E-07			

	Coefficients	*andard Erro*	*t Stat*	*P-value*	*Lower 95%*	*Upper 95%*	*ower 95.0%*	*Upper 95.0%*
Intercept	0.001448	0.000162	8.924844	0.012323	0.00075	0.002146	0.00075	0.002146
X Variable 1	-0.00093	0.000154	-6.07649	0.02603	-0.0016	-0.00027	-0.0016	-0.00027

SUMMARY OUTPUT

θ vs coefficient p_First 6 hours_Group b

Regression Statistics	
Multiple R	0.997091
R Square	0.99419
Adjusted R Square	0.991285
Standard Error	2.71E-06
Observations	4

ANOVA

	df	*SS*	*MS*	*F*	*ignificance F*
Regression	1	2.51E-09	2.51E-09	342.2528	0.002909
Residual	2	1.47E-11	7.34E-12		
Total	3	2.53E-09			

	Coefficients	*andard Erro*	*t Stat*	*P-value*	*Lower 95%*	*Upper 95%*	*ower 95.0%*	*Upper 95.0%*
Intercept	0.000102	3.69E-06	27.52105	0.001318	8.57E-05	0.000117	8.57E-05	0.000117
X Variable 1	-6.5E-05	3.5E-06	-18.5001	0.002909	-8E-05	-5E-05	-8E-05	-5E-05

SUMMARY OUTPUT

θ vs constant q_After 6 hours_Group b

Regression Statistics	
Multiple R	0.99783
R Square	0.995665
Adjusted R Square	0.993498
Standard Error	1.15E-05
Observations	4

ANOVA

	df	*SS*	*MS*	*F*	*ignificance F*
Regression	1	6.12E-08	6.12E-08	459.4051	0.00217
Residual	2	2.67E-10	1.33E-10		
Total	3	6.15E-08			

	Coefficients	*andard Erro*	*t Stat*	*P-value*	*Lower 95%*	*Upper 95%*	*ower 95.0%*	*Upper 95.0%*
Intercept	0.000504	1.57E-05	32.02007	0.000974	0.000436	0.000572	0.000436	0.000572
X Variable 1	-0.00032	1.49E-05	-21.4337	0.00217	-0.00038	-0.00026	-0.00038	-0.00026

Table 3-19. Result of regression analysis of relationship between fiber orientation angle and coefficient p or constant q before and after 6 hours.

In summary, the equations to be used for simulation to link curvature and time are derived as below:

For $0 \leq t \leq 6$,

Group a1	$\frac{1}{\rho} = 0.00168 \times t$	(Eq.8-a1-i)
Group a2~a5	$\frac{1}{\rho} = \left((-0.00021) \times \theta + 0.000324\right) \times t, \ (0 < \theta \leq 1.57)$	(Eq.8-a-i)
Group b1	$\frac{1}{\rho} = 0.00098 \times t$	(Eq.8-b1-i)
Group b2~b5	$\frac{1}{\rho} = \left((-0.00006) \times \theta + 0.000102\right) \times t, \ (0 < \theta \leq 1.57)$	(Eq.8-b-i)

For $6 < t \leq 24$,

Group a1	$\frac{1}{\rho} = 0.00001 \times t + 0.00911$	(Eq.8-a1-ii)
Group a2~a5	$\frac{1}{\rho} = 0.00002 \times t + (-0.00093) \times \theta + 0.001448, \ (0 < \theta \leq 1.57)$	(Eq.8-a-ii)
Group b1	$\frac{1}{\rho} = 0.00006 \times t + 0.00510$	(Eq.8-b1-ii)
Group b2~b5	$\frac{1}{\rho} = 0.00001 \times t + (-0.00032) \times \theta + 0.000504, \ (0 < \theta \leq 1.57)$	(Eq.8-b-ii)

where:

t = time in hours

θ = fiber orientation angle in radians

3.2.2 Software development & simulation

From the relationship obtained in the previous section above, the digital simulation comprises of two parts –

a) Scanning and drawing software for easy fabrication
b) Simulation of bending behavior of bi-layer wood surface

a) Scanning and drawing software for easy fabrication

As fabrication is part of the process, for people without skills to test the ideas, audit the necessary pieces to be cut and process the cutting easily, an interface was created using MATLAB. Part of the code is shown in Appendix 8.

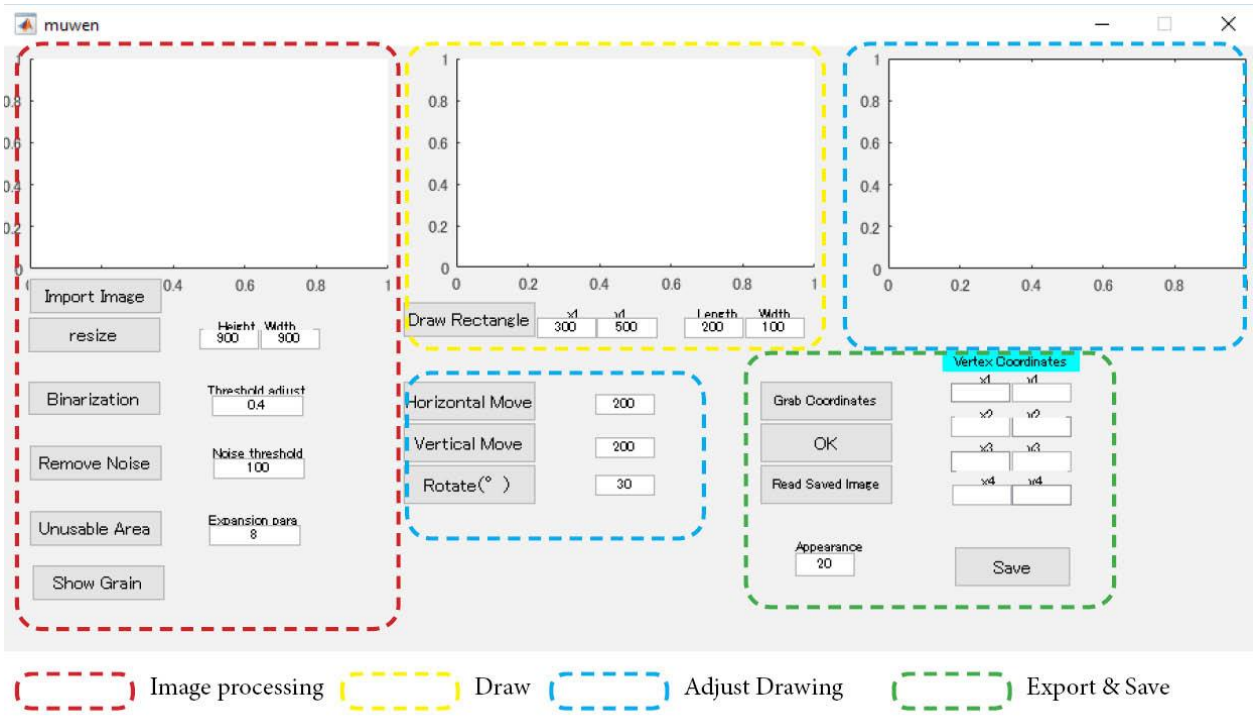

Figure 3-27. Interface of the scanning & drawing program.

The interface was categorized into four areas. Image processing, draw, adjust drawing and export & save (Figure 3-27). Image processing imports the image and identifies the major knots for users to avoid. Users then draw the desired rectangle shape by specify the location and size. Subsequently, the location of the drawn rectangle could be further adjusted by changing the location and rotating

drawing. Finally, both image and vertices of the rectangles could be exported for production. The steps to use the program is shown in Figure (3-28).

Step 1
Import photos taken.
Adjust the size of the photo similar to the size of the wood board to be cut.

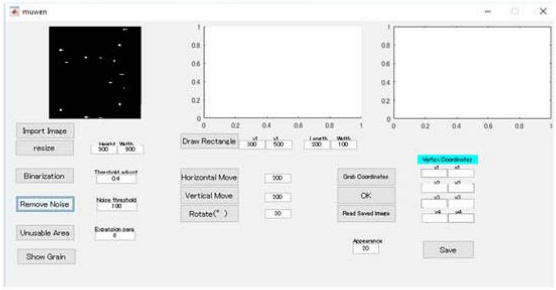

Step 2
Identify the obvious knots and tried to avoid them. Since the small knots will not affect the board (neither howllow up nor affect the bending), only the obvious ones are identified

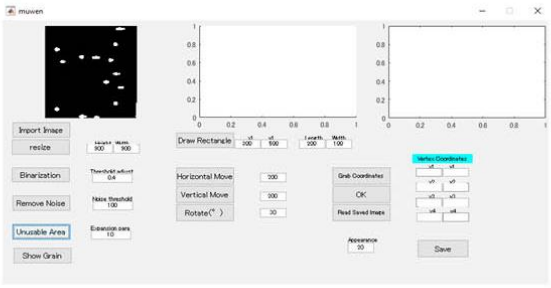

Step 3
Expand the area around the knot by controlling the expansion parameter.

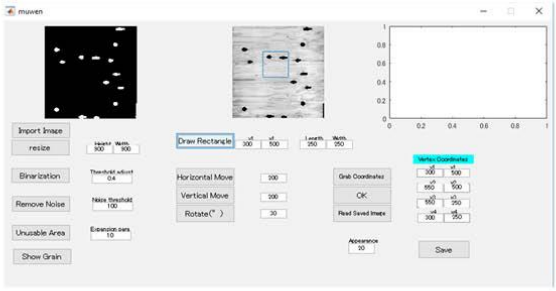

Step 4
Start drawing rectanlges.
x1 and y1 locate the left bottom corner of the retangle. The height and width can be adjusted.

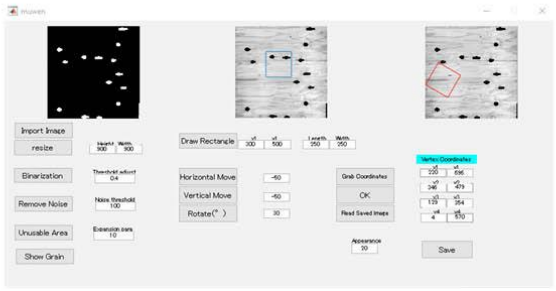

Step 5
Manipulate the rectangle drawn with horizontal, vertical move and rotate. Click OK to confirm and save image temporarily.

Figure 3-28. Steps to prepare for fabrication and audit the desired wood pieces using the program.

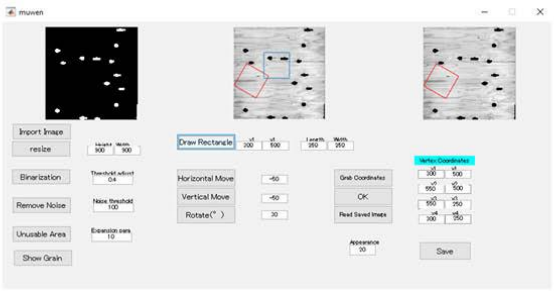

Step 6
Import the saved image in Step 5 and start to draw again.

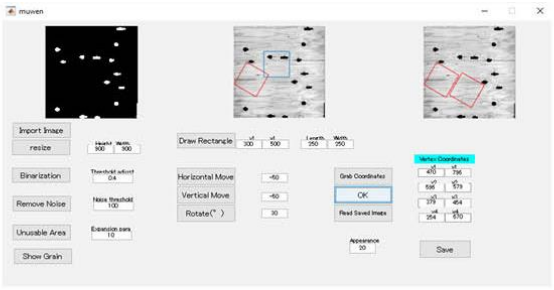

Step 7
Repeat Step 4-5 until satisfaction.

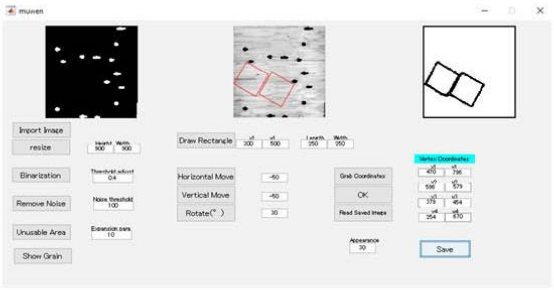

Step 8
Click Save to save the final output image for printing as a reference

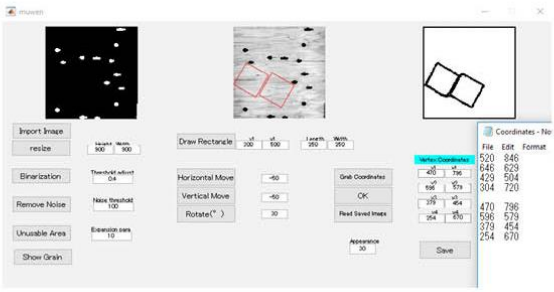

Step 9
The coordinates of each vertex could be displayed and saved as a text file. It could be used for further processing of wood.

Figure 3-28. Steps to prepare for fabrication and audit the desired wood pieces using the program. (continued)

b) Simulation of bending behaviour of bi-layer wood surface

From the relationship obtained from the analysis above, bending behaviour could be simulated for curvature over time. The structure of the simulation is shown in Figure 3-29 in which input, output and the equation used are differentiated in colors. Due to the above analyses, input in the simulation includes: fiber orientation of active layer (θ), thickness of restrictive layer (h_1) and active layer

(h_2), Young's Modulus of restrictive layer (E_1), expansion coefficient of restrictive layer (α_2), initial moisture content of active layer (c), relative humidity and temperature. Simulation is made through the Rhinoceros & Grasshopper interface.

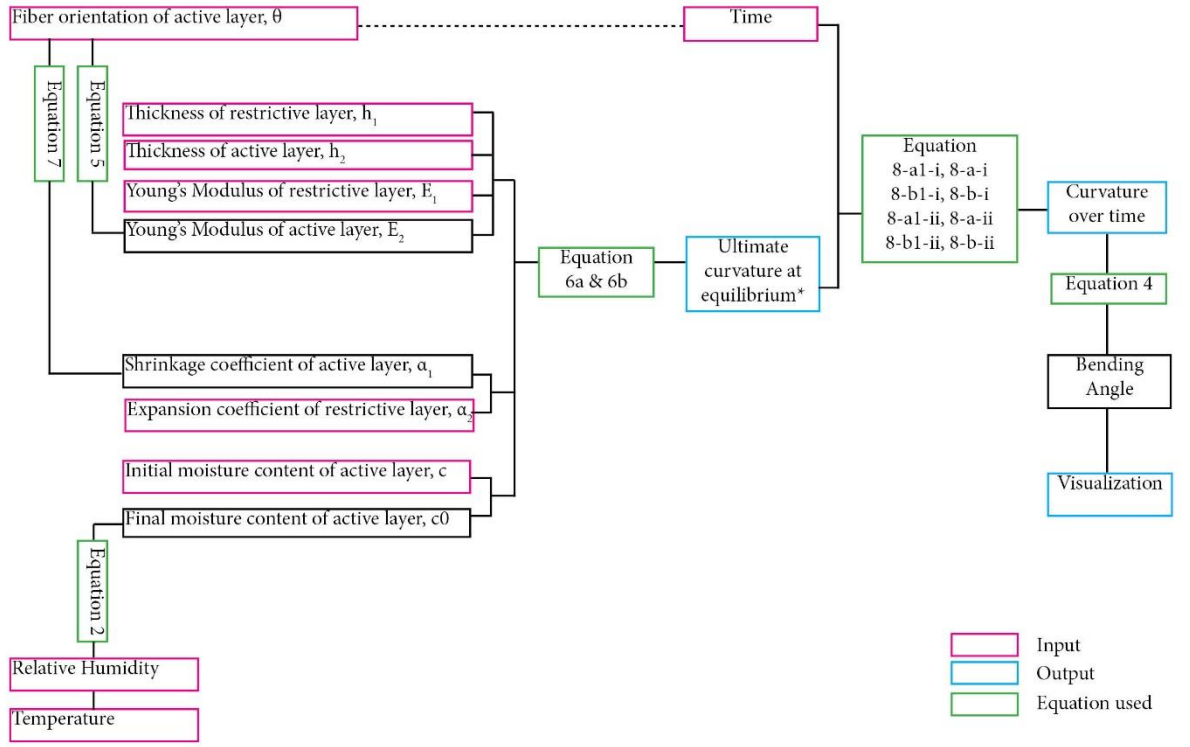

Figure 3-29. Structure flow of the simulation.

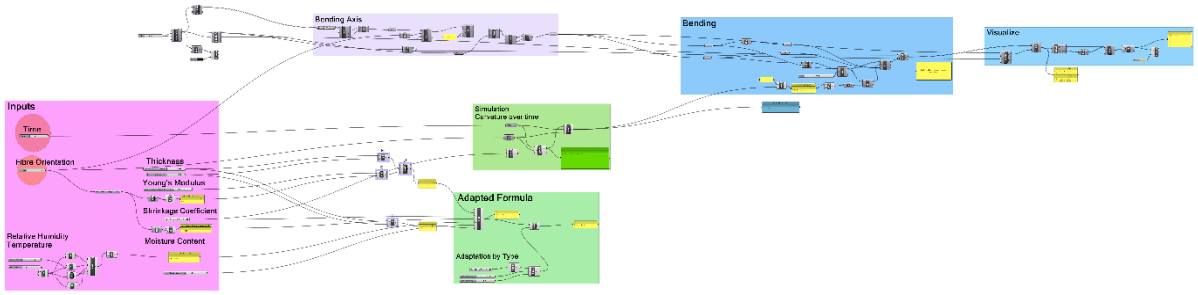

Figure 3-30. Overview of grasshopper definition of simulation following the color code of the figure above.

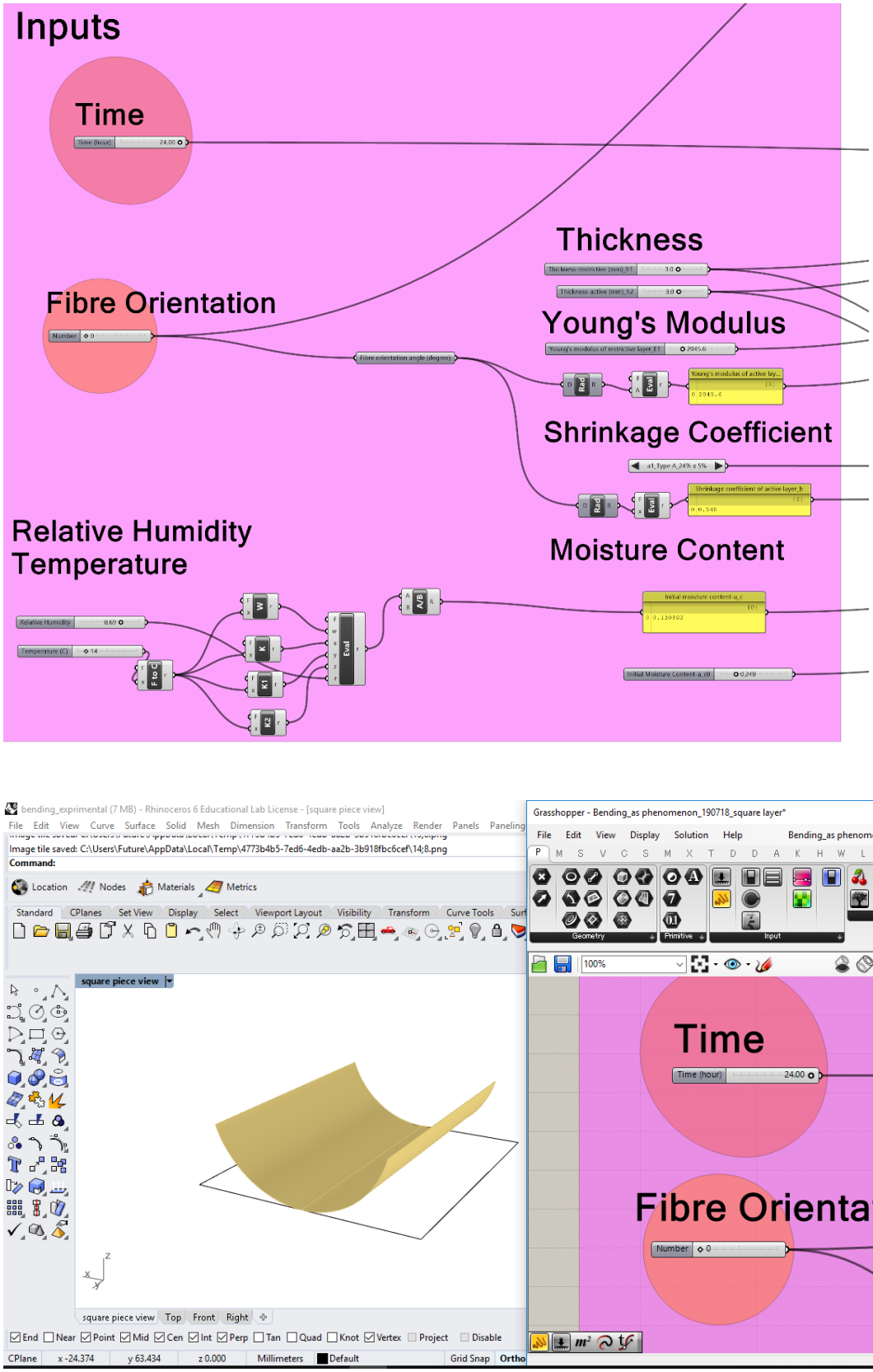

Figure 3-31. Top: Inputs includes the parameters that could be adjusted for the simulation. Bottom: Screenshot showing the simulation visualization with different time and fiber orientation.

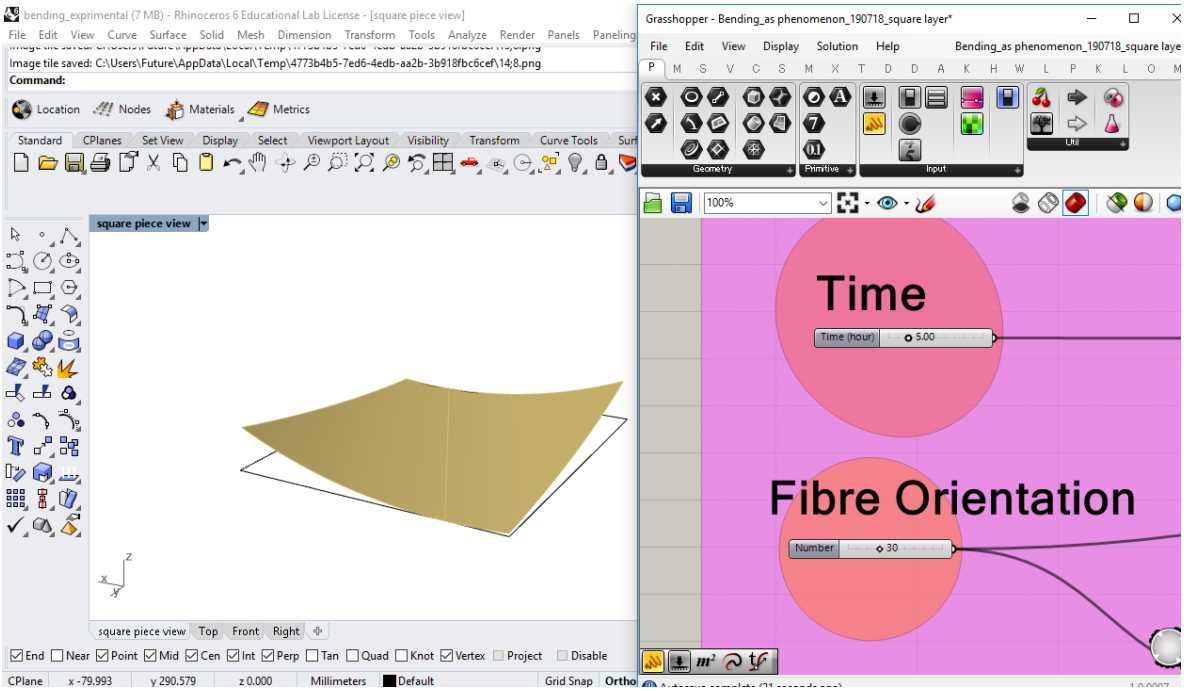

Figure 3-31. Top: Inputs includes the parameters that could be adjusted for the simulation. Bottom: Screenshot showing the simulation visualization with different time and fiber orientation. (continued)

The simulated curvature is then verified against the experiment curvature after 6 hours and for ultimate equilibrium with condition shown in Table 3-20a. The result showing a high correlation efficient of 0.953 and 0.938 for ultimate curvature for Type a and b (Table 3-20b). As for curvature over time, since in the experiments, since for all samples, the major curvature change happens within the first 6 hours, thickness has little effect on curvature over time. Group 3-3 is taken as an example for verification of curvature over time after 6 hours. (Table 3-20c)

Relative Humidity	69%
Temperature	14 C
Thickness of restrictive layer, h1	3 or 4mm
Thickness of active layer, h2	3 or 4mm
Young's Modulus of restrictive layer, E1	2.05GPa
Fiber orientation of active layer, θ	0,30,45,60,90
Initial moisture content of active layer, c	24%
Expansion coefficient of restrictive layer, α2	0.081

Table 3-20a. Input of simulation

Ultimate curvature

Type a

	Simulation	Experiment	Correlation
3-3-a1	0.01018	0.00864	0.953
3-3-a5	0.00318	0.00201	
3-3-a4	0.00140	0.00178	
3-3-a3	0.00027	0.00108	
3-3-a2	-0.00005	0.00000	
4-4-a1	0.00762	0.01039	
4-4-a5	0.00239	0.00124	
4-4-a4	0.00105	0.00054	
4-4-a3	0.00020	0.00051	
4-4-a2	-0.00004	0.00000	
3-4-a1	0.00854	0.01024	
3-4-a5	0.00273	0.00138	
3-4-a4	0.00123	0.00049	
3-4-a3	0.00025	0.00041	
3-4-a2	-0.00003	0.00000	

Type b

	Simulation	Experiment	Correlation
3-3-b1	0.00494	0.00339	0.938
3-3-b5	0.00168	0.00076	
3-3-b4	0.00085	0.00076	
3-3-b3	0.00030	0.00045	
3-3-b2	-0.00001	0.00000	
4-4-b1	0.00370	0.00434	
4-4-b5	0.00126	0.00082	
4-4-b4	0.00064	0.00024	
4-4-b3	0.00023	0.00010	
4-4-b2	-0.00002	0.00000	
3-4-b1	0.00415	0.00485	
3-4-b5	0.00144	0.00066	
3-4-b4	0.00075	0.00036	
3-4-b3	0.00029	0.00014	
3-4-b2	-0.00002	0.00000	

Table 3-20b. Simulation result of ultimate curvature was compared with experiment result. The correlation coefficient was calculated in Microsoft Excel. The simulation and experiment result had strong relationship, i.e., the simulation result was reliable.

Curvature after 6 hours

Type a

	Simulation	Experiment	Correlation
3-3-a1	0.00504	0.00766	0.999
3-3-a5	0.00128	0.00164	
3-3-a4	0.00095	0.00147	
3-3-a3	0.00063	0.00102	
3-3-a2	-0.00004	0.00000	

Type b

	Simulation	Experiment	Correlation
3-3-b1	0.00588	0.00269	0.985
3-3-b5	0.00042	0.00061	
3-3-b4	0.00033	0.00054	
3-3-b3	0.00024	0.00042	
3-3-b2	0.00005	0.00000	

Table 3-20c. Simulation result of curvature of time after 6 hours was compared with experiment result. The curvature over time for Type b after 6 hours was obtained by assuming a linear relationship between that at 4.5 hours and 16 hours during experiment.

3.3 Conclusion

In this Chapter, self-actuated bending experiments were conducted with the results analysed. Software for scanning the wood for easy fabrication and simulation of the self-actuated bending was completed. The workflow is shown in Figure 3-32 below. The goal of the experiment was to find out whether the proposed method of self-actuated bending was able to fit the bi-layer theory formula deducted by Ruggeberg & Burgert (Rüggeberg & Burgert, 2015). If not, the relationship should be further inferred and adapted to obtain a new formula to be used in the simulation.

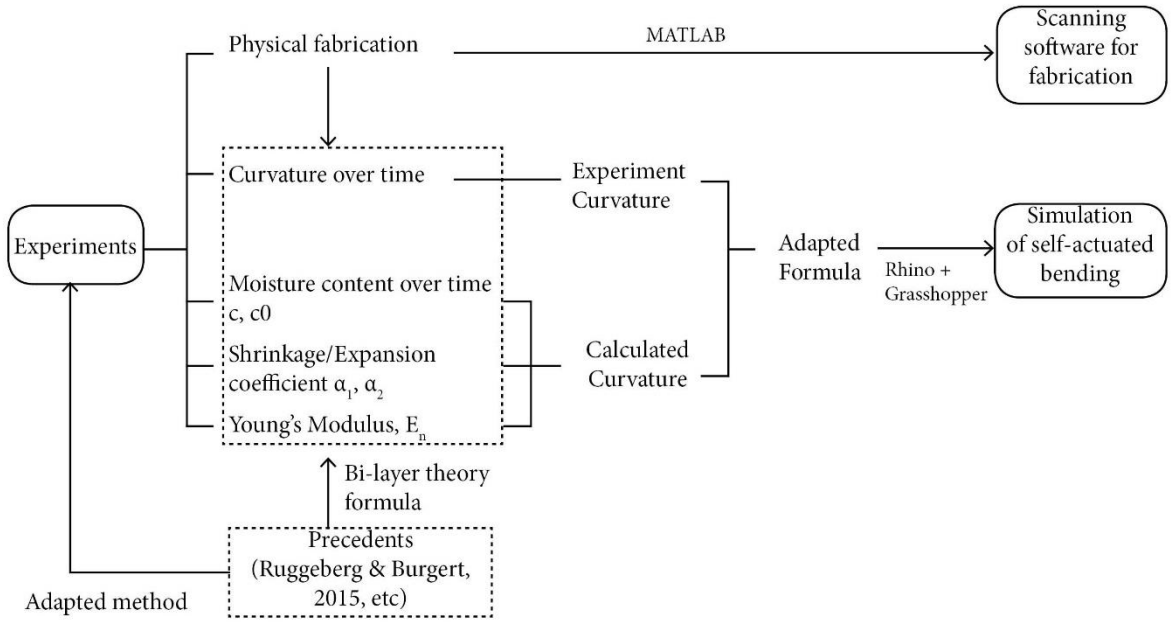

Figure 3-32. Workflow from research and experiment to the final outcome of software and simulation.

Regarding fabrication, as it took a lot of effort to get the coordinate of each vertex of the sample pieces, a software was designed to scan the wood by taking a photo, and the software is able to identify the knots and expand around the knot area to be avoided for drawing. One can adjust the size and orientation of the drawing for a desired piece to be cut and the coordinates of the vertices could be obtained for fabrication easily.

Regarding the design of the experiments, with the consideration of easily accessibility of the material, the widely used softwood cedar was used and the moisture content of the restrictive layer was purposely selected to be 5% which is a common moisture content for kiln dried wood and 12% which is a common moisture content in Japan for naturally air-dried wood.

The analysis of the experiment result has shown that the bi-layer theory formula has to be adapted for the simulation. On average, the experiment curvature for Type a and b was only 0.75 and 0.354 of the result calculated by bi-layer theory formula. This was mainly because of the modified method of producing the self-actuated bending. Instead of the original set-up in the precedents, i.e. different species and combination of tangential & longitudinal, to maximize the shrinkage difference between active and restrictive layer, the modified method prioritized the availability of the material and easiness for processing, resulting in different set-up that only single species and tangential & tangential combination were used. This has reduced the possible shrinkage difference between the active and restrictive layer. Hence, the experiment curvature was smaller than the calculated one and has to be adapted for simulation.

Also, as mentioned in Section 3.2.1a, there also observed an inverse relationship between the experiment curvature and initial moisture content of restrictive layer of Type a and Type b. However, the conclusion could not be drawn due to the limited types of samples. As the goal of this research was to explore the methodology of transformation from physical explorations to digital simulations, the discussion of the factors affecting the coefficient is out of the scope. However, the relationship between the coefficient and parameters could be discussed in future research.

Curvature over time, moisture over time, shrinkage/expansion coefficients and Young's Modulus were measured or derived through the experiments and analysis. Two new formulae were adapted from the bi-layer theory formula in the end and used in the simulation. Although the simulation was limited to the Type a and b

with specific initial moisture content for the restrictive layers, in general, the goal was achieved but with some limitations.

3.3.1 Limitations

Fabrication

During the fabrication process, as the wood pieces were thin and started to lose moisture content fast, glue with short fixation time was used. However, considering a more general application if the wood pieces become larger, the gluing process should be conducted at the ideal environment with constant relative humidity and temperature to keep the wood pieces in a constant moisture content. Fast gluing method such as spray may also be used to reduce the loss in the moisture content if such ideal environment is not available.

Curvature over time

Although data for curvature over time was taken diligently during the experiment, however, due to the limited number of samples, it is difficult to obtain a universal relationship for curvature over time. Also, for measurement of moisture content, an analogue-to-digital method was used in the experiment. However, this would not allow for constant monitoring of the curvature. The limited number of the data points resulted in a 2-step linear regression analysis. Although this analysis could explain the relationship between curvature before and after 6 hours, however, it is more meaningful to consider the stepped process as a whole. More data needs to be collected with a more constant frequency to deduct an overall relationship between curvature and time.

Applicability to a more generalized condition

This part of research and simulation considered only Japanese cedar as the material to conduct the self-actuated bending experiments. However, it is known that the magnitude of expansion and shrinkage of wood is also determined by the density of wood. Generally, the higher the density, the larger the extent of expansion or shrinkage due to the availability of more cell walls. However, the

moisture content also affects density as well ("Hygroexpansion in wood – shrinkage and swelling", n.d.). This complicates the matter which needs more experiment to drive a general relationship between density and moisture content for other species.

The design of the experiments prioritized the accessibility of wood with common moisture content. As a result, there was no thorough consideration of variations in initial moisture content. In the simulation, two modes of initial moisture content of 12% and 5% could be selected as a result of the research. However, considering future studies, the simulation should give more freedom for selection of material.

Chapter 4 – Kerf bending

While the self-actuated bending utilizes anisotropy of wood, the kerf pattern creates anisotropy in materials so as to facilitate bending with minimum requirements on equipment, energy, manpower, techniques and tools. Precedents in section 2.2.1 demonstrated extensive explorations of how kerf pattern could be used for a geometry deliberation of wood, but the subtractive action only happened locally so that structural strength depended mainly on the intact part of wood. Also, each component was relatively small. In this chapter, the relationship between kerf pattern and its structural strength are explored. With the availability of the technology producing plywood as long as 6 meters, the limit of kerf pattern bending was pushed to a larger scale. The outcome was a furniture-scale permanent installation named URO-CO in the office of Haseko Corporation[1]

4.1 Experiments

As kerf pattern can vary depending on the design requirement, top-down process is necessary for this study. As part of the URO-CO project, overall geometry was determined at first (Figure 4-1). As can be seen in the Figure 4-1, the side with smallest diameter 600mm required the structure to be able to sustain people's weight while the towards the largest diameter approximately 1500mm, the structure need to sustain self-weight by standing on themselves. These forms the primary goal of the experiments.

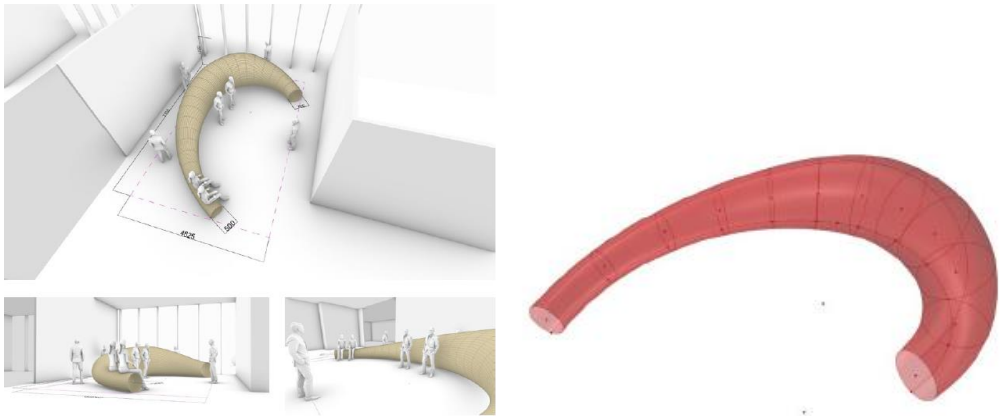

Figure 4-1. Overall geometry

[1] This project is completed as a joint research with Haseko Corporation in Japan, together with T_ADS and Kuma Laboratory of University of Tokyo. URO-CO means 'scale' in Japanese which reflects the pattern used.

The research regarding kerf pattern started from scratch from making small models to 1:1 mock-ups. In order to study the relationship between kerf pattern and structural strength without other disturbance, homogeneous materials, MDF boards and plywood were used respectively in the experiments.

4.1.1 Initial Studies

On pattern

Since making kerf pattern equates to add flexibility to wood with subtractive actions, there are plenty of ways to do so. However, as mentioned above, with the global geometry, the pattern requires to be **soft and strong** for bending into small radius roll, but **hard and porous** to be able to sustain self-weight and filter light. With consideration of both requirements, a pattern with moderate quality on softness, hardness and porosity is suitable for further development. A qualitative study was done first with some available patterns based on study of Aaron Porterfield to determine a pattern to be explored (Figure 4-2).

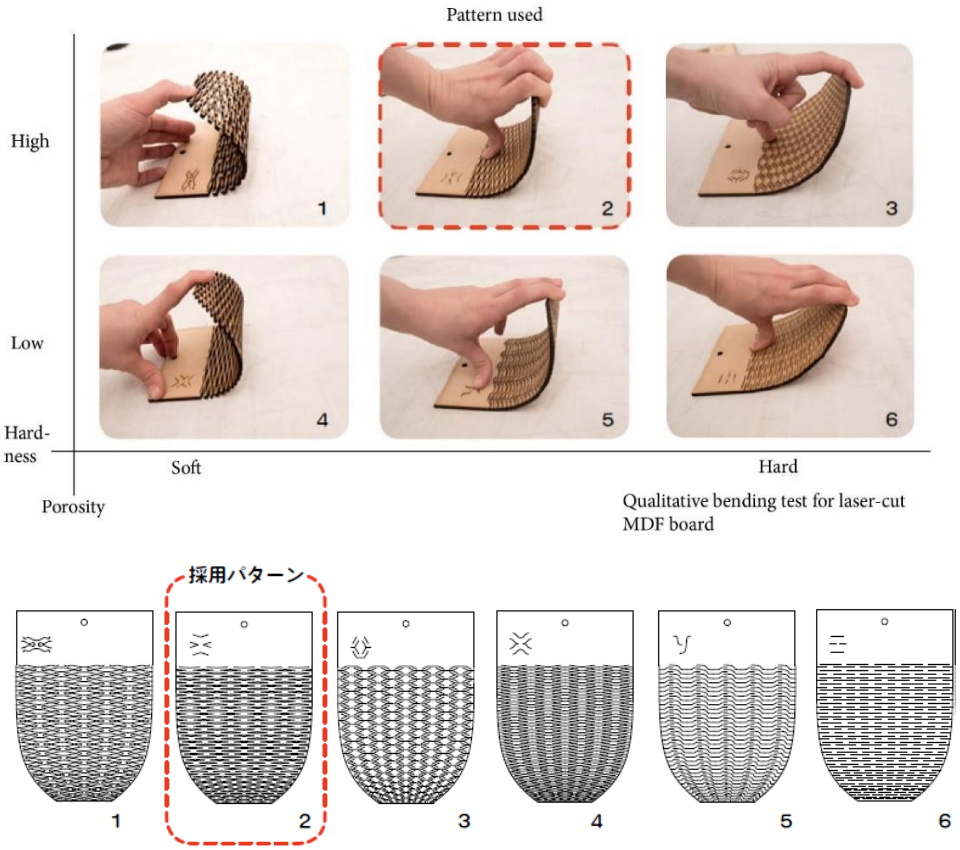

Figure 4-2. Six patterns were tested. Top: porosity increases from bottom to top while hardness increases from left to right. Bottom: drawings of each pattern (Porterfield, 2016)

On structural strength

With the pattern above, a 1:2 scale model was made to test the small diameter 600mm portion which requires the material to be soft and strong. The model is made with 6mm thick MDF boards. Loading test were carried out by putting weights over the model (Figure 4-3)

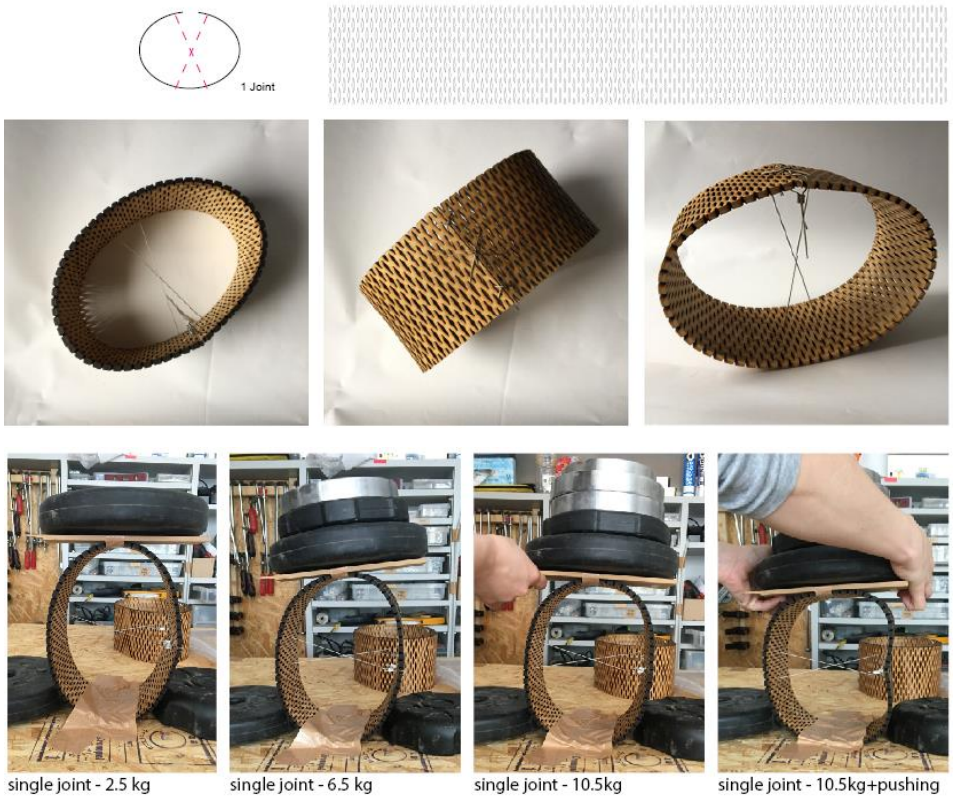

Figure 4-3. Top: pattern was made with a perforation rate of 17% and formed a ring of diameter 225 mm. Steel cables were used to close the ring but at the same it reinforced the structure which defeated the purpose of the experiment. Bottom: Loading test.

After this initial study, it was realized that the strength of wood depends much on the thickness of it. Even with a 1:2 scale model it is difficult to predict the behaviour of plywood in 1:1 scale. Thus, 1:1 prototypes and mock-ups were made for further development.

4.1.2 Prototypes and mock-ups

To make 1:1 prototypes, the following method was adopted to collect data for derivation of the relationship between pattern and structural strength (Figure 4-4).

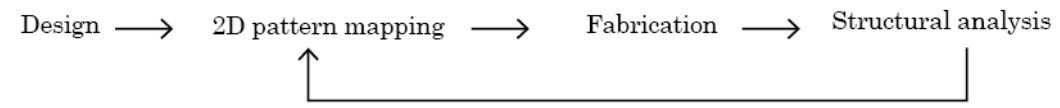

Figure 4-4. Method of exploring the relationship between the pattern and structural strength.

The test pieces were made with dimension 450mm x 1800mm in order to be able to form a ring with 600mm diameter. The plywood used were 10mm thick with 5 plies. Three tests were made to obtain the final result for this project. The process would be explained in chronical manner. Simple analysis will be explained in this section and used as a base for analysis in Section 4.2.
Rhinoceros and grasshopper are used to generate the pattern.

Test 1

The goal of this test was

- To find out the determinant parameters for structural strength other than perforation rate.
- To determine the fabrication method for processing wood.

Based on the initial studies, four sample pieces were proposed with similar perforation rate to the initial study to obtain the first set of data. Perforation rate were adjusted with the same h and l value where h is the height of the diamond and l is the length (Figure 4-5a & b). However, as the proposed sample took too long to be processed, only b & c & d were produced. Test pieces were processed both by CNC routers and laser-cutting machines.

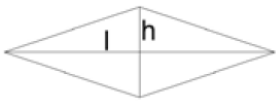

Figure 4-5a. Changing parameters for 2D pattern.

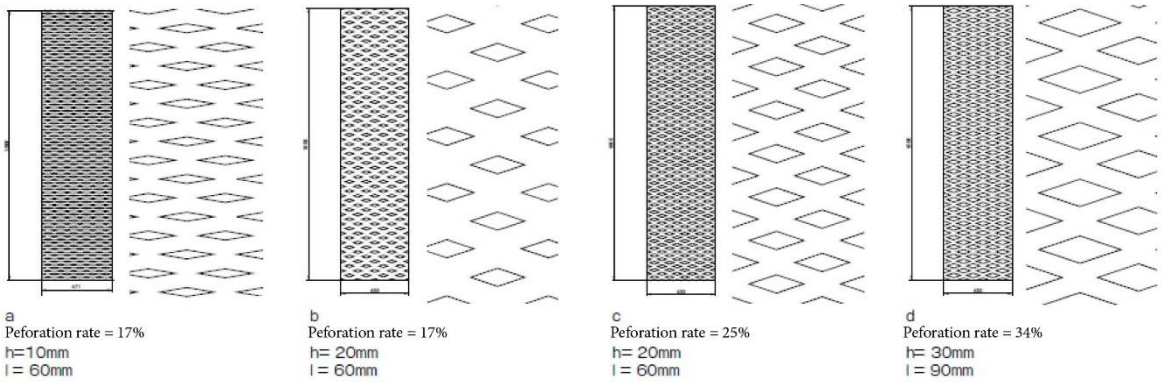

Figure 4-5b. Sample pieces.

Result of Test 1

- As the time spent for laser cutting is shorter (half of the time required for using CNC machines), and there was no need for after-treatment of the fringes of the board. Laser cutting was selected for the next tests.
- The samples were hard to bend (Figure 4-6).

Figure 4-6. The sample pieces were not able to be bento into a ring.

- The parameters were changed from h & l to h, l and w which is the distance between the cut holes (Figure 4-7)

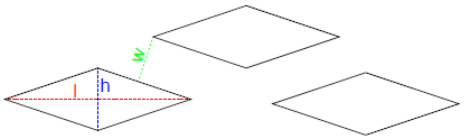

Figure 4-7. Parameters for Test 2

Test 2

With the updated parameters, sample pieces were planned in a more systematic way. The following Figure 4-8 shows the pattern of the three groups of sample pieces with:

Group A – keeping h and w constant, adjust length of l.

Group B – keeping w constant, adjust h and l.

Group C - keeping the position of the perforations while changing the size of them.

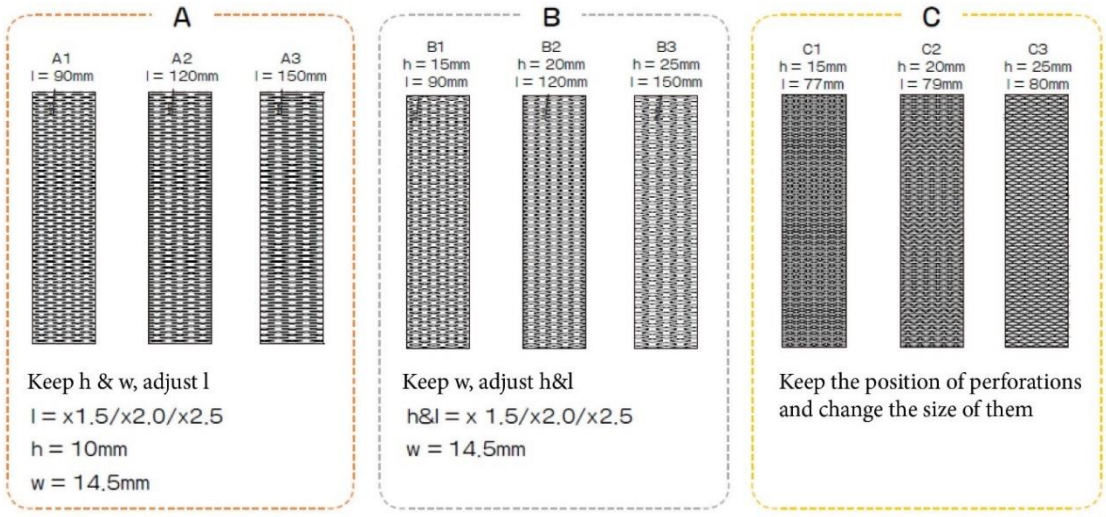

Figure 4-8. Left: group A – keeping h and w, adjust l. Center: group B – keeping w, adjust h and l. Right: group C – keeping the position of the perforations while changing the size of them.

Each one of them were bent with the minimum radius measured (Figure 4-9). As it was planned to bend the cut pieces manually for easy construction with minimum energy, the bending was done by hand.

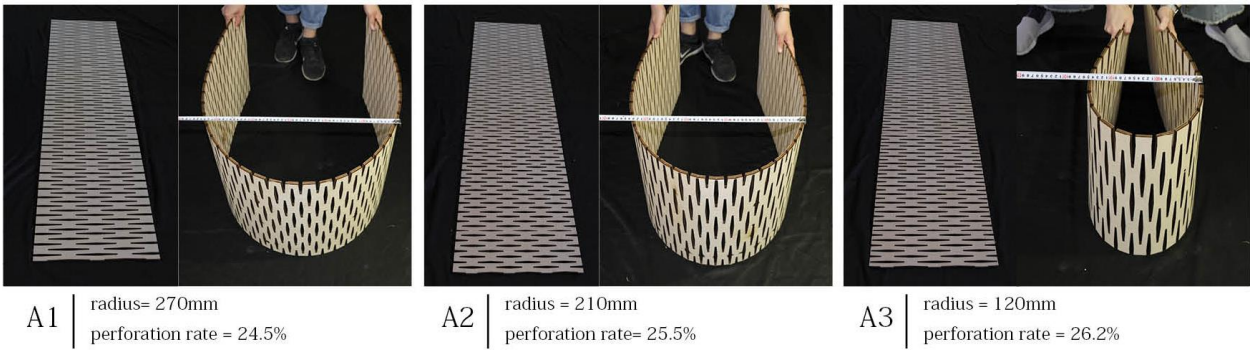

Figure 4-9. Example of bending sample pieces A1, A2 and A3.

The results were collated. Bending radius vs perforation rate was plotted (Figure 4-10)

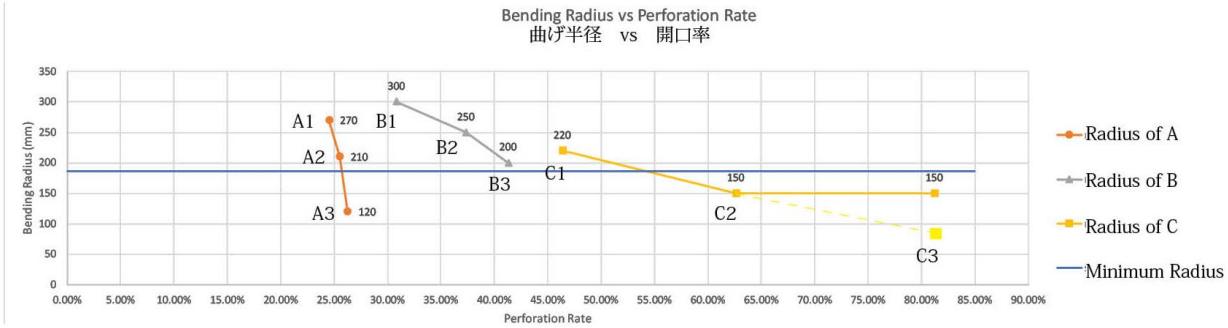

Figure 4-10. Curve showing relationship between bending radius and perforation rate. Sample C3 broke during bending, the bending radius was derived as 80mm.

Result of Test 2

Although the bending radius required was 300mm, however, the minimum radius represents the condition where the wood could not bend anymore, leaving it impossible to sustain extra stress when people sit on them. Thus, a safe radius was drawn and sample A3, C2 and C3 were used as a base for the next experiments. Amongst these three samples A3 had a low perforation rate while that of C2 and C3 were high, they were used as a base for the small radius part and large radius part of the structure respectively.

By comparing sample pieces of Group A, when parameters w & h were kept all the same, i.e. with the same number of units in y direction, the number of units in horizontal direction varied (Figure 4-11). This suggested that number of units is also a determinant of the bending radius. Thus, the parameters for the next experiment changed as shown in Figure 4-12.

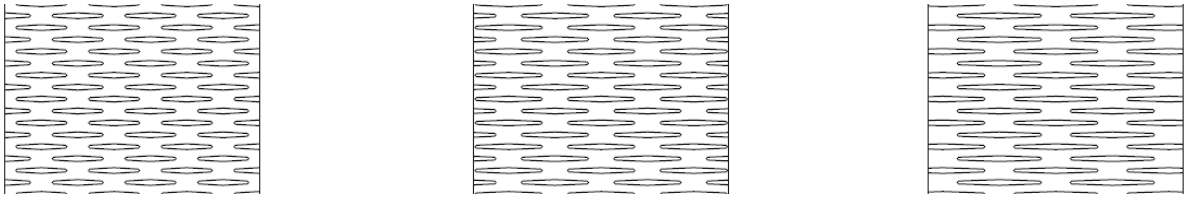

Figure 4-11. Left: sample A1 with 3.5 units in horizontal direction. Center: sample A2 with 2.5 units. Right: sample A3 with 2 units.

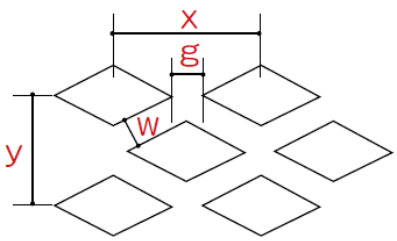

Figure 4-12. Parameters changed from h, l and w to x, y, g and w.

Test 3

While in Test 2, the sample pieces were tested with rectangular sections of 450mm x 1800mm, the final shape was much more complicated. The global geometry translated into a series of spirals so that they could connect to the next one without obvious dislocation (Figure 4-13). Thus, from Test 3, the 2D pattern mapping will not only happen in a rectangular shape but be applied and tested with the unrolled surface of the final structure.

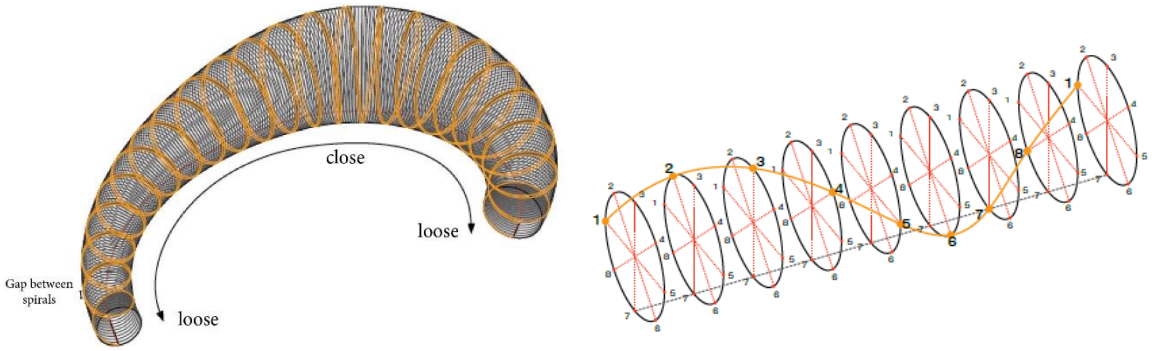

Figure 4-13. The global geometry was achieved by a series of spirals.

However, although each piece was different from each other, it was impossible test all the samples giving the time and budget limit. The first spiral, S1, of the smallest radius 300mm and the largest spiral, S14, of radius 750mm were selected as the benchmark for making the samples. The other spirals were adapted for the requirement shown in Figure 4-14. While S1 needs to be soft but strong, S14 needs to be porous and hard. With the updated parameters from Test 2, patterns were mapped to the unrolled surface. Due to the different alignment of the UV direction and the varying width within each piece, the pattern became uneven with each perforation different from each other (Figure 4-15).

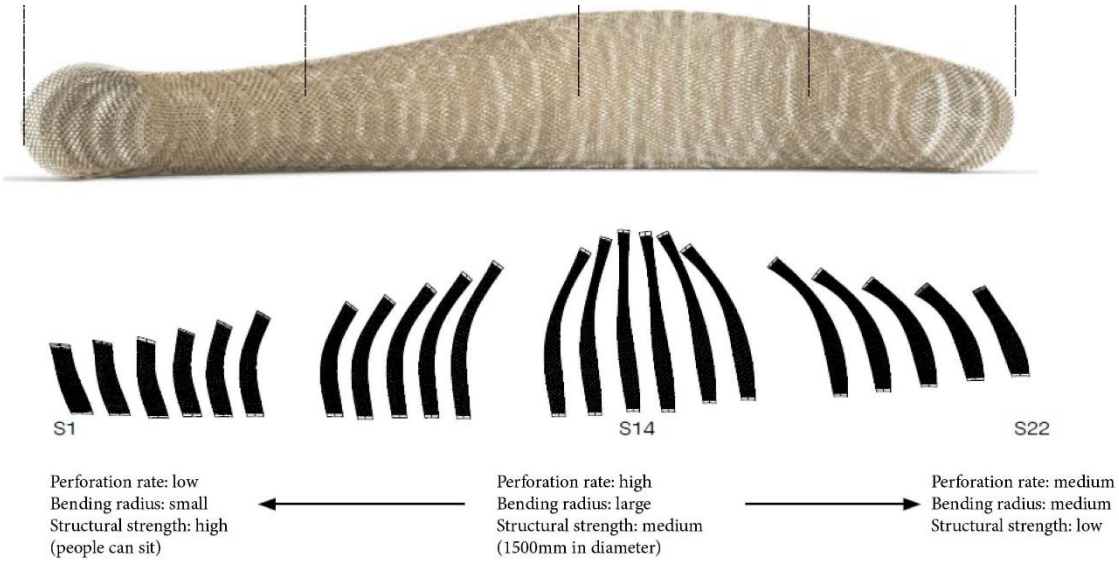

Figure 4-14. The requirement and arrangement of the spirals.

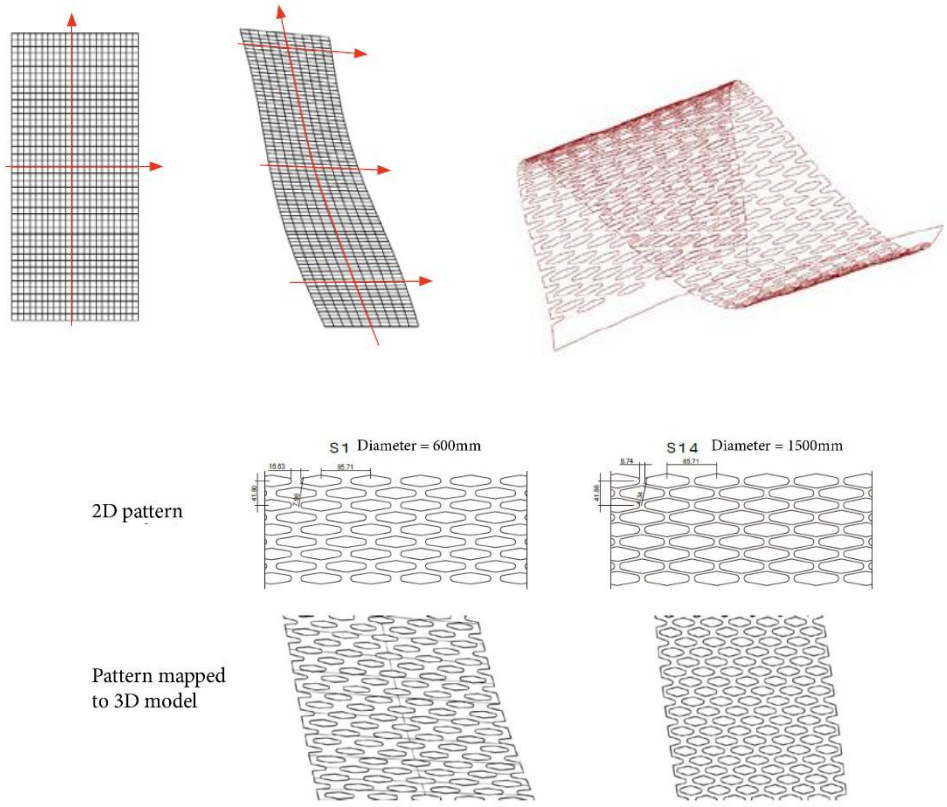

Figure 4-15. Mapping pattern onto unrolled surface of the spiral. After adjustment, the pattern was re-mapped back to the 3D model for visualization.

Sample pieces were made and tested (Figure 4-16). While sample for S1 could be bent but it broke after several times of bending it towards different directions,

sample for S4 underwent a tremendous increase in length such that it could not sustain its own weight.

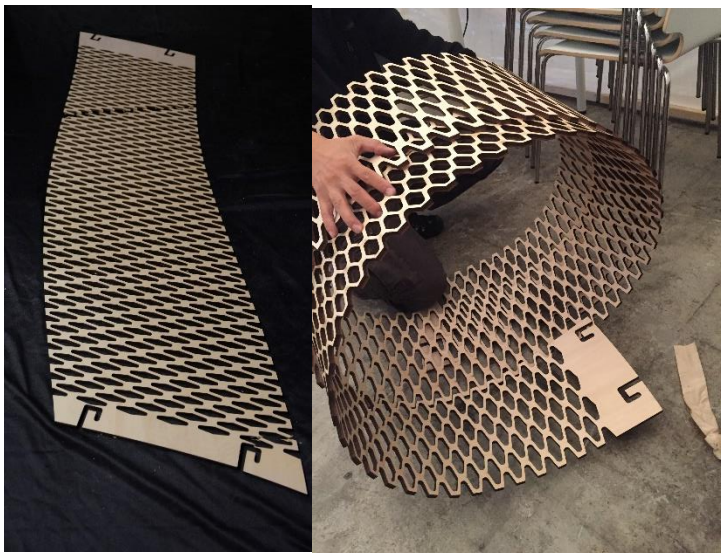

Figure 4-16. Sample for S1 and S4

Thus, modifications were made as shown in Figure 4-17. For S1, number of units per row and column were reduced by diminishing x and y to increase the flexibility of it, while g and w increased to add strength. For S14, number of units per row increased while that per column decreased so as to add more axial force in the longitudinal direction. Parameter g and w increased to add strength to the pattern.

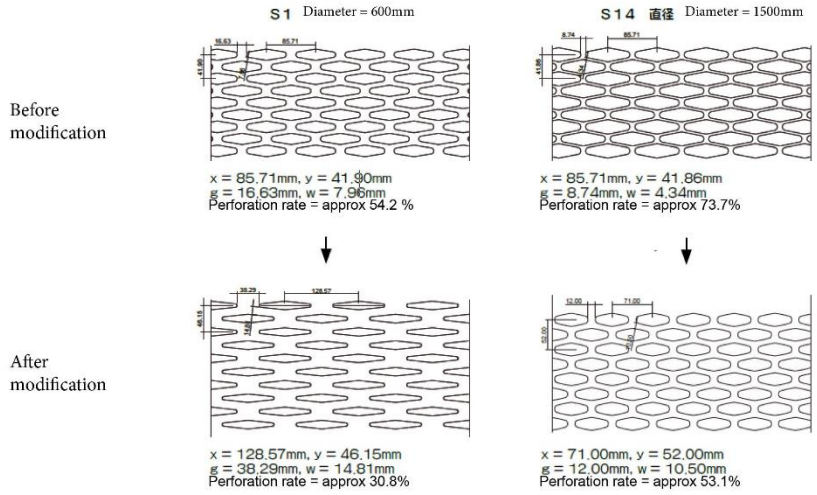

Figure 4-17. Modification of patterns using parameters x, y, w and g. The perforation rate was also monitored to meet the requirement on aesthetics.

For S1, two options were made while 4 options were made for S14 (Figure 4-18). For option 1 and 2 of S1 and options 1-3 of S14, variations happen in w ang g which is shown in Table 4-1. The sample pieces were tested by bending and the diameter of the bending measured.

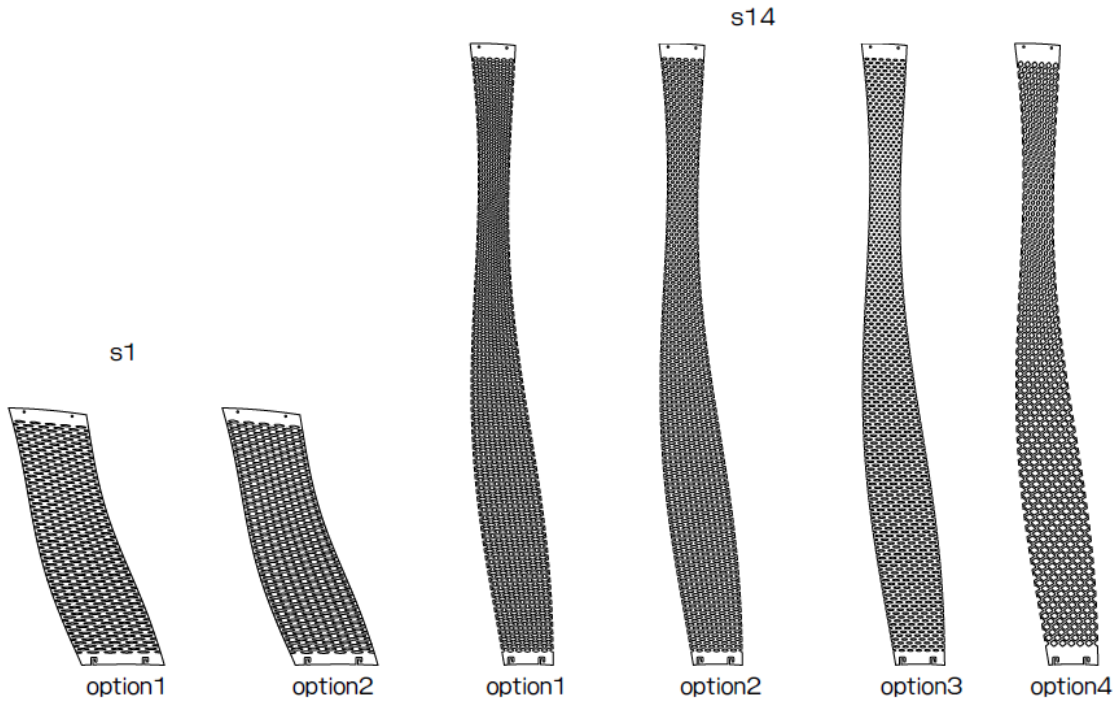

Figure 4-18. Two options for S1 and four options for S4.

Result of Test 3

Table 4-1 showed the result of Test 4. For S1, both option 1 and 2 were strong but option 2 was extremely difficult to bend. Considering manual construction, option 1 was selected. For option 1-3 of S4, as the drop in perforation rate did not give an increase in bending radius (Figure 4-19), and option 4 with a different value for y became soft with an increase in perforation rate even when x, w & g remained the same, thus option 1 was selected for final production.

S1

	w(mm)	g(mm)	perforation rate	diameter(mm)	Remarks
option 1	14.81	38	24.20%	600	difficult to bend but strong
option 2	11	38	33.21%	600	difficult to bend

S14

	w(mm)	g(mm)	perforation rate	diameter(mm)	Remarks
option 1	10.5	12	43.44%	1320	with screw attaching 2 layers together
option 2	14	16	33.50%	1350	
option 3	18	20.57	22.04%	1400	
option 4	10.5	12	46.30%	1340	feels soft(easy to deform when pressing)

Table 4-1. The parameters settings and result of the bending. Pink color marked the ones selected for final production.

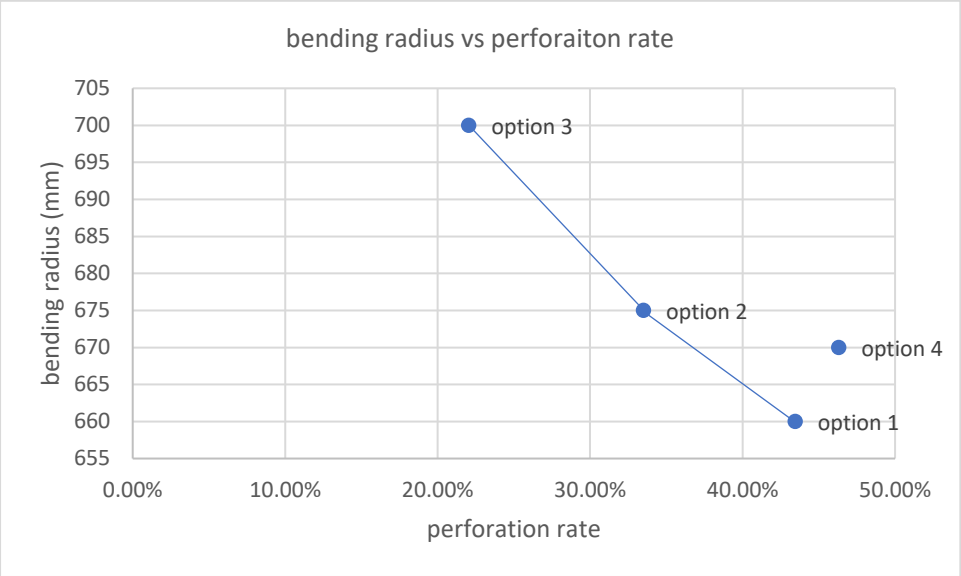

Figure 4-19. curve showing bending radius vs perforation rate for S4 samples.

With some more mock-ups and details (Figure 4-20), the final construction took only two and a half day to complete with one day setting up the site and move components to the site, one day rolling up the spirals and final half day to clean up (Figure 4-21). Since the details were not the scope of this research, they will not be discussed in detail here. The final outcome is shown in Figure 4-22. With overlaying at the small radius portion, it allowed people to sit without any other reinforcement. The gradient in porosity was also clear, especially with the light up.

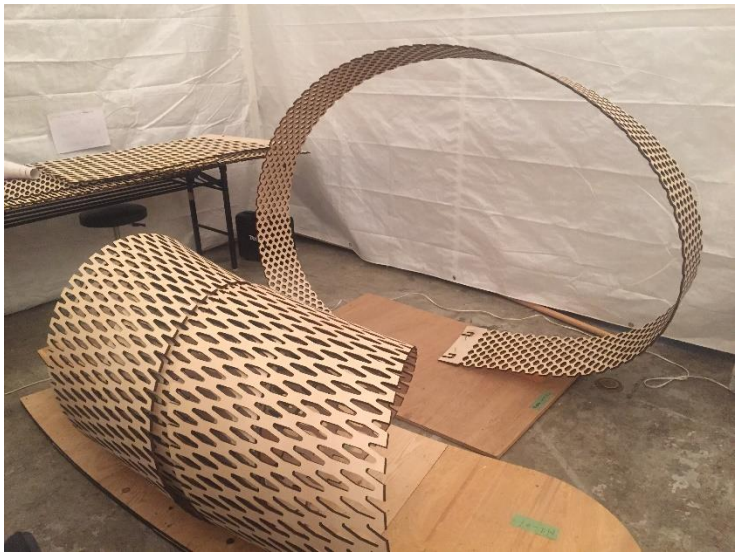

Figure 4-20. Mock up and details added in.

Figure 4-21. It took only one day to roll up all the spiral pieces.

Figure 4-22. The final outcome. People can sit at the end with overlaying of the spiral pieces. Bottom right picture showed a view of the space inside the structure.

4.2 Digital simulation

4.2.1 Relationship between pattern and bending radius

In previous section 4.1, the experiments were described in a chronicle order for a better understanding of the physical explorations. However, to build a mathematical model that relates the determinant parameters, results need to be re-collated for using the same variables. The result for tests in Test 2, Figure 4-10 of Section 4.1.2 and the final production parameters in Table 4-1 were the keys for generating the model. The results were re-summarized in Table below, where each parameter is shown in Figure 4-23.

	Angle θ (degree)	radius r(mm)	w (mm)
A1	6.3	270	14.5
A2	4.8	210	14.5
A3	3.8	120	14.5
B1	9.5	300	14.8
B2	9.5	250	14.8
B3	9.5	200	14.8
C1	11.0	220	10.4
C2	14.0	150	6.9
C3	17.4	80	3.4
S1	5.0	300	14.8
S14_op01	16.1	660	10.5
S14_op02	12.0	675	14
S14_op03	8.9	700	18
S14_op04	35.1	670	10.5

Table 4-2. Re-collated data for Test 2 in Section 4.1.2.

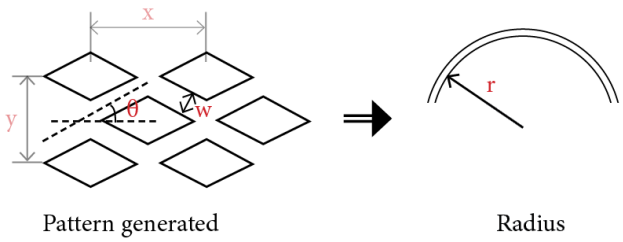

Figure 4-23. Parameters for plotting the graph. Angle is obtained from inverse tangent of x and y.

The data was plotted in 3D in MATLAB using curve fitting to derive a function of r, f (θ, w). The radius represents the stiffness of the sample. Since the radius can never be lower than 0, the firstly derived surface was adjusted to the upper and lower bounds of the data for a more precise result to be used in the simulation. The curve fit function optimized each of the coefficient using least squares method[2].

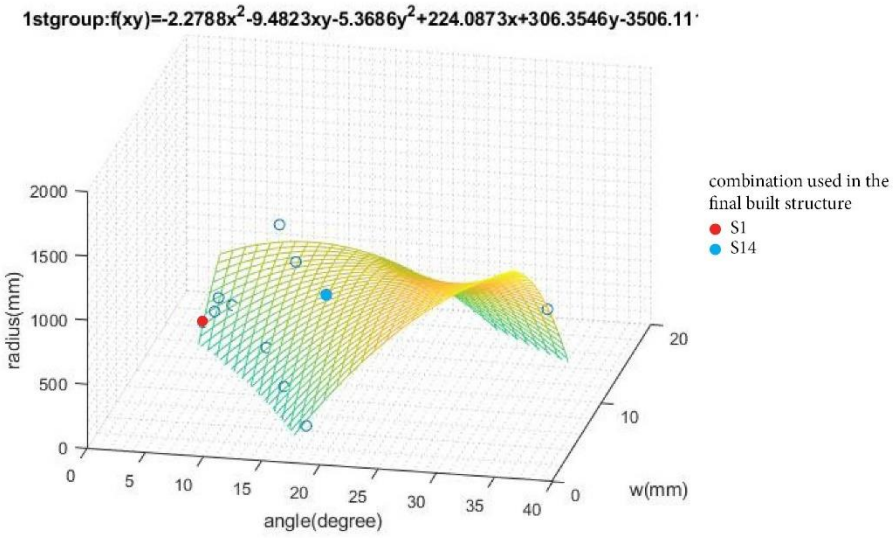

Figure 4-24. Image of result of curve fitting in MATLAB. Fitted surface with upper and lower bounds within the bounds of the data.

The function of r derived was:

$$r = f(\theta, w) = (-2.2788)\theta^2 - 9.4832\theta w - 5.3686w^2 + 224.0873\theta + 306.3546w - 3506.1111$$

[2] The documents of the function lsqcurvefit explains that x = lsqcurvefit(fun,x0,xdata,ydata) starts at x0 and finds coefficients x to best fit the nonlinear function fun(x, xdata) to the data ydata(in the least-squares sense).

where θ and w are the parameters shown in Figure 4-23. The function represents the radius that the kerf wood can be bent and should be always larger than 0. The code is shown in Appendix 13.

4.2.2 Simulation

Using the data obtained from above, grasshopper definition was written for the simulation of a piece of 10mm thick rectangular plywood to predict the radius it can be bent.

For the input, users can draw rectangle of any length and width. And set the value for x, y and w. x & y will give the angle θ, together with parameter w to define the pattern. For output, there are two parts: result and visualization. Users can find out the bending radius r and perforation rate as a result of the simulation. There is a flat surface ready to be fabricated and a visualization of the piece bent into its bending radius. The simulation structure is shown in Figure 4-25. The grasshopper definition and interface are shown in Figure 4-26.

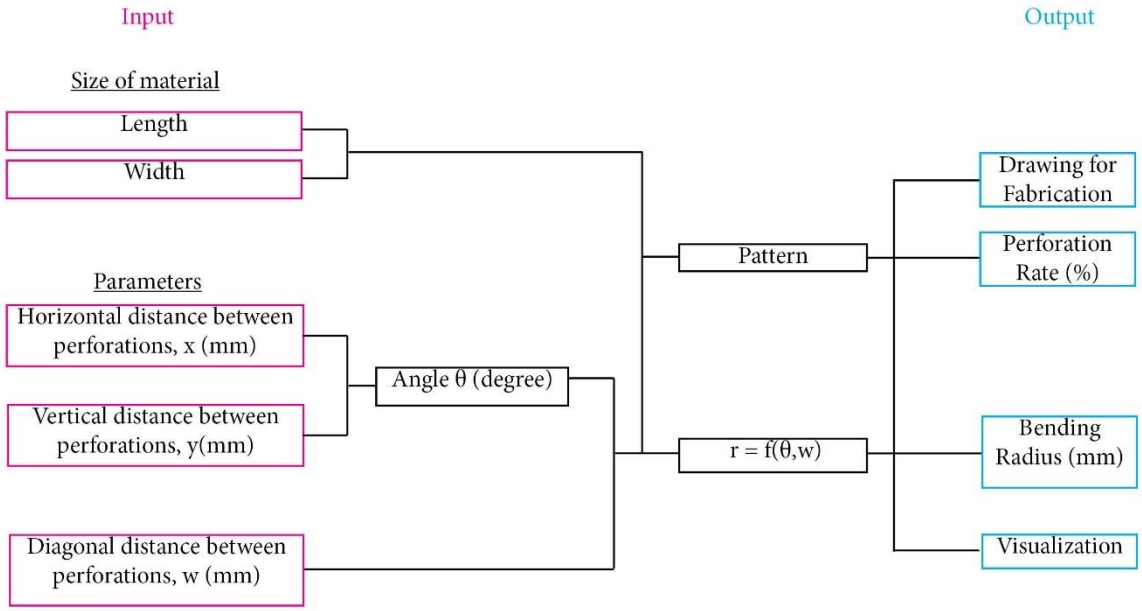

Figure 4-25. Structure of simulation

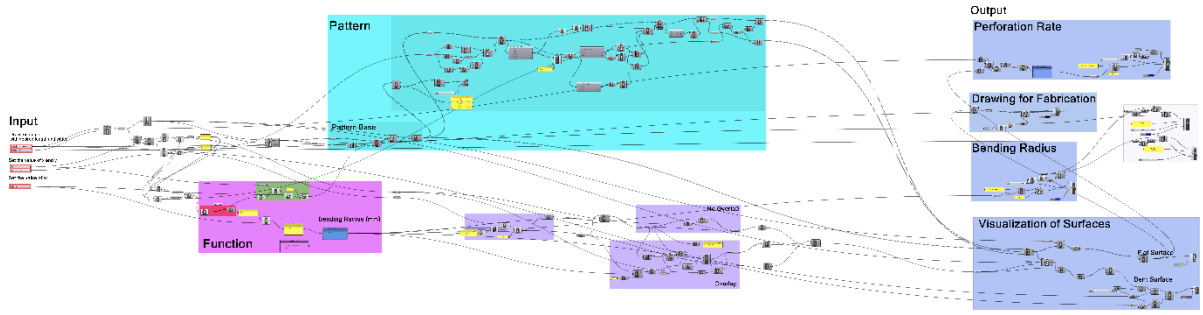

Figure 4-26. Grasshopper definition

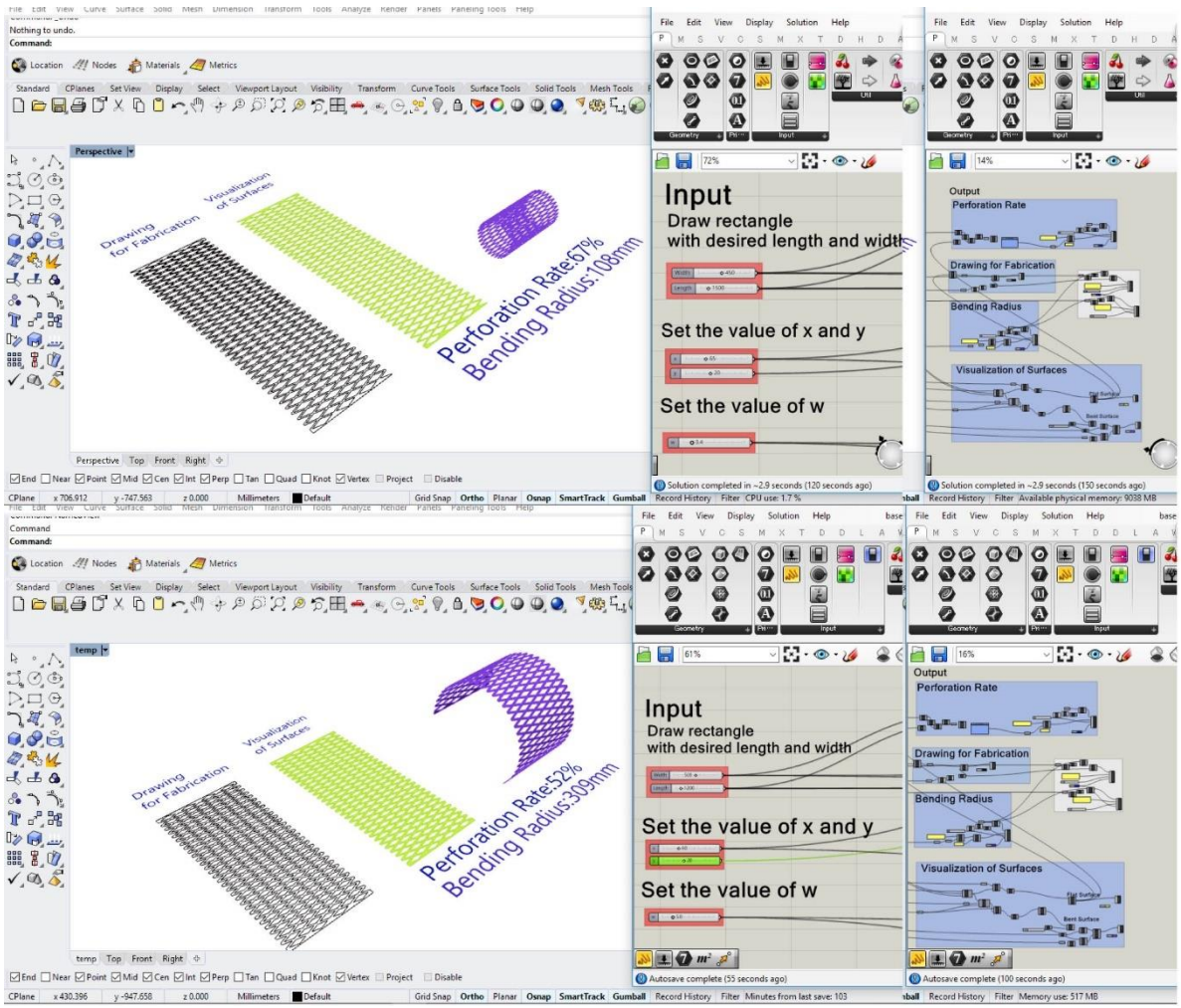

Figure 4-27. Screenshot of the Rhinoceros and Grasshopper interface.
Top: input values – width = 450mm, length = 1500mm, x = 65mm, y = 20mm, w = 3.4mm.
Output values – Perforation Rate = 67%, Bending Radius = 108mm.
Bottom: input values – width = 500mm, width = 1200mm, x = 60mm, y = 20mm, w = 5.0mm.
Output values – Perforation Rate = 52%, Bending Radius = 309mm.

4.3 Conclusion

In this chapter, kerf bending was explored with laser-cut kerf patterns on 10mm-thick plywood and ended up with a permanent installation standing in between furniture and architecture scale. As there was little quantifiable information available for the relationship between pattern and bending radius at this scale, there were also no precedents of making a structure out of full kerf pattern so that the structure with pattern could sustain its self-weight while bending, the studies were all made 1:1 to obtain realistic results. The parameters were updated for each round of test while the data was collected for analysis. The determinant parameters were then used to define the input to generate pattern in digital simulation. All the data from studies were used to derive a relationship between the parameters i.e. pattern and bending radius. It is a radius that could be bent to sustain self-weight by human forces. This workflow is shown in Figure 4-28 below.

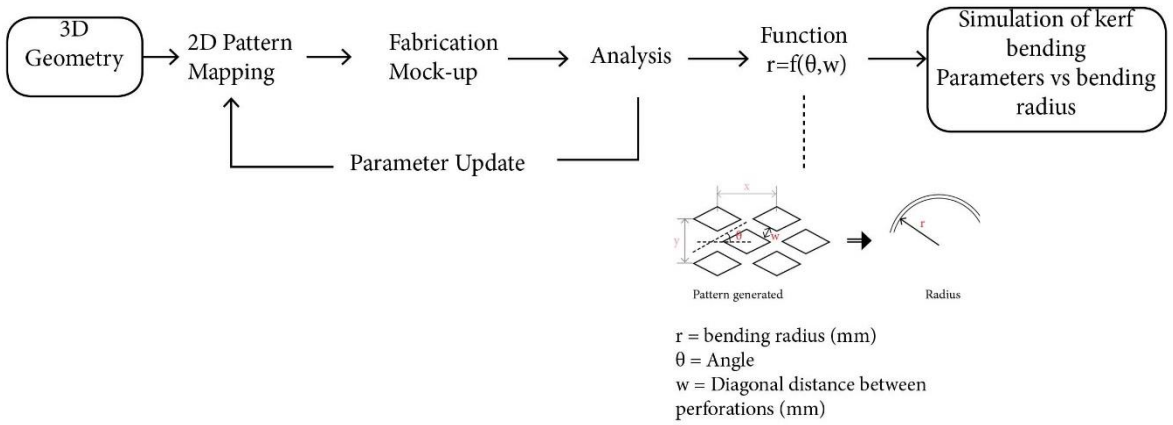

Figure 4-28. Workflow of the research on kerf bending.

The improvements of this research compared to other research is that it has deciphered the parameters that determines the bending radius and translated this set of data to a digital environment so that simulation can be used as a guidance for fabrication and design. The bending radius in the simulation serves as a guide for a match between the pattern applied to a bending radius that allows for the wood surface to be bent by people and sustain self-weight.

However, it has some limitations as well. Although the final result allowed for users to sit at the small end of the structure, due to the limitation of available material and budget, the load-bearing capacity was not included in the simulation. Thus, for a complete general application in future, structural test should be carried out to find out the extreme condition of the material. In addition, the data obtained were all for the thickness of 10mm plywood. Although the model and simulations worked for the limited number of ranges, but the sample size was too small to generate a model applicable for all. More time and budget are required to produce result for a more general application.

Chapter 5 – Discussion & Further studies

In the previous chapters, two methods that require minimum energy and manpower to bend wood – self-actuated bending and kerf bending – were investigated through physical models and digital simulations. The purpose of this research is not to deny the value of current widely used technologies for bending wood but to explore new ways to promote the use of wood which is an important resource for carbon storage. The requirement of energy, equipment and manpower for bending has refrained layman from bending wood surfaces. However, with the embedded intelligence of wood and simulations, it is possible to allow more people to access to the bending of wood surfaces. In addition, self-actuated bending, a bottom-up process, depends mainly on the environment and material, it provides little room for control and improvement. While kerf bending, a top-down process, provides total control over final bending radius. It is possible to combine these two methods such that the geometry potential of self-actuated bending can be maximized by applying the kerf pattern. Thus, in this chapter, the significance of this research will be discussed in two ways – as a more versatile design tool and as a contribution to the society. Further studies will be carried out to propose some design scenarios making use of the advantages of both methods.

5.1 A more versatile design tool

Compare to the existing researches such as those by Menges and Ruggeberg, this research approached self-actuated bending differently.

First of all, this research on self-actuated bending has less requirement in selection and processing wood. Existing researches require both softwood and hardwood cut in longitudinal and tangential directions so as to maximize the curvature that can be produced. However, this high requirement on species of wood and processing method was highly dependent on the availability of material for different regions and manufacturing skills. Instead, single material and rotary-cut processing method which is common for making veneers for plywood were used in this research. Variety of curvatures can be achieved by adjusting the moisture

content for active and restrictive layers and changing fiber orientations of active layer to create the unequal shrinkage. In addition, rotary-cutting has its limitations of unavoidable knots, providing difficulty in fabrication. Thus, a scanning-drawing soft was made to overcome this difficulty. In short, fewer restrictions on the selection and processing of wood may open self-actuated bending to more possibilities.

The comparison of this research with existing research is summarized in Figure 5-1.

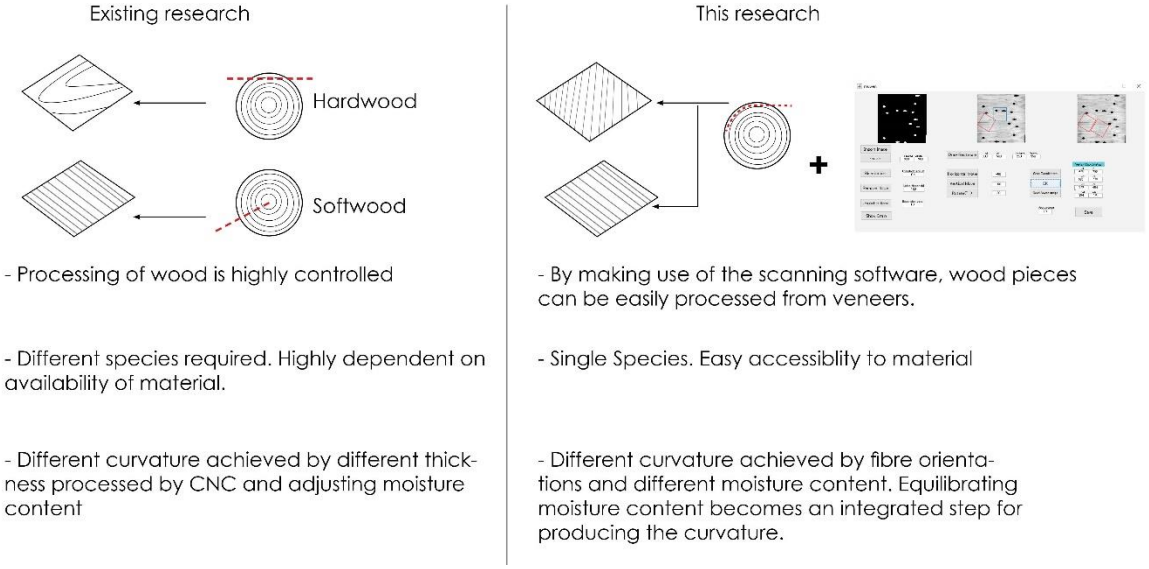

Figure 5-1. Comparison of this research with existing research

Secondly, geometry potential of self-actuated bending, hence possibilities of application, can be maximized through the application of kerf pattern. As mentioned before, the shrinkage/expansion of wood also depends on the density, i.e. the availability of cell wall of wood. Also, the study on kerf bending has demonstrated the impact of the pattern and hence perforation rate over bending radius. Thus, kerf pattern which is essentially a weakening of wood by removing the wood substances will have effect when it is applied to self-actuated bending. Hence, some further studies have been made to examine the potentials of the combination of these two techniques of bending and hence propose some possible design scenarios.

Study 1 – Apply kerf pattern to one of the bi-layer system

By applying the kerf pattern with different perforation rate to the active layers, it is possible to create different curvatures in one component as well (Figure 5-2). 250mm x 250mm samples were made with 3mm-thick Japanese cedar with active layer of moisture content of approximately 30% and restrictive layer of moisture content of 10%. Kerf pattern of perforation rate of 30%, 40% and 50% were applied to half of the active layers. After gluing, they were left in an outdoor environment with approximately 24 degree Celsius and relative humidity of 82% ("Meteorological Agency ｜Search past weather data", 2019) 48 hours for them to reach equilibrium. According to equation 1, the equilibrium moisture content reached was 16.6%. The curvatures were traced after 48 hours on a paper and drawn in AutoCAD. The result is summarized in Table 5-1.

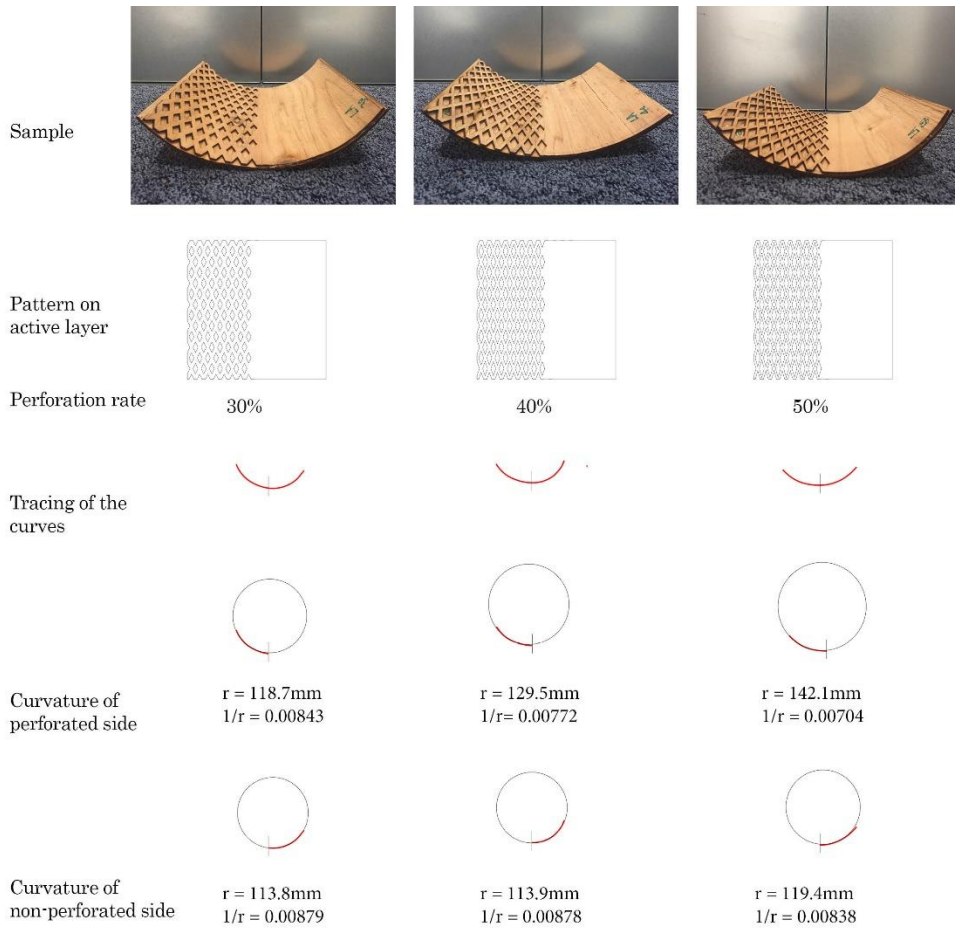

Figure 5-2. Studies on making kerf pattern on active layer. The curvature decreased when the perforation rate of active layer increased.

Perforated side of layer A

Perforation rate	curvature (mm-1)
30.0%	0.00842
40.0%	0.00772
50.0%	0.00704

Table 5-1. Summary of the result of study 1.

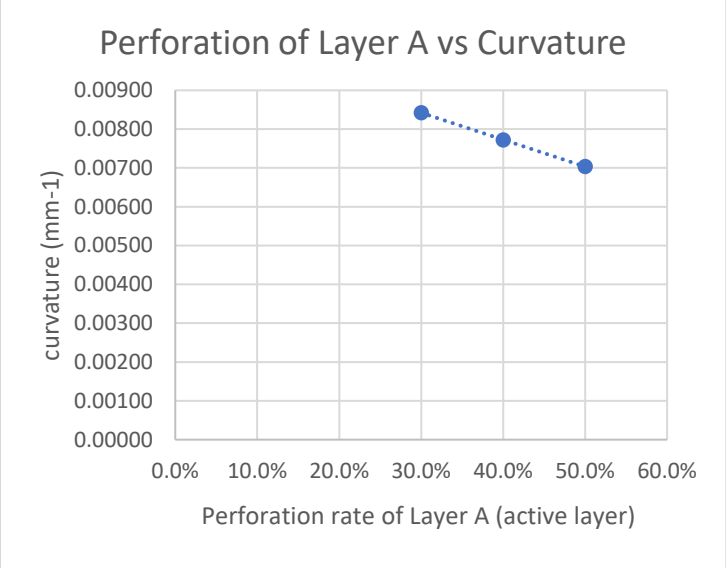

Figure 5-3. Graph of result of study 1

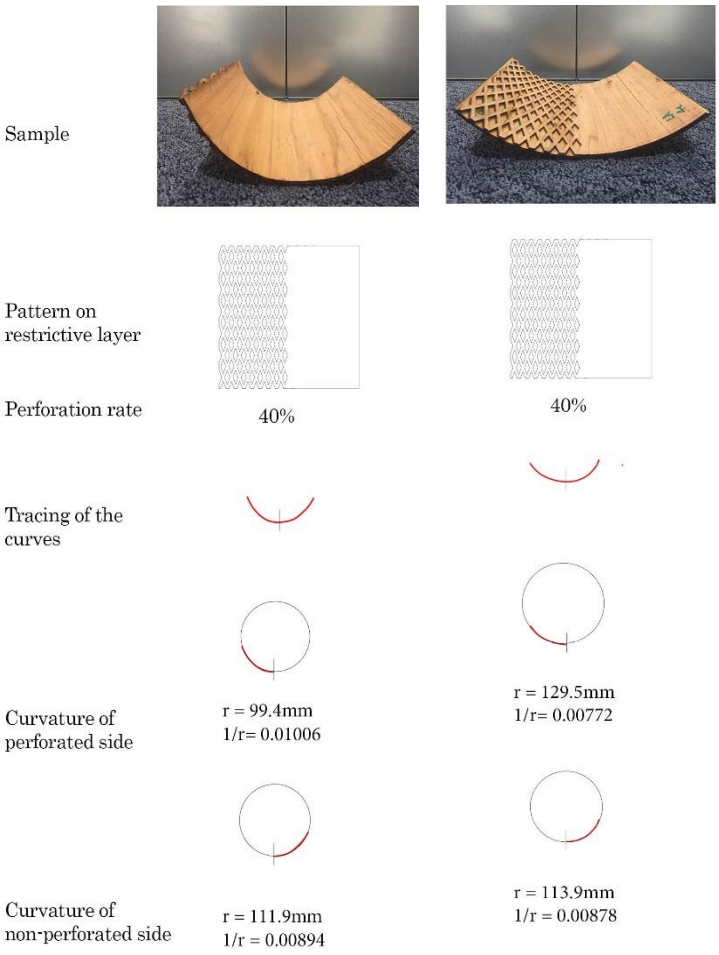

Figure 5-4. 40% perforation rate on the restrictive layer compared with that on the active layer. The side with perforation has a larger curvature than the side without perforation. A larger curvature could also be formed when the perforation is on the restrictive layer

Although there were too few samples to derive any numerical formula from the result, the result has shown a strong negative linear relationship between perforation rate and the bending radius (Figure 5-3). An increase in perforation rate will result in a decrease in curvature.

On the other hand, if the pattern is applied to the restrictive layer, the curvature on the perforated side will be larger than the non-perforated side due to a decrease in materials that restrict bending. In addition, by comparing with the active layer perforated with the same perforation rate, a perforation on the restrictive layer caused a larger perforation rate than that on the active layer. (Figure 5-4).

In this way, the range of curvature that could be achieved is widened beyond the limit that could be reached by different moisture content and fiber orientations in this research. The geometry potential of self-actuated bending has been expanded. This also widened its applicability to systems such as panelling or tessellation to create variations in the same system.

Study 2 – Apply kerf pattern to both layers of the bi-layer system

Samples were also made by applying kerf pattern on both active layer and restrictive layer of the bi-layer system (Figure 5-5). Half of the sample was applied with kerf pattern with perforation rate of 38%. There was no difference for the final curvature on both sides. As the active layer and restrictive layer has the same amount of material, unequal shrinkage of the two layers should occur the same way as the half without kerf pattern, i.e. the stress they incur is proportional to the ones without kerf pattern. Hence, the perforation does not change the final curvature when it reached equilibrium.

However, there were other dimensions added to the system. First of all, the envelope can be more refined to generate a more evenly lit indoor environment. This means the users inside the space have lower possibility to suffer from glare Secondly, the half with kerf pattern deformed faster due to less mass and smaller

gravity. This has expanded another dimension of self-actuated bending – the time scale. Taking the research by Menges & Reichert in 2012 as an example (Figure 5-6), not only but the time for each component or each leaf to open and close can be controlled (Figure 5-9, Figure 5-10). This can be beneficial especially for the indoor environment. A daylight simulation using Ladybug and Honeybee was carried out to demonstrate that, the façade openings can be designed to correspond to the sun position such that the openings at top can open faster to allow the sunlight to enter to the end of the room earlier (Figure 5-11).

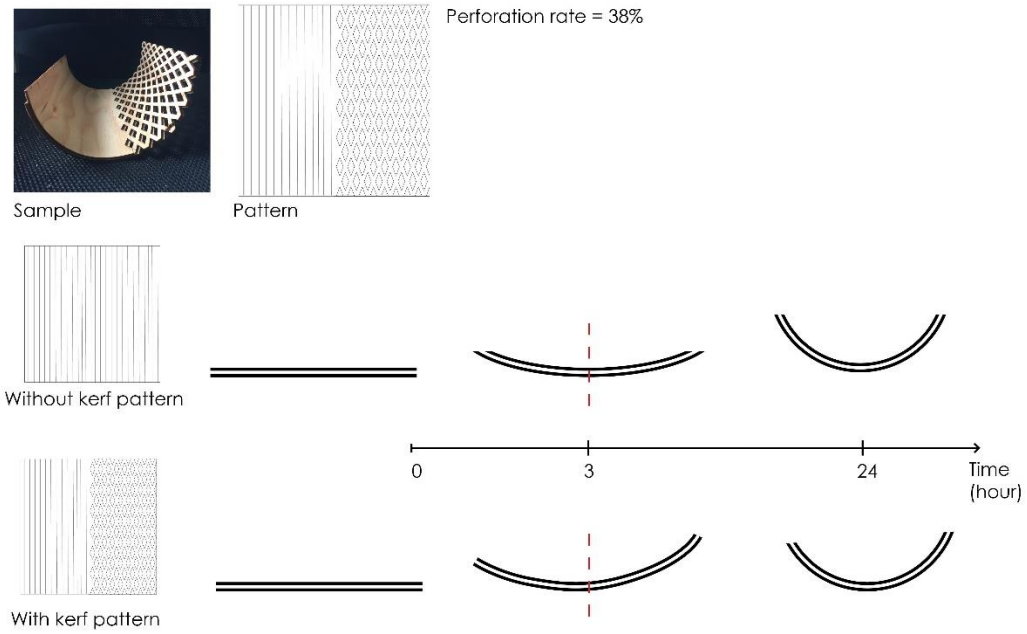

Figure 5-5. Both active and restrictive layers were applied with kerf pattern for half of the sample. The half with kerf pattern showed a faster deformation than the side without kerf pattern.

Figure 5-6. FAZ summer pavilion, openings responded to the weather changes. (Menges & Reichert, 2012)

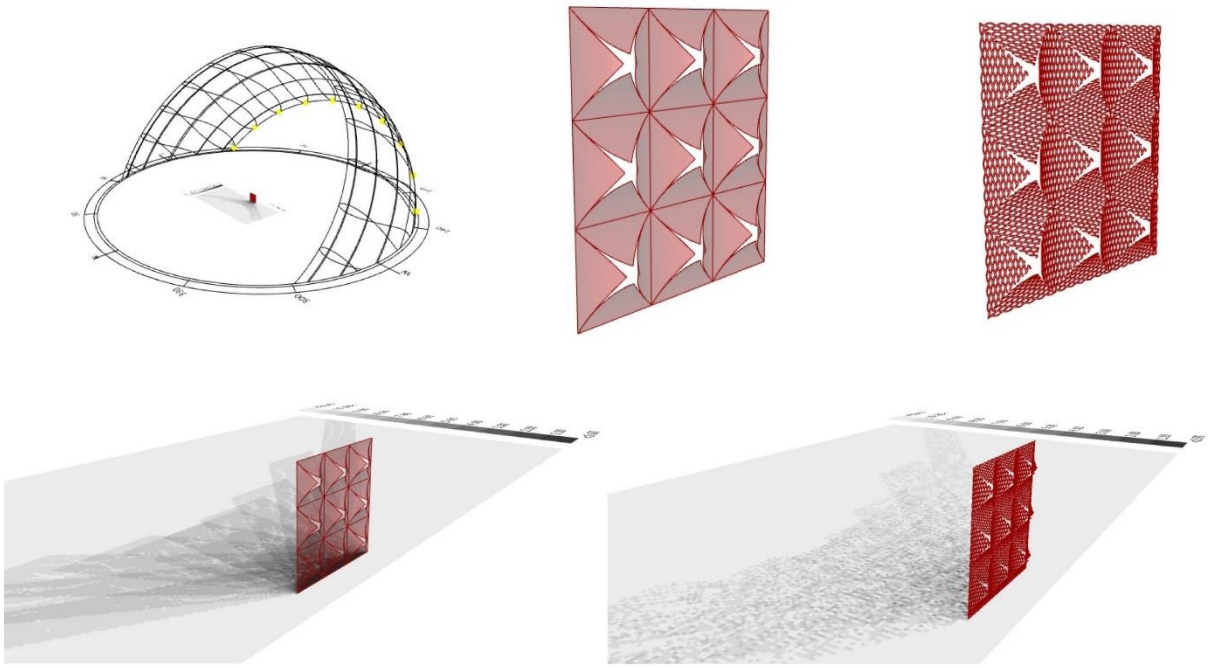

Figure 5-7. By doing a shadow analysis using Ladybug and Honeybee, the system with kerf pattern could cast a more refined shadow which could be a useful parameter as a design tool.

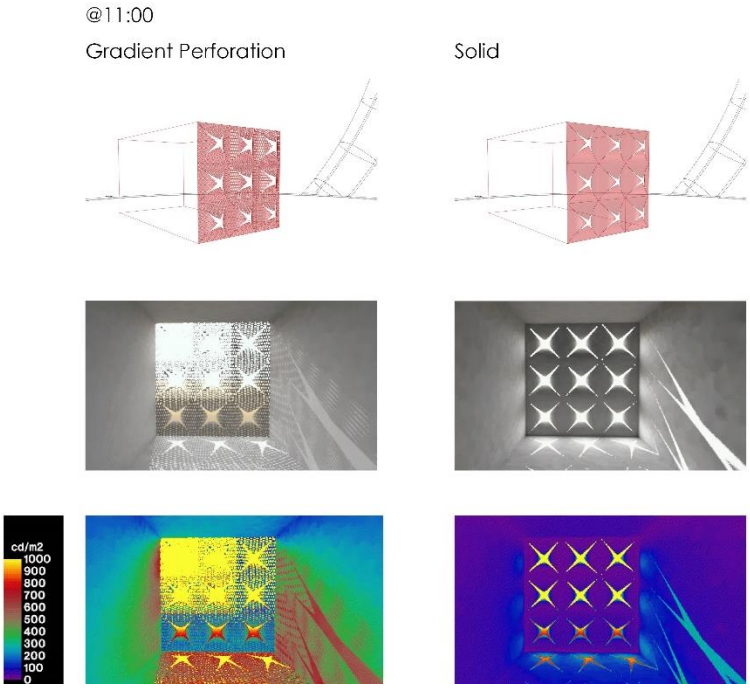

Figure 5-8. When this system was used to apply to the indoor environment, at the same point of time, the one with perforations makes the indoor space less prone to glare.

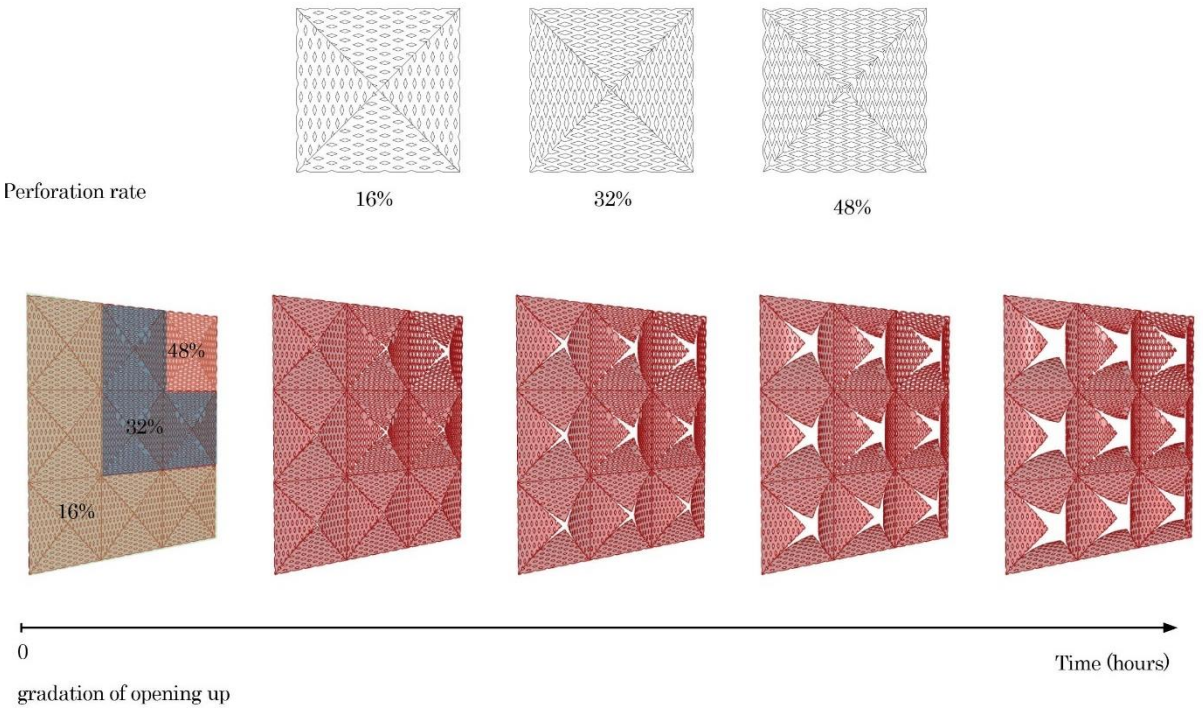

Figure 5-9. By adjusting the perforation rate of each component, the opening of the system could be gradual.

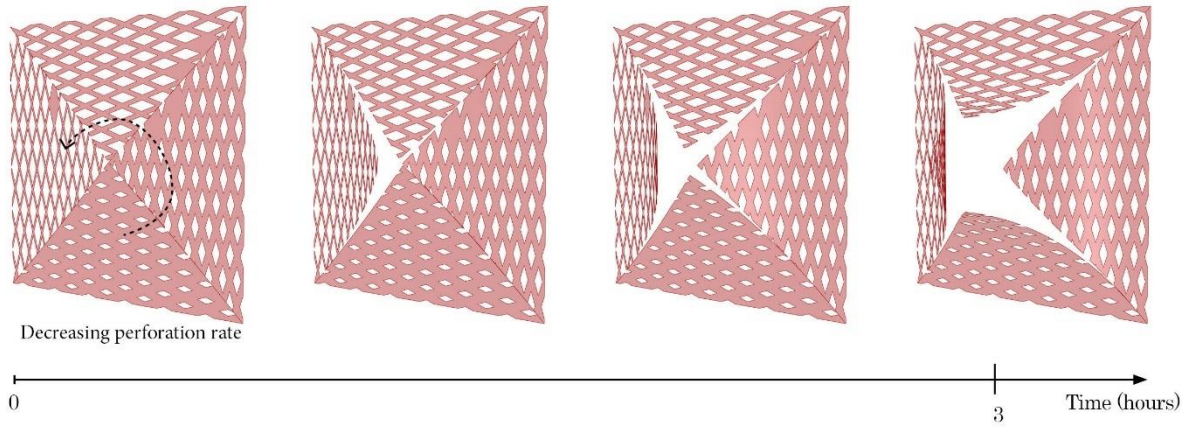

Figure 5-10. By adjusting the perforation rate of each leaf of each component, the componeng could open in a sequence as designed.

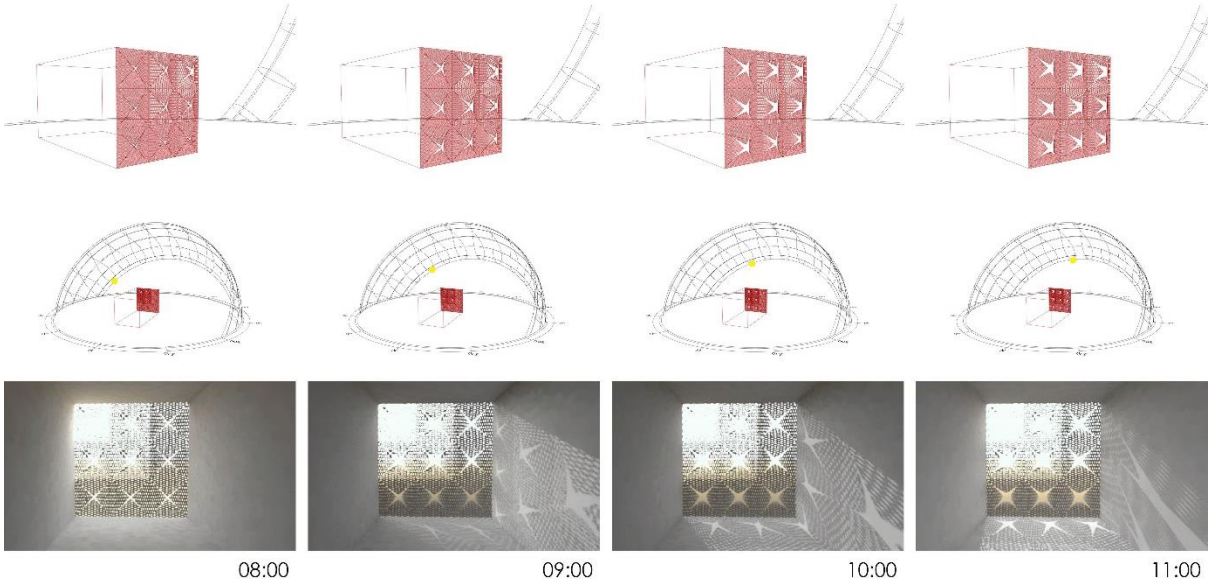

Figure 5-11. On winter solstice (21th December) in Tokyo, with larger openings at the top, light is able to reach the end of the room at an earlier time.

Both studies have demonstrated that although self-actuated bending has some limitations in a way that users has only partial control over the geometry change. However, with the aid of kerf pattern, the geometry potential could be maximized, making it an all-rounded design tool.

5.2 Contribution to the society

During World War II, annual forest cutting amount of Japan was 1,07.75 million cubic meter, 5 times of that of today (as of 2011). The forest and trees with usable size was depleted. Hence, Japan has to import wood from overseas, resulting in a drastic decrease in self-sufficiency rate (Figure 5-12). At the same time, since 1955, with the recovery of the economic activities, planted forest were planned to replace the natural forest for sustainable development in future. The planted forest consists mainly of softwood. With a half-century growth of planted forest, these softwoods have switched from the plantation period to the period of utilization. (Hayashi, 2012).

Thus, in June 2014, Japan announced Japan Revitalization Strategy to promote the use of wood and new demand for wood products in an attempt to transform forestry into a growth industry (Office of Prime Minister's Official Residence, 2014). The goal was to reach a self-sufficiency rate of 50% by 2020. Under this background, this research using Japanese cedar as the material has demonstrated its social significance in promoting the innovative way of using wood.

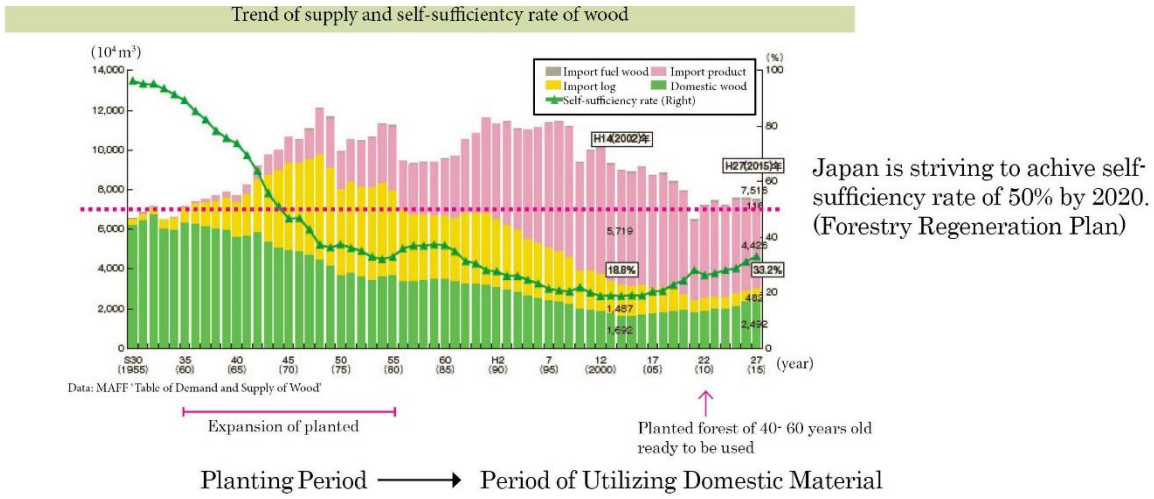

Figure 5-12. Trend of supply and self-sufficiency rate of wood in Japan (Ministry of Agriculture, Forestry and Fisheries, 2016) (Translated and modified)

In addition, this research is also trying to provide an alternative way for bending wood surfaces with minimum energy, equipment and manpower. The traditional

unpressurized steam bending involves the construction of a steam box usually fuelled by propane which is not environmentally friendly enough. The bending process also requires steaming the wood at 100 degree Celsius for one hour per 25mm of wood (“Lee Valley Tools - Woodworking Tools, Gardening Tools, Hardware”,2019). For pressurized steam bending, large equipment has to be invested, which hinders people from using. Other methods such as bending while laminating requires much formwork. From the perspective of promoting the use of wood for increasing carbon stock, self-actuated bending and kerf bending in this research provides a relatively ecological and easy way of bending wood surfaces.

Chapter 6 – Conclusion

Wood has been a material that human beings have dealt with for a long time. Ancient Egyptians laminated wood to make coffins so that they are not easily deformed. Steam bending is also used by ancient Egyptians to make military bows These have demonstrated that wood has been known as a flexible and a living material which could be tailored for the use of human beings. The emergence of wood processing machines and glue has enabled human beings to overcome the undesirable deformation of wood since World War I. The benefit these technologies brought us could not be denied. Wood has been used to make standardized products for military, architectural, and daily use which greatly increased the efficiency and longevity of wood products. The technological advancement before and during World War I has not only escalated the standardization of preventing undesired deformation of wood but also deciphered a standard way of making desirable bentwood. The creation of Thonet chair has marked the mass production of bentwood in the history and its legacy has continued until today. However, on the one hand, the emergence of lamination has tried to eliminate the hygroscopic property of wood, making it a homogeneous material which has little difference from other materials that are industrially produced such as steel except for the fragrance and touch. On the other hand, common bending technologies making use for the hygroscopic property of wood has involved much energy, equipment and manpower to produce the standardized bentwood. Although it is difficult to quantify how much energy is used for steam bending, this research has provided an alternative way of bending wood surfaces.

This research has surveyed two methods of bending wood, self-actuated bending and kerf bending, and the method of transforming the physical explorations into digital simulations.

For self -actuated bending, the pioneers such as Menges and Ruggeberg had provided a comprehensive methodology to apply bi-layer theory in the case of wood. However, the selection and processing of wood requires much precision by using

robotics or machineries which are not accessible for most people. Hence, this research attempted to use veneers of a single softwood, Japanese cedar, which could be obtained by rotary cut. The selection and fabrication processes are aided by a scanning and drawing software created. Simulation for the bending process was achieved by making experiments and linking the parameters which are difficult to obtain such as shrinking coefficient and Young's Modulus of active layer with different fiber orientation angle to simplify the inputs so as to push the simulation for easy use as much as possible.

The experiment result has shown that the bi-layer theory formula needs to be adapted for both Type a and Type b to fit the experiment data. The experiment result obtained a smaller curvature on average for both types than the result of calculated by bi-layer theory formula. This difference was mainly due to the modified method for self-actuated bending. While the original method maximized the shrinkage difference between active layer and restrictive layer by utilizing different species and grain orientation, the modified method put the local context and access to processing method in priority so that the potential shrinkage difference between active and restrictive layer were reduced, resulting in a milder curvature than the calculated ones using bi-layer theory formula. In addition, Type a and b were discussed separately due to the lack of statistical significance when they were discussed together as a whole. Although there were not enough types of sample to interpret further the relationship between the adapting coefficient and parameters, however, an inverse relationship could be observed between the adapting coefficient and initial moisture content of restrictive layer. This could be discussed further in future studies.

For kerf bending, it was researched through physical mockup as well. As there was little information on the relationship between the pattern and bending radius and sustainable self-weight, experiments were made to find out the determining parameters from scratch. The parameters were updated throughout the experiments and finally reached a conclusion for this pattern that diagonal distance between the perforations and the distance between the units were the determining parameters for the bending radius. The relationship was analysed

and obtained using digital tools such as MATLAB. The outcome was a built structure between furniture and architectural scale and a simulation for the bending behaviour with people having freedom to define the size of the material and pattern. However, for this simulation, it only discussed the plywood material with a thickness of 10mm. The relationship between the bending radius and thickness was not considered. In addition, although the final built structure allowed for people to sit on the smaller end of it, the loading capacity was not quantitively analysed as it is out of the scope for this research. However, it could add one more dimension for discussing geometry and structural strength. This could be an area of research in future.

These two methods of bending wood surfaces have their unique characteristics. Self-actuated bending depends heavily on the environment condition so that people have partial control over the final geometry. With kerf bending being able to introduce anisotropy into wood, it is used to help self-actuated bending to maximize its geometry potential under the same environment condition. Kerf pattern can be applied to one layer of the bi-layer to provide a wider range of possible curvatures, or applied to both layers to provide a refined shadow and time dimension to make self-actuated bending a more refined design tool.

In conclusion, the intention of this research is not trying to replace the current available methods for bending wood such as steam bending, but rather it is trying to promote the use of wood by embracing its embedded intelligence the material, providing an alternative way of bending wood surfaces. The common way of bending wood involves large investment of energy, equipment and manpower during the bending process. This has constrained bending of wood to be accomplished by only professionals and reduced the opportunities of using wood by ordinary people. However, by utilizing the properties of wood and with the help of computational technologies, the bending process of wood can be simulated and visualized. People are informed of the geometry outcome before proceeding to the selection of material and bending process. Instead of making a formwork and bending the wood afterwards, informed decisions can be made beforehand to make

the whole process more efficient. The material for formwork is also saved. As a result, instead of perceiving deformation of wood undesirable, wood is smart and designed to deform as how people wanted to be with the computational technologies. Wood does not only have a long history with us but a bright future as well.

Appendix 1 Drawings of all the samples cut for bi-layer experiment.

Thickness = 3mm

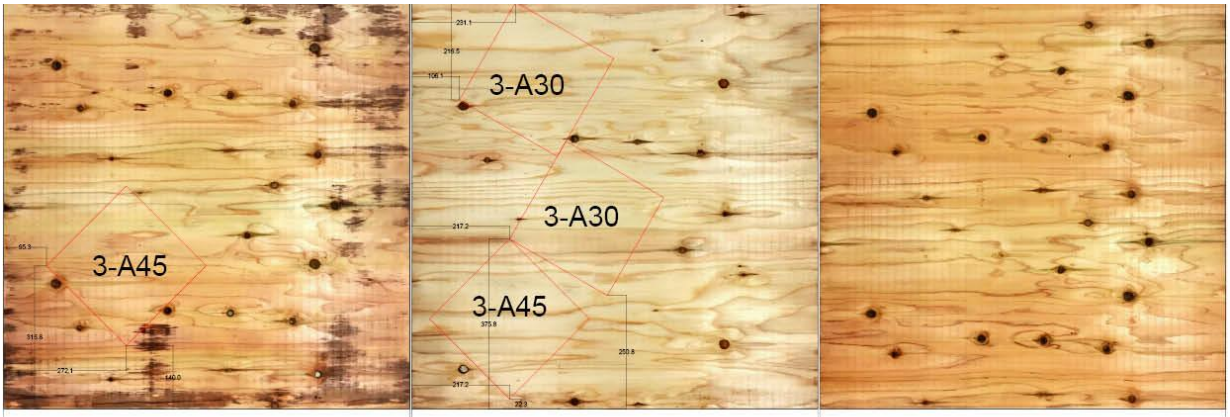

2a

2b

2c

2d

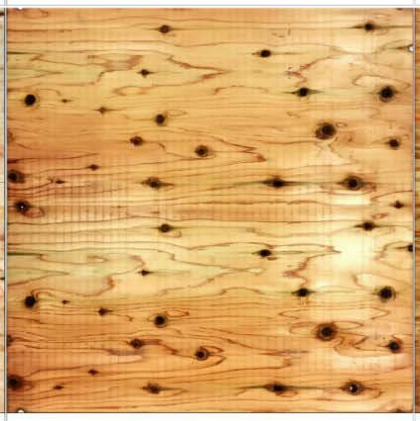

2e

2f

2g

2h

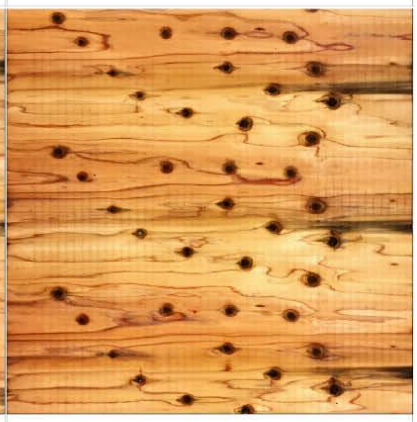

2i

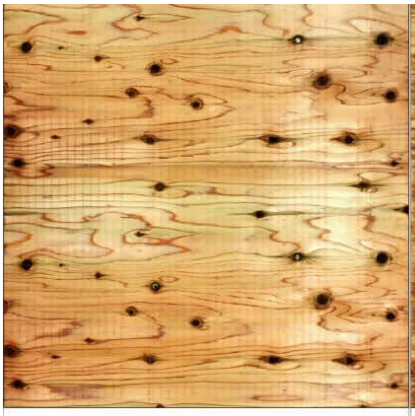

2j

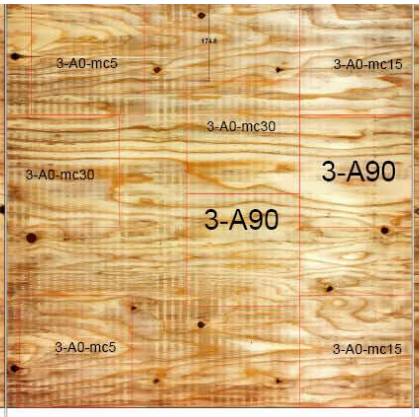
3-A0-mc5
3-A0-mc15
3-A0-mc30
3-A0-mc30
3-A90
3-A90
3-A0-mc5
3-A0-mc15

2k

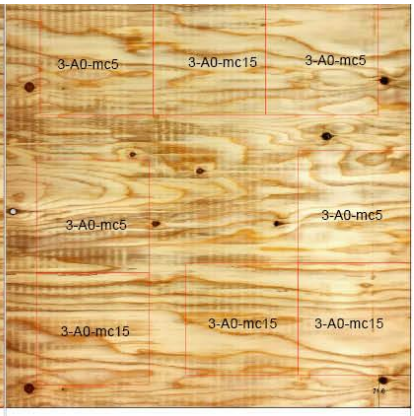
3-A0-mc5
3-A0-mc15
3-A0-mc5
3-A0-mc5
3-A0-mc5
3-A0-mc15
3-A0-mc15
3-A0-mc15

2l

2m

2n

Thickness = 3.5mm

3a

3b

3c

3d

3e

3f

3g

3h

3i


3.5-A0-mc5
3.5-A90
3.5-A90
3.5-A0-mc15
3.5-A0-mc15
3.5-A90

3j


3.5-A0-mc15
3.5-A0-mc30
3.5-A0-mc30

3k

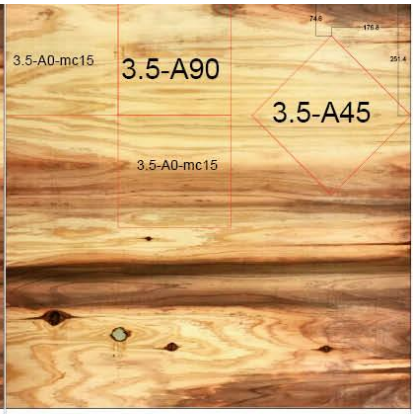
3.5-A0-mc15
3.5-A90
3.5-A45
3.5-A0-mc15

3l

Thickness = 4mm

4a

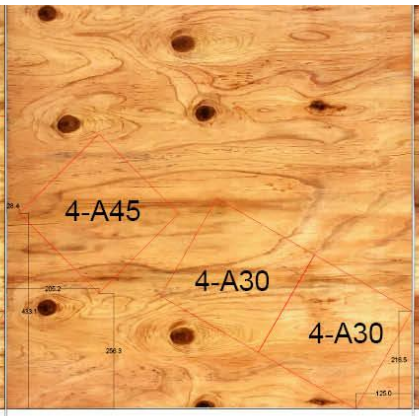

4b

4c

4d

4e

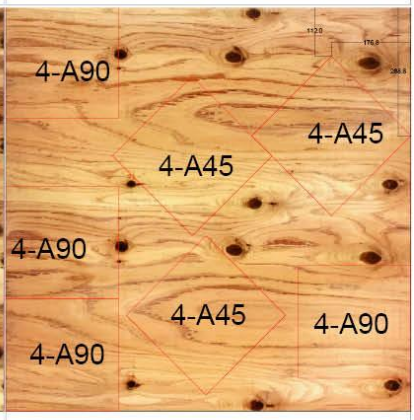

4f

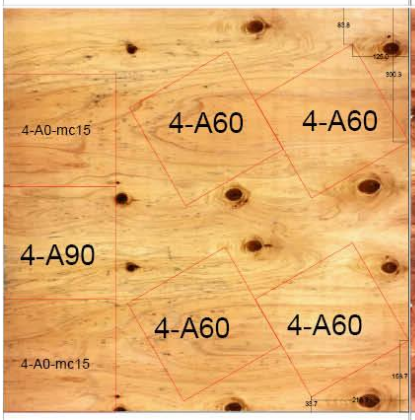

4g

4h

4i

	
4j	4k

Appendix 2 – Tools used in experiment

Figure p-2a. Thermo recorder TR-72U from T&D Corporation. (T&D Corporation, 2019)

Figure p-2b. Bosch Professional GLM 50C with precision of 0.1mm and could be connected to excel sheet via Bluetooth. (Bosch Professional, 2016)

Figure p-2c. Ultra Multi-purpose SU Premium Soft made from silylated urethane resin from Konishi Corporation. It allows for fixation within 15 minutes. ("Ultra Multi-purpose Special Site / Konishi Corporation", 2019)

Figure p-2d. Moisture meter of precision 0.1%. Shinwa Sokutei Corp. Ltd. Mode: 78636. (Shinwa Sokutei Co., Ltd., n.d.)

Appendix 3 – Mass measurements

Below are the original mass measured for all the samples.

Sample 3-3_3mm x 3mm

Name	Combination		Mass before glue(g)	Mass after glue(g)	Mass after 1.5 hr(g)	Mass after 3 hrs(g)	Mass after 4.5 hrs(g)	Mass after 6.0 hrs(g)	Mass after 16.0 hrs(g)	Mass after 19.5.hrs(g)	Mass after 24.5hrs(g)	Mass after 28hrs(g)	Mass after 52.5hrs(g)	Mass after 76hrs(g)	Mass after 111hrs(g)
3-3-a1	3-A0-mc5-1	3-A0-mc30-1	102.96	108.25	107.49	107.27	107.19	107.92	107.61	108.09	105.00	105.18	103.66	103.67	105.89
3-3-a2	3-A0-mc5-2	3-A90-mc30-1	101.59	106.77	107.24	106.31	105.22	107.07	106.02	104.72	103.19	103.56	102.05	102.08	103.34
3-3-a3	3-A0-mc5-3	3-A60-mc30-1	105.84	112.58	112.01	111.18	112.92	110.98	112.70	110.92	110.04	109.45	107.87	107.79	109.90
3-3-a4	3-A0-mc5-4	3-A45-mc30-1	106.68	113.05	111.51	112.96	112.82	111.51	112.78	111.19	111.05	109.78	108.17	108.10	110.10
3-3-a5	3-A0-mc5-5	3-A30-mc30-1	109.20	113.69	114.34	112.30	112.11	113.72	112.80	111.80	110.90	110.48	108.69	108.65	110.76
3-3-b1	3-A0-mc15-1	3-A0-mc30-2	106.22	111.89	111.53	109.25	110.17	108.56	109.56	108.18	106.25	106.45	104.38	104.07	106.20
3-3-b2	3-A0-mc15-2	3-A90-mc30-2	106.62	114.80	114.20	113.27	112.18	111.09	110.41	111.13	110.00	109.04	106.57	106.43	108.19
3-3-b3	3-A0-mc15-3	3-A60-mc30-2	113.14	120.28	119.33	118.90	118.37	116.47	116.70	115.56	114.20	114.04	111.46	111.30	114.01
3-3-b4	3-A0-mc15-4	3-A45-mc30-2	111.32	117.90	116.31	115.75	115.11	115.33	114.86	113.94	112.01	112.41	109.41	109.20	111.51
3-3-b5	3-A0-mc15-5	3-A30-mc30-2	108.37	113.02	111.67	110.18	109.95	109.27	110.86	109.99	108.36	107.69	104.98	104.81	107.06

Sample 4-4_4mm x 4mm

Name	Combination		Mass before glue(g)	Mass after glue(g)	Mass after 2.5 hrs(g)	Mass after 5.0 hrs(g)	Mass after 7.0 hrs(g)	Mass after 9.0 hrs(g)	Mass after 24 hrs(g)	Mass after 48 hrs(g)	Mass after 96 hrs(g)
4-4-a1	4-A0-mc5-1	4-A0-mc30-1	145.85	153.18	149.19	147.06	146.19	147.82	146.09	149.45	145.63
4-4-a2	4-A0-mc5-2	4-A90-mc30-1	143.68	150.71	146.79	147.11	145.91	145.13	144.60	147.84	145.29
4-4-a3	4-A0-mc5-3	4-A60-mc30-1	136.16	143.03	140.35	137.67	137.35	138.36	138.32	140.84	137.39
4-4-a4	4-A0-mc5-4	4-A45-mc30-1	141.51	146.91	143.25	143.06	141.73	142.55	141.28	144.56	140.83
4-4-a5	4-A0-mc5-5	4-A30-mc30-1	143.38	150.24	146.14	145.49	145.10	145.69	146.11	147.74	143.71
4-4-b1	4-A0-mc15-1	4-A0-mc30-2	155.07	161.01	154.96	152.66	152.61	150.50	151.60	153.49	147.61
4-4-b2	4-A0-mc15-2	4-A90-mc30-2	150.22	158.00	153.29	151.26	148.37	147.84	148.06	150.26	146.67
4-4-b3	4-A0-mc15-3	4-A60-mc30-2	147.54	151.80	147.61	145.57	144.92	144.42	142.85	145.73	140.29
4-4-b4	4-A0-mc15-4	4-A45-mc30-2	142.69	147.72	141.72	140.29	139.60	139.76	140.33	141.53	135.64
4-4-b5	4-A0-mc15-5	4-A30-mc30-2	142.50	148.85	144.29	141.01	141.29	140.56	140.48	142.72	136.62

Sample 3.5-3.5_3.5mm x 3.5mm

Name	Combination		Mass before glue(g)	Mass after glue(g)	Mass after 2.0 hr(g)	Mass after 4.5 hrs(g)	Mass after 6.5 hrs(g)	Mass after 8.5 hrs(g)	Mass after 24 hrs(g)	Mass after 48 hrs(g)	Mass after 96 hrs(g)
3.5-3.5-a1	3.5-A0-mc5-1	3.5-A0-mc30-1	133.41	139.62	135.48	134.91	134.66	134.56	134.95	137.38	133.55
3.5-3.5-a2	3.5-A0-mc5-2	3.5-A90-mc30-1	138.50	na	na	na	na	na	na	na	na
3.5-3.5-a3	3.5-A0-mc5-3	3.5-A60-mc30-1	135.77	140.29	135.76	135.01	134.62	134.29	134.48	136.66	132.93
3.5-3.5-a4	3.5-A0-mc5-4	3.5-A45-mc30-1	134.13	139.14	135.01	134.29	133.90	133.63	133.88	136.15	132.21
3.5-3.5-a5	3.5-A0-mc5-5	3.5-A30-mc30-1	137.73	142.67	138.52	137.92	137.50	137.37	137.75	140.28	136.00
3.5-3.5-b1	3.5-A0-mc15-1	3.5-A90-mc30-2	147.28	153.80	148.75	147.55	147.52	147.56	148.32	na	140.83
3.5-3.5-b2	3.5-A0-mc15-2	3.5-A90-mc30-2	na	na	na	na	na	na	na	na	na
3.5-3.5-b3	3.5-A0-mc15-3	3.5-A60-mc30-2	145.74	151.90	147.22	145.82	145.71	145.73	146.47	na	138.54
3.5-3.5-b4	3.5-A0-mc15-4	3.5-A45-mc30-2	148.99	154.99	149.90	148.59	148.57	148.62	149.38	na	141.30
3.5-3.5-b5	3.5-A0-mc15-5	3.5-A30-mc30-2	145.24	151.20	146.18	144.87	144.79	144.87	145.68	na	137.48

Sample 3-4_3mm x 4mm (active)

Name	Combination		Mass before glue(g)	Mass after glue(g)	Mass after 2.0 hr(g)	Mass after 4.5 hrs(g)	Mass after 6.5 hrs(g)	Mass after 8.5 hrs(g)	Mass after 24 hrs(g)	Mass after 48 hrs(g)	Mass after 96 hrs(g)
3-4-a1	3-A0-mc5-6	4-A0-mc30-3	125.00	132.15	128.37	126.57	125.15	125.81	125.41	128.00	124.51
3-4-a2	3-A0-mc5-7	4-A90-mc30-3	123.51	131.15	129.09	128.34	127.85	125.65	126.51	127.96	125.37
3-4-a3	3-A0-mc5-8	4-A60-mc30-3	124.36	131.37	130.21	127.62	127.82	126.11	126.38	128.86	125.49
3-4-a4	3-A0-mc5-9	4-A45-mc30-3	131.06	139.08	137.03	135.29	134.63	135.12	134.69	136.16	132.57
3-4-a5	3-A0-mc5-10	4-A30-mc30-3	131.12	138.27	133.73	131.63	132.06	131.06	131.98	134.21	130.22
3-4-b1	3-A0-mc15-6	4-A0-mc30-4	128.14	132.95	126.33	125.90	124.22	123.20	123.52	125.82	121.57
3-4-b2	3-A0-mc15-7	4-A90-mc30-4	128.87	134.78	129.39	129.19	128.70	126.57	127.29	128.24	124.87
3-4-b3	3-A0-mc15-8	4-A60-mc30-4	120.74	126.70	120.75	120.52	119.99	120.41	118.24	120.96	117.00
3-4-b4	3-A0-mc15-9	4-A45-mc30-4	126.10	132.68	127.24	125.81	125.26	124.85	125.19	126.67	122.44
3-4-b5	3-A0-mc15-10	4-A30-mc30-4	133.81	138.95	132.83	130.85	130.54	128.77	129.21	131.64	126.78

Sample 3-0.25_3mm (active) x 0.25mm (restrictive)

Name	Combination		Mass before glue(g)	Mass after glue(g)	Mass after 2.0 hr(g)	Mass after 4 hrs(g)	Mass after 6 hrs(g)	Mass after 24 hrs(g)	Mass after 72 hrs(g)
3-c1	0.25 veneer	3-A90-3	62.79	66.39	62.77	62.03	61.93	62.24	58.87
3.5-c1	0.25 veneer	3.5-A0-mc13	79.36	83.43	79.48	78.41	78.19	78.44	74.17
4-c1	0.25 veneer	4-A90-5	90.07	95.08	92.01	91.03	90.71	90.75	86.00

Sample 3-fiberglass cloth_3mm x fiberglass cloth (restrictive)

Name	Combination		Mass before glue(g)	Mass after glue(g)	Mass after 2.0 hr(g)	Mass after 4.0 hrs(g)	Mass after 6.0 hrs(g)	Mass after 24 hrs(g)	Mass after 48 hrs(g)
3-d1	fiber glass cloth	3-A90-4	71.73	75.88	63.64	61.37	61.42	61.98	59.58
3.5-d1	fiber glass cloth	3.5-A90-3	90.10	94.88	90.18	89.64	89.23	89.53	84.97
4-d1	fiber glass cloth	4-A90-6	93.46	97.54	93.60	92.98	92.59	92.74	88.30

Appendix 4a – Moisture content over time of samples

Sample 3-3-a Moisture Content over time

Time (hours)	0	1.5	3	4.5	6	16	19.5	24.5
RH	78%	78%	78%	78%	76%	75%	60%	56%
Temp (C)	15.0	15.0	15.0	15.0	15.3	14.9	24.0	25.6
3-3-a1	0-0							
MC-A_a1	24.0%	17.2%	15.3%	14.9%	14.8%	14.6%	14.0%	13.0%
MC-R_a1	5.0%	9.0%	11.0%	12.7%	12.6%	12.9%	12.3%	10.3%
3-3-a2	0-90							
MC-A_a2	24.0%	18.4%	16.4%	15.7%	14.9%	15.6%	14.9%	13.0%
MC-R_a2	5.0%	9.2%	10.9%	11.4%	12.1%	12.1%	11.4%	10.8%
3-3-a3	0-60							
MC-A_a3	24.0%	17.2%	15.8%	15.5%	15.2%	15.5%	14.9%	12.9%
MC-R_a3	5.0%	10.5%	11.6%	11.8%	12.1%	12.1%	11.5%	10.5%
3-3-a4	0-45							
MC-A_a4	24.0%	18.0%	15.9%	15.9%	15.7%	15.8%	15.3%	13.3%
MC-R_a4	5.0%	9.5%	12.9%	12.9%	13.1%	13.1%	12.6%	11.6%
3-3-a5	0-30							
MC-A_a5	24.0%	18.3%	16.3%	16.2%	16.1%	16.3%	15.7%	13.1%
MC-R_a5	5.0%	9.9%	11.4%	11.4%	11.5%	11.5%	10.9%	10.4%

Sample 3-3-b Moisture Content over time

Time (hours)	0	1.5	3	4.5	6	16	19.5	24.5
RH	78%	78%	78%	78%	76%	75%	60%	56%
Temp (C)	15.0	15.0	15.0	15.0	15.3	14.9	24.0	25.6
3-3-b1	0-0							
MC-A_b1	24.0%	20.1%	18.9%	17.8%	17.0%	16.2%	15.2%	14.7%
MC-R_b1	12.0%	12.5%	12.6%	12.8%	12.9%	13.0%	13.1%	10.5%
3-3-b2	0-90							
MC-A_b2	24.0%	20.1%	18.9%	17.8%	17.0%	16.2%	15.2%	13.6%
MC-R_b2	12.0%	12.5%	12.6%	12.8%	12.9%	13.0%	13.1%	11.6%
3-3-b3	0-60							
MC-A_b3	24.0%	19.5%	17.9%	16.7%	15.9%	15.2%	14.5%	12.4%
MC-R_b3	12.0%	12.6%	12.8%	12.9%	13.0%	13.1%	12.8%	11.7%
3-3-b4	0-45							
MC-A_b4	24.0%	20.2%	16.7%	15.4%	14.4%	13.5%	13.2%	12.0%
MC-R_b4	12.0%	12.5%	12.7%	12.8%	13.0%	13.1%	13.0%	11.7%
3-3-b5	0-30							
MC-A_b5	24.0%	20.5%	18.9%	17.7%	16.8%	15.9%	15.4%	13.3%
MC-R_b5	12.0%	12.4%	12.6%	12.8%	12.9%	13.0%	12.9%	12.3%

Table p-4a-1. Moisture content over time of 3-3-a & 3-3-b

Sample 4-4-a Moisture Content over time

Time (hours)	0	2.5	5	7	9	24
RH	50%	50%	49%	53%	51%	54%
Temp (C)	19.7	19.8	19.9	20.2	19.8	19.6
4-4-a1	0-0					
MC-A_a1	24.0%	17.2%	15.3%	14.9%	14.8%	14.6%
MC-R_a1	5.0%	6.1%	6.6%	6.8%	6.9%	6.8%
4-4-a2	0-0					
MC-A_a2	24.0%	17.5%	15.9%	15.0%	14.4%	14.0%
MC-R_a2	5.0%	5.8%	6.2%	6.4%	6.6%	6.6%
4-4-a3	0-60					
MC-A_a3	24.0%	17.2%	15.8%	15.5%	15.2%	15.5%
MC-R_a3	5.0%	5.8%	6.3%	6.5%	6.6%	6.5%
4-4-a4	0-45					
MC-A_a4	24.0%	18.0%	15.9%	15.9%	15.7%	15.8%
MC-R_a4	5.0%	5.8%	6.3%	6.4%	6.6%	6.5%
4-4-a5	0-30					
MC-A_a5	24.0%	18.3%	16.3%	16.2%	16.1%	16.3%
MC-R_a5	5.0%	5.7%	6.3%	6.5%	6.6%	6.6%

Sample 4-4-b Moisture Content over time

Time (hours)	0	2.5	5	7	9	24
RH	50%	50%	49%	53%	51%	54%
Temp (C)	19.7	19.8	19.9	20.2	19.8	19.6
4-4-b1	0-0					
MC-A_b1	24.0%	20.1%	18.9%	17.8%	17.0%	16.2%
MC-R_b1	12.0%	10.3%	9.8%	9.6%	9.5%	9.5%
4-4-b2	0-90					
MC-A_b2	24.0%	16.4%	13.6%	13.4%	12.9%	12.8%
MC-R_b2	12.0%	10.5%	9.9%	9.7%	9.6%	9.6%
4-4-b3	0-60					
MC-A_b3	24.0%	19.5%	17.9%	16.7%	15.9%	15.2%
MC-R_b3	12.0%	10.7%	10.2%	10.0%	9.9%	9.8%
4-4-b4	0-45					
MC-A_b4	24.0%	20.2%	16.7%	15.4%	14.4%	13.5%
MC-R_b4	12.0%	11.3%	10.2%	9.9%	9.7%	9.5%
4-4-b5	0-30					
MC-A_b5	24.0%	20.5%	18.9%	17.7%	16.8%	15.9%
MC-R_b5	12.0%	10.7%	10.1%	9.9%	9.8%	9.7%

Table p-4a-2. Moisture content over time of 4-4-a & 4-4-b

Sample 3-4-a Moisture Content over time

Time (hr)	0	2.5	4.5	6.5	8.5	24
RH (%)	54%	51%	50%	51%	52%	56%
Temp (C)	19.8	19.9	20.0	19.9	19.9	19.8
3-4-a1	0-0					
MC-A_a1	24.0%	16.2%	11.8%	10.5%	9.9%	10.0%
MC-R_a1	5.0%	6.0%	7.0%	7.2%	7.4%	7.4%
3-4-a2	0-90					
MC-A_a2	24.0%	19.1%	14.4%	13.1%	12.4%	11.3%
MC-R_a2	5.0%	6.2%	7.4%	7.7%	7.9%	7.6%
3-4-a3	0-60					
MC-A_a3	24.0%	18.6%	14.6%	13.3%	12.7%	12.7%
MC-R_a3	5.0%	6.3%	7.4%	7.7%	7.8%	7.8%
3-4-a4	0-45					
MC-A_a4	24.0%	18.2%	14.2%	13.0%	12.4%	12.1%
MC-R_a4	5.0%	6.4%	7.5%	7.7%	7.9%	7.9%
3-4-a5	0-30					
MC-A_a5	24.0%	17.1%	12.2%	10.8%	10.3%	10.3%
MC-R_a5	5.0%	5.7%	6.8%	7.1%	7.2%	7.2%

Sample 3-4-b Moisture Content over time

Time (hr)	0	2.5	4.5	6.5	8.5	24
RH (%)	54%	51%	50%	51%	52%	56%
Temp (C)	19.8	19.9	20.0	19.9	19.9	19.8
3-4-b1	0-0					
MC-A_b1	24.0%	14.6%	12.9%	11.9%	11.1%	10.7%
MC-R_b1	12.0%	11.4%	10.8%	10.4%	10.2%	10.1%
3-4-b2	0-0					
MC-A_b2	24.0%	16.0%	14.8%	13.8%	13.0%	11.6%
MC-R_b2	12.0%	11.6%	11.1%	10.8%	10.6%	10.4%
3-4-b3	0-60					
MC-A_b3	24.0%	15.4%	13.8%	12.8%	12.2%	11.6%
MC-R_b3	12.0%	11.1%	10.8%	10.6%	10.5%	10.4%
3-4-b4	0-45					
MC-A_b4	24.0%	16.5%	15.1%	14.1%	13.5%	12.8%
MC-R_b4	12.0%	11.6%	11.1%	10.8%	10.6%	10.4%
3-4-b5	0-30					
MC-A_b5	24.0%	15.3%	13.5%	12.4%	11.7%	11.1%
MC-R_b5	12.0%	11.6%	11.1%	10.9%	10.7%	10.6%

Table p-4a-3. Moisture content over time of 3-4-a & 3-4-b

Appendix 4b – Verification of moisture content

i) Mass calculated from moisture content is compared with mass measured from each sample (Table p-4b-1 ~ Table p-4b-6). Mass when full dry was obtained under the assumption that the starting moisture content was equilibrated at 24%, 12% and 5% effectively within one week. The comparison result is also plotted as histogram to compare the two sets of data side by side below (Figure p-4b). Generally, the result has shown a reliable moisture content obtained from moisture meter with correlation coefficient between 0.75 to 0.99. The variations in the coefficient may be due to the exchange of moisture content between the layers, especially the inexperienced application of glue at the start of the experiment.

Sample 3-3-a Mass from moisture content vs mass measurement

Time (hours)	0	1.5	3	4.5	6	16	19.5	24.5
RH	78%	78%	78%	78%	76%	75%	60%	56%
Temp (C)	15.0	15.0	15.0	15.0	15.3	14.9	24.0	25.6

3-3-a1	0-0							
MC-A_a1	24.0%	17.2%	15.3%	14.9%	14.8%	14.6%	14.0%	13.0%
MC-R_a1	5.0%	9.0%	11.0%	12.7%	12.6%	12.9%	12.3%	10.3%

Mass when full dry (g)	
A_a1	44.98
R_a1	44.94

Mass_A (g)	55.73	52.72	51.86	51.68	51.64	51.55	51.28	50.83
Mass_R (g)	47.23	48.99	49.89	50.64	50.61	50.75	50.48	49.56
Mass_A+R (g)	102.96	101.71	101.75	102.32	102.25	102.30	101.76	100.39
Mass_a1 (g)	102.96	102.20	101.98	101.90	102.63	102.32	102.80	99.71
Correlation	0.860							

3-3-a2	0-90							
MC-A_a2	24.0%	18.4%	16.4%	15.7%	14.9%	15.6%	14.9%	13.0%
MC-R_a2	5.0%	9.2%	10.9%	11.4%	12.1%	12.1%	11.4%	10.8%

Mass when full dry (g)	
A_a2	44.38
R_a2	44.35

Mass_A (g)	54.99	52.55	51.65	51.37	51.01	51.29	50.98	50.16
Mass_R (g)	46.60	48.42	49.17	49.41	49.73	49.73	49.42	49.14
Mass_A+R (g)	101.59	100.97	100.82	100.78	100.74	101.02	100.39	99.30
Mass_a2 (g)	101.59	102.06	101.13	100.04	101.89	100.84	99.54	98.01
Correlation	0.847							

3-3-a3	0-60							
MC-A_a3	24.0%	17.2%	15.8%	15.5%	15.2%	15.5%	14.9%	12.9%
MC-R_a3	5.0%	10.5%	11.6%	11.8%	12.1%	12.1%	11.5%	10.5%

Mass when full dry (g)	
A_a3	46.24
R_a3	46.20

Mass_A (g)	57.29	54.18	53.52	53.40	53.25	53.39	53.12	52.19
Mass_R (g)	48.55	51.03	51.58	51.66	51.78	51.78	51.51	51.05
Mass_A+R (g)	105.84	105.21	105.10	105.06	105.03	105.17	104.63	103.24
Mass_a3 (g)	105.84	105.27	104.44	106.18	104.24	105.96	104.18	103.30
Correlation	0.763							

3-3-a4	0-45							
MC-A_a4	24.0%	18.0%	15.9%	15.9%	15.7%	15.8%	15.3%	13.3%
MC-R_a4	5.0%	9.5%	12.9%	12.9%	13.1%	13.1%	12.6%	11.6%

Mass when full dry (g)	
A_a4	46.61
R_a4	46.57

Mass_A (g)	57.74	54.99	54.03	54.00	53.90	53.96	53.73	52.81
Mass_R (g)	48.94	50.99	52.56	52.58	52.66	52.66	52.42	51.97
Mass_A+R (g)	106.68	105.98	106.59	106.58	106.56	106.62	106.15	104.78
Mass_a4 (g)	106.68	105.14	106.59	106.45	105.14	106.41	104.82	104.68
Correlation	0.720							

3-3-a5	0-30							
MC-A_a5	24.0%	18.3%	16.3%	16.2%	16.1%	16.3%	15.7%	13.1%
MC-R_a5	5.0%	9.9%	11.4%	11.4%	11.5%	11.5%	10.9%	10.4%

Mass when full dry (g)	
A_a5	47.71
R_a5	47.67

Mass_A (g)	59.11	56.42	55.46	55.44	55.39	55.48	55.20	53.95
Mass_R (g)	50.09	52.39	53.11	53.11	53.15	53.15	52.86	52.61
Mass_A+R (g)	109.20	108.81	108.57	108.55	108.54	108.63	108.06	106.56
Mass_a5 (g)	109.20	109.85	107.81	107.62	109.23	108.31	107.31	106.41
Correlation	0.794							

Table p-4b-1. Sample 3-3-a Mass from moisture content vs mass measurement

Mass calculated from moisture content

Mass measured

Sample 3-3-b Mass from moisture content vs mass measurement

Time (hours)	0	1.5	3	4.5	6	16	19.5	24.5
RH	78%	78%	78%	78%	76%	75%	60%	56%
Temp (C)	15.0	15.0	15.0	15.0	15.3	14.9	24.0	25.6

3-3-b1	0-0							
MC-A_b1	24.0%	20.1%	18.9%	17.8%	17.0%	16.2%	15.2%	14.7%
MC-R_b1	12.0%	12.5%	12.6%	12.8%	12.9%	13.0%	13.1%	10.5%

Mass_A (g)	57.50	52.26	51.71	51.23	50.88	50.53	50.10	49.90
Mass_R (g)	48.72	52.15	52.23	52.29	52.34	52.38	52.44	51.22
Mass_A+R (g)	106.22	104.42	103.93	103.52	103.22	102.92	102.54	101.11
Mass_b1 (g)	106.22	105.86	103.58	104.50	102.89	103.89	102.51	100.58
Correlation	0.919							

Mass when full dry (g)
A_b1 43.50
R_b1 46.37

3-3-b2	0-90							
MC-A_b2	24.0%	20.1%	18.9%	17.8%	17.0%	16.2%	15.2%	13.6%
MC-R_b2	12.0%	12.5%	12.6%	12.8%	12.9%	13.0%	13.1%	11.6%

Mass_A (g)	57.71	52.46	51.90	51.42	51.07	50.72	50.29	49.61
Mass_R (g)	48.91	52.35	52.42	52.49	52.53	52.58	52.64	51.94
Mass_A+R (g)	106.62	104.81	104.33	103.91	103.61	103.30	102.93	101.55
Mass_b2 (g)	106.62	106.02	105.09	104.00	102.91	102.23	102.95	101.82
Correlation	0.917							

Mass when full dry (g)
A_b2 43.67
R_b2 46.54

3-3-b3	0-60							
MC-A_b3	24.0%	19.5%	17.9%	16.7%	15.9%	15.2%	14.5%	12.4%
MC-R_b3	12.0%	12.6%	12.8%	12.9%	13.0%	13.1%	12.8%	11.7%

Mass_A (g)	61.24	55.37	54.62	54.08	53.73	53.37	53.07	52.10
Mass_R (g)	51.90	55.59	55.69	55.76	55.81	55.86	55.70	55.18
Mass_A+R (g)	113.14	110.96	110.31	109.84	109.53	109.23	108.77	107.28
Mass_b3 (g)	113.14	112.19	111.76	111.23	109.33	109.56	108.42	107.06
Correlation	0.934							

Mass when full dry (g)
A_b3 46.34
R_b3 49.39

3-3-b4	0-45							
MC-A_b4	24.0%	20.2%	16.7%	15.4%	14.4%	13.5%	13.2%	12.0%
MC-R_b4	12.0%	12.5%	12.7%	12.8%	13.0%	13.1%	13.0%	11.7%

Mass_A (g)	60.26	54.80	53.22	52.63	52.18	51.73	51.62	51.05
Mass_R (g)	51.06	54.65	54.75	54.83	54.89	54.95	54.89	54.28
Mass_A+R (g)	111.32	109.45	107.97	107.46	107.07	106.68	106.51	105.33
Mass_b4 (g)	111.32	109.73	109.17	108.53	108.75	108.28	107.36	105.43
Correlation	0.937							

Mass when full dry (g)
A_b4 45.59
R_b4 48.59

3-3-b5	0-30							
MC-A_b5	24.0%	20.5%	18.9%	17.7%	16.8%	15.9%	15.4%	13.3%
MC-R_b5	12.0%	12.4%	12.6%	12.8%	12.9%	13.0%	12.9%	12.3%

Mass_A (g)	58.66	53.46	53.50	52.95	52.53	52.11	51.89	50.97
Mass_R (g)	49.71	53.19	50.62	50.69	50.74	50.79	50.75	50.45
Mass_A+R (g)	108.37	106.65	104.12	103.63	103.27	102.91	102.64	101.43
Mass_b5 (g)	108.37	107.02	105.53	105.30	104.62	106.21	105.34	103.71
Correlation	0.916							

Mass when full dry (g)
A_b5 44.38
R_b5 47.31

Table p-4b-2. Sample 3-3-b Mass from moisture content vs mass measurement

Mass calculated from moisture content

Mass measured

Sample 4-4-a Mass from moisture content vs mass measurement

Time (hours)	0	2.5	5	7	9	24
RH	50%	50%	49%	53%	51%	54%
Temp (C)	19.7	19.8	19.9	20.2	19.8	19.6

4-4-a1	0-0					
MC-A_a1	24.0%	17.2%	15.3%	14.9%	14.8%	14.6%
MC-R_a1	5.0%	6.1%	6.6%	6.8%	6.9%	6.8%

Mass when full dry (g)	
A_a1	63.67
R_a1	63.72

Mass_A (g)	78.95	74.62	73.41	73.15	73.09	72.96
Mass_R (g)	66.90	67.57	67.95	68.05	68.10	68.07
Mass_A+R (g)	145.85	142.19	141.36	141.20	141.19	141.03
Mass_a1 (g)	145.85	141.86	139.73	138.86	140.49	138.76
Correlation	0.963					

4-4-a2	0-90					
MC-A_a2	24.0%	17.5%	15.9%	15.0%	14.4%	14.0%
MC-R_a2	5.0%	5.8%	6.2%	6.4%	6.6%	6.6%

Mass when full dry (g)	
A_a1	62.72
R_a1	62.77

Mass_A (g)	77.77	73.67	72.68	72.14	71.72	71.50
Mass_R (g)	65.91	66.42	66.64	66.76	66.89	66.91
Mass_A+R (g)	143.68	140.09	139.32	138.90	138.61	138.41
Mass_a2 (g)	143.68	139.76	140.08	138.88	138.10	137.57
Correlation	0.970					

4-4-a3	0-60					
MC-A_a3	24.0%	17.2%	15.8%	15.5%	15.2%	15.5%
MC-R_a3	5.0%	5.8%	6.3%	6.5%	6.6%	6.5%

Mass when full dry (g)	
A_a1	59.44
R_a1	59.48

Mass_A (g)	73.70	69.65	68.80	68.65	68.45	68.63
Mass_R (g)	62.46	62.94	63.24	63.36	63.41	63.38
Mass_A+R (g)	136.16	132.59	132.04	132.01	131.87	132.01
Mass_a3 (g)	136.16	133.48	130.80	130.48	131.49	131.45
Correlation	0.926					

4-4-a4	0-45					
MC-A_a4	24.0%	18.0%	15.9%	15.9%	15.7%	15.8%
MC-R_a4	5.0%	5.8%	6.3%	6.4%	6.6%	6.5%

Mass when full dry (g)	
A_a1	61.77
R_a1	61.82

Mass_A (g)	76.60	72.88	71.62	71.58	71.44	71.52
Mass_R (g)	64.91	65.38	65.70	65.79	65.90	65.86
Mass_A+R (g)	141.51	138.26	137.32	137.36	137.35	137.39
Mass_a4 (g)	141.51	137.85	137.66	136.33	137.15	135.88
Correlation	0.947					

4-4-a5	0-30					
MC-A_a5	24.0%	18.3%	16.3%	16.2%	16.1%	16.3%
MC-R_a5	5.0%	5.7%	6.3%	6.5%	6.6%	6.6%

Mass when full dry (g)	
A_a1	62.59
R_a1	62.64

Mass_A (g)	77.61	74.02	72.76	72.74	72.67	72.79
Mass_R (g)	65.77	66.24	66.59	66.69	66.78	66.76
Mass_A+R (g)	143.38	140.26	139.35	139.43	139.45	139.55
Mass_a5 (g)	143.38	139.28	138.63	138.24	138.83	139.25
Correlation	0.985					

Table p-4b-3. Sample 4-4-a Mass from moisture content vs mass measurement

Mass calculated from moisture content

Mass measured

Sample 4-4-b Mass from moisture content vs mass measurement

Time (hours)	0	2.5	5	7	9	24
RH	50%	50%	49%	53%	51%	54%
Temp (C)	19.7	19.8	19.9	20.2	19.8	19.6

4-4-b1	0-0					
MC-A_b1	24.0%	20.1%	18.9%	17.8%	17.0%	16.2%
MC-R_b1	12.0%	10.3%	9.8%	9.6%	9.5%	9.5%

Mass when full dry (g)	
A_a1	67.69
R_a1	63.51

Mass_A (g)	83.94	81.32	80.45	79.71	79.17	78.63
Mass_R (g)	71.13	70.03	69.72	69.62	69.57	69.54
Mass_A+R (g)	155.07	151.35	150.18	149.33	148.74	148.17
Mass_b1 (g)	155.07	149.02	146.72	146.67	144.56	145.66
Correlation	0.980					

4-4-b2	0-90					
MC-A_b2	24.0%	16.4%	13.6%	13.4%	12.9%	12.8%
MC-R_b2	12.0%	10.5%	9.9%	9.7%	9.6%	9.6%

Mass when full dry (g)	
A_a1	65.57
R_a1	61.53

Mass_A (g)	81.31	76.36	74.51	74.36	74.03	73.97
Mass_R (g)	68.91	67.99	67.64	67.49	67.42	67.43
Mass_A+R (g)	150.22	144.35	142.15	141.85	141.46	141.40
Mass_b2 (g)	150.22	145.51	143.48	140.59	140.06	140.28
Correlation	0.956					

4-4-b3	0-60					
MC-A_b3	24.0%	19.5%	17.9%	16.7%	15.9%	15.2%
MC-R_b3	12.0%	10.7%	10.2%	10.0%	9.9%	9.8%

Mass when full dry (g)	
A_a1	64.40
R_a1	60.43

Mass_A (g)	79.86	76.95	75.92	75.16	74.67	74.18
Mass_R (g)	67.68	66.87	66.60	66.47	66.41	66.37
Mass_A+R (g)	147.54	143.82	142.52	141.64	141.08	140.55
Mass_b3 (g)	147.54	143.35	141.31	140.66	140.16	138.59
Correlation	0.994					

4-4-b4	0-45					
MC-A_b4	24.0%	20.2%	16.7%	15.4%	14.4%	13.5%
MC-R_b4	12.0%	11.3%	10.2%	9.9%	9.7%	9.5%

Mass when full dry (g)	
A_a1	62.29
R_a1	58.44

Mass_A (g)	77.24	74.86	72.70	71.90	71.29	70.68
Mass_R (g)	65.45	65.06	64.42	64.23	64.12	63.99
Mass_A+R (g)	142.69	139.91	137.12	136.12	135.41	134.66
Mass_b4(g)	142.69	136.69	135.26	134.57	134.73	135.30
Correlation	0.898					

4-4-b5	0-30					
MC-A_b5	24.0%	20.5%	18.9%	17.7%	16.8%	15.9%
MC-R_b5	12.0%	10.7%	10.1%	9.9%	9.8%	9.7%

Mass when full dry (g)	
A_a1	58.36
R_a1	142.50

Mass_A (g)	77.13	70.30	69.41	68.70	68.16	67.62
Mass_R (g)	65.37	64.60	64.26	64.14	64.08	64.01
Mass_A+R (g)	142.50	134.90	133.68	132.84	132.24	131.63
Mass_b5 (g)	142.50	137.94	134.66	134.94	134.21	134.13
Correlation	0.974					

Table p-4b-4. Sample 4-4-b Mass from moisture content vs mass measurement

Mass calculated from moisture content

Mass measured

Sample 3-4-a Mass from moisture content vs mass measurement

Time (hr)	0	2.5	4.5	6.5	8.5	24
RH (%)	54%	51%	50%	51%	52%	56%
Temp (C)	19.8	19.9	20.0	19.9	19.9	19.8

3-4-a1	0-0					
MC-A_a1	24.0%	16.2%	11.8%	10.5%	9.9%	10.0%
MC-R_a1	5.0%	6.0%	7.0%	7.2%	7.4%	7.4%

Mass when full dry (g)	
A_a1	62.18
R_a1	45.61

Mass_A (g)	77.11	72.26	69.52	68.73	68.35	68.43
Mass_R (g)	47.89	48.34	48.78	48.91	48.97	48.97
Mass_A+R (g)	125.00	120.60	118.31	117.64	117.32	117.39
Mass_a1 (g)	125.00	121.22	119.42	118.00	118.66	118.26
Correlation	0.992					

3-4-a2	0-90					
MC-A_a2	24.0%	19.1%	14.4%	13.1%	12.4%	11.3%
MC-R_a2	5.0%	6.2%	7.4%	7.7%	7.9%	7.6%

Mass when full dry (g)	
A_a1	64.16
R_a1	41.86

Mass_A (g)	79.56	76.40	73.42	72.56	72.10	71.41
Mass_R (g)	43.95	44.47	44.95	45.09	45.17	45.04
Mass_A+R (g)	123.51	120.87	118.37	117.65	117.27	116.45
Mass_a2 (g)	123.51	121.45	120.70	120.21	118.01	118.87
Correlation	0.929					

3-4-a3	0-60					
MC-A_a3	24.0%	18.6%	14.6%	13.3%	12.7%	12.7%
MC-R_a3	5.0%	6.3%	7.4%	7.7%	7.8%	7.8%

Mass when full dry (g)	
A_a1	61.86
R_a1	45.38

Mass_A (g)	76.71	73.38	70.88	70.10	69.74	69.71
Mass_R (g)	47.65	48.26	48.72	48.86	48.93	48.93
Mass_A+R (g)	124.36	121.64	119.59	118.96	118.66	118.64
Mass_a3 (g)	124.36	123.20	120.61	120.81	119.10	119.37
Correlation	0.953					

3-4-a4	0-45					
MC-A_a4	24.0%	18.2%	14.2%	13.0%	12.4%	12.1%
MC-R_a4	5.0%	6.4%	7.5%	7.7%	7.9%	7.9%

Mass when full dry (g)	
A_a1	65.20
R_a1	47.82

Mass_A (g)	80.85	77.08	74.45	73.67	73.26	73.08
Mass_R (g)	50.21	50.91	51.39	51.53	51.60	51.60
Mass_A+R (g)	131.06	127.98	125.84	125.20	124.87	124.68
Mass_a4 (g)	131.06	129.01	127.27	126.61	127.10	126.67
Correlation	0.990					

3-4-a5	0-30					
MC-A_a5	24.0%	17.1%	12.2%	10.8%	10.3%	10.3%
MC-R_a5	5.0%	5.7%	6.8%	7.1%	7.2%	7.2%

Mass when full dry (g)	
A_a1	65.23
R_a1	47.85

Mass_A (g)	80.88	76.36	73.15	72.30	71.92	71.98
Mass_R (g)	50.24	50.57	51.09	51.23	51.29	51.28
Mass_A+R (g)	131.12	126.93	124.24	123.53	123.21	123.25
Mass_a5 (g)	131.12	126.58	124.48	124.91	123.91	124.83
Correlation	0.978					

Table p-4b-5. Sample 3-4-a Mass from moisture content vs mass measurement

Mass calculated from moisture content

Mass measured

Sample 3-4-b Mass from moisture content vs mass measurement

Time (hr)	0	2.5	4.5	6.5	8.5	24
RH (%)	54%	51%	50%	51%	52%	56%
Temp (C)	19.8	19.9	20.0	19.9	19.9	19.8

3-4-b1	0-0					
MC-A_b1	24.0%	14.6%	12.9%	11.9%	11.1%	10.7%
MC-R_b1	12.0%	11.4%	10.8%	10.4%	10.2%	10.1%

Mass when full dry (g)	
A_a1	63.75
R_a1	43.84

Mass_A (g)	79.04	73.08	72.00	71.30	70.85	70.56
Mass_R (g)	49.10	48.82	48.57	48.41	48.31	48.24
Mass_A+R (g)	128.14	121.90	120.57	119.72	119.16	118.80
Mass_b1 (g)	128.14	121.52	121.09	119.41	118.39	118.71
Correlation	0.993					

3-4-b2	0-0					
MC-A_b2	24.0%	16.0%	14.8%	13.8%	13.0%	11.6%
MC-R_b2	12.0%	11.6%	11.1%	10.8%	10.6%	10.4%

Mass when full dry (g)	
A_a1	64.11
R_a1	44.09

Mass_A (g)	79.49	74.36	73.57	72.95	72.43	71.55
Mass_R (g)	49.38	49.18	49.00	48.86	48.74	48.67
Mass_A+R (g)	128.87	123.54	122.57	121.81	121.17	120.22
Mass_b2 (g)	128.87	123.48	123.28	122.79	120.66	121.38
Correlation	0.977					

3-4-b3	0-60					
MC-A_b3	24.0%	15.4%	13.8%	12.8%	12.2%	11.6%
MC-R_b3	12.0%	11.1%	10.8%	10.6%	10.5%	10.4%

Mass when full dry (g)	
A_a1	60.06
R_a1	41.30

Mass_A (g)	74.48	69.29	68.35	67.77	67.37	67.01
Mass_R (g)	46.26	45.91	45.78	45.70	45.65	45.60
Mass_A+R (g)	120.74	115.20	114.13	113.47	113.02	112.61
Mass_b3 (g)	120.74	114.79	114.56	114.03	114.45	112.28
Correlation	0.974					

3-4-b4	0-45					
MC-A_b4	24.0%	16.5%	15.1%	14.1%	13.5%	12.8%
MC-R_b4	12.0%	11.6%	11.1%	10.8%	10.6%	10.4%

Mass when full dry (g)	
A_a1	62.73
R_a1	43.14

Mass_A (g)	77.79	73.06	72.18	71.59	71.19	70.79
Mass_R (g)	48.31	48.14	47.93	47.80	47.70	47.61
Mass_A+R (g)	126.10	121.20	120.11	119.39	118.89	118.40
Mass_b4 (g)	126.10	120.66	119.23	118.68	118.27	118.61
Correlation	0.990					

3-4-b5	0-30					
MC-A_b5	24.0%	15.3%	13.5%	12.4%	11.7%	11.1%
MC-R_b5	12.0%	11.6%	11.1%	10.9%	10.7%	10.6%

Mass when full dry (g)	
A_a1	66.57
R_a1	45.78

Mass_A (g)	82.54	76.76	75.56	74.85	74.36	73.98
Mass_R (g)	51.27	51.09	50.88	50.76	50.67	50.61
Mass_A+R (g)	133.81	127.85	126.44	125.60	125.03	124.59
Mass_b5 (g)	133.81	127.69	125.71	125.40	123.63	124.07
Correlation	0.994					

Table p-4b-6. Sample 3-4-b Mass from moisture content vs mass measurement

Mass calculated from moisture content

Mass measured

Figure p-4b-1. Mass from moisture content vs mass measurement (3-3-a1 ~ 3-3-a4)

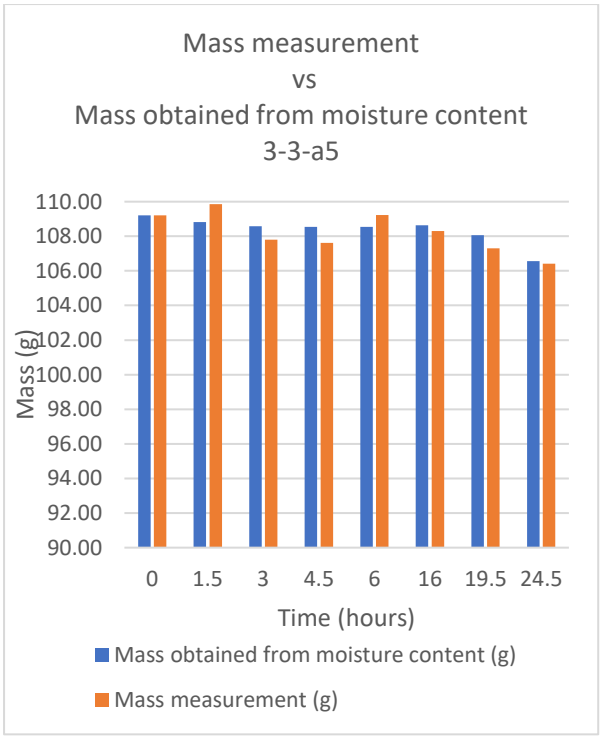

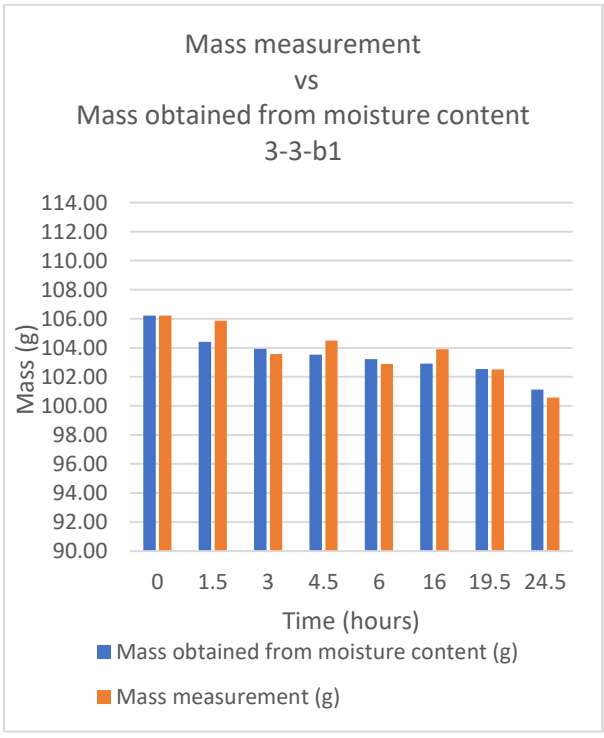

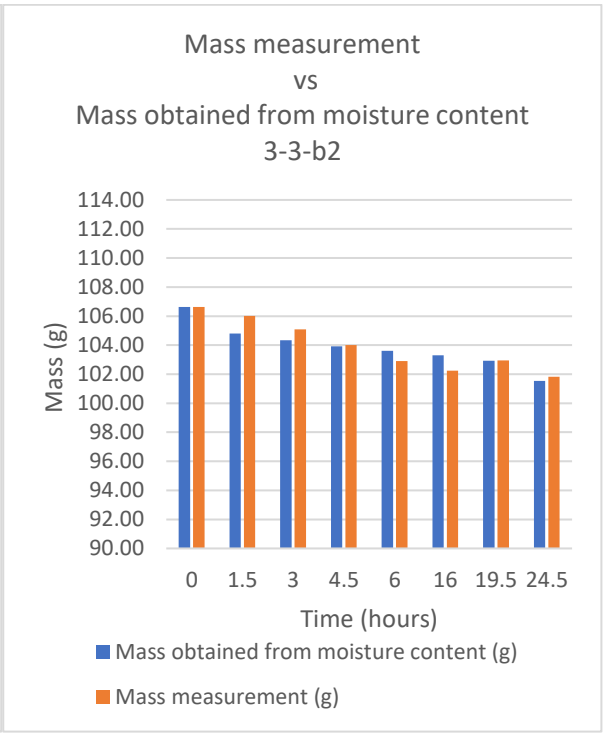

Figure p-4b-2. Mass from moisture content vs mass measurement (3-3-a5, 3-3-b1, 3-3-b2)

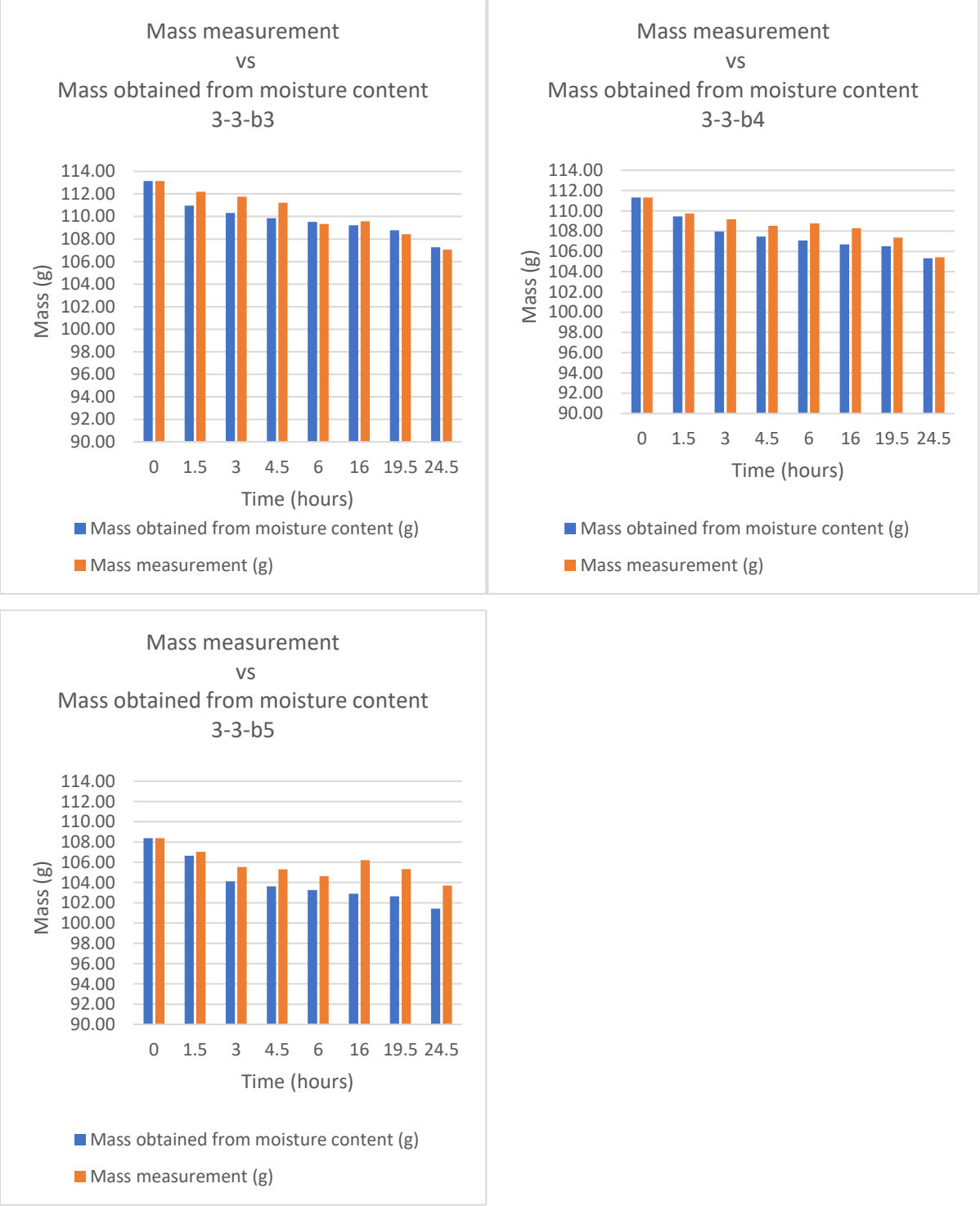

Figure p-4b-3. Mass from moisture content vs mass measurement (3-3-b3 ~ 3-3-b5)

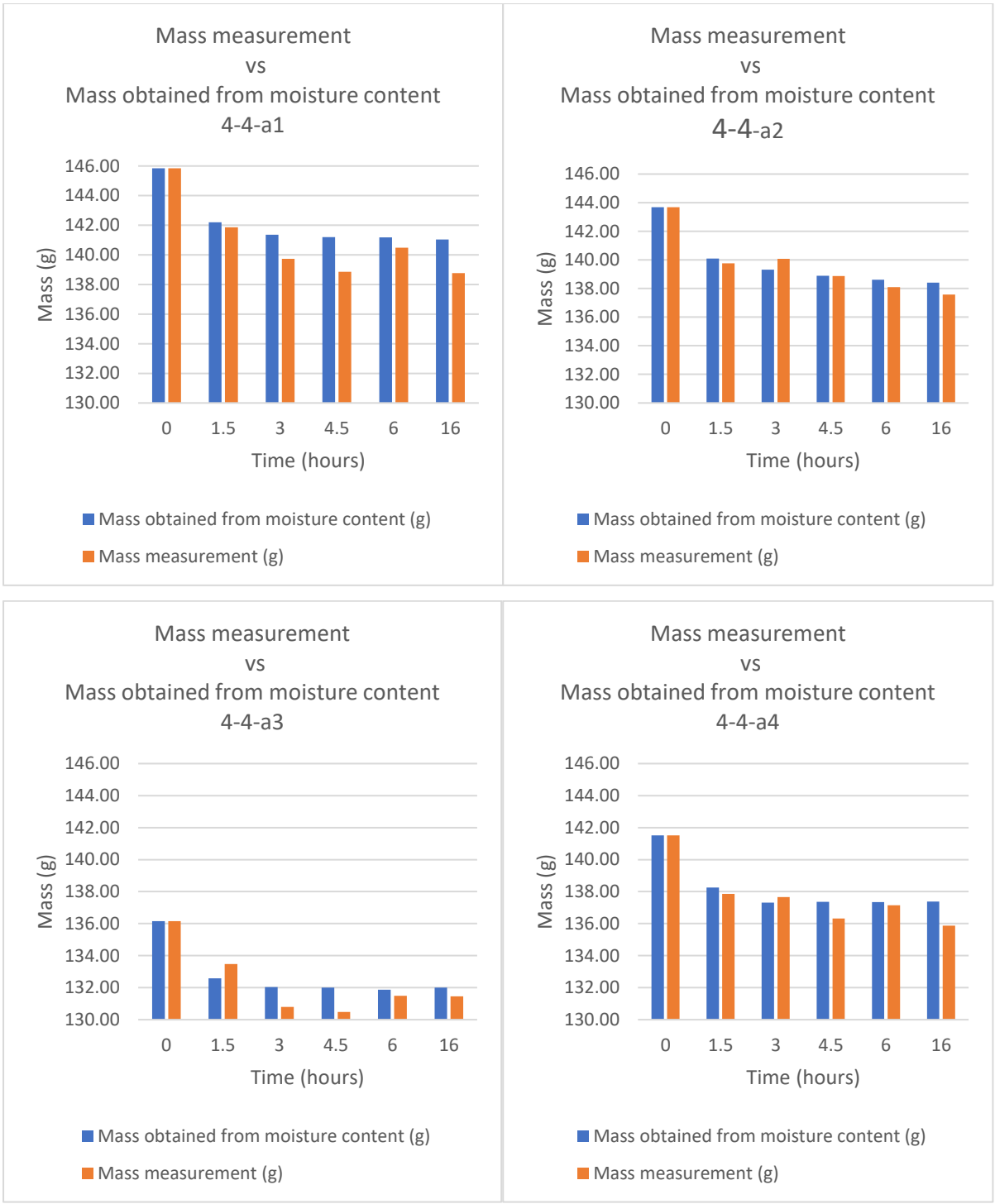

Figure p-4b-4. Mass from moisture content vs mass measurement (4-4-a1 ~ 4-4-a4)

Figure p-4b-5. Mass from moisture content vs mass measurement (4-4-a5, 4-4-b1, 4-4-b2)

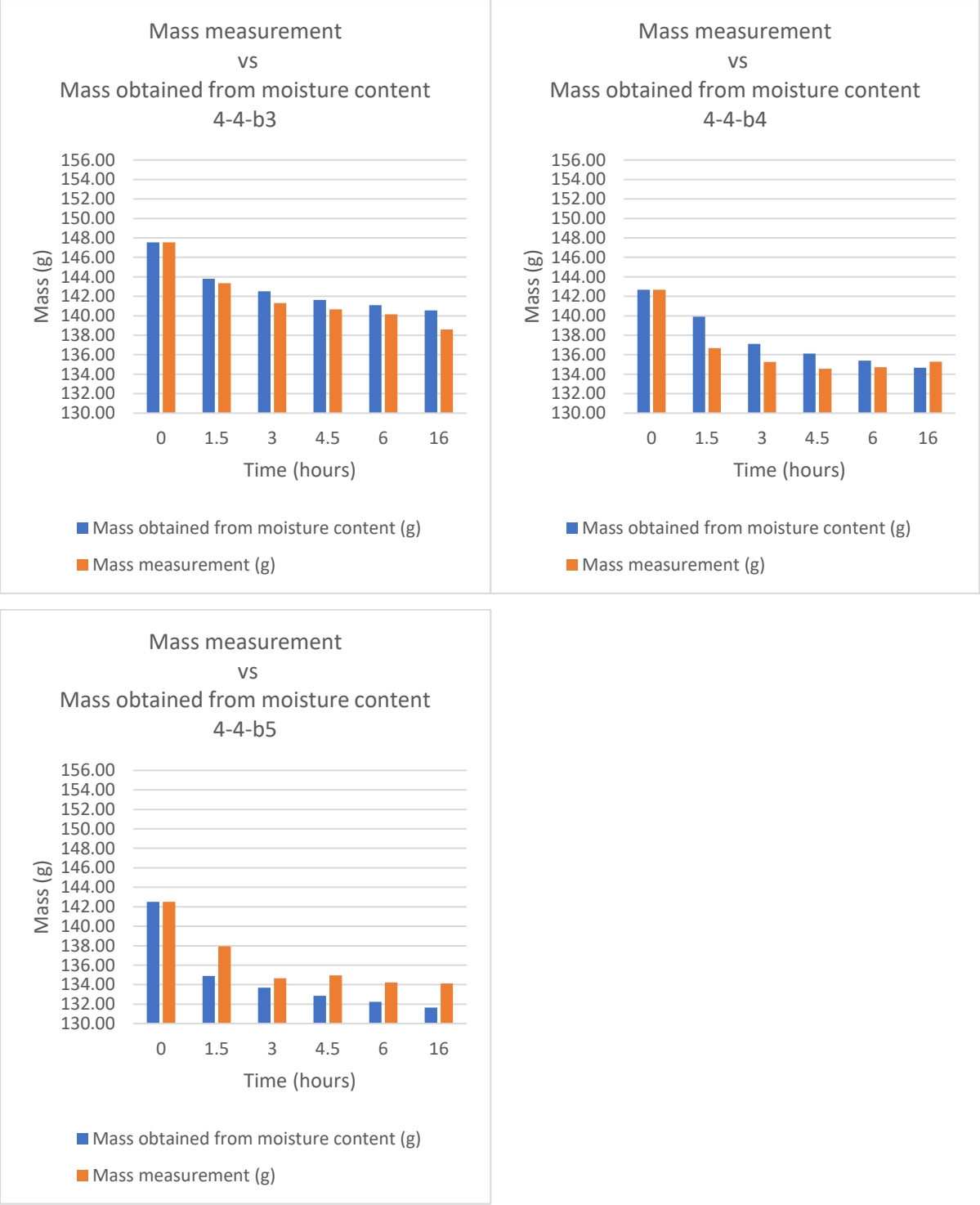

Figure p-4b-6. Mass from moisture content vs mass measurement (4-4-b3 ~ 4-4-b5)

Figure p-4b-7. Mass from moisture content vs mass measurement (3-4-a1 ~ 3-4-a4)

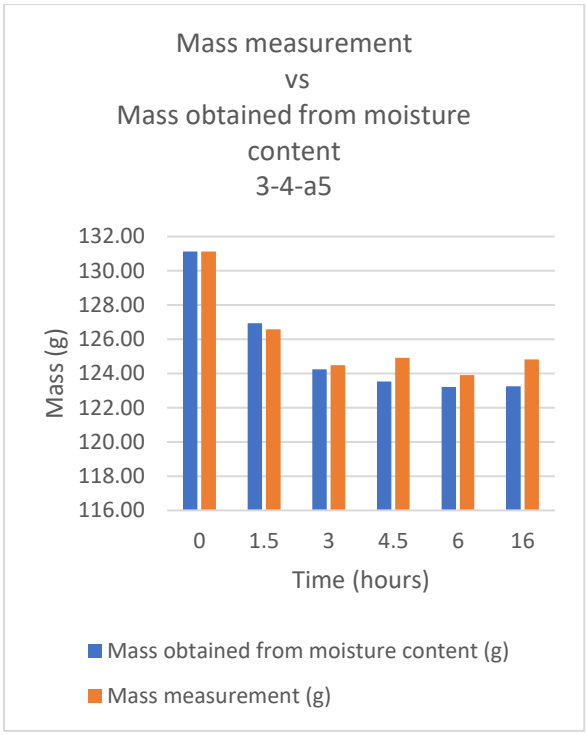

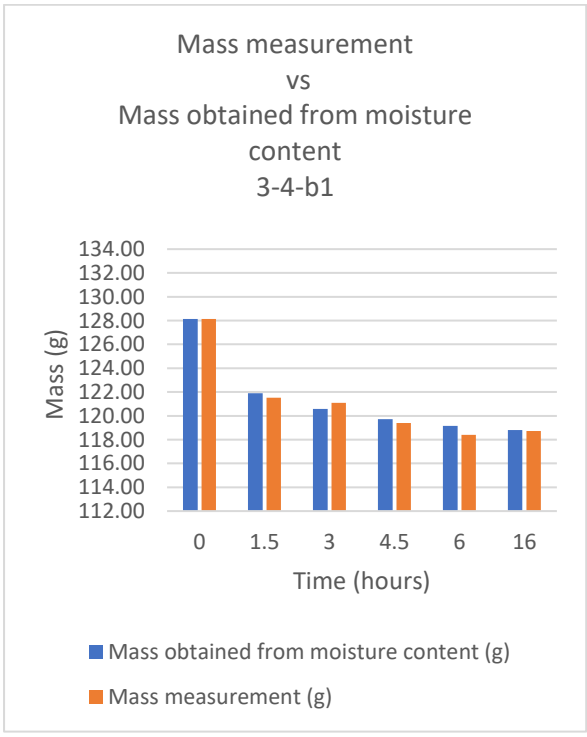

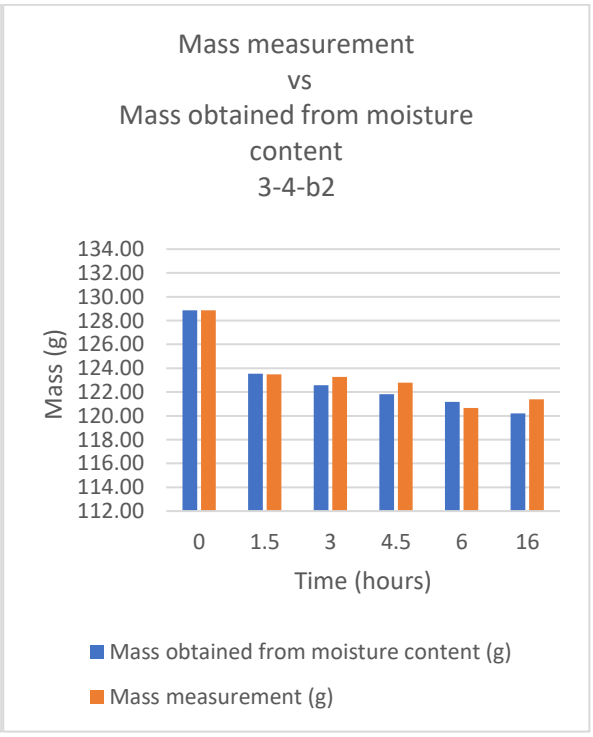

Figure p-4b-8. Mass from moisture content vs mass measurement (3-4-a5, 3-4-b1, 3-4-b2)

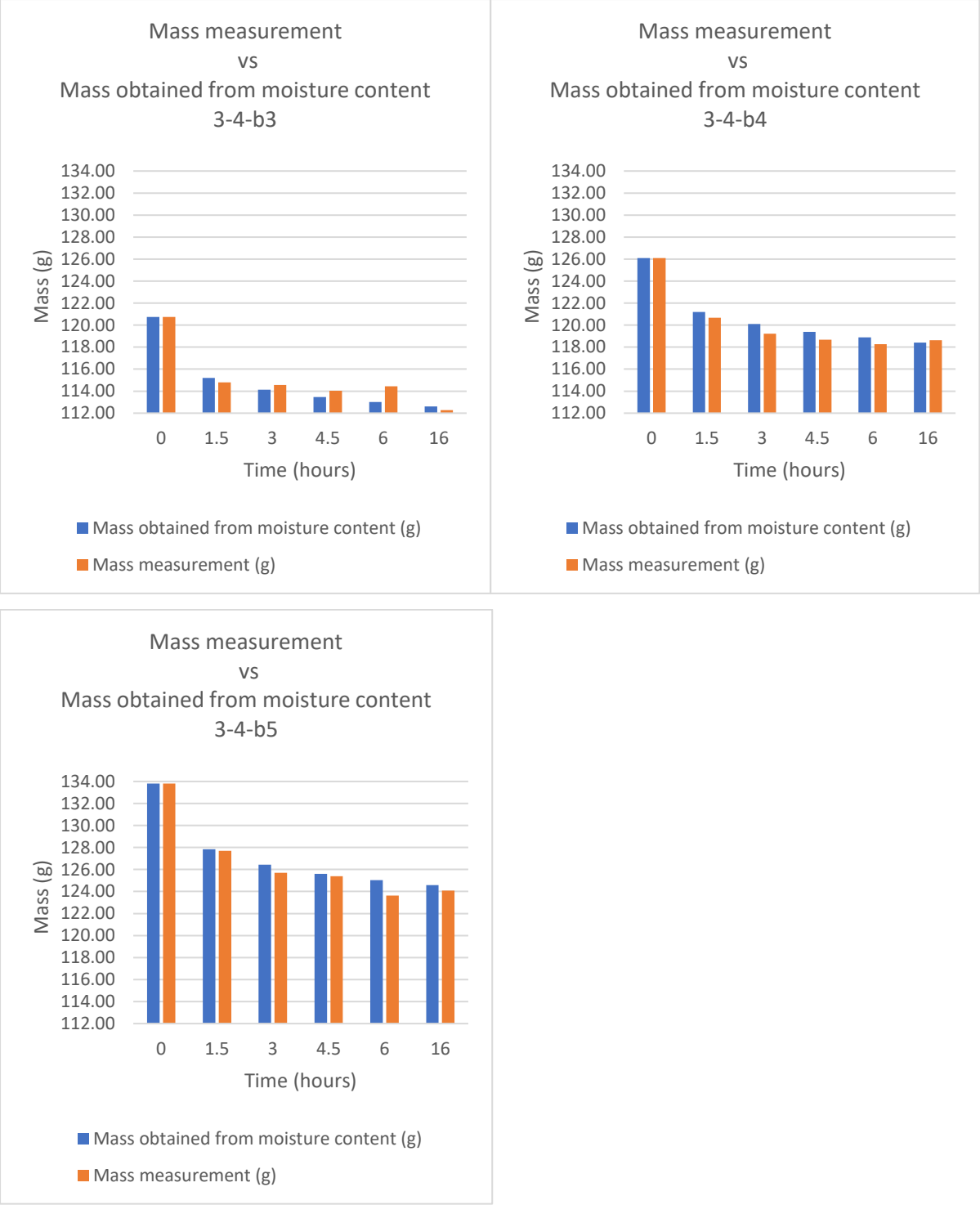

Figure p-4b-9. Mass from moisture content vs mass measurement (3-4-b3 ~3-4-b5)

ii) Moisture content over time graph trend compare with other researches.

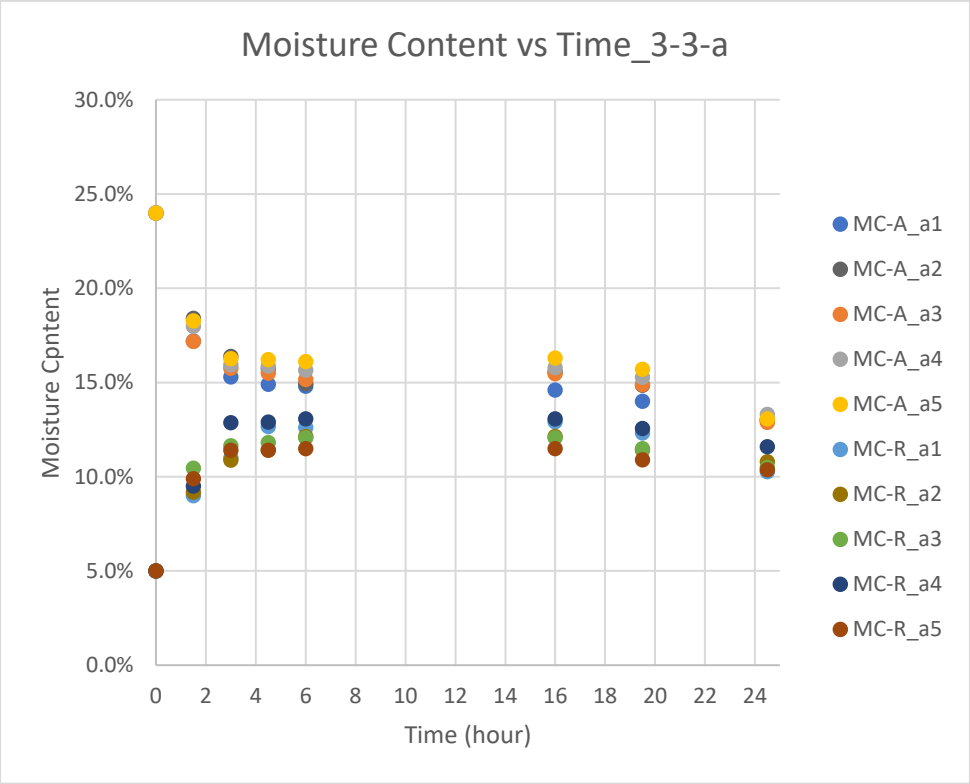

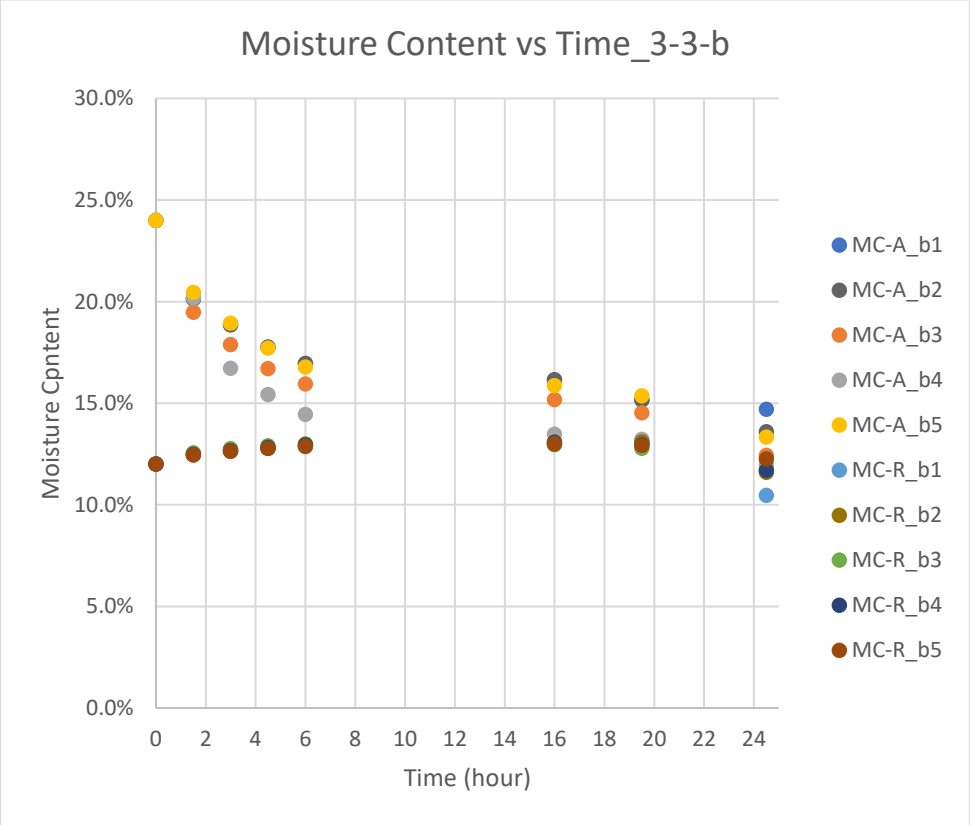

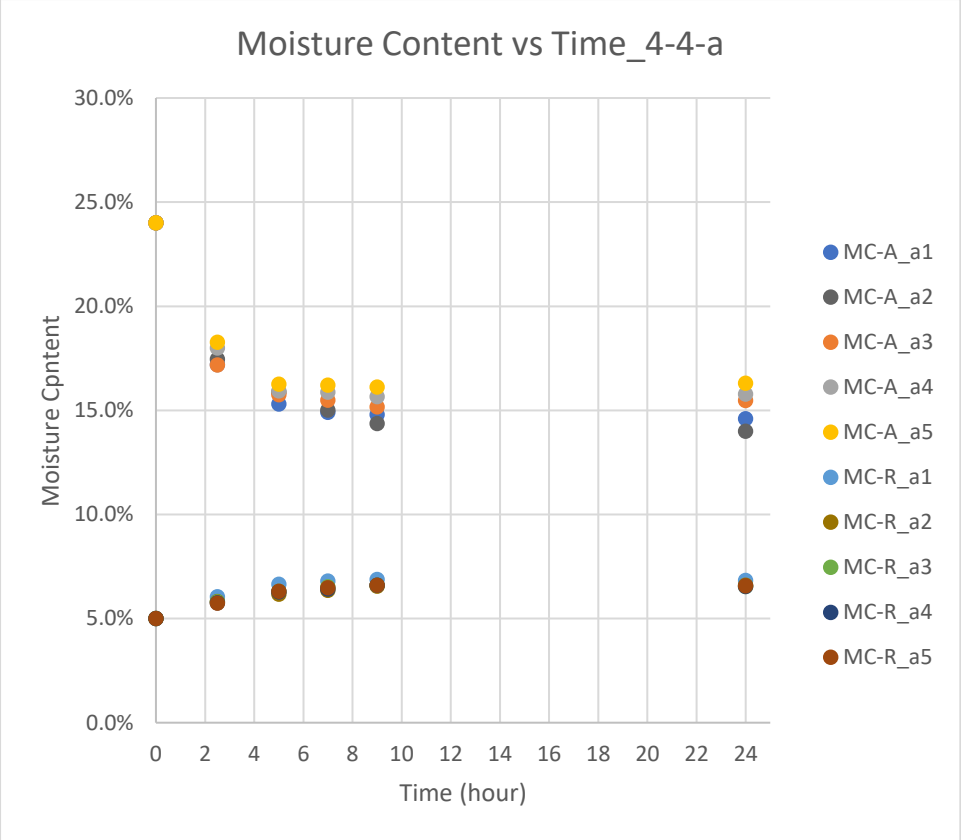
Moisture Content vs Time_4-4-a
Moisture Cpntent
30.0%
25.0%
20.0%
15.0%
10.0%
5.0%
0.0%
0 2 4 6 8 10 12 14 16 18 20 22 24
Time (hour)
MC-A_a1
MC-A_a2
MC-A_a3
MC-A_a4
MC-A_a5
MC-R_a1
MC-R_a2
MC-R_a3
MC-R_a4
MC-R_a5

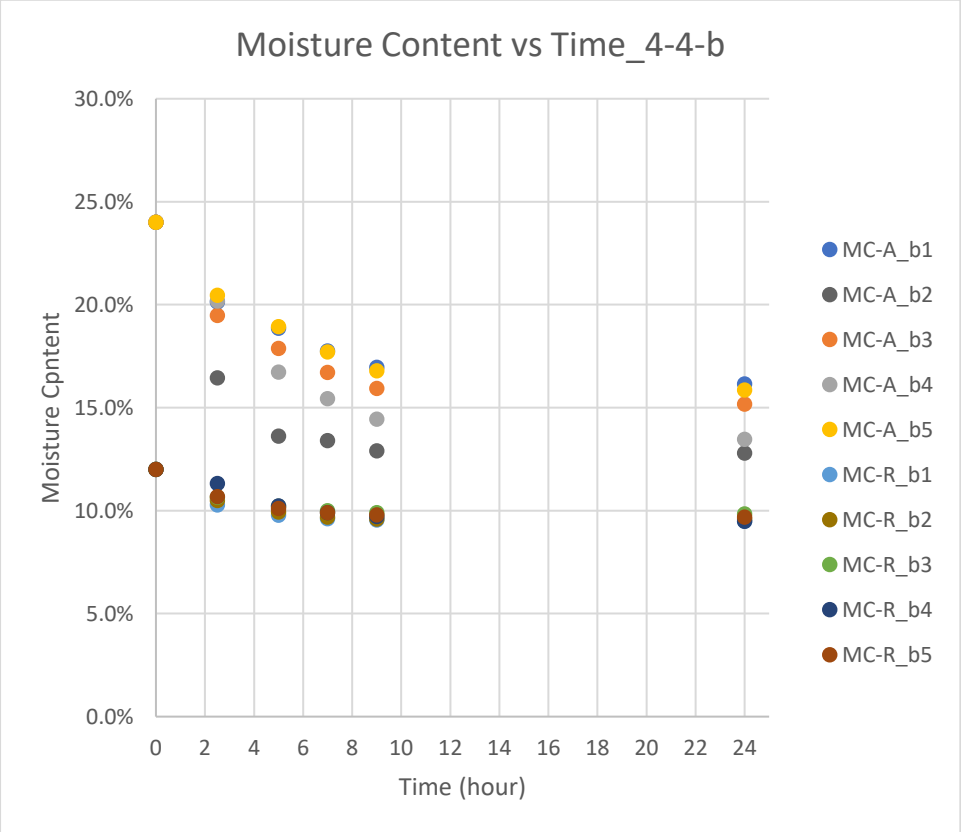
Moisture Content vs Time_4-4-b
Moisture Cpntent
30.0%
25.0%
20.0%
15.0%
10.0%
5.0%
0.0%
0 2 4 6 8 10 12 14 16 18 20 22 24
Time (hour)
MC-A_b1
MC-A_b2
MC-A_b3
MC-A_b4
MC-A_b5
MC-R_b1
MC-R_b2
MC-R_b3
MC-R_b4
MC-R_b5

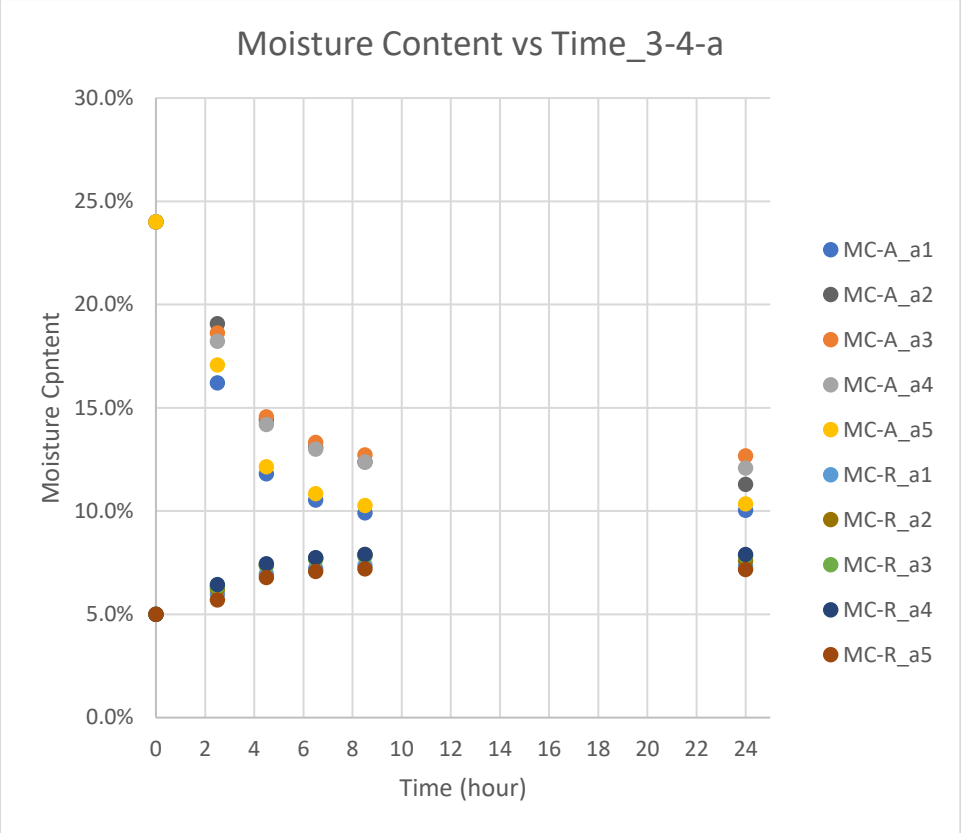

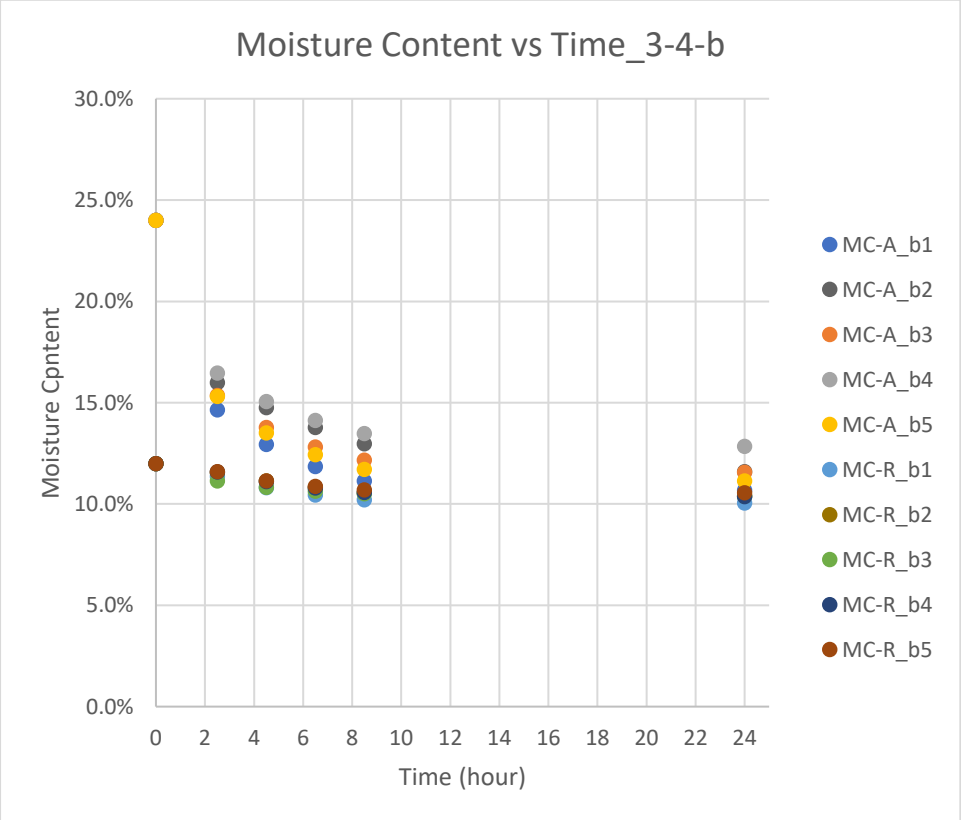

Figure p-4b-1. Graph of Group 3-3-a, 3-3-b, 4-4-a, 4-4-b and 3-4-a and 3-4-b. to compare with typical desorption and adsorption process shown below. The moisture content of restrictive layer of 3-4-b group has shown a desorption due to the environment condition has resulted in a lower equilibrium moisture content than the initial moisture content (Table p-3b).

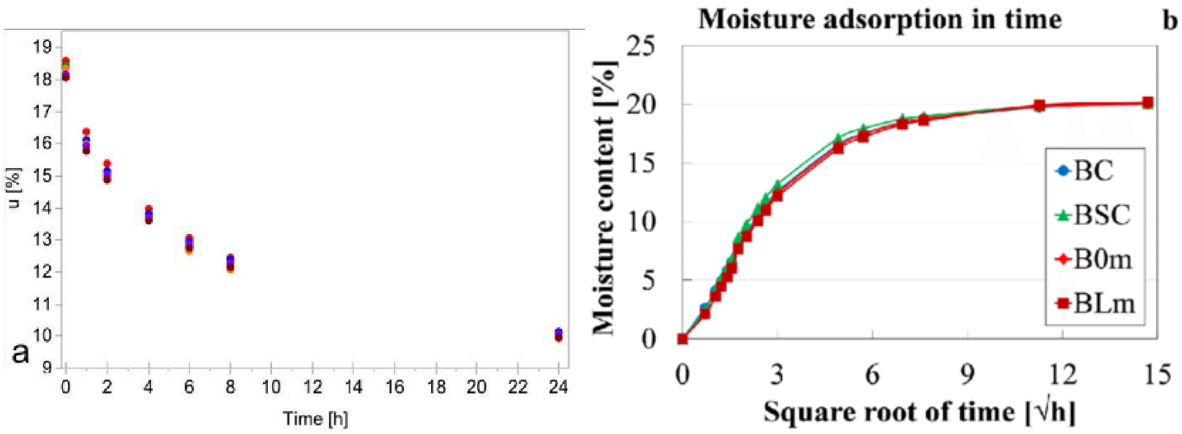

Figure p-4b-2: Typical desorption and adsorption curves over time.
Left: Desorption process of moisture content over time of the bi-layer component in an environment of relative humidity decreasing from 85% to 35% by Rüggeberg & Burgert, ETH 2015
Right: Adsorption process of moisture content over time of beech wood at 20 degree Celsius and relative humidity of 90% by Báder & Németh, 2017

Time (hr)	0	2.5	4.5	6.5	8.5	24
RH (%)	54%	51%	50%	51%	52%	56%
Temp (C)	19.8	19.9	20.0	19.9	19.9	19.8
EMC	9.8%	9.9%	9.4%	9.3%	9.4%	9.6%

Table p-4b. Condition for decreasing moisture content for 3-4-b group. Equilibrium moisture content (EMC) calculated using equation 1 in Chapter 1.

Appendix 4c – Collation of the measurements of moisture over time, curvature over time, relative humidity and temperature

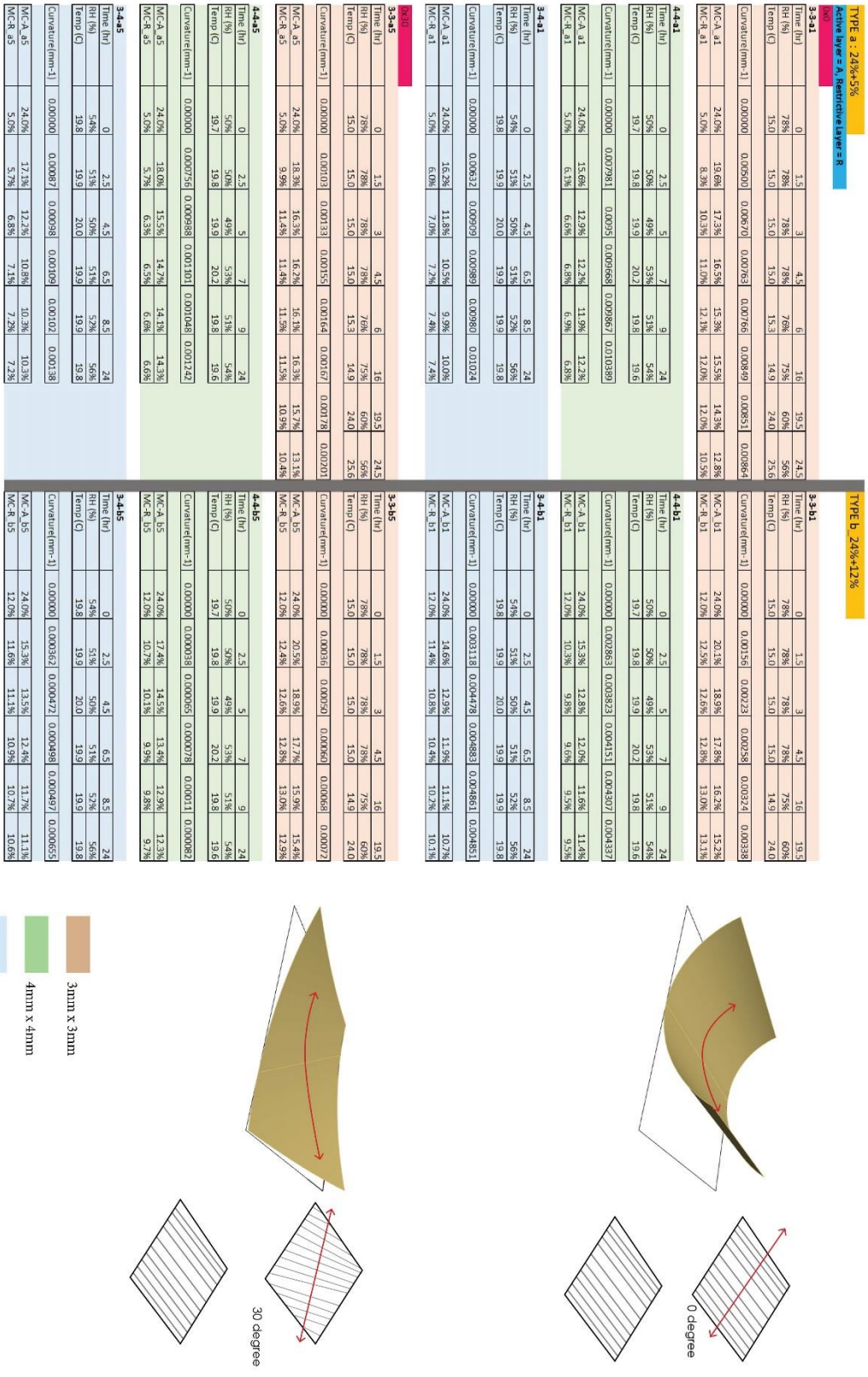

TYPE a : 24%+5%

Active layer = A, Restrictive Layer = R

0x45

3-3-a4

Time (hr)	0	1.5	3	4.5	6	16	19.5	24.5
RH (%)	78%	78%	78%	78%	76%	75%	60%	56%
Temp (C)	15.0	15.0	15.0	15.0	15.3	14.9	24.0	25.6
Curvature(mm-1)	0.00000	0.00082	0.00126	0.00135	0.00147	0.00172	0.00175	0.00178
MC-A_a4	24.0%	18.0%	15.9%	15.9%	15.7%	15.8%	15.3%	13.3%
MC-R_a4	5.0%	9.5%	12.9%	12.9%	13.1%	13.1%	12.6%	11.6%

4-4-a4

Time (hr)	0	2.5	5	7	9	24
RH (%)	50%	50%	49%	53%	51%	54%
Temp (C)	19.7	19.8	19.9	20.2	19.8	19.6
Curvature(mm-1)	0.00000	0.000131	0.000155	0.000142	0.000134	0.000139
MC-A_a4	24.0%	18.0%	15.6%	15.0%	14.3%	14.6%
MC-R_a4	5.0%	5.8%	6.3%	6.4%	6.6%	6.5%

3-4-a4

Time (hr)	0	2.5	4.5	6.5	8.5	24
RH (%)	54%	51%	50%	51%	52%	56%
Temp (C)	19.8	19.9	20.0	19.9	19.9	19.8
Curvature(mm-1)	0.00000	0.00017	0.00029	0.00027	0.00023	0.00019
MC-A_a4	24.0%	18.2%	14.2%	13.0%	12.4%	12.1%
MC-R_a4	5.0%	6.4%	7.5%	7.7%	7.9%	7.9%

0x60

3-3-a3

Time (hr)	0	1.5	3	4.5	6	16	19.5	24.5
RH (%)	78%	78%	78%	78%	76%	75%	60%	56%
Temp (C)	15.0	15.0	15.0	15.0	15.3	14.9	24.0	25.6
Curvature(mm-1)	0.00006	0.00064	0.00081	0.00093	0.00102	0.00115	0.00112	0.00108
MC-A_a3	24.0%	17.2%	15.8%	15.5%	15.2%	15.5%	14.9%	12.9%
MC-R_a3	5.0%	10.5%	11.6%	11.8%	12.1%	12.1%	11.5%	10.5%

4-4-a3

Time (hr)	0	2.5	5	7	9	24
RH (%)	50%	50%	49%	53%	51%	54%
Temp (C)	19.7	19.8	19.9	20.2	19.8	19.6
Curvature(mm-1)	0.00000	0.0002	0.000348	0.000406	0.00047	0.00051
MC-A_a3	24.0%	17.5%	15.2%	14.6%	14.3%	14.8%
MC-R_a3	5.0%	5.8%	6.3%	6.5%	6.6%	6.5%

3-4-a3

Time (hr)	0	2.5	4.5	6.5	8.5	24
RH (%)	54%	51%	50%	51%	52%	56%
Temp (C)	19.8	19.9	20.0	19.9	19.9	19.8
Curvature(mm-1)	0.00000	0.00027	0.00034	0.00036	0.00038	0.00041
MC-A_a3	24.0%	18.6%	14.6%	13.3%	12.7%	12.7%
MC-R_a3	5.0%	6.3%	7.4%	7.7%	7.8%	7.8%

TYPE b_24%+12%

3-3-b4

Time (hr)	0	1.5	3	4.5	16	19.5
RH (%)	78%	78%	78%	78%	75%	60%
Temp (C)	15.0	15.0	15.0	15.0	14.9	24.0
Curvature(mm-1)	0.00000	0.00033	0.00041	0.00052	0.00061	0.00072
MC-A_b4	24.0%	20.2%	18.6%	17.3%	15.3%	15.1%
MC-R_b4	12.0%	12.5%	12.7%	12.8%	13.1%	13.0%

4-4-b4

Time (hr)	0	2.5	5	7	9	24
RH (%)	50%	50%	49%	53%	51%	54%
Temp (C)	19.7	19.8	19.9	20.2	19.8	19.6
Curvature(mm-1)	0.00000	0.000152	0.000206	0.000252	0.000264	0.00024
MC-A_b4	24.0%	18.1%	15.9%	15.2%	14.7%	14.2%
MC-R_b4	12.0%	11.3%	10.2%	9.9%	9.7%	9.5%

3-4-b4

Time (hr)	0	2.5	4.5	6.5	8.5	24
RH (%)	54%	51%	50%	51%	52%	56%
Temp (C)	19.8	19.9	20.0	19.9	19.9	19.8
Curvature(mm-1)	0.00000	0.000057	6.70E-05	0.00006	3.80E-05	0.000036
MC-A_b4	24.0%	16.5%	15.1%	14.1%	13.5%	12.8%
MC-R_b4	12.0%	11.6%	11.1%	10.8%	10.6%	10.4%

3-3-b3

Time (hr)	0	1.5	3	4.5	16	19.5
RH (%)	78%	78%	78%	78%	75%	60%
Temp (C)	15.0	15.0	15.0	15.0	14.9	24.0
Curvature(mm-1)	0.00000	0.00029	0.00038	0.00041	0.00044	0.00044
MC-A_b3	24.0%	19.5%	17.9%	16.7%	15.2%	14.5%
MC-R_b3	12.0%	12.6%	12.8%	12.9%	13.1%	12.8%

4-4-b3

Time (hr)	0	2.5	5	7	9	24
RH (%)	50%	50%	49%	53%	51%	54%
Temp (C)	19.7	19.8	19.9	20.2	19.8	19.6
Curvature(mm-1)	0.00000	0.000036	0.00007	0.000079	0.000081	0.000096
MC-A_b3	24.0%	17.2%	15.0%	13.9%	13.5%	13.1%
MC-R_b3	12.0%	10.7%	10.2%	10.0%	9.9%	9.8%

3-4-b3

Time (hr)	0	2.5	4.5	6.5	8.5	24
RH (%)	54%	51%	50%	51%	52%	56%
Temp (C)	19.8	19.9	20.0	19.9	19.9	19.8
Curvature(mm-1)	0.00000	0.000061	0.000092	0.000124	0.00013	0.00014
MC-A_b3	24.0%	15.4%	13.8%	12.8%	12.2%	11.6%
MC-R_b3	12.0%	11.1%	10.8%	10.6%	10.5%	10.4%

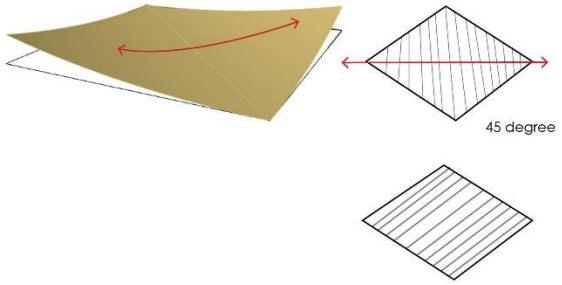

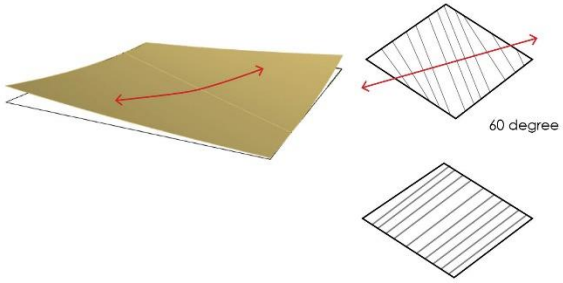

3mm x 3mm

4mm x 4mm

3mm x 4mm

TYPE a : 24%+5%

Active layer = A, Restrictive Layer = R

0x90

3-3-a2

Time (hr)	0	1.5	3	4.5	6	16	19.5	24.5
RH (%)	78%	78%	78%	78%	76%	75%	60%	56%
Temp (C)	15.0	15.0	15.0	15.0	15.3	14.9	24.0	25.6
Curvature(mm-1)	0.00000	0.00000	0.00000	0.00000	0.00000	0.00000	0.00000	0.00000
MC-A_a2	24.0%	18.4%	16.4%	15.7%	14.9%	15.6%	14.9%	13.0%
MC-R_a2	5.0%	9.2%	10.9%	11.4%	12.1%	12.1%	11.4%	10.8%

4-4-a2

Time (hr)	0	2.5	5	7	9	24
RH (%)	50%	50%	49%	53%	51%	54%
Temp (C)	19.7	19.8	19.9	20.2	19.8	19.6
Curvature(mm-1)	0.00000	0.00000	0.00000	0.00000	0.00000	0.00000
MC-A_a2	24.0%	17.5%	15.9%	15.0%	14.4%	14.0%
MC-R_a2	5.0%	5.8%	6.2%	6.4%	6.6%	6.6%

3-4-a2

Time (hr)	0	2.5	4.5	6.5	8.5	24
RH (%)	54%	51%	50%	51%	52%	56%
Temp (C)	19.8	19.9	20.0	19.9	19.9	19.8
Curvature(mm-1)	0.00000	0.00000	0.00000	0.00000	0.00000	0.00000
MC-A_a2	24.0%	19.1%	14.4%	13.1%	12.4%	11.3%
MC-R_a2	5.0%	6.2%	7.4%	7.7%	7.9%	7.6%

TYPE b_24%+12%

3-3-b2

Time (hr)	0	1.5	3	4.5	16	19.5
RH (%)	78%	78%	78%	78%	75%	60%
Temp (C)	15.0	15.0	15.0	15.0	14.9	24.0
Curvature(mm-1)	0.00000	0.00000	0.00000	0.00000	0.00000	0.00000
MC-A_b2	24.0%	20.1%	18.9%	17.8%	16.2%	15.2%
MC-R_b2	12.0%	12.5%	12.6%	12.8%	13.0%	13.1%

4-4-b2

Time (hr)	0	2.5	5	7	9	24
RH (%)	50%	50%	49%	53%	51%	54%
Temp (C)	19.7	19.8	19.9	20.2	19.8	19.6
Curvature(mm-1)	0.00000	0.00000	0.00000	0.00000	0.00000	0.00000
MC-A_b2	24.0%	16.4%	13.6%	13.4%	12.9%	12.8%
MC-R_b2	12.0%	10.5%	9.9%	9.7%	9.6%	9.6%

3-4-b2

Time (hr)	0	2.5	4.5	6.5	8.5	24
RH (%)	54%	51%	50%	51%	52%	56%
Temp (C)	19.8	19.9	20.0	19.9	19.9	19.8
Curvature(mm-1)	0.00000	0.00000	0.00000	0.00000	0.00000	0.00000
MC-A_b2	24.0%	16.0%	14.8%	13.8%	13.0%	11.6%
MC-R_b2	12.0%	11.6%	11.1%	10.8%	10.6%	10.4%

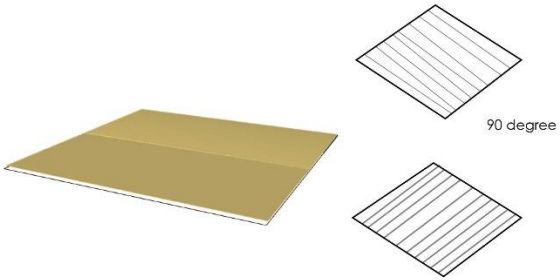

3mm x 3mm

4mm x 4mm

3mm x 4mm

Appendix 5a – Graph of curvature of time plotted by groups and time.

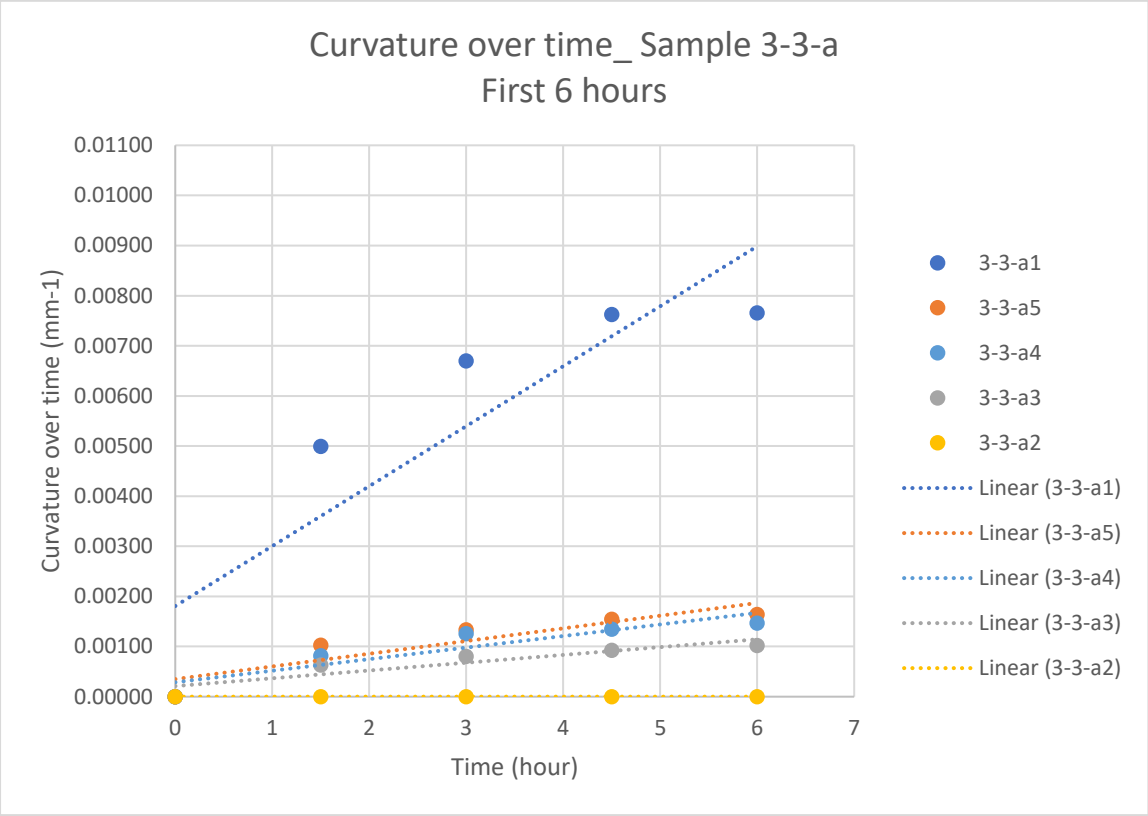

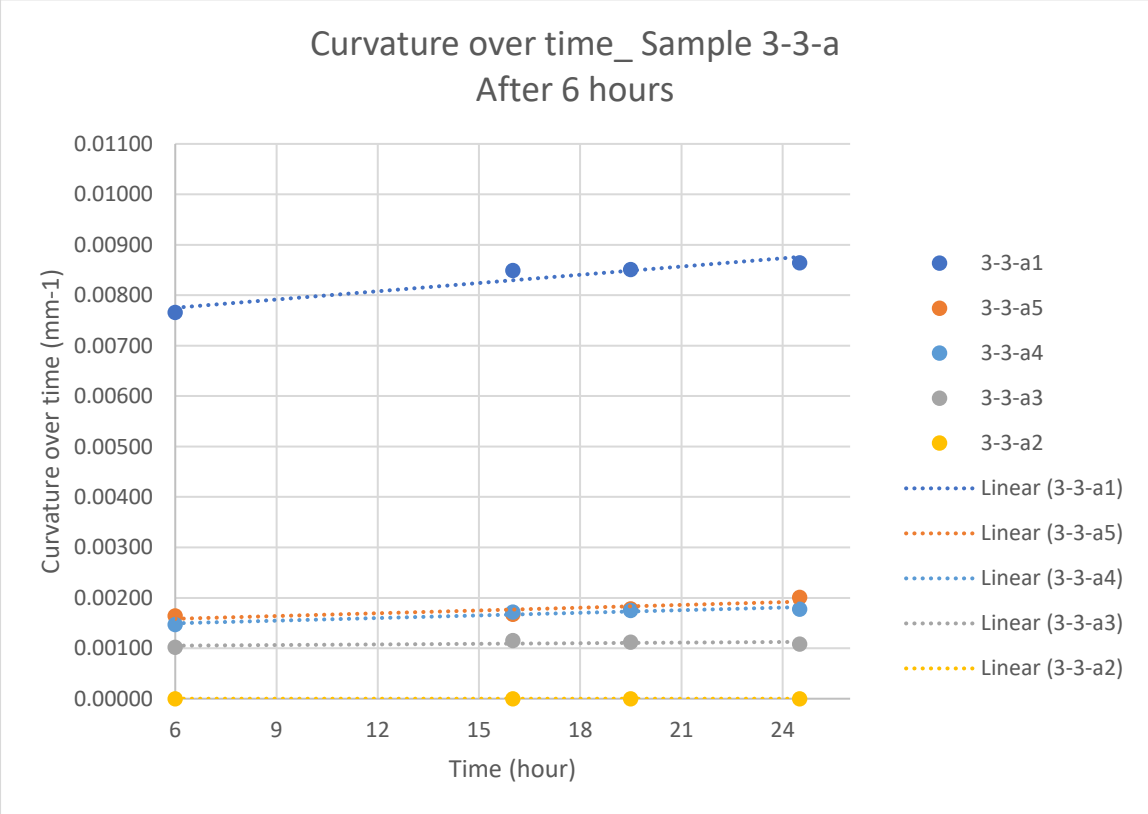

Figure p-5a. Curvature over time plotted before and after 6 hours

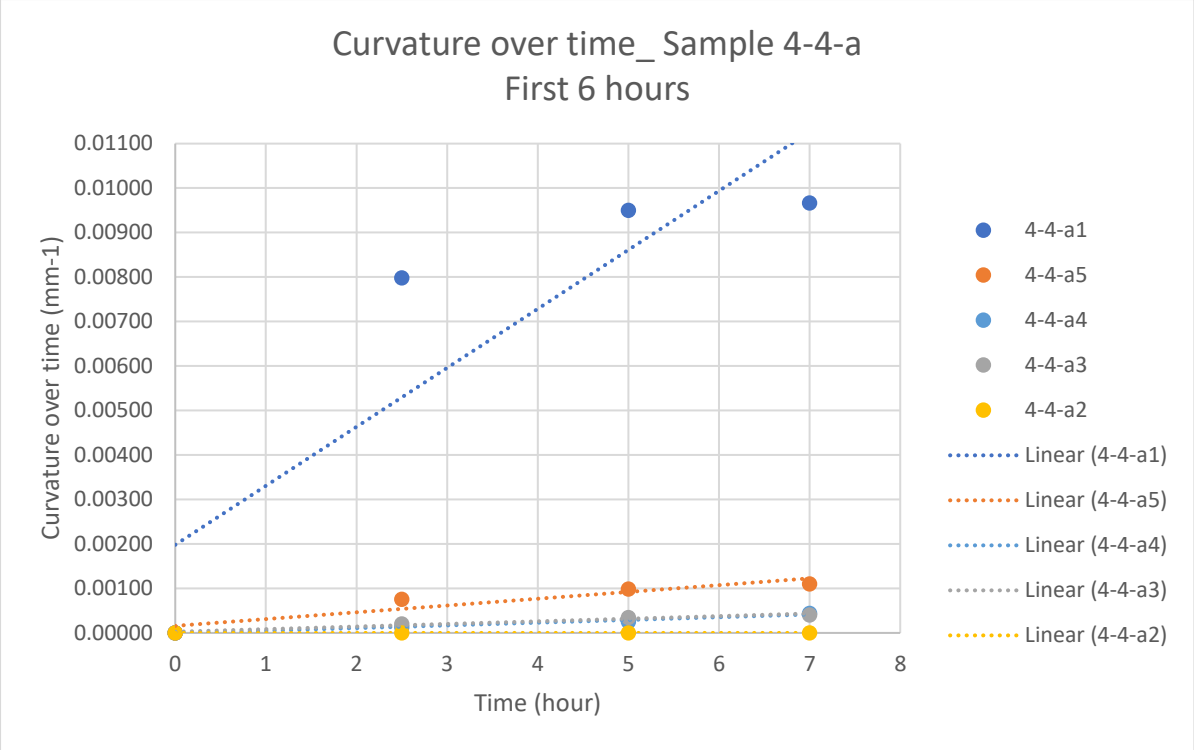

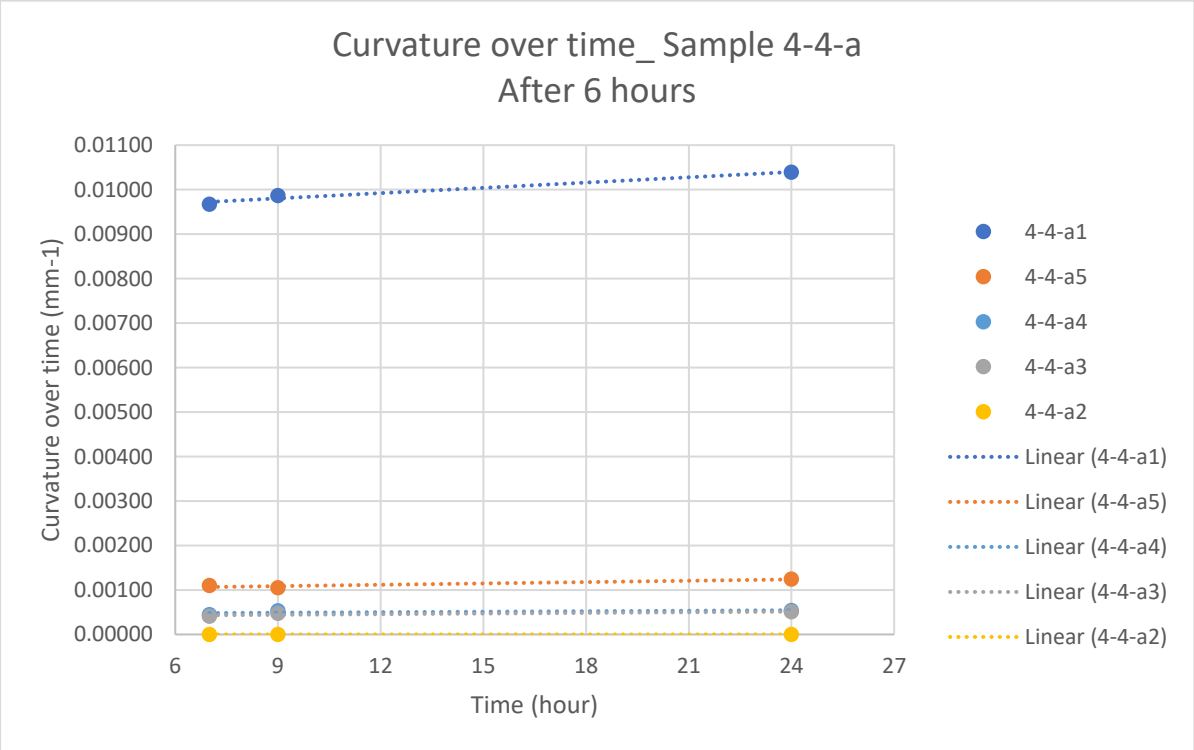

Figure p-5a. Curvature over time plotted before and after 6 hours (continued)

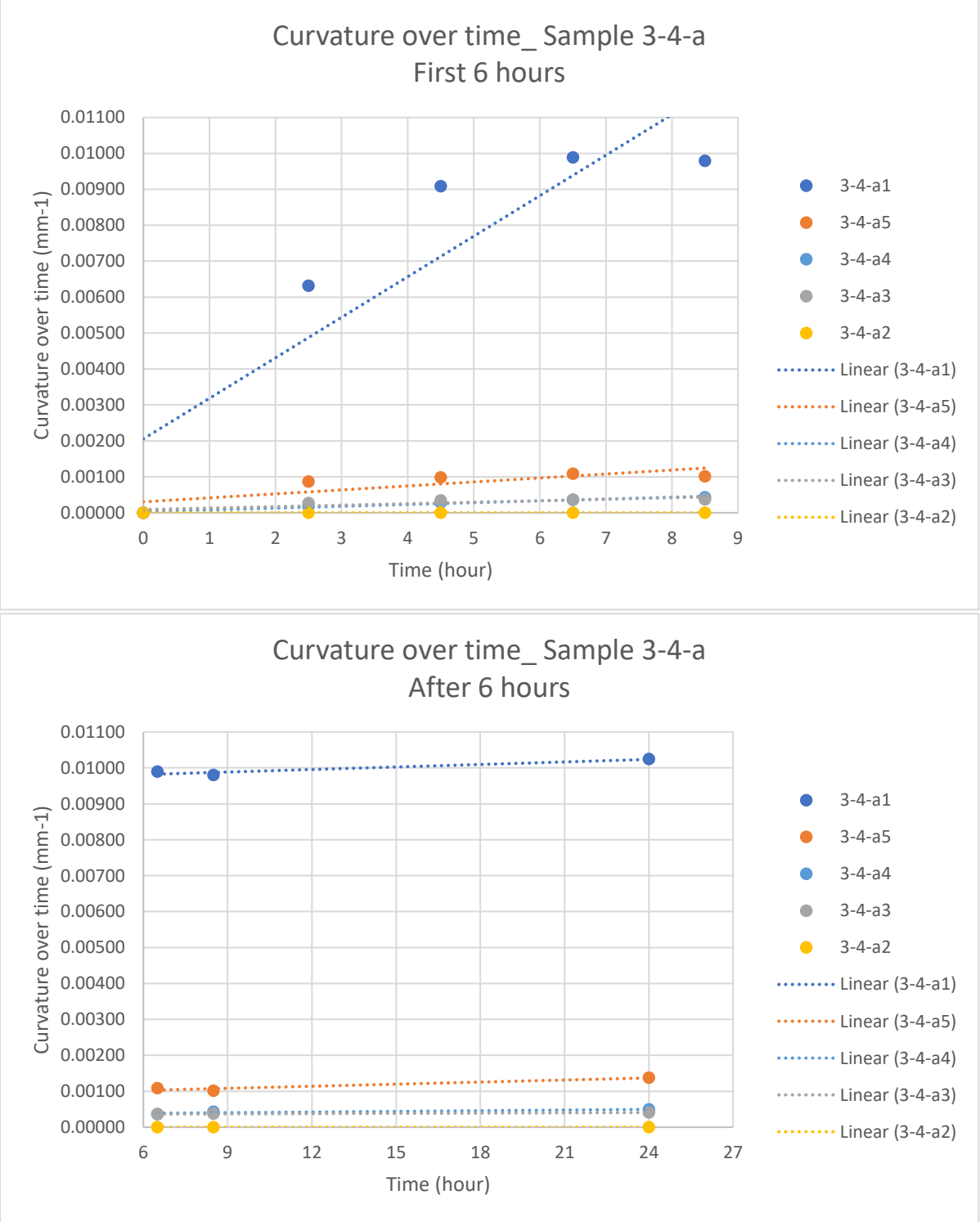

Figure p-5a. Curvature over time plotted before and after 6 hours (continued).

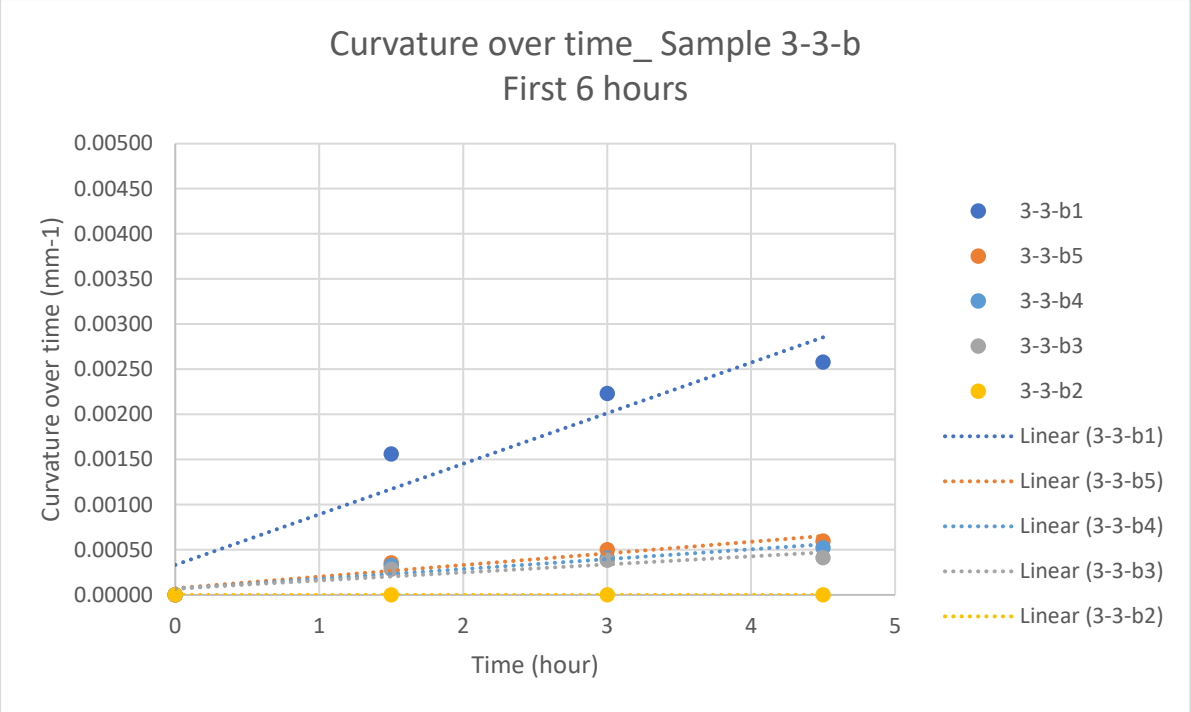

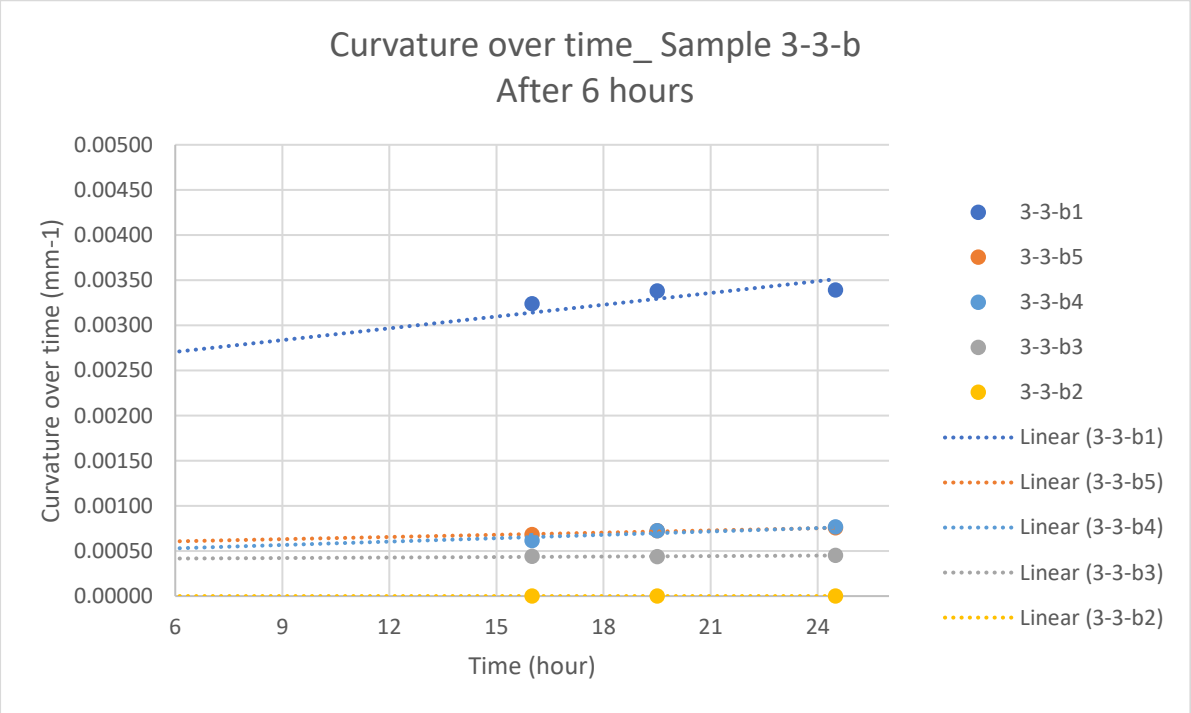

Figure p-5a. Curvature over time plotted before and after 6 hours (continued).

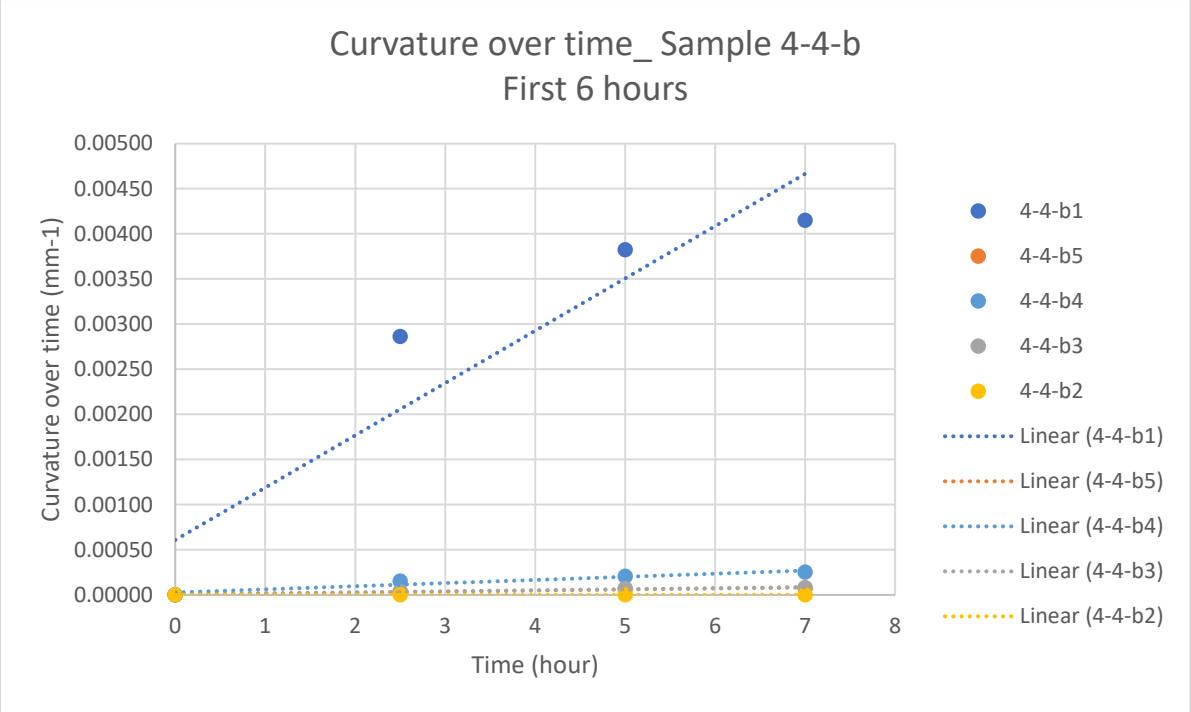

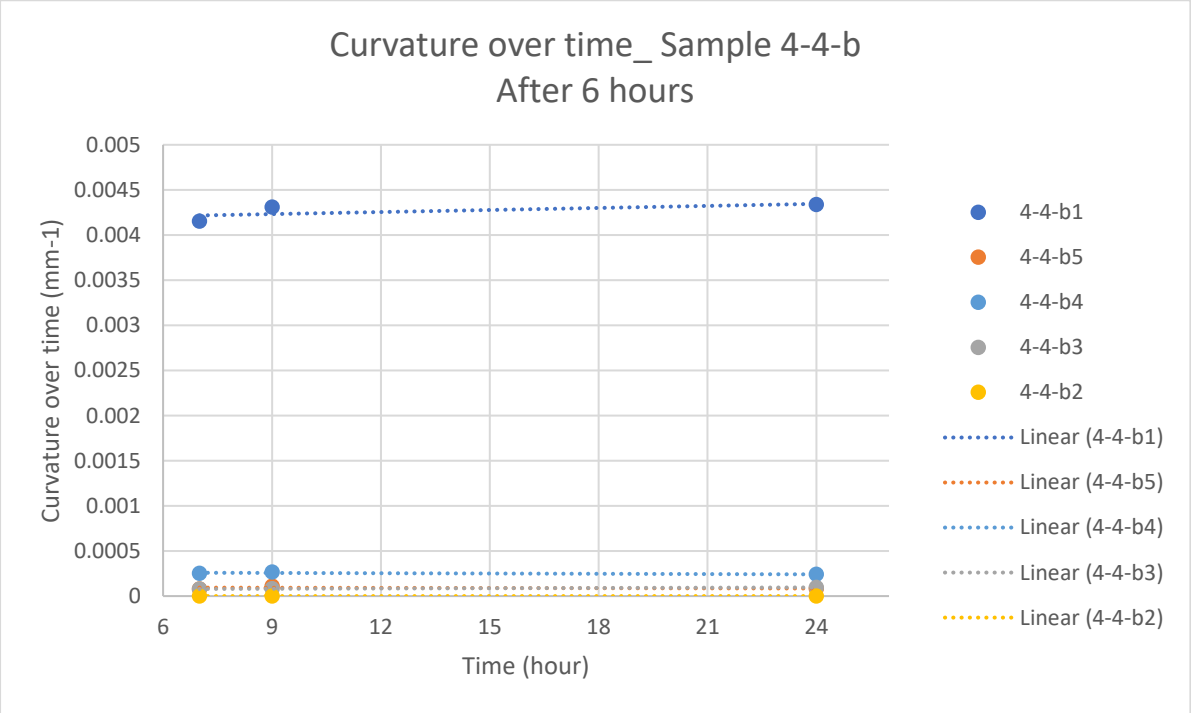

Figure p-5a. Curvature over time plotted before and after 6 hours (continued).

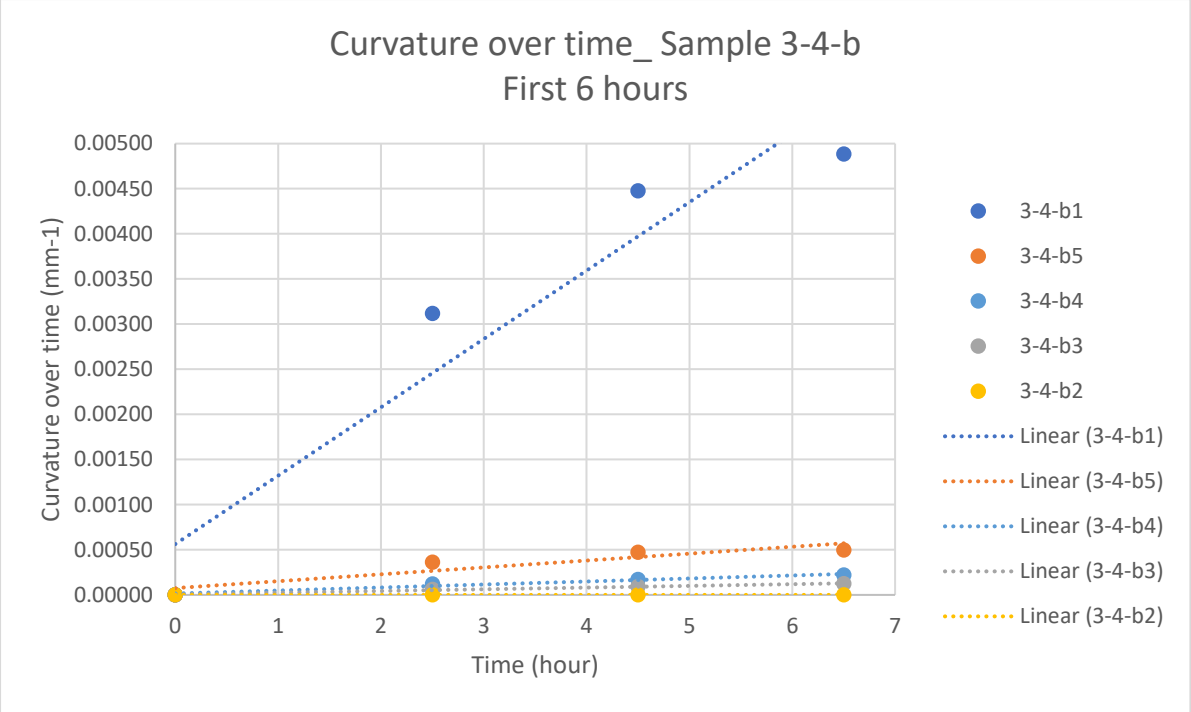

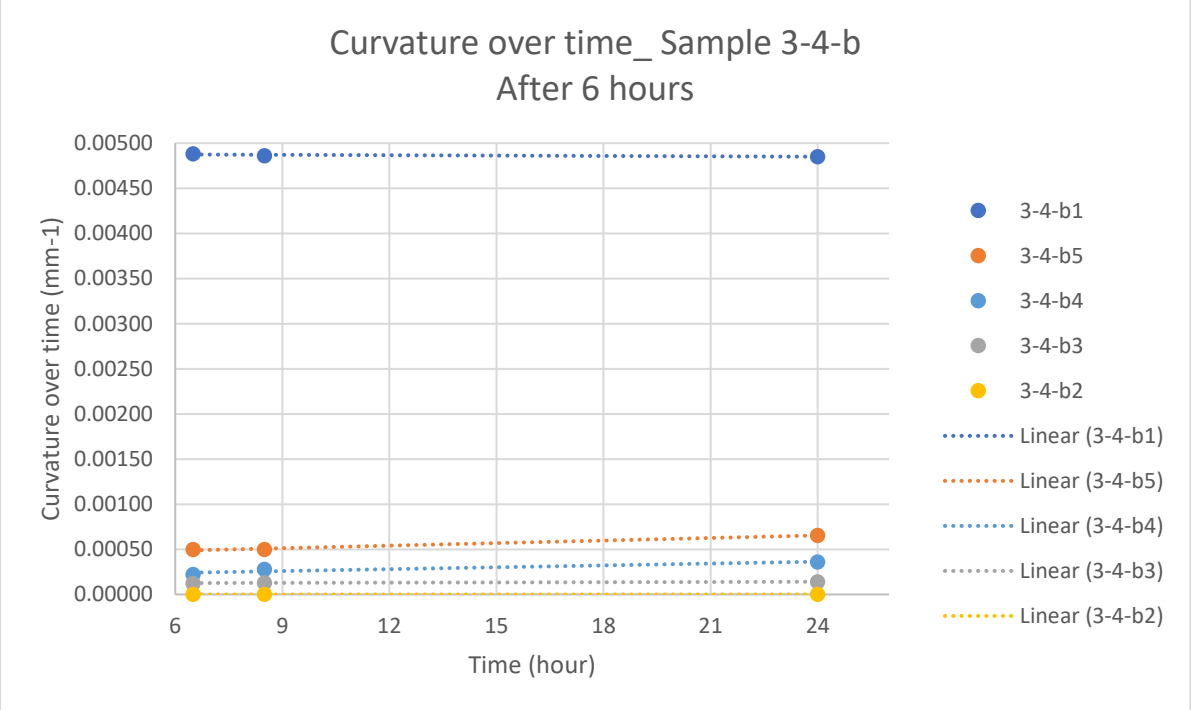

Figure p-5a. Curvature over time plotted before and after 6 hours (continued).

Appendix 5b – Graph of curvature of time plotted by thickness.

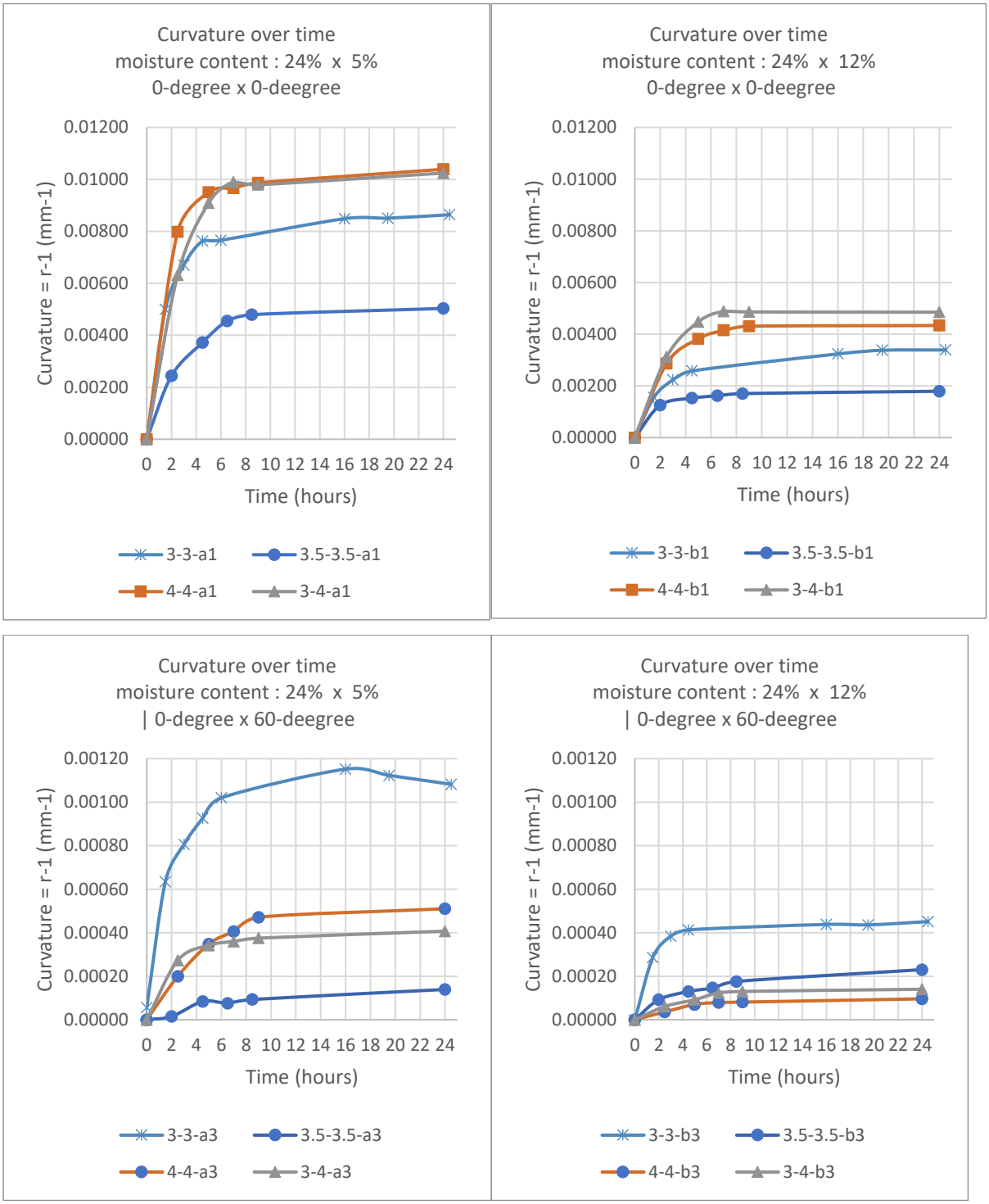

Figure p-5b. curvature over time of samples of the same orientation and moisture content but different thicknesses.

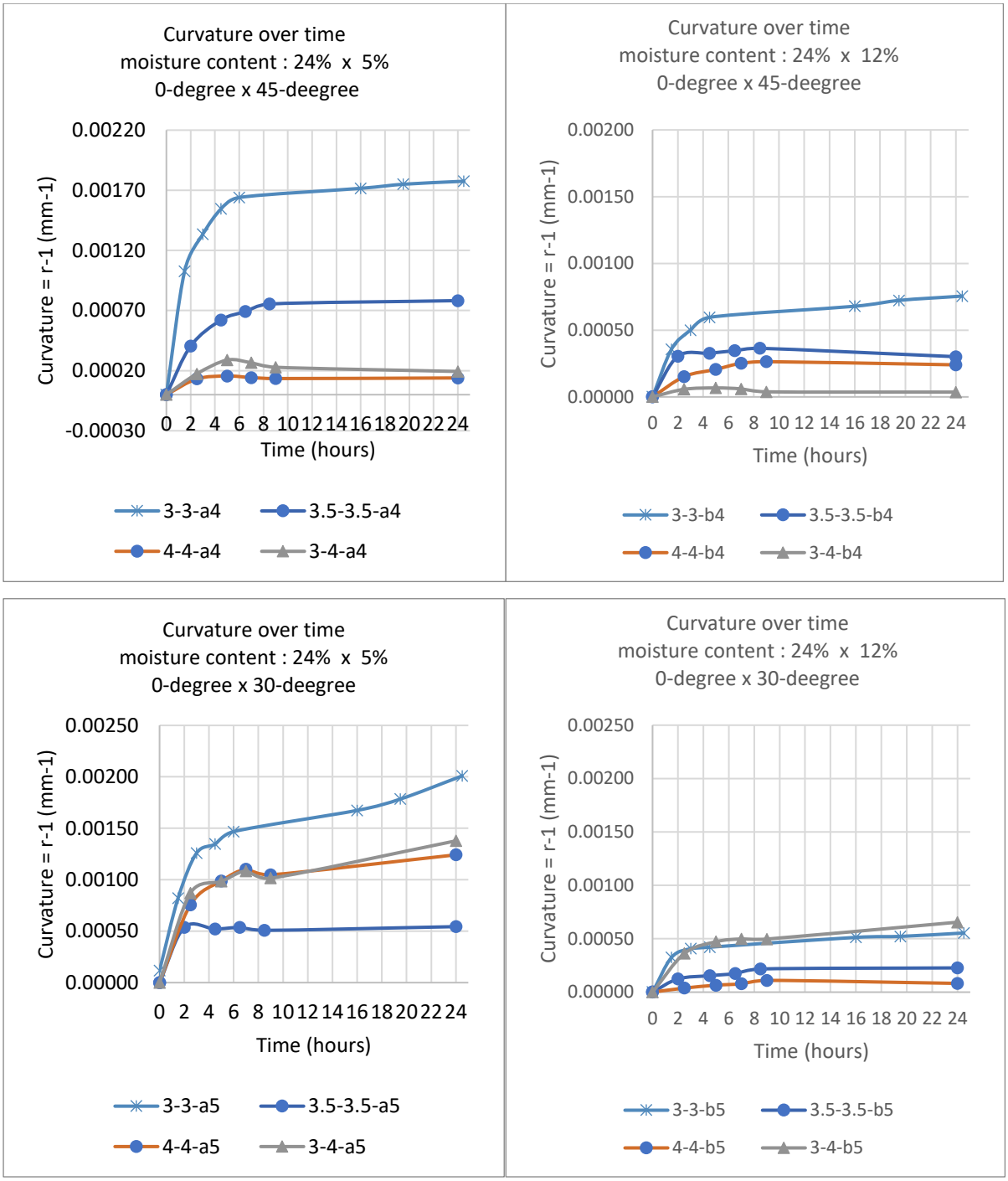

Figure p-5b. curvature over time of samples of the same orientation and moisture content but different thicknesses. (continued)

Appendix 6 – Deformation measurement data

Measurement data of samples of 3-3-a group are shown below.

Sample 3-3-a2 was lacking data for the last measurement as there was no deformation due to the perpendicular combination of the fiber orientations.

Sample 3-3-a1

17:30	19:01	20:31	22:11	23:34	9:09	12:47	16:27	20:02	20:39	20:14	13:00+1day
94.55 mm	81.75 mm	71.55 mm	67.20 mm	60.45 mm	54.60 mm	54.25 mm	48.25 mm	49.60 mm	45.40 mm	43.15 mm	44.65 mm
88.75 mm	94.65 mm	93.40 mm	92.10 mm	90.35 mm	89.65 mm	86.95 mm	89.85 mm	90.25 mm	89.55 mm	87.60 mm	91.05 mm
86.50 mm	97.10 mm	97.90 mm	97.95 mm	98.60 mm	99.05 mm	98.30 mm	97.15 mm	97.20 mm	97.95 mm	98.00 mm	97.50 mm
87.65 mm	85.70 mm	84.65 mm	84.70 mm	86.85 mm	87.15 mm	88.50 mm	80.50 mm	77.70 mm	77.05 mm	80.25 mm	75.75 mm
94.10 mm	57.75 mm	50.80 mm	44.60 mm	47.45 mm	44.70 mm	48.95 mm	55.85 mm	55.15 mm	47.45 mm	25.15 mm	27.95 mm
95.00 mm	79.40 mm	70.55 mm	64.50 mm	59.00 mm	53.70 mm	53.70 mm	47.90 mm	48.35 mm	44.25 mm	42.70 mm	45.80 mm
89.45 mm	94.30 mm	93.25 mm	92.10 mm	90.35 mm	88.90 mm	87.15 mm	89.75 mm	90.25 mm	89.90 mm	87.90 mm	91.35 mm
86.00 mm	97.20 mm	98.30 mm	97.35 mm	98.10 mm	98.80 mm	98.25 mm	97.25 mm	97.65 mm	97.65 mm	97.90 mm	98.65 mm
87.65 mm	86.90 mm	85.40 mm	83.80 mm	86.90 mm	87.60 mm	88.20 mm	80.40 mm	79.00 mm	77.00 mm	81.20 mm	75.95 mm
94.25 mm	60.00 mm	50.65 mm	46.10 mm	49.40 mm	45.60 mm	46.65 mm	54.40 mm	54.90 mm	48.15 mm	28.55 mm	27.10 mm
94.75 mm	80.95 mm	70.00 mm	65.15 mm	58.50 mm	52.75 mm	53.25 mm	47.60 mm	47.35 mm	45.10 mm	40.70 mm	43.55 mm
89.00 mm	94.60 mm	93.50 mm	91.45 mm	89.35 mm	88.65 mm	86.35 mm	89.20 mm	89.55 mm	89.25 mm	86.90 mm	91.50 mm
86.50 mm	97.85 mm	98.10 mm	97.70 mm	97.95 mm	98.00 mm	97.80 mm	97.80 mm	97.35 mm	98.70 mm	98.30 mm	97.95 mm
87.70 mm	86.70 mm	85.40 mm	84.95 mm	87.10 mm	86.65 mm	88.20 mm	80.90 mm	78.85 mm	78.20 mm	81.40 mm	76.00 mm
95.45 mm	59.85 mm	51.85 mm	47.20 mm	49.25 mm	46.05 mm	46.85 mm	54.00 mm	53.80 mm	48.15 mm	30.15 mm	27.80 mm
93.85 mm	79.75 mm	69.70 mm	63.50 mm	57.50 mm	51.40 mm	51.40 mm	45.90 mm	47.15 mm	45.27 mm	40.15 mm	42.50 mm
88.85 mm	94.25 mm	92.00 mm	91.55 mm	88.90 mm	88.85 mm	85.85 mm	89.00 mm	89.35 mm	89.05 mm	86.05 mm	91.80 mm
86.10 mm	98.00 mm	98.00 mm	98.05 mm	98.10 mm	98.00 mm	97.75 mm	97.90 mm	97.85 mm	98.20 mm	98.00 mm	97.45 mm
87.95 mm	87.75 mm	85.30 mm	84.70 mm	86.95 mm	87.05 mm	87.80 mm	81.40 mm	78.60 mm	78.25 mm	81.15 mm	74.45 mm
94.45 mm	61.10 mm	53.25 mm	47.35 mm	50.20 mm	46.25 mm	48.20 mm	54.40 mm	54.45 mm	49.50 mm	29.85 mm	27.85 mm
94.25 mm	79.95 mm	67.50 mm	62.60 mm	57.15 mm	50.55 mm	48.20 mm	44.25 mm	46.75 mm	46.35 mm	38.75 mm	40.65 mm
88.15 mm	94.15 mm	91.60 mm	89.80 mm	88.80 mm	87.80 mm	85.85 mm	87.85 mm	89.15 mm	88.70 mm	85.15 mm	91.90 mm
85.10 mm	97.85 mm	97.55 mm	98.40 mm	97.95 mm	97.65 mm	97.45 mm	97.75 mm	97.75 mm	97.90 mm	98.90 mm	96.90 mm
88.05 mm	87.85 mm	86.75 mm	86.60 mm	88.05 mm	85.95 mm	88.10 mm	82.25 mm	80.00 mm	77.90 mm	82.65 mm	72.35 mm
94.00 mm	61.65 mm	53.40 mm	48.30 mm	50.65 mm	45.95 mm	47.10 mm	53.60 mm	54.50 mm	50.55 mm	29.00 mm	28.80 mm

Sample 3-3-a2

17:36	19:05	20:35	22:14	23:36	9:11	12:50	16:30	20:05	20:42	20:28
98.30 mm	97.15 mm	97.10 mm	97.75 mm	98.00 mm	98.25 mm	97.55 mm	97.80 mm	98.10 mm	98.70 mm	98.10 mm
97.85 mm	97.65 mm	98.70 mm	98.70 mm	98.75 mm	98.35 mm	98.20 mm	98.35 mm	98.00 mm	98.75 mm	98.65 mm
97.35 mm	98.30 mm	98.50 mm	98.95 mm	98.45 mm	98.65 mm	98.70 mm	97.95 mm	98.00 mm	98.20 mm	98.40 mm
96.95 mm	97.40 mm	97.90 mm	96.70 mm	97.65 mm	97.95 mm	97.70 mm	97.05 mm	96.80 mm	97.45 mm	98.20 mm
98.10 mm	97.00 mm	96.30 mm	96.65 mm	96.55 mm	96.90 mm	95.90 mm	95.90 mm	96.20 mm	96.05 mm	96.05 mm
98.80 mm	98.10 mm	97.75 mm	97.25 mm	97.15 mm	98.00 mm	97.90 mm	96.95 mm	97.45 mm	98.20 mm	97.70 mm
98.60 mm	98.30 mm	98.20 mm	98.10 mm	98.00 mm	98.40 mm	98.10 mm	97.70 mm	98.15 mm	98.05 mm	97.90 mm
98.50 mm	97.90 mm	98.35 mm	97.90 mm	98.45 mm	98.25 mm	98.05 mm	97.55 mm	97.50 mm	98.35 mm	98.70 mm
98.50 mm	97.10 mm	97.10 mm	97.45 mm	97.40 mm	97.75 mm	97.10 mm	97.05 mm	97.35 mm	97.75 mm	97.75 mm
98.50 mm	96.95 mm	97.05 mm	96.95 mm	97.10 mm	96.70 mm	96.40 mm	96.50 mm	96.55 mm	96.80 mm	96.95 mm
97.95 mm	96.95 mm	96.75 mm	96.85 mm	96.70 mm	96.40 mm	97.30 mm	97.00 mm	97.20 mm	97.60 mm	96.90 mm
98.20 mm	97.25 mm	97.45 mm	97.70 mm	97.30 mm	97.75 mm	97.70 mm	96.75 mm	97.15 mm	97.55 mm	97.60 mm
97.70 mm	97.30 mm	97.40 mm	97.25 mm	97.35 mm	98.00 mm	97.55 mm	96.75 mm	97.35 mm	97.80 mm	97.15 mm
98.25 mm	97.55 mm	97.20 mm	97.80 mm	97.80 mm	97.20 mm	97.40 mm	97.10 mm	97.30 mm	97.45 mm	96.90 mm
98.20 mm	96.25 mm	96.75 mm	96.70 mm	97.45 mm	97.50 mm	96.55 mm	96.00 mm	96.50 mm	96.75 mm	97.25 mm
97.00 mm	96.80 mm	96.80 mm	96.95 mm	96.90 mm	96.50 mm	96.80 mm	96.40 mm	96.55 mm	97.30 mm	97.50 mm
97.35 mm	97.70 mm	97.70 mm	97.75 mm	97.30 mm	97.30 mm	97.45 mm	96.80 mm	97.40 mm	97.95 mm	100.30 mm
97.60 mm	97.60 mm	97.45 mm	97.75 mm	97.30 mm	97.55 mm	97.45 mm	97.00 mm	97.55 mm	98.05 mm	98.10 mm
97.40 mm	97.20 mm	97.45 mm	97.55 mm	97.40 mm	97.55 mm	97.30 mm	97.05 mm	97.25 mm	97.50 mm	97.45 mm
97.40 mm	96.35 mm	96.90 mm	97.15 mm	97.30 mm	96.85 mm	96.50 mm	96.60 mm	96.75 mm	97.00 mm	97.25 mm
96.70 mm	97.55 mm	96.75 mm	96.65 mm	96.55 mm	96.90 mm	96.35 mm	96.50 mm	96.85 mm	97.15 mm	97.50 mm
96.90 mm	97.85 mm	97.45 mm	96.60 mm	97.25 mm	97.50 mm	97.05 mm	97.00 mm	97.40 mm	97.70 mm	97.30 mm
96.35 mm	98.00 mm	97.90 mm	97.30 mm	97.70 mm	97.65 mm	97.40 mm	96.80 mm	97.45 mm	97.95 mm	97.70 mm
96.40 mm	97.65 mm	97.30 mm	97.00 mm	97.60 mm	97.65 mm	96.80 mm	96.85 mm	97.20 mm	97.55 mm	97.25 mm
96.45 mm	97.15 mm	96.75 mm	96.85 mm	96.75 mm	97.15 mm	96.70 mm	96.10 mm	96.50 mm	96.75 mm	96.30 mm

Table p-6. Deformation measurement data

Sample 3-3-a3

17:40	19:07	20:38	22:16	23:44	9:14	12:53	16:33	20:07	20:44	20:23	13:02
97.45 mm	93.85 mm	91.25 mm	89.70 mm	89.05 mm	89.40 mm	88.80 mm	89.10 mm	90.25 mm	90.45 mm	89.55 mm	89.75 mm
98.10 mm	95.70 mm	94.50 mm	94.45 mm	93.45 mm	94.35 mm	94.00 mm	94.05 mm	94.00 mm	93.95 mm	93.80 mm	95.10 mm
98.00 mm	97.90 mm	97.75 mm	97.25 mm	97.60 mm	97.55 mm	97.40 mm	97.20 mm	97.00 mm	96.55 mm	96.05 mm	97.70 mm
97.70 mm	98.65 mm	98.30 mm	98.85 mm	98.90 mm	99.20 mm	98.65 mm	98.45 mm	98.60 mm	98.30 mm	97.45 mm	98.85 mm
98.85 mm	98.25 mm	98.80 mm	98.35 mm	97.40 mm	98.20 mm	98.55 mm	98.20 mm	97.55 mm	99.15 mm	98.90 mm	97.75 mm
98.15 mm	94.10 mm	93.35 mm	92.05 mm	91.65 mm	91.55 mm	91.75 mm	92.00 mm	92.30 mm	92.75 mm	92.70 mm	91.90 mm
97.70 mm	96.55 mm	95.95 mm	95.85 mm	95.40 mm	96.55 mm	95.50 mm	95.80 mm	95.40 mm	95.45 mm	95.85 mm	96.30 mm
97.40 mm	98.15 mm	97.95 mm	98.50 mm	97.45 mm	98.05 mm	97.85 mm	97.85 mm	97.70 mm	97.55 mm	97.40 mm	97.45 mm
97.60 mm	98.70 mm	98.40 mm	98.95 mm	98.15 mm	98.00 mm	98.80 mm	98.55 mm	97.50 mm	97.80 mm	98.10 mm	97.75 mm
98.30 mm	97.30 mm	96.65 mm	96.95 mm	96.05 mm	96.30 mm	96.50 mm	97.05 mm	96.25 mm	95.90 mm	96.65 mm	95.45 mm
97.90 mm	95.20 mm	95.45 mm	94.40 mm	93.90 mm	93.85 mm	94.10 mm	94.10 mm	94.15 mm	94.20 mm	94.65 mm	94.55 mm
97.60 mm	96.85 mm	97.40 mm	96.85 mm	97.40 mm	96.55 mm	96.35 mm	96.45 mm	96.70 mm	96.70 mm	96.85 mm	96.55 mm
97.45 mm	98.10 mm	97.25 mm	97.10 mm	97.35 mm	97.60 mm	97.25 mm	97.30 mm	97.30 mm	97.60 mm	97.50 mm	97.35 mm
98.50 mm	97.65 mm	97.10 mm	97.75 mm	97.60 mm	96.50 mm	97.40 mm	97.45 mm	96.85 mm	97.35 mm	96.75 mm	96.50 mm
98.15 mm	95.65 mm	95.45 mm	95.50 mm	94.25 mm	93.90 mm	93.55 mm	93.55 mm	93.75 mm	94.55 mm	94.60 mm	93.10 mm
98.35 mm	96.60 mm	96.10 mm	95.95 mm	95.55 mm	95.90 mm	95.50 mm	95.85 mm	96.05 mm	96.70 mm	95.90 mm	95.75 mm
97.70 mm	97.60 mm	97.60 mm	98.45 mm	98.15 mm	97.85 mm	97.65 mm	97.35 mm	97.30 mm	97.80 mm	97.30 mm	97.70 mm
97.95 mm	97.45 mm	97.30 mm	97.70 mm	97.10 mm	97.55 mm	97.40 mm	97.30 mm	97.25 mm	96.75 mm	97.40 mm	96.95 mm
96.90 mm	96.55 mm	96.35 mm	95.50 mm	95.45 mm	95.20 mm	95.10 mm	94.75 mm	94.75 mm	94.90 mm	95.20 mm	94.70 mm
97.55 mm	94.15 mm	92.75 mm	92.55 mm	91.05 mm	89.90 mm	90.40 mm	90.35 mm	91.05 mm	91.70 mm	92.35 mm	90.25 mm
97.65 mm	97.65 mm	97.75 mm	96.70 mm	97.10 mm	97.40 mm	96.85 mm	97.30 mm	97.30 mm	97.35 mm	97.40 mm	97.95 mm
97.15 mm	97.60 mm	97.50 mm	97.90 mm	97.95 mm	98.05 mm	97.70 mm	96.85 mm	97.85 mm	97.55 mm	97.55 mm	98.00 mm
96.85 mm	97.05 mm	96.90 mm	97.00 mm	96.55 mm	96.50 mm	96.30 mm	96.00 mm	95.30 mm	96.15 mm	96.15 mm	95.90 mm
98.20 mm	95.65 mm	93.70 mm	93.70 mm	93.60 mm	92.80 mm	92.50 mm	92.05 mm	92.25 mm	93.05 mm	92.90 mm	92.45 mm
98.05 mm	91.35 mm	90.25 mm	88.55 mm	88.45 mm	86.00 mm	86.30 mm	86.35 mm	86.65 mm	87.40 mm	88.10 mm	86.20 mm

Sample 3-3-a4

17:46	19:11	20:40	22:20	23:46	9:17	12:55	16:37	20:09	20:45	20:26	13:03
93.85 mm	84.25 mm	80.95 mm	78.55 mm	76.20 mm	76.10 mm	75.60 mm	76.90 mm	76.65 mm	76.15 mm	76.50 mm	76.95 mm
94.35 mm	91.25 mm	90.05 mm	88.70 mm	87.90 mm	87.90 mm	87.60 mm	87.85 mm	87.60 mm	86.65 mm	86.60 mm	88.20 mm
94.70 mm	96.25 mm	95.25 mm	95.30 mm	95.45 mm	95.60 mm	95.35 mm	94.60 mm	94.85 mm	94.35 mm	94.60 mm	95.20 mm
96.10 mm	97.70 mm	98.75 mm	97.50 mm	97.90 mm	97.70 mm	98.00 mm	97.55 mm	97.35 mm	97.90 mm	97.65 mm	97.40 mm
98.00 mm	96.30 mm	95.85 mm	95.35 mm	95.10 mm	94.55 mm	95.25 mm	94.65 mm	94.60 mm	96.50 mm	96.45 mm	95.15 mm
95.40 mm	86.40 mm	84.50 mm	83.30 mm	81.65 mm	80.20 mm	80.00 mm	81.55 mm	81.75 mm	80.85 mm	80.30 mm	80.80 mm
95.10 mm	93.15 mm	92.20 mm	91.55 mm	90.85 mm	90.60 mm	90.85 mm	90.75 mm	91.25 mm	89.55 mm	90.10 mm	90.45 mm
95.90 mm	96.30 mm	96.65 mm	96.35 mm	96.25 mm	96.05 mm	96.35 mm	95.80 mm	95.40 mm	95.30 mm	95.00 mm	96.05 mm
96.40 mm	96.80 mm	96.40 mm	96.40 mm	96.85 mm	96.15 mm	96.40 mm	95.50 mm	95.60 mm	95.80 mm	96.80 mm	95.90 mm
97.00 mm	95.35 mm	93.95 mm	93.15 mm	92.90 mm	91.40 mm	92.75 mm	91.20 mm	91.45 mm	93.25 mm	93.25 mm	92.30 mm
96.75 mm	89.95 mm	87.90 mm	86.75 mm	85.45 mm	85.60 mm	84.35 mm	86.30 mm	86.15 mm	85.30 mm	85.30 mm	84.90 mm
95.10 mm	94.65 mm	94.10 mm	94.65 mm	93.75 mm	93.45 mm	93.70 mm	94.00 mm	92.85 mm	92.85 mm	93.00 mm	93.30 mm
95.40 mm	97.25 mm	97.15 mm	96.65 mm	96.85 mm	96.45 mm	96.45 mm	96.00 mm	96.10 mm	95.95 mm	95.75 mm	95.35 mm
95.85 mm	95.65 mm	95.60 mm	94.25 mm	94.80 mm	93.95 mm	95.75 mm	93.60 mm	93.40 mm	94.25 mm	94.40 mm	94.20 mm
97.40 mm	93.00 mm	91.25 mm	90.10 mm	89.65 mm	89.15 mm	89.55 mm	86.85 mm	87.45 mm	89.90 mm	89.95 mm	88.10 mm
96.75 mm	92.25 mm	91.30 mm	90.45 mm	89.85 mm	89.05 mm	89.15 mm	90.50 mm	90.15 mm	89.75 mm	91.45 mm	89.85 mm
94.80 mm	96.20 mm	96.00 mm	95.70 mm	95.20 mm	95.30 mm	95.60 mm	95.75 mm	95.70 mm	95.20 mm	95.10 mm	94.90 mm
95.75 mm	96.80 mm	95.90 mm	95.65 mm	95.25 mm	95.90 mm	96.05 mm	94.95 mm	94.85 mm	95.55 mm	96.70 mm	95.35 mm
95.95 mm	95.15 mm	93.60 mm	92.50 mm	92.55 mm	91.75 mm	92.35 mm	90.30 mm	90.70 mm	91.90 mm	91.55 mm	90.55 mm
97.05 mm	90.90 mm	88.60 mm	86.40 mm	86.70 mm	85.15 mm	85.85 mm	83.80 mm	83.60 mm	86.40 mm	86.20 mm	85.30 mm
97.25 mm	94.65 mm	94.90 mm	94.05 mm	93.40 mm	93.45 mm	92.80 mm	94.30 mm	94.45 mm	93.65 mm	94.85 mm	93.00 mm
95.70 mm	97.05 mm	96.50 mm	96.35 mm	96.75 mm	97.00 mm	96.75 mm	96.70 mm	96.60 mm	97.05 mm	96.95 mm	96.75 mm
95.10 mm	96.20 mm	95.50 mm	94.85 mm	95.25 mm	95.05 mm	95.25 mm	93.35 mm	93.70 mm	94.70 mm	94.65 mm	95.00 mm
95.50 mm	93.55 mm	91.85 mm	89.95 mm	90.70 mm	89.55 mm	89.75 mm	87.10 mm	87.70 mm	89.05 mm	89.35 mm	89.05 mm
96.75 mm	88.85 mm	85.25 mm	82.50 mm	82.30 mm	81.25 mm	81.85 mm	78.60 mm	78.90 mm	81.60 mm	82.15 mm	81.05 mm

Table p-6. Deformation measurement data. (continued)

Sample 3-3-a5

17:48	19:15	20:43	22:23	23:51	9:19	12:57	16:39	20:11	20:47	20:27	13:05
97.75 mm	83.10 mm	75.75 mm	72.10 mm	71.50 mm	67.80 mm	66.60 mm	64.55 mm	63.15 mm	61.65 mm	62.25 mm	65.55 mm
96.95 mm	93.45 mm	91.10 mm	88.60 mm	89.25 mm	88.40 mm	87.75 mm	86.25 mm	85.80 mm	85.25 mm	85.00 mm	86.85 mm
96.50 mm	98.00 mm	96.90 mm	97.30 mm	97.60 mm	97.10 mm	96.90 mm	96.85 mm	95.90 mm	96.75 mm	96.65 mm	96.85 mm
97.10 mm	97.45 mm	98.10 mm	97.85 mm	97.35 mm	97.10 mm	97.40 mm	97.65 mm	97.60 mm	98.20 mm	98.15 mm	97.75 mm
96.55 mm	94.00 mm	92.35 mm	91.25 mm	91.05 mm	90.25 mm	89.35 mm	90.30 mm	90.80 mm	95.00 mm	94.20 mm	90.80 mm
97.80 mm	86.55 mm	80.40 mm	78.40 mm	77.05 mm	75.00 mm	73.50 mm	72.40 mm	71.25 mm	70.10 mm	70.70 mm	72.85 mm
97.35 mm	94.35 mm	92.20 mm	97.05 mm	91.25 mm	91.20 mm	90.80 mm	90.45 mm	89.45 mm	89.05 mm	89.35 mm	90.75 mm
97.20 mm	97.55 mm	97.45 mm	95.95 mm	97.65 mm	97.40 mm	96.90 mm	97.25 mm	97.10 mm	97.05 mm	97.35 mm	97.55 mm
97.20 mm	96.80 mm	96.00 mm	96.30 mm	95.95 mm	95.25 mm	95.65 mm	95.30 mm	95.45 mm	96.15 mm	96.55 mm	95.60 mm
97.70 mm	92.75 mm	90.30 mm	89.20 mm	87.60 mm	87.25 mm	87.25 mm	87.25 mm	87.80 mm	91.05 mm	91.30 mm	87.40 mm
97.80 mm	89.05 mm	84.90 mm	82.75 mm	82.20 mm	80.25 mm	79.40 mm	78.80 mm	78.35 mm	77.95 mm	78.25 mm	78.85 mm
97.65 mm	95.10 mm	94.35 mm	97.05 mm	93.30 mm	93.10 mm	93.15 mm	93.00 mm	92.55 mm	92.35 mm	91.60 mm	92.75 mm
96.85 mm	97.20 mm	97.75 mm	97.45 mm	97.45 mm	97.05 mm	97.60 mm	96.80 mm	96.80 mm	96.95 mm	97.00 mm	97.20 mm
96.90 mm	94.95 mm	93.80 mm	93.00 mm	92.55 mm	92.90 mm	92.45 mm	92.35 mm	92.10 mm	93.60 mm	93.50 mm	92.75 mm
98.45 mm	90.90 mm	88.05 mm	86.10 mm	85.15 mm	84.55 mm	83.40 mm	83.25 mm	83.30 mm	87.00 mm	88.15 mm	85.10 mm
96.40 mm	90.95 mm	87.95 mm	87.35 mm	85.70 mm	85.05 mm	84.80 mm	85.50 mm	84.35 mm	83.95 mm	84.10 mm	84.50 mm
96.25 mm	96.40 mm	95.20 mm	95.65 mm	95.00 mm	95.35 mm	94.95 mm	95.45 mm	94.60 mm	94.70 mm	95.10 mm	95.70 mm
95.65 mm	97.10 mm	97.15 mm	96.50 mm	97.25 mm	97.05 mm	97.00 mm	95.90 mm	96.55 mm	96.40 mm	96.95 mm	96.85 mm
96.95 mm	93.85 mm	92.55 mm	92.10 mm	91.20 mm	90.80 mm	90.55 mm	89.50 mm	89.80 mm	90.90 mm	91.20 mm	90.40 mm
98.30 mm	89.20 mm	84.95 mm	83.00 mm	81.75 mm	80.70 mm	79.95 mm	78.35 mm	78.85 mm	83.40 mm	84.20 mm	81.00 mm
95.95 mm	93.05 mm	90.75 mm	90.55 mm	90.40 mm	89.05 mm	88.70 mm	90.30 mm	89.95 mm	89.85 mm	90.15 mm	89.40 mm
94.30 mm	97.45 mm	96.75 mm	96.85 mm	97.40 mm	96.95 mm	96.90 mm	97.10 mm	97.30 mm	97.40 mm	97.50 mm	97.25 mm
94.65 mm	95.75 mm	96.15 mm	96.05 mm	95.20 mm	95.60 mm	95.80 mm	94.60 mm	94.60 mm	95.00 mm	95.25 mm	95.00 mm
96.10 mm	93.00 mm	91.55 mm	90.35 mm	89.20 mm	88.95 mm	88.45 mm	86.90 mm	87.80 mm	89.55 mm	90.40 mm	88.75 mm
96.90 mm	86.75 mm	80.90 mm	78.85 mm	77.90 mm	75.95 mm	75.45 mm	72.55 mm	73.85 mm	78.15 mm	79.10 mm	76.00 mm

Table p-6. Deformation measurement data. (continued)

Appendix 7 – Shrinkage coefficient measurement and calculation data

Type a = 24% x 5%

3mm x 3mm

Active Layer	orientation (degree)	initial moisture content	final moisture content	initial length (mm)	final length (mm)	percentage shrinkage	shrinkage coefficient
		c	c0	l1	l2	n	α1
3-3-a1-A	0	24.0%	12.80%	25.0	23.5	5.6%	0.500
3-3-a5-A	30	24.0%	13.10%	25.0	24.3	2.5%	0.233
3-3-a4-A	45	24.0%	13.30%	25.0	24.5	1.8%	0.167
3-3-a3-A	60	24.0%	12.90%	25.0	24.7	1.1%	0.100
3-3-a2-A	90	24.0%	13.03%	25.0	24.9	0.4%	0.033
Restrictive Layer	orientation (degree)	initial moisture content	final moisture content	initial length (mm)	final length (mm)	percentage expansion	expansion coefficient
		c	c0	l1	l2	n	α2
3-3-a1-R	0	5.0%	10.5%	25.0	25.1	0.6%	0.100
3-3-a5-R	0	5.0%	10.4%	25.0	25.1	0.4%	0.080
3-3-a4-R	0	5.0%	11.6%	25.0	25.1	0.5%	0.078
3-3-a3-R	0	5.0%	10.5%	25.0	25.1	0.3%	0.059
3-3-a2-R	0	5.0%	10.8%	25.0	25.1	0.4%	0.065

Table p-7a. Calculation of shrinkage coefficient α1 and expansion coefficient α2 of Type a

Active Layer	orientation (degree)	initial moisture content	final moisture content	initial length (mm)	final length (mm)	percentage shrinkage	shrinkage coefficient
		c	c0	l1	l2	n	α1
4-4-a1-A	0	24.0%	12.2%	25.0	26.5	6.1%	0.520
4-4-a5-A	30	24.0%	14.3%	25.0	25.5	2.0%	0.210
4-4-a4-A	45	24.0%	14.6%	25.0	25.4	1.5%	0.160
4-4-a3-A	60	24.0%	14.8%	25.0	25.3	1.1%	0.120
4-4-a2-A	90	24.0%	14.0%	25.0	25.1	0.3%	0.033
Restrictive Layer	orientation (degree)	initial moisture content	final moisture content	initial length (mm)	final length (mm)	percentage expansion	expansion coefficient
		c	c0	l1	l2	n	α2
4-4-a1-R	0	5.0%	6.8%	25.0	25.0	0.2%	0.100
4-4-a5-R	0	5.0%	6.6%	25.0	25.0	0.1%	0.090
4-4-a4-R	0	5.0%	6.5%	25.0	25.0	0.1%	0.082
4-4-a3-R	0	5.0%	6.5%	25.0	25.0	0.1%	0.067
4-4-a2-R	0	5.0%	6.6%	25.0	25.0	0.1%	0.090

Active Layer	orientation (degree)	initial moisture content	final moisture content	initial length (mm)	final length (mm)	percentage shrinkage	shrinkage coefficient
		c	c0	l1	l2	n	α1
3-4-a1-A	0	24.0%	10.0%	25.0	26.8	7.1%	0.510
3-4-a5-A	30	24.0%	10.3%	25.0	25.7	2.6%	0.190
3-4-a4-A	45	24.0%	12.1%	25.0	25.5	2.0%	0.166
3-4-a3-A	60	24.0%	12.7%	25.0	25.3	1.4%	0.120
3-4-a2-A	90	24.0%	11.3%	25.0	25.1	0.4%	0.033
Restrictive Layer	orientation (degree)	initial moisture content	final moisture content	initial length (mm)	final length (mm)	percentage expansion	expansion coefficient
		c	c0	l1	l2	n	α2
3-4-a1-R	0	5.0%	7.4%	25.0	25.1	0.2%	0.100
3-4-a5-R	0	5.0%	7.2%	25.0	25.0	0.2%	0.090
3-4-a4-R	0	5.0%	7.9%	25.0	25.1	0.2%	0.078
3-4-a3-R	0	5.0%	7.8%	25.0	25.0	0.2%	0.063
3-4-a2-R	0	5.0%	7.6%	25.0	25.0	0.2%	0.070

Type b = 24% x 12%

Table p-7b. Calculation of shrinkage coefficient α1 and expansion coefficient α2 of Type b

Active Layer	orientation (degree)	initial moisture content	final moisture content	initial length (mm)	final length (mm)	percentage shrinkage	shrinkage coefficient
		c	c0	l1	l2	n	α1
3-3-b1-A	0	24.0%	14.7%	25.0	23.7	4.0%	0.433
3-3-b5-A	30	24.0%	13.3%	25.0	24.9	0.4%	0.033
3-3-b4-A	45	24.0%	13.8%	25.0	24.8	0.7%	0.067
3-3-b3-A	60	24.0%	12.4%	25.0	24.6	1.5%	0.133
3-3-b2-A	90	24.0%	13.6%	25.0	24.3	2.4%	0.233
Restrictive Layer	orientation (degree)	initial moisture content	final moisture content	initial length (mm)	final length (mm)	percentage expansion /shrikage	expansion /shrinkage coefficient
		c	c0	l1	l2	n	α2
3-3-b1-R	0	12.0%	10.5%	25.0	25.0	0.1%	0.049
3-3-b5-R	0	12.0%	12.3%	25.0	25.0	0.0%	0.047
3-3-b4-R	0	12.0%	11.7%	25.0	25.0	0.0%	0.042
3-3-b3-R	0	12.0%	11.7%	25.0	25.0	0.0%	0.048
3-3-b2-R	0	12.0%	11.6%	25.0	25.0	0.0%	0.043

Active Layer	orientation (degree)	initial moisture content	final moisture content	initial length (mm)	final length (mm)	percentage shrinkage	shrinkage coefficient
		c	c0	l1	l2	n	α1
4-4-b1-A	0	24.0%	11.4%	25.0	26.3	5.4%	0.425
4-4-b5-A	30	24.0%	12.3%	25.0	25.6	2.5%	0.211
4-4-b4-A	45	24.0%	14.2%	25.0	25.3	1.2%	0.125
4-4-b3-A	60	24.0%	13.1%	25.0	25.2	0.8%	0.069
4-4-b2-A	90	24.0%	12.8%	25.0	25.1	0.3%	0.031
Restrictive Layer	orientation (degree)	initial moisture content	final moisture content	initial length (mm)	final length (mm)	percentage expansion /shrikage	expansion /shrinkage coefficient
		c	c0	l1	l2	n	α2
4-4-b1-R	0	12.0%	9.5%	25.0	25.0	0.1%	0.050
4-4-b5-R	0	12.0%	9.7%	25.0	25.0	0.2%	0.080
4-4-b4-R	0	12.0%	9.5%	25.0	25.0	0.2%	0.078
4-4-b3-R	0	12.0%	9.8%	25.0	25.0	0.1%	0.060
4-4-b2-R	0	12.0%	9.6%	25.0	25.0	0.1%	0.060

Active Layer	orientation (degree)	initial moisture content	final moisture content	initial length (mm)	final length (mm)	percentage shrinkage	shrinkage coefficient
		c	c0	l1	l2	n	α1
3-4-b1-A	0	24.0%	10.7%	25.0	26.4	5.5%	0.412
3-4-b5-A	30	24.0%	11.1%	25.0	25.6	2.6%	0.200
3-4-b4-A	45	24.0%	12.8%	25.0	25.4	1.4%	0.128
3-4-b3-A	60	24.0%	11.6%	25.0	25.2	0.8%	0.067
3-4-b2-A	90	24.0%	11.6%	25.0	25.1	0.3%	0.028
Restrictive Layer	orientation (degree)	initial moisture content	final moisture content	initial length (mm)	final length (mm)	percentage expansion /shrikage	expansion /shrinkage coefficient
		c	c0	l1	l2	n	α2
3-4-b1-R	0	12.0%	10.1%	25.0	25.0	0.1%	0.047
3-4-b5-R	0	12.0%	10.6%	25.0	25.0	0.1%	0.070
3-4-b4-R	0	12.0%	10.4%	25.0	25.0	0.1%	0.078
3-4-b3-R	0	12.0%	10.4%	25.0	25.0	0.1%	0.063
3-4-b2-R	0	12.0%	10.4%	25.0	25.0	0.1%	0.050

Appendix 8 - Bending test data

As there was too much data, only part of the data of sample D4 is shown here as an example.

20181214_Future積層板曲げ実験_5体目(D4)								
名前	測定日時	荷重(アム	◎荷重(ロ	変位(CDP5	変位(CDP5	変位(CDP1	◎変位_平	荷重[N]
1	2018/12/14 21:11	0	0	0.0005	0.0005	0	0.0005	0
2	2018/12/14 21:11	0	0	0.0025	0.0005	0	0.0015	0
3	2018/12/14 21:11	0.0025	0	0.003	0.0005	0	0.00175	0
4	2018/12/14 21:11	0.005	0	0.0035	0.0005	0	0.002	0
5	2018/12/14 21:11	0.0075	0	0.004	0.0005	0	0.00225	0
6	2018/12/14 21:11	0.0025	0	0.004	0.0005	0	0.00225	0
7	2018/12/14 21:11	0.0075	0	0.005	0.0005	0.001	0.00275	0
8	2018/12/14 21:11	0.0075	0	0.0055	0.0005	0.002	0.003	0
9	2018/12/14 21:11	0.005	0	0.0055	0	0.001	0.00275	0
10	2018/12/14 21:11	-0.005	0	0.0085	0	0.001	0.00425	0
11	2018/12/14 21:11	0.0075	0	0.0355	0	0.019	0.01775	0
12	2018/12/14 21:11	0.005	0	0.0705	0	0.032	0.03525	0
13	2018/12/14 21:11	0.005	0	0.113	0.001	0.058	0.057	0
14	2018/12/14 21:11	0.01	0	0.1655	0.0015	0.087	0.0835	0
15	2018/12/14 21:11	0.015	0.000125	0.2075	0.002	0.114	0.10475	0.125
16	2018/12/14 21:11	0.005	0.000125	0.257	0.003	0.143	0.13	0.125
17	2018/12/14 21:11	0.01	0.000125	0.308	0.0035	0.171	0.15575	0.125
18	2018/12/14 21:11	0.01	0.000375	0.35	0.0055	0.201	0.17775	0.375
19	2018/12/14 21:11	0.0125	0.000375	0.382	0.01	0.229	0.196	0.375
20	2018/12/14 21:11	0.0125	0.0005	0.417	0.014	0.251	0.2155	0.5
21	2018/12/14 21:11	0.0175	0.00075	0.4425	0.0245	0.278	0.2335	0.75
22	2018/12/14 21:11	0.005	0.00075	0.4565	0.044	0.299	0.25025	0.75
23	2018/12/14 21:11	0.005	0.000875	0.4705	0.067	0.327	0.26875	0.875
24	2018/12/14 21:11	0.01	0.001	0.482	0.088	0.351	0.285	1
25	2018/12/14 21:11	0.0075	0.001125	0.4945	0.1065	0.378	0.3005	1.125
26	2018/12/14 21:11	0.0025	0.00125	0.505	0.1225	0.405	0.31375	1.25
27	2018/12/14 21:11	0.01	0.001375	0.5145	0.1355	0.433	0.325	1.375
28	2018/12/14 21:11	0.01	0.0015	0.5255	0.1505	0.465	0.338	1.5
29	2018/12/14 21:11	0.01	0.001625	0.536	0.162	0.497	0.349	1.625
30	2018/12/14 21:11	0.005	0.001625	0.545	0.1755	0.525	0.36025	1.625
31	2018/12/14 21:11	0.0025	0.00175	0.555	0.1885	0.555	0.37175	1.75
32	2018/12/14 21:11	0.0075	0.00175	0.566	0.2085	0.586	0.38725	1.75
33	2018/12/14 21:11	0.01	0.001875	0.579	0.229	0.615	0.404	1.875
34	2018/12/14 21:11	0.0125	0.002	0.593	0.2515	0.641	0.42225	2
35	2018/12/14 21:11	0.0075	0.002125	0.606	0.275	0.667	0.4405	2.125
36	2018/12/14 21:11	0.005	0.00225	0.62	0.3025	0.694	0.46125	2.25
37	2018/12/14 21:11	0.0075	0.0025	0.636	0.3355	0.724	0.48575	2.5
38	2018/12/14 21:11	0.0075	0.002625	0.649	0.3635	0.751	0.50625	2.625
39	2018/12/14 21:11	0.005	0.002875	0.664	0.3925	0.777	0.52825	2.875
40	2018/12/14 21:11	0.0125	0.003125	0.681	0.425	0.806	0.553	3.125
41	2018/12/14 21:11	0.005	0.00325	0.6965	0.4575	0.832	0.577	3.25
42	2018/12/14 21:11	0.01	0.0035	0.7095	0.4875	0.855	0.5985	3.5
43	2018/12/14 21:11	0.0075	0.00375	0.725	0.524	0.884	0.6245	3.75
44	2018/12/14 21:11	0.0125	0.004	0.7385	0.5545	0.91	0.6465	4
45	2018/12/14 21:11	0.005	0.004	0.7525	0.5875	0.939	0.67	4
46	2018/12/14 21:12	0.005	0.004375	0.7665	0.6165	0.964	0.6915	4.375
47	2018/12/14 21:12	0.005	0.0045	0.779	0.6485	0.991	0.71375	4.5
48	2018/12/14 21:12	0.0075	0.00475	0.7925	0.6835	1.02	0.738	4.75

Table p-8. Part of the bending test data

Appendix 9 – Attempt to adapt formula by combining Type a and b

	Calculated	Experiment
3-3-a1	0.01100	0.00864
3-3-a5	0.00416	0.00291
3-3-a4	0.00230	0.00178
3-3-a3	0.00100	0.00108
3-3-a2	-0.00005	0.00000
4-4-a1	0.01239	0.01039
4-4-a5	0.00290	0.00124
4-4-a4	0.00178	0.00054
4-4-a3	0.00107	0.00051
4-4-a2	-0.00008	0.00000
3-4-a1	0.01406	0.01024
3-4-a5	0.00341	0.00138
3-4-a4	0.00262	0.00049
3-4-a3	0.00155	0.00041
3-4-a2	-0.00012	0.00000
3-3-b1	0.00894	0.00339
3-3-b5	0.00496	0.00076
3-3-b4	0.00226	0.00076
3-3-b3	0.00048	0.00045
3-3-b2	-0.00002	0.00000
4-4-b1	0.01181	0.00434
4-4-b5	0.00381	0.00082
4-4-b4	0.00112	0.00024
4-4-b3	0.00022	0.00010
4-4-b2	-0.00005	0.00000
3-4-b1	0.01214	0.00485
3-4-b5	0.00417	0.00066
3-4-b4	0.00136	0.00036
3-4-b3	0.00010	0.00014
3-4-b2	-0.00004	0.00000

Table p-9.

Top: Summary of calculated curvature vs Experiment curvature for all samples of Type a and Type b

Bottom: Regression analysis showing an R square of 0.87 which is not good enough for such a small amount of sample.

Type a & b

Regression Statistics	
Multiple R	0.932691
R Square	0.869913
Adjusted R Square	0.835431
Standard Error	0.001273
Observations	30

Type a & b
ANOVA

	df	*SS*	*MS*	*F*	*ignificance F*
Regression	1	0.000314	0.000314	193.9284	4.12E-14
Residual	29	4.7E-05	1.62E-06		
Total	30	0.000361			

	Coefficients	*andard Erro*	*t Stat*	*P-value*	*Lower 95%*	*Upper 95%*	*ower 95.0%*	*Upper 95.0%*
Intercept	0	#N/A	#N/A	#N/A	#N/A	#N/A	#N/A	#N/A
X Variable 1	0.571832	0.041063	13.92582	2.25E-14	0.487849	0.655814	0.487849	0.655814

Appendix 10 – Linear regression prediction of relationship of shrinkage coefficient and fiber orientation angle.

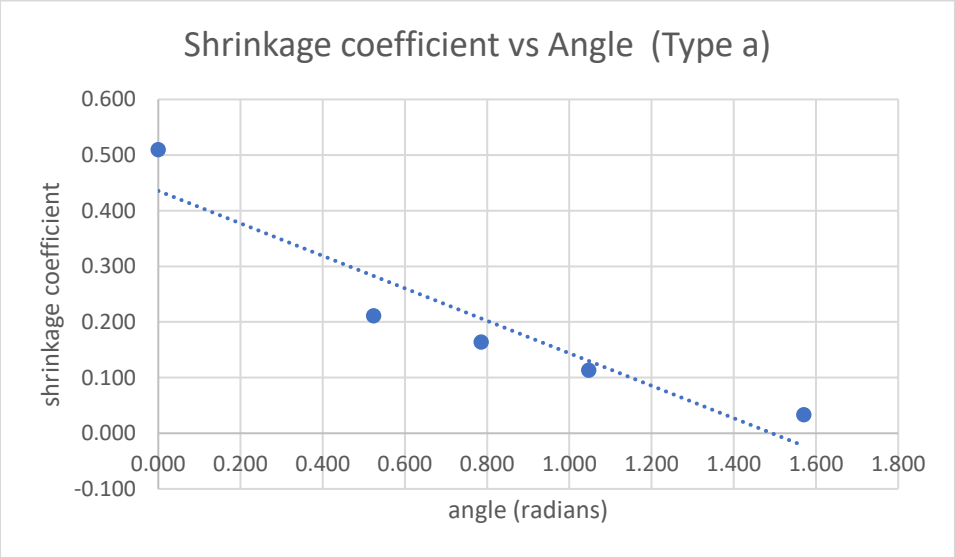

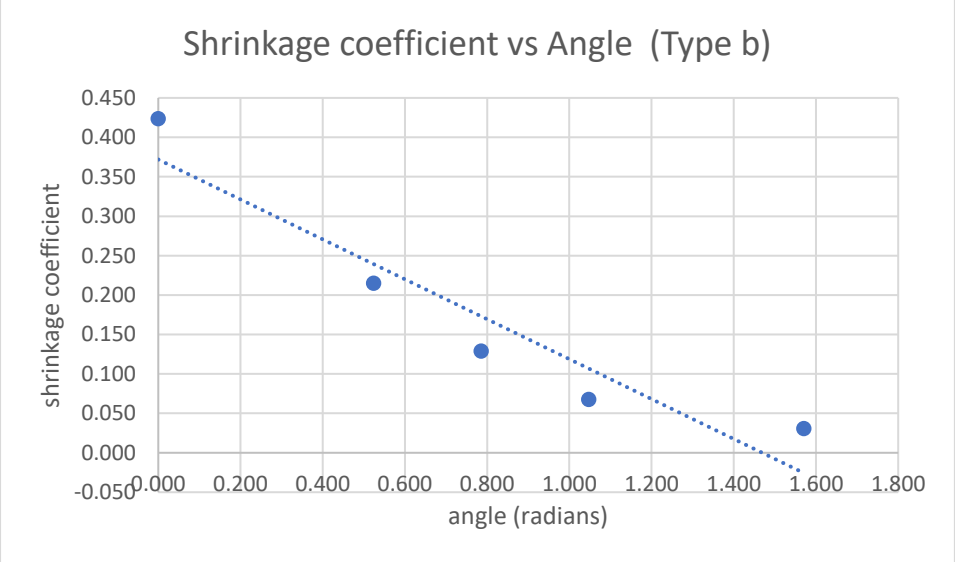

Figure p-10. Regression line fitting to the data.

Shrinkage coefficient vs angle

Type a		Type b	
Regression Statistics		*Regression Statistics*	
Multiple R	0.938196	Multiple R	0.947684
R Square	0.880212	R Square	0.898105
Adjusted R Square	0.840283	Adjusted R Square	0.86414
Standard Error	0.072761	Standard Error	0.05763
Observations	5	Observations	5

Table p-10. Regression analysis for shrinkage coefficient vs angle. An R square values were not good enough for small samples like this. Exponential curve was used then used for expressing the relationship between shrinkage coefficient and angle.

Appendix 11 – Regression analysis for curvature over time for all samples

Figure p-11. regression analysis of curvature over time

Figure p-11. regression analysis of curvature over time. (continued)

Figure p-11. regression analysis of curvature over time. (continued)

Figure p-11. regression analysis of curvature over time. (continued)

Figure p-11. regression analysis of curvature over time. (continued)

Figure p-11. regression analysis of curvature over time. (continued)

Figure p-11. regression analysis of curvature over time. (continued)

Appendix 12 - Part of software code for scanning and drawing program

Below shows part of the code for image processing, treating the knot on board

```
I=imread('2b.jpg');
I=imresize(I,[900 900]);


figure(1),imshow(I)
I1=rgb2gray(I);
figure(2),imshow(I1)
bw=im2bw(I1,graythresh(I1)-0.4);
figure(3),imshow(bw);
bw2=imfill(~bw,'holes');
figure(4),imshow(bw2)
bw3=bwareaopen(bw2,100);
figure(5),imshow(bw3)

bw4=imdilate(bw3,strel('disk',8));
figure,imshow(bw4)
beijing=uint8(~bw4).*rgb2gray(I);
figure,imshow(beijing)



bwrgb=cat(3,~bw3,~bw3,~bw3);
beijing=uint8(bwrgb).*I;
figure(6),imshow(beijing)

Lrgb = label2rgb(bw3, 'jet', 'k', 'shuffle');
figure; imshow(I), hold on
 imshow(I+Lrgb);



hold on
ellipse(200,100,  0*pi/180,500,300,[],4)
%%
% [X Y]=[450 450]
% X=[450-200; 450; 450+200; 450];
% Y=[450;   450+100; 450 ; 450-100];



% [X Y]=[500 300]
```

```
X=[500-200; 500; 500+200; 500];
Y=[300;   300+100; 300 ; 300-100];
X=[300;300+200;300+200;300]
Y=[500;500;500-100;500-100]

n = length(X);
X=round(X);
Y=round(Y);
X=[X;X(1)];Y=[Y;Y(1)];
side = [];
for i=1:n
    aa = LxyLine(X(i),Y(i),X(i+1),Y(i+1));
    side = [side;aa];
    clear aa;
end
plot(side(:,1),side(:,2))
%plot(side(:,1),side(:,2),'r.')

%Tlength= str2num(get(handles.edit10, 'String'));
Tlength=200;
side(:,1)=side(:,1)-Tlength;
plot(side(:,1),side(:,2),'r-')
hold on;
side(:,2)=side(:,2)+Tlength;
plot(side(:,1),side(:,2),'r-')
hold off;

Angle=100;
A=180/Angle;
M=[cos(pi/A)   sin(pi/A);
   -sin(pi/A)   cos(pi/A);];

R1=[side(:,1)';side(:,2)'];
R2=M*R1;
hold on;
plot(R2(1,:),R2(2,:),'r-')
side=R2';
```

Appendix 13. Code for derivation of function for kerf bending in MATLAB

```
Data_g1 = [
    6.3 270 14.5
4.8 210 14.5
3.8 120 14.5
9.5 300 14.8
9.5 250 14.8
9.5 200 14.8
11.0    220 10.4
14.0    150 6.9
17.4    80  3.4
5.0 300 14.8
16.1    660 10.5
12.0    675 14
8.9 700 18
35.1    670 10.5];


xy = Data_g1(:,[1,3]);
z = Data_g1(:,[2]);
fun = @(x,xdata)(  x(1)*xdata(:,1).^2 + x(2)*xdata(:,1).*xdata(:,2) + ...
    x(3)*xdata(:,2).^2 +  x(4)*xdata(:,1) + x(5)*xdata(:,2) + x(6) );

x0 = [1 1 1 1 1 1];
lb = [-inf -inf -inf -inf -inf -inf];
ub = [inf inf inf inf inf inf];

[x_g1,r_norm_g1,r_g1] = lsqcurvefit(fun,x0,xy,z,lb,ub);

x_range = linspace( min(xy(:,1)), max(xy(:,1)) ,30);
y_range = linspace( min(xy(:,2)), max(xy(:,2)) ,30);
[x_mesh,y_mesh] = meshgrid(x_range,y_range);
z_mesh = zeros(size(x_mesh));
[N,M] = size(z_mesh );
fun_g1 = @(xy)( fun(x_g1,xy)  );
for i = 1:N
    for j = 1:M
        z_mesh(i,j) = fun_g1( [x_mesh(i,j),y_mesh(i,j)] );
    end
end

figure
hold on
scatter3(xy(:,1),xy(:,2),z)
mesh(x_mesh,y_mesh,z_mesh)
grid minor
view(12,32)
zlim( [0,2000] )

C1 = cell(6,1);
C2 = {'x^2','xy','y^2','x','y'};
for i = 1:6
    if x_g1(i)>0
        C1{i,1} = [ '+',num2str(x_g1(i))];
    else
        C1{i,1} = [ num2str(x_g1(i)) ];
    end
end
titlename = [];
```

```
for i = 1:5
    titlename = [titlename, C1{i,1},C2{1,i}];
end
titlename = [titlename,C1{6,1}];
title(['1stgroup:f(xy)=',titlename])
xlabel('angle(degree)')
ylabel('w(mm)')
zlabel('radius(mm)')
disp( 'first_group_deviation')
fun(x_g1,xy)-z
```

Bibliography

Abdelmohsen, S., Adriaenssens, S., El-Dabaa, R., Gabriele, S., Olivieri, L., & Teresi, L. (2019). A multi-physics approach for modeling hygroscopic behavior in wood low-tech architectural adaptive systems. *Computer-Aided Design*, *106*, 43-53. doi: 10.1016/j.cad.2018.07.005

Applied Science. (2015). *Extreme wood bending with ammonia* [Video]. Retrieved from https://www.google.com/search?q=bending+wood+ammonia&oq=bending+wood+ammonia&aqs=chrome..69i57j0l4.3825j1j4&sourceid=chrome&ie=UTF-8#kpvalbx=1

Báder, M., & Németh, R. (2017). Hygroscopicity of Longitudinally Compressed Wood. *Acta Silvatica Et Lignaria Hungarica*, *13*(2), 135-144. doi: 10.1515/aslh-2017-0010

Breakdown of Country and Forest Area, Trend of Growth of Forest Stock (From MAFF). (2018). Retrieved from https://tech.nikkeibp.co.jp/atcl/nxt/column/18/00461/102400004/?SS=imgview&FD=1420933308

Bosch Professional. (2016). [Image]. Retrieved from http://www.bosch-professional.com/za/en/laser-measure-glm-50-c-241456-0601072c00.html

Definition of KERF. (2019). Retrieved from https://www.merriam-webster.com/dictionary/kerf

Digital Moisture Meter For Wood - Hold function for max/min values - Shinwa Sokutei Co., Ltd. Retrieved from https://www.shinwasokutei.co.jp/products/78636/

Fathis, Z. (2018). [Image]. Retrieved from https://www.instagram.com/zaqifathis/

Guzelci, O., Alaçam, S., & Bacınoğlu, S. (2017). THREE-STEP EXPERIMENTATION ON EMBEDDING CURVATURE TO RIGID PLANAR MATERIALS THROUGH CUT PATTERNS. *Gestão & Tecnologia De Projetos*, *12*(3), 93. doi: 10.11606/gtp.v12i3.134543

Harvard GSD. (2010). *Kerf-Based Complex Wood Systems* [Image]. Retrieved from http://www.achimmenges.net/?p=5006

Happold, E., & Liddell, I. (1975). Timber lattice roof for the Mannheim Bundesgartenschau. *The Structural Engineer*, *3*(3), 99-135. Retrieved from http://people.bath.ac.uk/abscjkw/Berus2018/Happold%20&%20Liddell%20Mannheim.pdf

Hayashi, Tomoyuki. 2012. Puro Demo Igai Ni Shiranai Ki No Chishiki. Gakugeishuppansha.

Hokkaido Research Organization, Forest Research Department Products Research Institute. (2006). *Three directions of wood* [Image]. Retrieved from https://www.hro.or.jp/list/forest/research/fpri/dayori/0603/5.htm

Hygroexpansion in wood – shrinkage and swelling. Retrieved from https://is.mendelu.cz/eknihovna/opory/zobraz_cast.pl?cast=19372

Iwai, H. (1994). Magemono (p. 227). Tokyo: Hosei Daigaku Shuppankyoku.
MIT Architecture. (2012). *Kerf Pavilion* [Image]. Retrieved from https://architecture.mit.edu/architecture-and-urbanism/project/kerf-pavilion

Kabel, M. (2008). *The wood roof shingles on this onion dome were bent to match the curves of the dome. The church is in a compound known as the Kizhi Pogost.* [Image]. Retrieved from https://en.wikipedia.org/wiki/Steam_bending

Kodai Sangyo Co. Ltd. 2007. Foot Spa Bucket. Image. http://www.kodaimokuty.co.jp/en/products/bathware.

Lee Valley Tools - Woodworking Tools, Gardening Tools, Hardware. (2019). Retrieved from http://www.leevalley.com/us/home.aspx

Making curved beams. (2017). [Video]. Retrieved from https://www.youtube.com/watch?v=eqlEY8ifILc&t=126s

Menges, A., & Reichert, S. (2012). Material Capacity: Embedded Responsiveness. Architectural Design, 82(2), 52-59. doi: 10.1002/ad.1379

Meteorological Agency ｜Search past weather data. (2019). Retrieved from https://www.data.jma.go.jp/obd/stats/etrn/view/mb5daily_s1.php?prec_no=45&block_no=47682&year=2019&month=06&day=01&view=p1

Miller, Hugh. 2015. Japanese Wooden Craftsmanship. Ebook. Winston Churchill Memorial Trust. https://www.wcmt.org.uk/sites/default/files/report-documents/Miller%20H%20Report%202015%20Final.pdf.

Ministry of Agriculture, Forestry and Fisheries. (2016). *Trend of supply and self-sufficiency rate of wood in Japan* [Image]. Retrieved from http://www.rinya.maff.go.jp/j/kikaku/hakusyo/28hakusyo_h/summary/s05.html

Mitchell, P. (2017). Calculating the Equilibrium Moisture Content for Wood Based on Humidity Measurements. *Bioresources*, *13*(1). doi: 10.15376/biores.13.1.171-175

Moholy-Nagy, L. (1975). *The New Vision* (pp. 45-47). Mineola: Dover Publications.

Nicholson, P., & Shaw, I. (2000). *Ancient Egyptian Materials and Technology* (pp. 356-357). London: Cambridge University Press.

Office of Prime Minister's Official Residence. (2014). *Japan Revitalization Strategy*(p. 157). Tokyo.

Overview of the survey (31 March, 2012) : MAFF. (2012). Retrieved from http://www.rinya.maff.go.jp/j/keikaku/genkyou/h24/2.html

PLIABILITY | meaning in the Cambridge English Dictionary. (2019). Retrieved from https://dictionary.cambridge.org/dictionary/english/pliability

Porterfield, A. (2016). Curved Laser Bent wood. Retrieved from https://www.instructables.com/id/Curved-laser-bent-wood/

Richardson, J. (2011). HYGROSCOPICITY. Retrieved from http://www.thermopedia.com/content/869/

Rüggeberg, M., & Burgert, I. (2015). Bio-Inspired Wooden Actuators for Large Scale Applications. *PLOS ONE*, *10*(4), e0120718. doi: 10.1371/journal.pone.0120718

Shinwa Sokutei Co., Ltd. [Image]. Retrieved from https://www.shinwasokutei.co.jp/products/78636/

Steam bending examples. (2019). [Image]. Retrieved from https://bendingwood.wordpress.com/2012/09/13/steam-bending-examples/#jp-carousel-25

Stew MacDonald. *Bending Iron | Stew MacDonald* [Image]. Retrieved from https://www.stewmac.com/Luthier_Tools/Tools_by_Job/Tools_for_Bending_Sides/Bending_Iron.html

T&D Corporation. (2019). [Image]. Retrieved from https://www.tandd.co.jp/ondotori_25th/

THONET. *An ingenious distribution idea* [Image]. Retrieved from http://en.thonet.de/inspirations/magazine/thonet-the-story/the-thonet-principle.html

Timoshenko, S. (1925). Analysis of Bi-Metal Thermostats. *Journal Of The Optical Society Of America*, *11*(3), 233. doi: 10.1364/josa.11.000233

Well formwork found in 2013. [Image]. Retrieved from http://www.shijonawate-rekishi.jp/iseki/nakano-ido/1-ido.htm

Wood, D., Correa, D., Krieg, O., & Menges, A. (2016). Material computation—4D timber construction: Towards building-scale hygroscopic actuated, self-constructing timber surfaces. *International Journal Of Architectural Computing*, *14*(1), 49-62. doi: 10.1177/1478077115625522

Wood, D., Vailati, C., Menges, A., & Rüggeberg, M. (2018). Hygroscopically actuated wood elements for weather responsive and self-forming building parts – Facilitating upscaling and complex shape changes. Construction And Building Materials, 165, 782-791. doi: 10.1016/j.conbuildmat.2017.12.134

Ultra Multi-purpose Special Site / Konishi Corporation. (2019). Retrieved from http://www.bond.co.jp/bond/special/su/lineup_soft/